

TEMPORAL AND MOLECULAR INSIGHTS INTO THE PATHOPHYSIOLOGY OF
CDKL5 DEFICIENCY DISORDER

Barbara Terzic

A DISSERTATION

in

Neuroscience

Presented to the Faculties of the University of Pennsylvania

in

Partial Fulfillment of the Requirements for the

Degree of Doctor of Philosophy

2020

Supervisor of Dissertation

Zhaolan Zhou, Ph.D.

Professor of Genetics

Graduate Group Chairperson

Joshua I. Gold, Ph.D., Professor of Neuroscience

Dissertation Committee

Marc V. Fuccillo, M.D., Ph.D., Assistant Professor of Neuroscience

Erika Holzbaur, Ph.D., Professor of Physiology

Wenqin Luo, M.D., Ph.D., Associate Professor of Neuroscience

Eric D. Marsh, M.D., Ph.D., Associate Professor of Neurology

TEMPORAL AND MOLECULAR INSIGHTS INTO THE PATHOPHYSIOLOGY OF CDKL5
DEFICIENCY DISORDER

COPYRIGHT

2020

Barbara Terzic

This work is licensed under the
Creative Commons Attribution-
NonCommercial-ShareAlike 4.0
License

To view a copy of this license, visit
<https://creativecommons.org/licenses/by-nc-sa/4>.

ABSTRACT

TEMPORAL AND MOLECULAR INSIGHTS INTO THE PATHOPHYSIOLOGY OF CDKL5 DEFICIENCY DISORDER

Barbara Terzic

Zhaolan Zhou

CDKL5 deficiency disorder (CDD) is a severe, neurodevelopmental disorder associated with lesions in the X-linked cyclin-dependent kinase-like 5 (*CDKL5*) gene. Despite the simple genetic etiology of CDD its pathophysiology remains poorly understood, and the treatability of specific CDD symptoms is untested. Using genetically modified mouse models of CDD, we demonstrate that aberrant glutamatergic signaling through NMDA receptors underlies the disrupted circuit hyperexcitability connected to several CDD-related deficits in mice. We also temporally manipulated endogenous *Cdkl5* expression, and find that post-developmental loss of CDKL5 disrupts numerous behavioral domains, hippocampal circuit communication, and dendritic spine morphology, demonstrating an indispensable role for CDKL5 in the adult brain. Accordingly, adult restoration of *Cdkl5* in knockout mice significantly ameliorates CDD-related behavioral impairments and aberrant NMDA receptor signaling. These results demonstrate that adult neural function requires CDKL5, and suggest chronic treatment may be required in CDD. Furthermore, our results uncover a broad therapeutic time window for numerous CDD-related deficits, and substantiate aberrant NMDA receptor signaling as underlying numerous CDD pathologies. These discoveries expand upon our current understanding of CDKL5 in regulating neurological function, and comprise a critical foundation for future studies aiming to develop therapeutics for CDD patients, especially beyond the early developmental time window.

TABLE OF CONTENTS

ABSTRACT	III
LIST OF TABLES	VIII
LIST OF ILLUSTRATIONS.....	IX
CHAPTER 1 – INTRODUCTION.....	1
Overview.....	1
The Genetics and Clinical Features of CDKL5 Deficiency Disorder.....	2
A history of the classification of CDKL5 Deficiency Disorder	2
Clinical presentations and phenotypic variations in CDKL5 Deficiency Disorder.....	3
Genetic characteristics of CDKL5 Deficiency Disorder patients	5
Animal Models of CDKL5 Deficiency.....	6
Molecular Features and Signaling Pathways of the CDKL5 Protein.....	8
CDKL5 protein characteristics.....	8
CDKL5 transcript isoforms and expression pattern	9
CDKL5 interacting proteins and signaling pathways.....	10
Cellular Phenotypes Resulting from CDKL5 Loss	13
Synaptic, Circuit, and Network Phenotypes of CDKL5-Deficient Mice	14
Synaptic phenotypes regulated by CDKL5.....	14
Disrupted circuit activity with loss of CDKL5	16
Network activity and epilepsy in models of CDKL5 deficiency	17
Tables.....	20
CHAPTER 2 – ALTERED NMDAR SIGNALING UNDERLIES AUTISTIC-LIKE FEATURES IN MOUSE MODELS OF CDKL5 DEFICIENCY DISORDER.....	22
Abstract	22
Introduction.....	23
Results	25
CDKL5 GABAergic deletion results in autistic-like features.....	25
Dlx-cKO mice show aberrant circuit activation	26
Dlx-cKO mice show enhanced excitatory synaptic transmission	28
Dlx-cKO mice have an increase in postsynaptic NMDA receptors	29

NMDAR blockade ameliorates autistic-like features in Dlx-cKO	29
NMDAR blockade improves autistic-like features in CDKL5 R59X	30
Discussion	31
Materials and Methods.....	35
Figures	48
CHAPTER 3 – CDKL5 IS ESSENTIAL IN THE POST-DEVELOPED BRAIN TO MAINTAIN MULTIPLE BEHAVIORAL DOMAINS, HIPPOCAMPAL CIRCUIT COMMUNICATION, AND SYNAPTIC MORPHOLOGY	63
Abstract	63
Introduction.....	64
Results	66
Post-developmental loss of CDKL5 results in behavioral deficits similar to germline knockout mice.....	66
Adult loss of CDKL5 disrupts hippocampal, low-frequency event-related neuronal oscillations similar to germline knockout mice.....	68
Germline, but not adult, loss of CDKL5 disrupts dendritic complexity of hippocampal CA1 pyramidal neurons.....	69
CDKL5 is required for the maintenance of dendritic spine morphology on hippocampal CA1 pyramidal neurons.....	70
CDKL5 continuously regulates phosphorylation of the microtubule end-binding 2 protein.....	73
Discussion	75
Adult neural function requires CDKL5.....	75
Loss of CDKL5 influences dendritic arborization of CA1 pyramidal neurons during a critical time window in development.....	78
CDKL5 is required for the maintenance of hippocampal dendritic spine morphology	80
Materials and Methods.....	82
Figures	92
CHAPTER 4 – LATE RESTORATION OF CDKL5 EXPRESSION IS SUFFICIENT TO RESCUE CDD-RELATED BEHAVIORAL IMPAIRMENTS AND ABBERANT NMDA-RECEPTOR SIGNALING	107
Abstract	107
Introduction.....	108
Results	109
Adult restoration of CDKL5 rescues numerous CDD-related behavioral deficits in hemizygous male knockout mice	109

Adult restoration of CDKL5 abrogates NMDA-induced hyperexcitability and aberrant NMDAR-mediated synaptic responses.....	112
Adult restoration of <i>Cdkl5</i> expression ameliorates CDD-related behavioral deficits in heterozygous female mouse models of CDD	114
Discussion	115
Adult restoration of CDKL5 ameliorates several loss-of-function deficits	115
CDKL5 and NMDA receptor signaling.....	117
Modeling and treating CDD-related phenotypes in heterozygous female mice.....	118
Materials and Methods.....	119
Figures	130
CHAPTER 5 – X-LINKED CELLULAR MOSAICISM UNDERLIES AGE-DEPENDENT SEIZURE OCCURRENCE IN MOUSE MODELS OF CDKL5 DEFICIENCY DISORDER	140
Abstract	140
Introduction.....	141
Results	143
Female mice heterozygous for mutations in <i>Cdkl5</i> exhibit seizure-like events in an age-dependent manner	143
Seizure-like event frequency and severity in <i>Cdkl5</i> heterozygous females increases with age with a concomitant reduced life span	146
Heterozygous mosaic, but not homozygous or hemizygous, loss of CDKL5 underlies spontaneous seizure development.....	149
Restoration of <i>Cdkl5</i> expression prevents and reverses the evolution of seizure-like events in heterozygous female models of CDD	150
Discussion	151
Late-onset of epilepsy phenotype in female CDD mouse models	152
Disturbance-associated nature of CDD mouse seizure phenotypes	154
Mosaic loss of CDKL5 drives the overt presentation of spontaneous seizures	155
Seizure treatment in mouse models of CDD.....	156
Materials and Methods.....	157
Figures	163
CHAPTER 6 – EXTENDED DISCUSSION AND FUTURE DIRECTIONS	172
Cellular Origins of CDKL5 Deficiency Disorder-Related Phenotypes	172
Generation of CDKL5-TAVI knock-in mice for the investigation of CDKL5 molecular targets and signaling pathways.....	173
Synaptic Convergence of CDKL5 Loss-of-Function Phenotypes	174

Temporal Dissection of CDKL5 Deficiency Disorder Pathophysiology	176
Therapeutic Insights for CDKL5 Deficiency Disorder	178
Materials and Methods.....	179
Figures	182
BIBLIOGRAPHY	184

LIST OF TABLES

Chapter 1

Table 1. Behavioral phenotypes reported across various mouse models of <i>Cdkl5</i> deficiency.....	p20
Table 2. Summary of all reported CDKL5 interacting proteins and targets.....	p21

Chapter 5

Table 1. Modified Racine scale used for behavioral seizure scoring.....	p163
---	------

LIST OF ILLUSTRATIONS

Chapter 2

Figure 1. Generation and validation of mice lacking CDKL5 selectively in forebrain GABAergic neurons (Dlx-cKO).....	p47
Figure 2. Dlx-cKO mice show unaltered growth, locomotion, anxiety-related behavior, and motor coordination.....	p48
Figure 3. Dlx-cKO mice exhibit an autistic-like phenotype.....	p49
Figure 4. Dlx-cKO mice show aberrant paired-pulse facilitation.....	p51
Figure 5. VSDI responses in regions of the dentate gyrus at 400 μ A stimulation intensity.....	p53
Figure 6. Enhanced excitatory synaptic transmission but unaltered inhibitory synaptic transmission in Dlx-cKO mice.....	p54
Figure 7. Unaltered mEPSC and mIPSC kinetics in Dlx-cKO mice.....	p55
Figure 8. Dlx-cKO mice have an upregulation of NMDA receptors at the postsynaptic membrane.....	p56
Figure 9. Acute NMDAR blockade ameliorates autistic-like features in Dlx-cKO mice.....	p57
Figure 10. R59X mice have an upregulation of NMDA receptors at the postsynaptic membrane.....	p58
Figure 11. Loss of full-length CDKL5 protein in R59X knock-in mice.....	p59
Figure 12. Acute NMDAR blockade ameliorates autistic-like features, but not learning and memory, in CDKL5-deficient mice.....	p60

Chapter 3

Figure 1: Post-developmental loss of CDKL5 disrupts multiple behavioral domains in mice.....	p91
Figure 2. Timecourse of CDKL5 protein knockdown with tamoxifen.....	p93
Figure 3. Additional behavioral domains analyzed upon adult deletion of <i>Cdkl5</i>	p94

Figure 4: Post-developmental loss of *Cdkl5* disrupts hippocampal event-related potentials.....p95

Figure 5: Germline, but not adult, loss of *Cdkl5* results in decreased dendrite length and complexity of CA1 pyramidal neurons.....p97

Figure 6. Germline or post-developmental deletion of *Cdkl5* does not alter dendritic spine density on hippocampal CA1 neurons.....p99

Figure 7. Post-developmental deletion of *Cdkl5* disrupts hippocampal CA1 dendritic spine morphology.....p100

Figure 8: Post-developmental loss of *Cdkl5* results in cell-autonomous disruption of dendritic spine morphology on CA1 pyramidal neurons.....p101

Figure 10. AKO mice do not demonstrate disrupted AKT/mTOR pathway signaling.....p103

Figure 9. Germline and post-developmental deletion of *Cdkl5* abrogate EB2 phosphorylation.....p104

Figure 11. EB2 phosphorylation is developmentally regulated and correlates with CDKL5.....p105

Chapter 4

Figure 1: Adult restoration of *Cdkl5* expression rescues CDD-associated behavioral deficits.....p129

Figure 2. STOP mice are behaviorally similar to *Cdkl5* germline knock-in mice by postnatal day 42.....p131

Figure 3. Rapid, but not gradual, reversal of *Cdkl5* expression is associated with significant lethality.....p132

Figure 4. Additional behavioral domains analyzed upon adult rescue of *Cdkl5*.....p133

Figure 5. Partial restoration of CDKL5 protein is capable of rescuing multiple behavioral domains.....p134

Figure 6: Adult restoration of CDKL5 abrogates aberrant NMDAR-mediated synaptic responses.....p136

Figure 7: Adult restoration of *Cdkl5* expression ameliorates several CDD-associated behavioral deficits in heterozygous female CDD mice.....p138

Chapter 5

Figure 1. Disturbance-associated seizure-like events in heterozygous CDD female mice.....p163

Figure 2. Prevalence and severity of disturbance-associated seizure-like events in R59X/+ females increases with age.....p164

Figure 3. Prevalence and severity of disturbance-associated seizure-like events in KO/+ females increases with age.....p165

Figure 4. Seizure-like events are confined to *Cdkl5* heterozygous female knockout mice and are independent of estrous cycle and parity.....p166

Figure 5: Prevention of seizure phenotype in heterozygous *Cdkl5* knockout female mice with early gene restoration.....p167

Figure 6: Reversal of seizure phenotype in heterozygous *Cdkl5* knockout female mice with late gene restoration.....p168

Figure 7: Reversal of seizure phenotype in heterozygous females of an independent *Cdkl5* knockout mouse line with late gene restoration.....p169

Supplemental Videos are all accessible in a DropBox folder linked [here](#).

(<https://www.dropbox.com/sh/f4vi37yo03rf0yy/AABqNzzJLmv5gsYz9MLzCr03a?dl=0>)

Chapter 6

Figure 1. Generation and validation of CDKL5-TAVI mice.....p181

CHAPTER 1 – INTRODUCTION

Overview

CDKL5 deficiency disorder (CDD) is a severe, childhood epileptic encephalopathy associated with pathogenic variants in the X-linked cyclin-dependent kinase-like 5 (*CDKL5*) gene (Fehr et al., 2013; Kalscheuer et al., 2003; Tao et al., 2004; Weaving et al., 2004). Currently, CDD has a reported incidence of one in 40,000 to 50,000 live births, making it one of the most common genetic causes of epilepsy in children (López-Rivera et al., 2020; H. E. Olson et al., 2019). The majority of cases are heterozygous females who carry a constellation of debilitating phenotypes including early-onset seizures, global neurodevelopmental delay, motor dysfunction, intellectual disability, and several autonomic dysfunctions (e.g., feeding and gastrointestinal problems, sleep disturbances, and breathing abnormalities) (H. E. Olson et al., 2019). Despite the strong genetic link, the evolution of CDD pathophysiology and neurological impairments resulting from disrupted CDKL5 function remain unclear.

Several animal models of CDD have been generated and characterized to date, demonstrating a general overlap in phenotypic presentation and highlighting the importance of CDKL5 in establishing proper brain development and neurological function (Amendola et al., 2014; Okuda et al., 2018; I. T. Wang et al., 2012). Importantly, these animal models have also provided an *in vivo* setting to discover and validate the molecular, cellular, and circuit disruptions associated with loss of CDKL5 function. Despite this progress, the time course of CDD pathogenesis, specific roles for CDKL5 in nervous system development versus maintenance, and reversibility of CDD-related phenotypes remain undetermined. Thus, there remains a pressing need to address these unknowns, and thereby support future examinations into CDKL5 function as well as therapeutic efforts aimed towards treating CDD.

The Genetics and Clinical Features of CDKL5 Deficiency Disorder

A history of the classification of CDKL5 Deficiency Disorder

CDKL5 Deficiency Disorder (CDD) only became recognized as an independent clinical entity in 2013, however, clinical reports of patients presenting with an “atypical” pattern of Rett syndrome date back as early as the 1980s(Fehr et al., 2013). In 1985, Dr. Folker Hanefeld reported on a case in which a young girl presented with atypical infantile spasms in conjunction with progressive Rett-like symptoms, now known to be characteristic of CDD(Hanefeld, 1985). As early seizures are unusual in the evolution of Rett syndrome, and infantile spasms had yet to be reported in these patients, this collection of phenotypes was hereafter referred to as the early-onset-seizure, or “atypical,” variant of Rett syndrome. In 2003, Kalscheuer et al. reported an association between lesions in the X-linked *CDKL5* gene and severe infantile spasms coupled to global neurodevelopmental delay(Kalscheuer et al., 2003). The two, severely affected, female patients in this case report carried *de novo* X chromosome translocations, both of which disrupted the (then named) serine-threonine kinase 9 gene, *STK9* (since renamed *CDKL5*)(Montini et al., 1998). The neurological impairments and infantile spasms presented by these two patients carried characteristics of X-linked West syndrome, also referred to as X-linked infantile spasms (ISSX), which presents with early-onset generalized seizures, hypsarrhythmia, and mental retardation(Bienvenu, 2002). Thus, disruptions in *STK9/CDKL5* were grouped with previously-reported *ARX* mutations, and postulated to serve as a second X-chromosomal locus for ISSX(Kalscheuer et al., 2003).

Independently, and shortly thereafter, Weaving et al. reported on two additional, unrelated families carrying mutations in *CDKL5* whose children (including one male) presented with severe neurodevelopmental delay and infantile spasms(Weaving et al., 2004). This study, published in 2004, also examined the *CDKL5* locus within *MECP2*-mutation negative Rett syndrome patients, and found an additional female patient reported to present with the early-onset-seizure variant of Rett to carry a *de novo* *CDKL5* splice-site mutation (*CDKL5* IVS13-

1G→A). In this same 2004 issue of *American Journal of Human Genetics*, an independent clinical report demonstrated further evidence linking *de novo* mutations in the *CDKL5/STK9* gene to early-onset infantile spasms, intellectual disability, and severe neurodevelopmental delay (Tao et al., 2004). Although ~80% of Rett syndrome patients carry a mutation in the X-linked *MECP2*, only ~20-40% of patients presenting with atypical Rett syndrome have reported *MECP2* mutations. This study reported previously-unidentified *CDKL5* mutations in several *MECP2*-mutation negative atypical Rett syndrome patients, further linking lesions in *CDKL5* to the atypical clinical features associated with this subtype of Rett. Therefore, these early studies comprised a seminal foundation for connecting lesions in *CDKL5* to the etiology of this distinct constellation of features characterized by early-onset seizures/infantile spasms, severe neurodevelopmental delay, and autistic features. Although it would be another ten years before CDD became classified as an independent clinical entity, distinct from Rett syndrome (Fehr et al., 2013).

Clinical presentations and phenotypic variations in CDKL5 Deficiency Disorder

The most updated reports of the clinical features of CDKL5 Deficiency Disorder (CDD) currently classify it as a developmental encephalopathy (H. E. Olson et al., 2019). This class of diseases share a common constellation of features beyond traditional autism spectrum disorders or intellectual disability, most notably refractory epilepsy as well as motor and autonomic dysfunctions (Paciorkowski, Seltzer, & Neul, 2018). The current incidence of reported pathogenic variants in *CDKL5* is one in 40,000 to 50,000 live births, making it only half as prevalent as traditional Rett syndrome, and as an X-linked disorder CDD predominately afflicts young females over males (~4:1) (López-Rivera et al., 2020; H. E. Olson et al., 2019).

One of the hallmark features of CDD, refractory epilepsy, significantly impacts patient and family quality of life, with 80% of CDD patients presenting with daily seizures and fewer than half reporting more than 2 months of sustained seizure freedom (Fehr et al., 2013; Fehr, Wong, et al., 2016). Most families report a median age of onset at 6 weeks of age, with 90% of patients developing seizures by three months of age. This severe, early-onset feature of CDD can also

have profound impact on neurodevelopment and carries a high risk of behavioral and cognitive comorbidities(Fehr et al., 2015; Fehr et al., 2013; Mangatt et al., 2016). Thus, seizure treatment in CDD has been a central focus of recent therapeutic endeavors. The epilepsy of CDD typically progresses in three stages across the first several years of life: 1) early-onset infantile spasms, 2) epileptic encephalopathy with hypsarrhythmia, and finally 3) refractory multifocal and myoclonic epilepsy. The evolving epilepsy phenotype in CDD appears to be mixed focal and generalized, with spasms, tonic, and tonic-clonic seizures being the most common(Bahi-Buisson, Kaminska, et al., 2008). The autonomic dysfunctions associated with CDD, such as irregular respirations and apnea, can also arise during this time(H. E. Olson et al., 2019). Broad spectrum antiseizure medications are most commonly prescribed including clobazam, valproate, topiramate, levetiracetam, and vigabatrin in combination with a ketogenic diet(Fehr, Wong, et al., 2016; Muller et al., 2016). Cannabidiol has been more recently explored with regards to the treatment of motor seizure frequency, and is in phase 2 of clinical trials for use in CDD(Devinsky et al., 2018). However, seizure management remains an issue for the majority patients, and the efficacy of most therapies does not appear to extend beyond 12 months for most individuals(Muller et al., 2016).

Unlike Rett syndrome, CDD patients do not typically carry a developmental regression, and instead present with severe global developmental delays and intellectual disability(Bahi-Buisson, Nectoux, et al., 2008; Fehr et al., 2013; Liang et al., 2011; D. Mei et al., 2010; H.E. Olson & Poduri, 2012). Only 22-23% of reported female patients can independently walk, and 26% of individuals could produce spoken language with only 7.5% speaking in sentences(Fehr, Downs, et al., 2016; Fehr et al., 2015). However, microcephaly is only reported in fewer than 10% of individuals(Fehr et al., 2013; H.E. Olson & Poduri, 2012). The cortical visual impairment reported for CDD also limits the use of nonverbal communication and eye gaze(H. E. Olson et al., 2019). Accordingly, although autistic features are commonly reported in CDD, a diagnosis of autism spectrum disorder is infrequently provided given the significance of global developmental

impairments(Bahi-Buisson, Nectoux, et al., 2008; Liang et al., 2011; D. Mei et al., 2010; Nemos et al., 2009; H.E. Olson & Poduri, 2012).

Over 80% of CDD individuals also present with hand stereotypies such as self-stimulatory behavior as well as repetitive leg crossing, and hypotonia is a nearly universal feature for most patients(Fehr et al., 2013; Fehr, Wong, et al., 2016; H. E. Olson et al., 2019),. Gastrointestinal symptoms such as constipation, reflux, and air swallowing are reported in up to 86.5% of patients along with dysphagia, with only 5.3% able to eat and drink independently(Fehr et al., 2013; Mangatt et al., 2016). Furthermore, sleep difficulties for CDD individuals are reported by over 85% of parents often comorbid with breathing abnormalities and hyperventilation(Mangatt et al., 2016).

Together, these clinical reports highlight a heterogeneous assortment of phenotypes, including treatment-resistant epilepsy, autistic traits, and severe cognitive and motor developmental delays, that can comprise CDD. However, significant phenotypic heterogeneity has been reported, and growing efforts in diagnosis and variant mapping of CDD patients will hopefully lead to better genotype-phenotype correlations(H. E. Olson et al., 2019). With further clinical and preclinical studies, there is hope that future drug and therapy development will ultimately provide more efficacious treatments for this devastating and debilitating disorder.

Genetic characteristics of CDKL5 Deficiency Disorder patients

CDD is associated with mutations, typically *de novo*, in the X-linked cyclin-dependent kinase-like 5 (*CDKL5*) gene(Archer et al., 2006; Evans et al., 2005; Fehr et al., 2013; Kalscheuer et al., 2003; H.E. Olson & Poduri, 2012). *CDKL5* resides on the distal portion of the short arm of the X chromosome (Xp22), and encodes a serine-threonine kinase of the same name, CDKL5(Montini et al., 1998). Pathogenic missense variants mapped to date occur exclusively within the catalytic domain of the protein, and deletion and truncating variants nearly universally cause CDD(R.D. Hector et al., 2017). There have also been reports of patients carrying *CDKL5*

duplications, which are typically associated with macrocephaly and learning disability without epilepsy(Szafranski et al., 2015).

As mentioned, there is at times significant phenotypic heterogeneity amongst CDD patients, however, genotype-phenotype correlations are limited. Individuals carrying early truncating variants, compared with some pathogenic missense variants, appear to have a more severe disorder(Bahi-Buisson et al., 2012; Fehr, Downs, et al., 2016; Fehr et al., 2015; Fehr, Wong, et al., 2016). Being an X-linked disorder, some of the phenotypic heterogeneity observed in CDD female patients may be due to variable X-chromosome inactivation (XCI), however, the influence of somatic CDKL5 mosaicism on the clinical phenotype of CDD remains unknown(R.D. Hector et al., 2017; H. E. Olson et al., 2019; Stosser et al., 2018). In the Weaving et al. clinical reported discussed above, one female patient demonstrated slightly skewed XCI that favored expression of the normal CDKL5 allele, however, the XCI pattern of blood leukocytes profiled in this study may not accurately reflect XCI patterns in the brain(Weaving et al., 2004). In fact, the same study reported twin sisters displaying similar XCI patterns in peripheral blood, yet completely different clinical features. Furthermore, mosaic exon deletions and mosaic *de novo* variants have been reported in both male and female CDD patients, and although their exact incidence remains undetermined, they may be an underappreciated phenomenon in CDD(Stosser et al., 2018).

Animal Models of CDKL5 Deficiency

In 2012, the first knockout mouse model of CDD was generated and found to recapitulate several of the cardinal phenotypes of the human disease including learning and memory impairments, motor deficits, and autistic-like behaviors but not overt seizures(I. T. Wang et al., 2012). This line carries a deletion of *Cdkl5* exon 6, mimicking a reported CDD patient splice site mutation resulting in exon 6 skipping and loss of protein(Archer et al., 2006). The male mice examined in this report exhibited normal growth, brain and body weight, and a lack of gross brain pathology. Several additional knockout and knock-in lines have since been generated with

behavioral assessments, despite a few discrepancies, highlighting a general overlap of phenotype presentation across different *Cdkl5* knockout models. These include three independent *Cdkl5* knockout lines (*Cdkl5* Δ 4, *Cdkl5* Δ 2, and *Cdkl5*^{STOP} (first reported in this study; Chapter 4)) as well as a knock-in line, *Cdkl5*^{R59X}, modeling a reported patient nonsense mutation resulting in early truncation and loss of CDKL5 protein (Amendola et al., 2014; Okuda et al., 2018; Tang et al., 2019; Yennawar, White, & Jensen, 2019). A summary of the behavioral phenotypes evaluated across various CDD mouse models is summarized in Table 1.

CDKL5 is expressed throughout various cell types in the heterologous brain highlighting the importance of dissecting any cell type-specific and circuit-level network disruptions relevant to CDD (Chen et al., 2010; Johnson et al., 2017; Rusconi et al., 2008; I. T. Wang et al., 2012; Zeisel et al., 2015). There have accordingly been *Cdkl5* conditional knockout studies wherein *Cdkl5* was ablated selectively from either forebrain glutamatergic (Nex-cKO) or forebrain GABAergic (Dlx-cKO; Chapter 2) neurons (Tang et al., 2019; Tang et al., 2017). These two studies, as discussed further in Chapter 2 below, reflect a general segregation of *Cdkl5* constitutive knockout phenotypes with Nex-cKO mice selectively demonstrating impaired learning and memory (reminiscent of the intellectual disability of CDD), and Dlx-cKO mice selectively demonstrating autistic-like features. Prior to this work, Amendola et al. had also performed a conditional deletion of *Cdkl5* from forebrain glutamatergic neurons and glial cells (Emx1-cKO) versus GABAergic (Dlx-cKO) neurons, but only evaluated general locomotion, finding a selective decrease in activity in Dlx-cKO males (Amendola et al., 2014). Although the results of cell-type-specific loss of CDKL5 within different circuits and brain regions remain to be expanded upon, these data reveal that distinct phenotypes in *Cdkl5* knockout mouse models can be mapped to diverse forebrain neuronal populations.

Interestingly, although early-onset epilepsy is one of the hallmark features of CDD, no overt seizure phenotype or abnormal basal EEG pattern was reported in any of the hemizygous knockout male mice observed in the above-mentioned studies. However, a recent finding by our group suggests that spontaneous seizure activity in CDD mouse models is confined to aged,

heterozygous knockout females (Chapter 5). This highlights X-linked mosaicism as a potential driver for overt, spontaneous seizure activity and underscores why previous reports to date may not have observed this phenotype. Further details on the EEG and network phenotypes reported in *Cdkl5*-deficient animal models is discussed in the 'Synaptic, Circuit, and Network Phenotypes of CDKL5-Deficient Mice' section below. Despite these multitude of behavioral and EEG characterizations of various CDD mouse models, the endogenous function of CDKL5 and its role in nervous system development, maintenance, and CDD pathogenesis remain undetermined.

Molecular Features and Signaling Pathways of the CDKL5 Protein

CDKL5 protein characteristics

The CDKL5 protein is serine-threonine kinase highly conserved among vertebrates, carrying 99% identity within its 960 amino acids between mouse and human orthologues of CDKL5 (Montini et al., 1998). As mentioned, all pathogenic missense mutations appear to cluster within the region of *CDKL5* encoding the amino(N)-terminal kinase domain, suggesting that disrupted kinase function likely underlies disease pathophysiology (R.D. Hector et al., 2017). The CDKL5 kinase domain carries significant homology to those of the cyclin-dependent kinase (CDK) and mitogen-activated protein (MAP) kinase families, however, it is distinct from these and other cyclin-dependent kinase like (CDKL) family members in that it also possess a long, proline-rich carboxy(C)-terminal domain of about 700 amino acids (Canning et al., 2018; R. D. Hector et al., 2016). Previous *in vitro* and heterologous cell line studies have suggested this C-terminal domain to serve as a negative regulator of CDKL5 kinase activity as well as to affect protein sub-cellular localization (Bertani et al., 2006; Lin, Franco, & Rosner, 2005). In addition, the CDKL5 protein carries two predicted nuclear localization sequences (NLS) and a nuclear export sequence (NES), suggesting that it may shuttle between the nuclear and cytoplasmic compartments (Bertani et al., 2006; Rusconi et al., 2008). More recently, visualization of CDKL5 in neuronal cultures as well as post-synaptic density fractionation from brain tissues has suggested that CDKL5 is enriched at the post-synaptic density of neurons (Bayés et al., 2012; Reim et al.,

2017; Ricciardi et al., 2012; Zhu et al., 2013). However, the *in vivo* relevance of these findings has yet to be tested, and the limited availability of tools to visualize and tag the endogenous CDKL5 make these results difficult to corroborate.

CDKL5 transcript isoforms and expression pattern

Analysis of the human and mouse *CDKL5/Cdkl5* transcript sets has identified at least five unique isoforms(R. D. Hector et al., 2016). *hCDKL5_1/mCdkl5_1* is the predominant isoform in the brains of humans and mice, respectively, with detectable levels in additional tissues (particularly testis), albeit at significantly lower levels. Alternative CDKL5 mRNA isoforms (*hCDKL5_2-5*; *mCdkl5_2* & *mCdkl5_6-8*) arise from the inclusion of additional 3' exons as well as alternative splicing of exon 17, however, in mice, their expression pattern appears to be mostly restricted to the testis. The human *hCDKL5_2* (inclusion of exon 17) and *hCDKL5_3* (alternative splicing of exon 11) are also detectable in brain tissues, but are only predicted to constitute ~10% of *CDKL5* transcripts in brain(R. D. Hector et al., 2016). Therefore, the 960 amino acid protein product of isoform 1 is thought to be the predominant product regulating neuronal function in both mouse and human.

In rodents, the CDKL5 protein is most highly expressed in the central nervous system, particularly within regions of the forebrain (e.g., cortex, striatum, amygdala, and hippocampus)(Chen et al., 2010; Rusconi et al., 2008; I. T. Wang et al., 2012; Zeisel et al., 2015). More recent findings have also demonstrated a role for CDKL5 within the peripheral nervous system in the regulation of pain perception by sensory neurons of the dorsal root ganglia(Paolo La Montanara et al., 2020). Our lab and others have also observed detectable, but significantly lower, CDKL5 protein levels in additional tissues of mice such as lung, kidney, and testis(Lin et al., 2005; Rusconi et al., 2008). Interestingly, a recent kinome-wide screen identified CDKL5 as a critical regulator of a stress-response pathway in renal tubular epithelial cell death during acute kidney injury, highlighting the potential importance of CDKL5 in additional tissues(Kim et al., 2020). The role of CDKL5 and its various isoforms in additional tissues remains ripe for

exploration, however, the remainder of this report will focus on its role in neurological function with relation to CDD.

RNA-sequencing analysis of mouse embryonic brain tissue finds *Cdkl5* transcripts significantly detectable by embryonic day 15 (Smith CM, 2019). This embryonic expression pattern is supported by post-mortem, human brain transcriptome data reflecting a significant expression of *CDKL5* RNA within several brain regions by the second trimester of gestation (H. J. Kang et al., 2011). Several groups have previously reported on the developmental expression pattern of CDKL5 protein within the rodent brain, albeit with conflicting conclusions likely due to the lack of a specific CDKL5 antibody. These reports range from suggesting the kinase to be detectable in brain as early as embryonic day 7.5 to expression being restricted until the postnatal period, and then usually peaking in expression during the critical period of synaptogenesis for several brain regions in mice (i.e. postnatal day 10-14) (Lin et al., 2005; Rusconi et al., 2008; Zhu et al., 2013). Despite slight embryonic discrepancies, our group and others have consistently demonstrated that CDKL5 remains stably expressed throughout life in the forebrain of mice (Chapter 3). These results ultimately motivated our exploration of the post-developmental role of CDKL5 in neurological function (Chapter 3).

CDKL5 interacting proteins and signaling pathways

As mentioned above, CDKL5, unlike its family members CDKL1-4, is expressed predominantly in post-mitotic neurons as opposed to dividing cells, likely conferring a distinct set of signaling targets and pathways (Canning et al., 2018; Dubos, Pannetier, & Hanauer, 2008; He et al., 2020; Li et al., 2014; Qin et al., 2017; Smith CM, 2019). To date, several *in vitro* and cell culture studies have identified a variety of CDKL5 interacting proteins. Given the clinical overlap between Rett syndrome and CDD, it was initially postulated that CDKL5 and MECP2 might function within the same molecular pathway. In fact, it was shown in an *in vitro* kinase assay that CDKL5 was capable of interacting with and phosphorylating MECP2 (Mari et al., 2005). However, this finding has yet to be replicated by other groups or *in vivo*, and more recent reports suggest

the two proteins likely function within unique molecular signaling networks(Lin et al., 2005). Thus, the clinical overlap between CDD and Rett syndrome may simply occur due to converging disruptions at the cellular or network levels.

In line with the idea of a nuclear function for CDKL5, additional nuclear binding partners and targets have been postulated, mainly identified via *in vitro* kinase assays or through work in heterologous cell lines. These include the DNA methyltransferase 1 (DNMT1), as well as a role for CDKL5 in regulating mRNA splicing activity via its association with the nuclear speckle component SC35(Kameshita et al., 2008; Ricciardi et al., 2009). A more recent, phosphoproteomic screen for direct CDKL5 substrates also highlighted proteins involved in the DNA damage response, such as centrosomal protein 131 (CEP131)(Munoz et al., 2018). These findings align with the increase in cell death and DNA damage-associated biomarkers reported with CDKL5 deletion in mouse hippocampal cultures and human neuroblastoma (SH-SY5Y) cell lines(Barbiero et al., 2017; Fuchs et al., 2019; Loi et al., 2020).

Additional hypotheses have focused on a synaptic role for CDKL5 within neurons. In rat primary neuron cultures, knockdown of CDKL5 was found to disrupt neuronal morphogenesis and neurite outgrowth upon BDNF-induced actin remodeling via its association with Rac1(Chen et al., 2010). Similarly, two independent reports highlighted a role for CDKL5 in dendritic spine morphology in cultured hippocampal neurons via its interaction with components of the postsynaptic compartment such as phosphorylating netrin-G1 ligand (NGL-1) and co-localizing with palmitoylated post synaptic density protein 95 (PSD-95)(Ricciardi et al., 2012; Zhu et al., 2013). CDKL5 was also linked to the phosphorylation of amphiphysin 1 at the pre-synaptic terminal, again, using an *in vitro* system(Katayama, Sueyoshi, & Kameshita, 2015; Sekiguchi et al., 2013). Furthermore, a yeast two-hybrid screen identified an interaction of CDKL5 with shootin1, a regulator of neuronal polarization during axon development(Nawaz et al., 2016). Interestingly, a mind bomb 1 (Mib1) interactome screen that identified CDKL5 demonstrated that CDKL5 is ubiquitinated by Mib1 and targeted for degradation by the proteasome(Mertz et al.,

2015). The direct relevance of these synaptic and axonal targets *in vivo* has yet to be validated, again likely due to the limitation of tools to visualize and tag the endogenous CDKL5.

More recently, a chemical-genetic approach was leveraged to identify direct CDKL5 kinase targets by harnessing an ATP analog-specific CDKL5 mutant in mouse brain tissue lysates coupled with thiophosphopeptide-targeted mass spectrometry. This study reported that CDKL5 directly phosphorylates peptides at the RPXS* motif that mapped to proteins associated with the microtubule network of neurons (Lucas L. Baltussen et al., 2018). These targets included the microtubule associated protein RP/EB family member 2 (MAPRE2/EB2), the microtubule associated protein 1S (MAP1S), and Rho guanine nucleotide exchange factor 2 (ARHGEF2). These results were corroborated by an independent group performing a global, TMT-based phosphoproteomic screen for CDKL5 substrates. This second study confirm the enrichment of CDKL5 phosphorylated proteins as involved in the actin cytoskeleton and microtubule-associated proteins, including MAP1S (Munoz et al., 2018). Together, these findings highlight a novel, activity-dependent molecular pathway in dendritic microtubule regulation that may underlie the pathology of CDD. These more recent results also align with some of the cellular and synaptic phenotypes reported in CDKL5-deficient models (see 'CDKL5 Loss-of-Function Cellular Phenotypes' section below). A summary of all reported CDKL5 interacting proteins and targets identified to date is listed in Table 2.

Loss of CDKL5 was shown to disrupt signaling of the AKT-mammalian target of rapamycin (mTOR) cascade within several brain region tissue lysates of the first *Cdkl5* knockout mouse (*Cdkl5Δ6*) (I. T. Wang et al., 2012). Similar findings were reported in whole brain extracts of an independent knockout mouse line (*Cdkl5Δ4*) with reduced phosphorylation of AKT and ribosomal protein S6 reflecting an overall disruption of neuronal growth/plasticity and protein translation (Amendola et al., 2014). More specifically, altered AKT/GSK-3β signaling was also reported within *Cdkl5* knockout mouse hippocampal tissue, concomitant with a significant reduction of dendritic arborization and length (Fuchs et al., 2014). However, the direct role of

CDKL5 within the action of these pathways, as opposed to compensatory or non-specific AKT/mTOR disruptions, has not been tested.

Cellular Phenotypes Resulting from CDKL5 Loss

At the cellular level, loss of CDKL5 has been reported to result in morphological deficits such as reduced dendritic arborization and complexity as well as aberrant spine morphology/stability in pyramidal neurons. In culture models, shRNA knockdown of CDKL5 impairs neurite outgrowth in rat primary hippocampal neurons, and several *Cdkl5* knockout mice have been reported to display reduced dendritic complexity in the hippocampus (Amendola et al., 2014; Chen et al., 2010; Okuda et al., 2018; Tang et al., 2017). Our group recently demonstrated little effect on dendritic morphology upon post-developmental deletion of CDKL5, bringing into question the timing or specificity of this phenotype to CDKL5 loss. These results are discussed further in Chapter 3.

The effects of CDKL5 loss on spine dynamics/stability, however, remain inconclusive. Ricciardi et al. demonstrated that shRNA-mediated knockdown of CDKL5 in primary mouse hippocampal neuron cultures leads to an increased density of filipodia-like, or immature, spine protrusions that is corroborated by a decreased frequency of miniature excitatory postsynaptic currents (mEPSCs), and this was recapitulated by Zhu et al. in 2013 (Ricciardi et al., 2012; Zhu et al., 2013). In line with these culture studies, Okuda et al. reported a significantly increased length and density of spines on hippocampal pyramidal neurons of *Cdkl5* knockout mice, and similarly, conditional knockout of CDKL5 selectively from forebrain excitatory cells resulted in an increased spine density and frequency of mEPSCs in this same region (Okuda et al., 2018; Tang et al., 2017). However, additional studies have demonstrated that loss of CDKL5 in mice reduced dendritic spine stability and density in somatosensory cortex and reduced excitatory synaptic puncta markers in visual cortex (Della Sala et al., 2016; Pizzo et al., 2016). In the visual cortex, loss of CDKL5 was associated with a decrease in excitatory puncta markers associated with PSD-95 and Homer with a concomitant increase in parvalbumin-positive interneurons, suggestive

of a disruptive synaptic organization within this region(Pizzo et al., 2016). Conflicting results on these cellular phenotypes between groups is likely due to regional differences within the brain as well as *in vitro* versus *in vivo* variability on circuit activity and spine dynamics. Furthermore, the *in vivo* functional effects of these synaptic morphological abnormalities associated with CDKL5 loss remain unresolved.

As mentioned, more recent molecular advances have begun to reveal a potential mechanistic role for CDKL5 within the microtubule network of neurons, supporting the above-mentioned morphological phenotypes. However, the *in vivo* relevance and cellular defects that directly result from CDKL5-mediated disruption of microtubule dynamics remain poorly understood. In particular, *in vivo* and genetic models such as knockout mice do not allow for a mechanistic dissection of kinase roles in the brain that are direct versus a result of network and developmental compensation.

Synaptic, Circuit, and Network Phenotypes of CDKL5-Deficient Mice

Synaptic phenotypes regulated by CDKL5

As highlighted above, several studies to date in both knockout mouse models and knockdown cell culture systems have demonstrated an altered synaptic density and morphology with loss of CDKL5. In hippocampal primary neurons and *in vivo*, CDKL5 knockout appears to lead to an increased proportion of thin, filipodia-like, or morphologically immature, dendritic spines(Della Sala et al., 2016; Ricciardi et al., 2012; Zhu et al., 2013). These have been supported by a decreased frequency and amplitude of mEPSCs in hippocampal neuron cultures and onto pyramidal neurons *in vivo* within somatosensory cortex(Della Sala et al., 2016; Ricciardi et al., 2012; Zhu et al., 2013). Surprisingly, selective loss of CDKL5 from forebrain excitatory neurons was reported to increase both spine density and the frequency of mEPSC in the hippocampal CA1 region(Tang et al., 2017). In parallel, selective loss of CDKL5 from GABAergic forebrain neurons also leads to an increased mEPSC frequency onto hippocampal pyramidal

neurons coupled with circuit hyperexcitability in the form of aberrant paired-pulse facilitation (Tang et al., 2019). Whether these varied results are the outcome of region-specific effects of CDKL5 loss, *in vitro* versus *in vivo* models, or the effects of conditional versus whole-network CDKL5 deletion remains to be confirmed, but highlight a potentially context-specific role for CDKL5. Regardless, these previous findings have established precedence for altered synaptic signaling with loss of CDKL5.

Okuda et al. reported an increased postsynaptic localization of GluN2B-containing NMDA receptors in the hippocampus of *Cdkl5* knockout mice. This finding was supported by an increased ratio of NMDAR/AMPA-mediated EPSCs, and in particular, a significantly larger decay time constant of NMDA receptor-mediated EPSCs reflective of an increased contribution of GluN2B-containing NMDARs. Accordingly, this aberrant NMDAR signaling activity was mitigated by the GluN2B-selective antagonist ifenprodil, further highlighting NMDAR subunit mislocalization within this circuit upon CDKL5 loss (Okuda et al., 2017).

In an independent study of *Cdkl5* knock-in mice (*Cdkl5^{R59X}*), there was no reported alterations in the postsynaptic localization of NMDAR subunits measured by protein quantification. Instead, this study reported a decrease in GluA2 protein within postsynaptic density fractions of knockout mice, highlighting an increased contribution of GluA2-lacking AMPA receptors that was accompanied by an increased rectification ratio of AMPAR-mediated EPSCs within the CA1. Interestingly, a GluA2-lacking-specific AMPAR blocker (IEM-1460) was capable of rescuing several behavioral deficits in this mouse model such as context-dependent memory (Yennawar et al., 2019).

These synaptic phenotypes may arise through CDKL5's regulation of postsynaptic proteins such as NGL-1, SAP-102, or PSD-95, or alternatively, due to a disruption of microtubule network-mediated receptor trafficking and synaptic maturation. However, the direct association between CDKL5 loss, postsynaptic protein and receptor trafficking, and these synaptic phenotypes has yet to be confirmed.

Disrupted circuit activity with loss of CDKL5

Despite the lack of overt, behavioral seizures in animal models of CDD reported to date, several groups have observed synaptic and circuit-level hyperexcitability in various brain regions as well as altered sensitivity to specific chemoconvulsants. Constitutive loss of CDKL5 was found to result in enhanced long-term potentiation in the hippocampus by a misregulation of postsynaptic GluN2B-containing NMDA receptor localization(Okuda et al., 2017). In line with this, *Cdkl5* KO mice exhibit significant hyperexcitability to NMDA, and this NMDA-sensitivity phenotype was recapitulated in an independent *Cdkl5* knock-in line (*Cdkl5^{R59X}*; reported in Chapter 2)(Tang et al., 2019). In contrast, a different study demonstrated impaired long-term potentiation in somatosensory cortex of *Cdkl5* knockout mice coupled to decreased dendritic spine stability and mEPSC frequency(Della Sala et al., 2016).

Furthermore, conditional deletion of CDKL5 from forebrain excitatory neurons was reported to disrupt hippocampal microcircuitry with an increased frequency of both mEPSCs and mIPSCs onto CA1 pyramidal neurons but no change in their amplitude(Tang et al., 2017). Specifically, voltage-sensitive dye imaging (VSDI) demonstrated spatio-temporally-distinct increases in depolarization and inhibition within the *stratum radiatum* and *stratum pyramidale/oriens* highlighting a differential spatial distribution of aberrant excitation and inhibition within the hippocampus. This disrupted hippocampal microcircuit was associated with the impaired learning and memory phenotype selectively demonstrated by these conditional knockout mice(Tang et al., 2017). A follow-up study of this conditional knockout line demonstrated overall hippocampal circuit hypo-excitability in the form of aberrant paired-pulse depression(Tang et al., 2019). In contrast, in the same study we demonstrate that conditional deletion of CDKL5 from forebrain inhibitory neurons (Dlx-cKO; Chapter 2) leads to aberrant circuit hyperactivity within the hippocampus in the form of aberrant paired-pulse facilitation(Tang et al., 2019). Intriguingly, these Dlx-cKO mice also exhibited significantly enhanced frequency of mEPSCs onto pyramidal

neurons of the hippocampus, highlighting a likely non cell-autonomous mechanisms for disruptions of excitatory signaling via conditional CDKL5 loss from inhibitory neurons.

Network activity and epilepsy in models of CDKL5 deficiency

The drug-resistant, refractory, and high burden nature of the seizures associated with CDD make them a particularly debilitating aspect of the disorder for both patients and their families(H. E. Olson et al., 2019). However, until this year, no animal models to date had been reported to recapitulate the spontaneous seizures that are a hallmark feature of the disorder. Establishing animal models with stronger face validity for this epilepsy within CDD will be imperative in order to dissect the nature of the seizures associated with mutations in *Cdkl5* as well as further preclinical development/screening of more targeted therapeutics to manage seizure occurrence.

Hippocampal electroencephalographic (EEG) recordings in postnatal day (P) 70-90 male *Cdkl5Δ6* knockout mice demonstrated disruptions in event-related neuronal oscillations in response to auditory stimuli, however, chronic video-EEG recordings revealed no spontaneous seizure activity(I. T. Wang et al., 2012). Furthermore, basal EEG patterns and power distribution across various oscillation frequencies were unchanged in these hemizygous male *Cdkl5* knockout mice versus littermate controls. Shortly afterwards, Amendola et al. developed and characterized the *Cdkl5Δ4* deletion mouse that also results in early reading frame truncation and loss of CDKL5 function(Amendola et al., 2014). Similarly to the exon 6 deletion mouse, EEG recordings in this novel knockout line did not reveal spontaneous epileptiform activity in hemizygous male *Cdkl5* knockout mice. More recently, an exon 2 deletion mouse of *Cdkl5* (*Cdkl5Δ2*; also resulting in constitutive knockout) was created, and although it was reported that these animals carried an increased sensitivity to NMDA-induced seizures, no overt spontaneous seizure activity was reported(Okuda et al., 2017). In summary, despite the presence of multiple behavioral and

neurophysiological impairments, no spontaneous seizure activity has been reported across three, independent constitutive *Cdkl5* knockout mouse lines.

It was long purported that the lack of a robust seizure phenotype in CDD mouse models was due to neural network differences between human and mouse brains. Despite this, several groups have observed synaptic and circuit-level hyperexcitability in various brain regions (described above) as well as altered sensitivity to specific chemoconvulsants. Although high-dose kainic acid induces overt seizures in *Cdkl5* hemizygous knockout males at similar latency to wild-type littermates, the mean duration of these epileptic EEG bursts is reported to be longer (Amendola et al., 2014). *Cdkl5* KO mice have also been reported to display decreased latency to seizure upon low-dose pentylenetetrazol administration (Yennawar et al., 2019). Although EEG recordings in loss-of-function models of CDD have not revealed spontaneous seizures, the majority of these studies have been limited to hemizygous males or young/adolescent animals. These early findings suggest that seizure susceptibility may in fact be altered in the absence of CDKL5, but perhaps only under certain environmental conditions or even specific periods of development and aging.

In Chapter 5, we describe the first report of overt, myoclonic behavioral seizures in two distinct mouse models of CDD: the *Cdkl5 Δ 6* and *Cdkl5^{R59X}*. These events are specific to aged, female mice heterozygous for mutations in *Cdkl5*, with no hemizygous knockout male mice, homozygous knockout female mice, or wild-type mice displaying spontaneous seizure activity. This suggests that X-linked mosaicism of *Cdkl5* deficiency may be a driving factor of the seizure phenotype in mouse models of CDD. A simultaneous report, in collaboration with our lab, characterized the ictal and interictal EEG features of epileptic spasms in these female *Cdkl5* heterozygous knockout mice, finding them to be most frequently associated with generalized slow-wave activity during sleep (Mulcahey et al., 2020). The precise mechanisms driving this mosaicism-linked seizure phenotype remain to be dissected. Nonetheless, these seminal findings not only contribute to our understanding of the effects of CDKL5 loss on network hyperactivity in

mice, but also strengthen the face validity of current CDD models for future therapeutic development.

Tables

Table 1: Behavioral phenotyping of mouse models of CDKL5 deficiency

Model	Allele	Study	Sex(es) studied	General physiology	Age upon assessment	Motor				Sensory				Cognitive		Socio-emotional		
						Locomotor activity	Limb clasping and gait abnormalities	Motor coordination and learning	Stereotyped behaviors	Olfaction	Vision	Hearing	Learning and memory	Social behavior and communication	Anxiety and aggression			
Constitutive knockout	exon 6 deletion (Cdk5l ^{Δ6})	Wang et al. 2012	Male only	Normal gross physical appearance and brain size	9-12 weeks	Hyporeactivity (60min beam break assay)	Hindlimb and forelimb clasping	Impaired motor coordination (Rotarod)	Not assessed	Unaltered odor discrimination	Not assessed	Impaired auditory event-related potentials; unaltered brainstem response	Impaired context- and cue-dependent learning (lear conditioning)	Reduced sociability (three-chamber assay) and nest building	Reduced anxiety (elevated zero maze)			
	exon 4 deletion (Cdk5l ^{Δ4})	Amendola et al. 2014	Male and female	Normal body and brain weight at 6 weeks of age	6-8 weeks	Hyporeactivity in home cage (day monitoring) but no change in open arena (30min assay)	Hindlimb clasping	Not assessed	Not assessed	Not assessed	Impaired optokinetic response and optokinetic evoked potentials	Not assessed	Not assessed	Not assessed				
	exon 4 deletion (Cdk5l ^{Δ4})	Fuchs et al. 2014 & 2015	Male and female	Not assessed	8 weeks		Not assessed	Not assessed	Not assessed	Not assessed	Not assessed	Not assessed	Impaired working memory (Y-maze), impaired spatial learning (Morris water maze)	Not assessed	Not assessed			
	exon 6 deletion (Cdk5l ^{Δ6} ; Wang et al. 2012)	Jiang et al. 2017	Male only	Not assessed	4-5 weeks	Hyperactivity (16min open field assay)	Not assessed	Impaired motor coordination (Rotarod)	Increased stereotyped digging behavior	Not assessed	Not assessed	Not assessed	Impaired spatial learning (Barnes maze)	Reduced sociability (three-chamber assay); reduced USVs in adult and juvenile mice	Unaltered anxiety (open field assay), but increased aggression (resident-intruder test)			
	exon 6 deletion (Cdk5l ^{Δ6} ; Wang et al. 2012)	PsychoGenics 2016	Male and female	Decreased body weight at 5.5 weeks; reduced respiration rate	5-15 weeks	Hyporeactivity (24hr PhenoCube assay)	Hindlimb clasping; gait abnormalities (NeuroCube)	Unaltered motor coordination (single-day Rotarod)	Not assessed	Not assessed	Impaired optokinetic response	Not assessed	Impaired context- and cue-dependent learning (lear conditioning)	Reduced social interaction (PhenoCube)	Not assessed			
	exon 6 deletion (Cdk5l ^{Δ6} ; Wang et al. 2012)	Yernawar et al. 2019	Male only	Normal gross physical appearance and brain size	12-16 weeks	Hyperactivity (10min open field assay)	Hindlimb clasping	Impaired motor coordination (Rotarod)	Not assessed	Unaltered odor discrimination	Not assessed	Not assessed	Impaired context-dependent learning (lear conditioning) and working memory (Y-maze)	Reduced sociability (three-chamber assay)	Increased anxiety (open field periphery time)			
Conditional knockout using <i>Enx1-Cre</i> & <i>Dlx5/6-Cre</i>	exon 4 deletion (Cdk5l ^{Δ4})	Amendola et al. 2014	Male and female	Normal body and brain weight at 6 weeks of age	6-8 weeks	Hyporeactivity in home cage (4day monitoring) in Dlx5/6- <i>cKO</i> male mice	Hindlimb clasping in <i>Enx1-cKO</i> male and female mice	Not assessed	Not assessed	Not assessed	Impaired optokinetic response in <i>Enx1-cKO</i> male mice	Not assessed	Not assessed	Not assessed	Not assessed			
Conditional knockout using <i>Nes-Cre</i>	exon 6 deletion (Cdk5l ^{Δ6})	Tang et al. 2017	Male only	Normal gross physical appearance, body weight, and brain size	9-12 weeks	Context-dependent hyperactivity (three-chamber assay and Y-maze only)	Hindlimb clasping	Unaltered motor coordination and learning (Rotarod)	Unaltered stereotyped behavior	Unaltered odor discrimination	Not assessed	Impaired spatial learning (Barnes maze) and impaired working memory (Y-maze)	Unaltered social behavior (three-chamber assay) and nest-building	Unaltered anxiety (zero maze)				
Conditional knockout using <i>Dlx-Cre</i>	exon 6 deletion (Cdk5l ^{Δ6})	Tang et al. 2019	Male only	Normal gross physical appearance, body weight, and brain size	9-12 weeks	normal locomotion	No hindlimb clasping	Unaltered motor coordination and learning (Rotarod)	Increased repetitive behaviors (grooming in a homecage-like environment)	Unaltered odor discrimination	Not assessed	unaltered working memory (Y-Maze) and unaltered learning (Barnes Maze), but increased error probe	decreased sociability during a 3-chambered social choice test and dyadic interaction test	Unaltered anxiety (zero maze)				

Table 2. Putative protein interactions and signaling pathways involving CDKL5 (results in bold have been validated <i>in vivo</i>)		
Putative Protein Interaction	Experimental method	Reference(s)
MeCP2	Co-immunoprecipitation of overexpressed GFP-CDKL5 and endogenous MeCP2 in HEK293T cells; GST pull-down assay of GST-MeCP2 with 35S-hCDKL5 & co-immunoprecipitation of GFP-CDKL5 with myc-MeCP2 in 293T cells	Mari et al. 2005; Lin et al. 2005; Bertani et al. 2006; Williamson et al. 2012
DNMT1	Pull-down assay using GST-DNMT1(1-290) incubated with mouse brain extract, followed by fractionation and LC-MS/MS	Kameshita et al. 2008
SC35	Co-immunoprecipitation of YFP-SC35 with GFP-CDKL5 in NIH3T3 cells	Ricciardi et al. 2009
Rac 1	Pull-down assay using GST-CDKL5(670-934) in COS-7 cells	Chen et al. 2010
NGL-1	Co-immunoprecipitation of NGL-1 using a CDKL5 antibody in P4 mouse brain synaptosome extract	Ricciardi et al. 2012
Amphiphysin 1	Liquid-phase isoelectric focusing, followed by an <i>in vitro</i> kinase assay using incubation with CDKL5(1-352)	Sekiguchi et al. 2013
PSD-95	Co-immunoprecipitation from rat brain synaptosomes using CDKL5 and PSD-95 antibodies	Zhu et al. 2013
Mind Bomb 1	Affinity purification of rat brain lysate using GST-Mib1, followed by sequential elution and LC-MS/MS analysis	Mertz et al. 2015
Shootin-1	Co-immunoprecipitation from P5-7 mouse brain lysate using CDKL5 and Shootin-1 antibodies	Nawaz et al. 2016
HDAC4	Co-immunoprecipitation of overexpressed CDKL5-FLAG with endogenous HDAC4 in SH-SY5Y cells	Trazzi et al. 2016
MAP1S, EB2, and ARHGEF2	chemical-genetic identification of direct CDKL5 substrates, followed by validation of reduced phosphorylation in <i>Cdkl5</i> knockout mouse brain	Baltussen et al. 2018
MAP1S, CEP131, and DLG5	TMT-based CDKL5 phosphoproteomic screening in U2OS osteosarcoma cells followed by validation of reduced phosphorylation in CDKL5 KD HEK293 cells	Muñoz et al. 2018
Signaling Pathway Alteration	Experimental method	Reference(s)
Decreased AKT and mTOR phosphorylation	Western blotting of whole mouse brain lysate; kinome profiling	Wang et al. 2012; Amendola et al. 2014; Fuchs et al. 2014
Decreased GSK3-β phosphorylation	Western blotting of mouse hippocampal lysate	Fuchs et al. 2014
Increased levels of GluN2B and SAP102	Western blotting of PSD fraction from adult mouse hippocampus and quantification of GluN2B and SAP102 protein level	Okuda et al. 2017; Tang et al. 2019
Decreased levels of GluA2	Western blotting of PSD fraction from adult mouse hippocampus and quantification of GluA2 protein level	Yennawar et al. 2019

CHAPTER 2 – ALTERED NMDAR SIGNALING UNDERLIES AUTISTIC-LIKE FEATURES IN MOUSE MODELS OF CDKL5 DEFICIENCY DISORDER

Adapted from: Tang S*, Terzic B*, Wang ITJ, Sarmiento N, Sizov K, Yue C, Takano H, Marsh ED, Zhou Z. Altered NMDAR signaling underlies autistic-like features in mouse models of CDKL5 deficiency disorder. *Nature Communications*. 2019 Jun;10:2655

*these two authors contributed equally to this work

Abstract

CDKL5 deficiency disorder (CDD) is characterized by epilepsy, intellectual disability, and autistic features, and CDKL5-deficient mice exhibit a constellation of behavioral phenotypes reminiscent of the human disorder. We previously found that CDKL5 dysfunction in forebrain glutamatergic neurons results in deficits in learning and memory. However, the pathogenic origin of the autistic features of CDD remains unknown. Here, we find that selective loss of CDKL5 in GABAergic neurons leads to autistic-like phenotypes in mice accompanied by excessive glutamatergic transmission, hyperexcitability, and increased levels of postsynaptic NMDA receptors. Acute, low-dose inhibition of NMDAR signaling ameliorates autistic-like behaviors in GABAergic knockout mice, as well as a novel mouse model bearing a CDD-associated nonsense mutation, CDKL5 R59X, implicating the translational potential of this mechanism. Together, our findings suggest that enhanced NMDAR signaling and circuit hyperexcitability underlie autistic-like features in mouse models of CDD and provide a new therapeutic avenue to treat CDD-related symptoms.

Introduction

Mutations in cyclin-dependent kinase-like 5 (*CDKL5*) cause a severe neurodevelopmental disorder characterized by early-onset seizures, intellectual disability, and autistic features (Kalscheuer et al., 2003; Tao et al., 2004; Weaving et al., 2004). Mouse models of CDD have recapitulated numerous aspects of the human disorder, and despite a subtle overall degree of impairment, they show behavioral deficits such as impaired learning, reduced sociability, motor dysfunction, and altered anxiety-related behaviors (Amendola et al., 2014; Jhang, Huang, Hsueh, & Liao, 2017; Okuda et al., 2018; I. T. Wang et al., 2012). The extent to which these behavioral deficits arise from common or distinct mechanisms, however, remains unclear.

CDKL5 protein expression is enriched in the forebrain, primarily in glutamatergic and GABAergic neurons (Chen et al., 2010; Johnson et al., 2017; Rusconi et al., 2008; I. T. Wang et al., 2012; Zeisel et al., 2015). In glutamatergic neurons, CDKL5 has been found at the postsynaptic density, where it interacts with PSD-95 and NGL-1 (Ricciardi et al., 2012; Zhu et al., 2013). In addition, loss of CDKL5, both *in vitro* and *in vivo*, is associated with changes in dendritic morphology, spine density, excitatory synaptic transmission, and synaptic plasticity (Della Sala et al., 2016; Okuda et al., 2017; Ricciardi et al., 2012; Tang et al., 2017). Mice lacking CDKL5 selectively in forebrain glutamatergic neurons (Nex-cKO) show impaired learning and memory, reminiscent of the intellectual disability found in CDD (Tang et al., 2017). Interestingly, Nex-cKO mice did not show other behavioral deficits found in *Cdkl5* constitutive knockout mice, such as alterations in sociability, stereotypic behavior, locomotion, motor coordination, and anxiety-related behavior (Tang et al., 2017). These findings imply that distinct, cell-type specific etiologies underlie CDD-related behavioral phenotypes in mice.

Mice lacking CDKL5 show numerous functional changes at the synaptic and circuit levels. A recent study found that *Cdkl5* constitutive knockout mice demonstrated increased NMDA-dependent synaptic transmission and enhanced long-term potentiation at hippocampal

synapses(Okuda et al., 2017). In contrast, long-term potentiation is decreased in the somatosensory cortex of *Cdkl5* knockout mice(Della Sala et al., 2016). Furthermore, selectively ablating CDKL5 from glutamatergic neurons leads to increased glutamatergic and GABAergic synaptic transmission, disrupted microcircuit dynamics, and learning and memory impairment(Tang et al., 2017). While some of these differences are potentially attributable to different genetic backgrounds of mouse models of CDD, the differences between *Cdkl5* constitutive knockout mice and Nex-cKO mice suggest the existence of additional, non-glutamatergic mechanisms that may mediate CDD-related behavioral deficits. Notably, the function of CDKL5 in forebrain GABAergic neurons, where CDKL5 is also highly expressed, has yet to be elucidated(Johnson et al., 2017).

Here, we selectively ablate CDKL5 expression in forebrain GABAergic neurons (Dlx-cKO). We found that these mice exhibit an autistic-like phenotype, but, in contrast to Nex-cKO mice, show preserved learning and memory(Tang et al., 2017). In addition, Dlx-cKO mice show an enhancement of excitatory synaptic transmission and circuit-level hyperexcitability, coupled with elevated levels of NMDA receptors. Reducing NMDAR activity using an uncompetitive antagonist, memantine, significantly mitigated the behavioral deficits found in Dlx-cKO mice. To examine the translational potential of these findings, we generated a novel CDD model bearing a patient mutation and found that these mice, similarly to Dlx-cKO mice, show an elevation of NMDA receptors. Importantly, acute, low-dose NMDAR blockade selectively ameliorates autistic-like features in this CDD model. Taken together, our findings support a novel mechanism by which CDKL5 loss in GABAergic neurons leads to excessive NMDAR signaling and contribute to the etiology of autistic-like behaviors in mouse models of CDD.

Results

CDKL5 GABAergic deletion results in autistic-like features

Our previous findings showed that CDD-related learning and memory impairment has origins in forebrain glutamatergic neurons in mice (Tang et al., 2017). Given that CDKL5 is also highly expressed in forebrain GABAergic neurons, we generated conditional knockout mice selectively lacking CDKL5 in this cell population (Dlx-cKO) using the *Dlx-5/6* Cre driver (Figure 1A, B) (Monory et al., 2006). Dlx-cKO mice showed normal growth and body weight through adulthood and no obvious physical abnormalities (Figure 2A). We then performed a battery of behavioral assays, similar to those in previous studies of *Cdkl5* constitutive KO and *Nex*-cKO mice (Tang et al., 2017; I. T. Wang et al., 2012). Compared to WT controls, Dlx-cKO showed no changes in locomotor activity, anxiety-related behaviors, and motor coordination (Fig. 2B–D).

In contrast, Dlx-cKO mice demonstrated significantly reduced social interaction on the three-chamber social approach assay, showing diminished preference for investigating a social stimulus as compared to an object (Fig. 3a, b). When allowed the opportunity for direct interaction with a novel stimulus mouse, Dlx-cKO mice also spent significantly less time initiating contact in comparison to wild-type controls (Fig. 3c). To rule out the involvement of an olfactory deficit underlying reduced social preference, we conducted the olfactory habituation-dishabituation test. Dlx-cKO mice showed an intact ability to discriminate between different scents but spent reduced time sniffing a social scent, a feature consistent with a reduced interest in social stimuli (Fig. 3d).

In addition to social deficits, another defining feature of human autism spectrum disorders (ASDs) is the presence of repetitive or stereotypic behaviors. We next assessed repetitive behaviors in Dlx-cKO mice. In a home-cage like environment, Dlx-cKO mice showed significantly increased time engaging in stereotypic behaviors such as grooming and digging (Fig. 3e), and also exhibited a nesting deficit (considered by some to be a home-cage social behavior) compared to littermate controls (Fig. 3f).

We next assessed learning and memory, a behavioral domain significantly impaired in both *Cdkl5* constitutive knockout mice and Nex-cKO mice. Interestingly, Dlx-cKO showed no impairment in spontaneous alternation behavior on the Y-maze, suggesting intact working memory (Fig. 3g, h). On the Barnes maze, an assay of spatial learning and memory, Dlx-cKO did not show a significant difference from wild-type controls in the number of errors made on probe trials (Fig. 3i). However, when the target hole location was altered to the opposite side of the maze after acquisition (reversal probe trials), Dlx-cKO mice demonstrated a significant impairment in adjusting to this new target hole (Fig. 3j). In addition, Dlx-cKO mice show an increased number of perseverations on reversal probe trials, or visits to the previous target hole location (Fig. 3k). These results suggest that Dlx-cKO mice have intact learning and memory, but impaired cognitive flexibility, another feature reminiscent of autism spectrum disorders.

Taken together, Dlx-cKO mice show a set of autistic-like features with relatively preserved learning and memory that stand in contrast to previous findings in Nex-cKO mice, which exclusively show impaired learning and memory (Tang et al., 2017). These results demonstrate a segregation of behavioral deficits in *Cdkl5* conditional knockout mice, suggesting that impaired learning and autistic-like features have distinct cellular origins in CDD.

Dlx-cKO mice show aberrant circuit activation

In previously established mouse models of ASD, the finding of excitation-inhibition (E/I) imbalance has emerged as a prominent theme underlying patterns of circuit and network dysfunction (Bourgeron, 2015; Rubenstein & Merzenich, 2003). Specifically, hyperexcitability at the circuit and network levels has been found to be associated with many of the autistic-like features reported in these models. Importantly, reversal of hyperexcitability in these models is often sufficient to ameliorate disease phenotypes, demonstrating a causal role for E/I imbalance in generating the features of social impairment and stereotypy (Chung et al., 2015; Yizhar et al., 2011).

The exhibition of autistic-like features in *Dlx*-cKO mice, coupled to the previous findings of E/I imbalance in other models of ASD, prompted us to investigate any circuit irregularities in CDD mouse models. We first used voltage-sensitive dye imaging (VSDI), a technique that has been consistently used in mouse models of neurologic disease to assess circuit function with high spatiotemporal resolution (Ang, 2005; Ang, Carlson, & Coulter, 2006; Calfa, Hablitz, & Pozzo-Miller, 2011; Carlson & Coulter, 2008; Tang et al., 2017). We conducted our experiments with WT, *Dlx*-cKO, and *Nex*-cKO mice, to facilitate a side-by-side comparison of circuit function in the context of the distinct behavioral profiles of *Dlx*-cKO and *Nex*-cKO mice.

We began by interrogating the function of the perforant path-dentate gyrus pathway, a hippocampal microcircuit often perturbed in disease states that critically relies on both excitation and inhibition for proper function (Douglas A. Coulter et al., 2011; Dengler & Coulter, 2016; Goldberg & Coulter, 2013). Using VSDI responses as a readout, we assessed the layer-specific responses of the molecular layer, granule cell layer, as well as the downstream hilar region in response to perforant path stimulation (Fig. 4a). We used a paired-pulse paradigm, which assesses both the baseline excitability of the circuit and its short-term plasticity. We first focused our analysis on the response of the granule cell layer (Fig. 4b–e), which contains the cell bodies of the principal neurons of the dentate gyrus. WT mice showed comparable responses in the granule cell layer to the first and second stimuli without significant facilitation or depression (Fig. 4b–d), showing a paired-pulse ratio that was not significantly different from one (Fig. 4e). Neither *Nex*-cKO or *Dlx*-cKO mice showed a significant difference from WT in their peak responses to the first stimulation, suggesting similar baseline excitability of the dentate gyrus (Fig. 4b, c). Interestingly, *Nex*-cKO mice showed a diminished peak response to the second stimulus, with a paired-pulse ratio significantly less than one (Fig. 4b, d, e). In contrast to *Nex*-cKO mice, *Dlx*-cKO mice exhibited paired-pulse facilitation, evident by an increase in depolarization upon a second successive stimulus and a peak ratio significantly greater than one (Fig. 4d, e). Importantly, this aberrant paired-pulse facilitation in *Dlx*-cKO was also observed in an upstream input region (molecular layer) and downstream output region (hilus) (Fig. 4f–k). Furthermore, we repeated this

experiment at a second stimulation intensity and observed similar results (Fig. 5). Taken together, our findings reveal that the distinct behavioral phenotypes of *Cdkl5* conditional knockout mice are accompanied by contrasting patterns of circuit dysfunction. Specifically, *Dlx*-cKO mice show circuit hyperexcitability in the form of aberrant paired-pulse facilitation, whereas *Nex*-cKO mice show circuit hypo-excitability in the form of aberrant paired-pulse depression.

Dlx-cKO mice show enhanced excitatory synaptic transmission

Given the finding of circuit hyperexcitability in *Dlx*-cKO mice, we next investigated the synaptic origins of this E/I imbalance. Previous studies have found enhanced synaptic transmission and long-term potentiation in the hippocampal CA1 region of *Cdkl5* constitutive knockout mice (Okuda et al., 2017). Interestingly, these changes were not fully recapitulated in the glutamatergic conditional knockout mice, suggesting that CDKL5 function in other neuronal populations, such as GABAergic neurons, may contribute to synaptic hyperexcitability (Tang et al., 2017). Therefore, using whole-cell patch-clamp recordings, we assessed both excitatory and inhibitory synaptic transmission in the hippocampal CA1 region in *Dlx*-cKO mice. We found that *Dlx*-cKO mice exhibited significantly enhanced frequency of miniature spontaneous excitatory postsynaptic currents (mEPSCs), but no changes in amplitude or kinetics of these events (Fig. 6a–e and Fig. 7A, B). In contrast, miniature spontaneous inhibitory postsynaptic currents (mIPSCs) were not significantly different in either amplitude, frequency, or kinetics between *Dlx*-cKO and WT mice (Fig. 6f–j and Fig. 7C, D). This suggests that despite CDKL5 loss in GABAergic neurons, adult *Dlx*-cKO mice do not show a significant alteration of inhibitory signaling at CA1 pyramidal neurons. In turn, synaptic transmission between excitatory neurons is enhanced upon selective loss of CDKL5 in GABAergic neurons. Taken together, our results support a shift in E/I balance in *Dlx*-cKO mice toward hyperexcitability that is consistent with our circuit findings.

Dlx-cKO mice have an increase in postsynaptic NMDA receptors

The finding of excess glutamatergic synaptic transmission in Dlx-cKO mice suggests a potential alteration in the molecular composition of postsynaptic receptors. Indeed, previous studies have suggested a role for CDKL5 in regulating synaptic receptor composition and homeostasis (P. La Montanara et al., 2015; Okuda et al., 2017). For example, excessive glutamatergic synaptic transmission can result from an enhancement of postsynaptic AMPA receptors (AMPA), NMDA receptors (NMDAR), or both. We therefore examined the composition of major ionotropic glutamate receptors in postsynaptic density membrane preparations from Dlx-cKO and WT mice, including GluA1, GluA2, GluN1, GluN2A, and GluN2B. Interestingly, we found a selective increase in the protein level of NMDARs, but not AMPARs in Dlx-cKO mice (Fig. 8). Specifically, the NMDAR subunits GluN1 and GluN2B were significantly elevated in Dlx-cKO mice. (Fig. 8d, f). These findings are consistent with results from *Cdkl5* constitutive knockout mice and suggest a non-cell autonomous mechanism underlying the enhancement of glutamatergic synaptic transmission through CDKL5 loss from GABAergic neurons (Okuda et al., 2017).

NMDAR blockade ameliorates autistic-like features in Dlx-cKO

Our findings in Dlx-cKO mice raised the possibility that enhanced NMDAR signaling may underlie the autistic-like phenotype exhibited by these mice. We first investigated the extent to which NMDAR signaling is responsible for the repetitive behavior phenotype in Dlx-cKO mice. We used low doses of memantine, a non-competitive NMDA receptor blocker that has been previously found to rescue behavioral deficits in numerous mouse models of neurodevelopmental disorders (Chung et al., 2015; Figueiredo et al., 2013; J. Kang & Kim, 2015). We observed that acute memantine administration (5 mg kg⁻¹, intraperitoneal) ameliorated excessive grooming in Dlx-cKO mice, significantly reducing both total time spent grooming and the duration of the longest grooming bout (Fig. 9a, b). Next, we employed a modified dyadic interaction assay to quantitatively assess social interactions in drug- and vehicle-treated Dlx-cKO mice. Whereas vehicle-administered Dlx-cKO mice showed significantly reduced social interaction, memantine

ameliorated this deficit, significantly increasing the time spent by Dlx-cKO mice in social interaction (Fig. 9c). This effect was specific to Dlx-cKO mice, as memantine normalized the ratio of time spent in social interaction in pairs of Dlx-cKO and WT control mice co-tested side-by-side in identical cages (Fig. 9d). Taken together, these results suggest that enhanced NMDAR signaling underlies, at least in part, the autistic-like features of Dlx-cKO mice, and that an acute reduction of NMDAR activity can ameliorate these phenotypes.

NMDAR blockade improves autistic-like features in CDKL5 R59X

To investigate the translational potential of our findings in Dlx-cKO mice, we generated a novel mouse model of CDD, *Cdkl5*^{R59X} (referred to as R59X). R59X mice bear a knock-in mutation mimicking a human CDD nonsense mutation at arginine 59, leading to the loss of CDKL5 kinase function (Fig. 10a). We found that full-length CDKL5 protein expression was abolished in R59X mice, similar to a knockout model we previously developed (Fig. 11)(I. T. Wang et al., 2012). Similar to Dlx-cKO mice and other mouse models of CDD, R59X mice demonstrate autistic-like features, including increased repetitive behaviors and diminished social interaction (Fig. 12).

We next investigated the extent to which enhanced NMDAR signaling is also present in R59X mice. Using a similar approach as for Dlx-cKO mice, we examined the protein levels of NMDAR and AMPAR subunits in postsynaptic density fractions (Fig. 10b–g). In R59X mice, we found an upregulation of NMDAR subunit levels, with a selective increase in GluN2B, mirroring previous findings in *Cdkl5* constitutive knockout mice (Fig. 10g)(Okuda et al., 2017).

Using R59X mice as a model of CDD, we next examined the extent to which enhanced NMDA signaling is responsible for CDD-related behavioral deficits. We first tested the possibility that enhanced NMDAR signaling may underlie impaired learning and memory in CDKL5-deficient mice. Using the Y-maze assay, we found that R59X mice demonstrated a robust working memory deficit, demonstrated by reduced spontaneous alternation behavior, similar to our previous

findings in both *Cdkl5* constitutive KO and Nex-cKO mice (Fig. 12a)(Tang et al., 2017; I. T. Wang et al., 2012). Notably, acute memantine administration at a range of doses (1.25–10 mg kg⁻¹, intraperitoneal) did not ameliorate this behavioral deficit, suggesting that excess NMDAR signaling is unlikely to be the major mechanism underlying learning and memory deficits in R59X mice (Fig. 12a).

In contrast, we observed that acute memantine administration (5 mg kg⁻¹, intraperitoneal) rescued excessive stereotypic behaviors in R59X mice, significantly reducing both total time spent grooming and the duration of the longest grooming bout to a level similar to that of WT mice (Fig. 12b, c). Similarly, whereas vehicle-treated R59X mice showed significantly reduced social interaction, memantine ameliorated this deficit, significantly increasing the time spent by R59X mice in social interaction (Fig. 12d). This effect was specific to R59X mice, as memantine normalized the ratio of time spent in social interaction in pairs of R59X and WT control mice co-tested side-by-side in identical cages (Fig. 12e). Taken together, these results suggest that enhanced NMDAR signaling underlies the autistic-like features, but not learning and memory deficits, in CDKL5-deficient mice, and reveal the translational potential of this pathway in the treatment of CDD.

Discussion

Our behavioral studies in *Dlx*-cKO mice revealed an autistic-like phenotype characterized by reduced social preference and increased stereotypic behaviors, but relative preservation of other behaviors such as learning and memory, motor coordination, and anxiety-related behaviors. This behavioral profile stands in contrast to our previous findings in Nex-cKO mice, which exhibit selectively impaired learning and memory. Our results delineate the distinct cellular origins of CDD-related behavioral phenotypes: whereas impaired learning primarily originates from the loss of CDKL5 in forebrain glutamatergic neurons, autistic-like features primarily originate from the loss of CDKL5 in forebrain GABAergic neurons. Interestingly, anxiety-related behavior, locomotion, and motor coordination were not altered in either Nex-cKO or *Dlx*-cKO mice. These

additional phenotypes may be mediated by 1) CDKL5 function in other cell populations and brain regions and/or 2) the synergistic functions of CDKL5 in forebrain glutamatergic and GABAergic neurons.

Our findings in *Cdkl5* conditional knockout mice support a model whereby CDKL5 loss in glutamatergic and GABAergic neurons lead to divergent changes in E/I balance that generate distinct behavioral deficits. We show that in *Dlx*-cKO mice, hippocampal circuit hyperexcitability is coupled with autistic-like features, a finding corroborated in numerous other mouse models of autism (Chung et al., 2015; Lee, Lee, & Kim, 2017; Sacha & Valakh, 2015; Yizhar et al., 2011). In specific cases, autistic-like behaviors have been linked to a dysfunction of inhibitory neuronal transmission (Chao et al., 2010; Han et al., 2012; Rothwell et al., 2014). In contrast, we show that in *Nex*-cKO mice, hippocampal circuit hypo-excitability is linked to learning and memory deficits. Interestingly, reduced E/I ratio has been demonstrated in numerous mouse models of intellectual disability (Dierssen, 2012; Fernandez & Garner, 2007). Therefore, our studies reveal a novel avenue toward treating specific CDD-related symptoms, but also suggest that modulation of E/I balance in CDD may be a double-edged sword. To date, the majority of reported CDD patients have been predicted to carry loss-of-function mutations, such as nonsense, indels, or missense mutations abolishing CDKL5 kinase activity, suggesting that our knockout and R59X knockin mouse models may carry a high translational relevance. In order to develop targeted therapies for CDD, additional studies are needed to elucidate the specific signaling pathways and neural circuits responsible for each of the behavioral symptoms.

In our VSDI studies of *Nex*- and *Dlx*-cKO mice, we employed a paired-pulse stimulation paradigm, which assesses the integration of excitatory and inhibitory synaptic transmission in the dentate gyrus. Interestingly, previous work has shown that NMDA signaling is a necessary component for the paired-pulse facilitation response in the dentate gyrus, suggesting a potential mechanism for circuit excitability in *Dlx*-cKO mice (Joy & Albertson, 1993). On the other hand, the aberrant paired-pulse depression in *Nex*-cKO mice may result from enhanced inhibition, given

that feedforward and feedback inhibition play key roles in regulating the activity of the dentate gyrus (Amaral, Scharfman, & Lavenex, 2007; D.A. Coulter & Carlson, 2007; Tang et al., 2017). In our electrophysiologic studies of *Dlx*-cKO mice, the most prominent change was, surprisingly, an enhancement in glutamatergic synaptic transmission. This change likely arises from a non-cell autonomous mechanism, especially in the absence of a concomitant change in GABAergic-glutamatergic inhibitory synaptic transmission. For example, the loss of CDKL5 in GABAergic interneurons may lead to a modulation of presynaptic release probability at glutamatergic synapses. Alternatively, enhanced excitatory synaptic transmission may be a homeostatic response to a transient alteration of GABAergic signaling during early development. Supporting this notion, a previous study has found that GABAergic transmission cooperates with NMDA receptor activation during development for excitatory synapse formation (D. D. Wang & Kriegstein, 2008). Furthermore, the loss of CDKL5 may lead to different disruptions in distinct populations of forebrain interneurons that as of yet we are unable to dissect from our *Dlx5/6*-Cre-driven dissection. Future studies looking into the role of CDKL5 at specific sub-populations of interneurons will provide clarity on its non-cell autonomous roles.

Interestingly, despite the findings of synaptic and circuit-level hyperexcitability, we did not observe spontaneous seizure-like behaviors in *Dlx*-cKO mice during our routine assays, at least in male mice and at the ages examined. This is similar to what has been observed in constitutive loss-of-function models of CDD where EEG recordings have not revealed spontaneous seizures (Amendola et al., 2014; Okuda et al., 2017; I. T. Wang et al., 2012). However, this does not exclude the possibility that seizure susceptibility is altered in the absence of CDKL5 under certain environmental conditions and during specific periods in development and aging. Thus far, the lack of a robust seizure phenotype in CDD mouse models suggests that neural network differences between human and mouse brains may prevent the development of overt seizures in CDKL5-deficient mice. In addition, given the contrasting profiles of hypo- and hyperexcitability in *Nex*-cKO and *Dlx*-cKO mice, respectively, the state of circuit excitability in constitutive loss-of-function models of CDD remains to be further characterized. Indeed, previous studies have

revealed changes in synapse density, distribution, and plasticity of both excitatory and inhibitory neurons (Della Sala et al., 2016; Okuda et al., 2017). Therefore, it is possible that both pro- and anti-epileptogenic changes occur in the CDKL5-deficient brain, each playing a distinct role in mediating the various behavioral deficits of CDD.

The finding of enhanced NMDAR signaling reveals a novel synaptic mechanism that may potentially underlie the behavioral deficits of mouse models of CDD. Our results in *Dlx-cKO* mice suggest that GABAergic dysfunction leads to an enhancement of NMDAR signaling, which in turn is responsible for autistic-like features. We validate this mechanism in *R59X* mice, demonstrating that the acute reduction of NMDAR signaling ameliorates select CDD-related behavioral deficits. Whereas acute memantine administration specifically rescued repetitive behavior and significantly improved social interaction in *R59X* mice, it did not positively affect the learning and memory deficit in *R59X* mice. Altogether with our previous findings in *Nex-cKO* mice, our studies suggest that distinct subsets of CDD-related phenotypes are mediated by distinct synaptic and circuit mechanisms (Tang et al., 2017). Future studies are expected to refine these mechanisms by testing brain region- and circuit-specific mechanisms for specific CDD-related phenotypes. For example, given that we found enhanced NMDAR subunit levels in our postsynaptic density membrane fractions, we cannot rule out the possibility that extra-synaptic NMDAR levels are also altered in *Dlx-cKO* and *R59X* mice. Indeed, memantine is known to act at both synaptic and extra-synaptic receptors in a dose-dependent manner, and its effects on behavior may be mediated by both mechanisms (Beconi et al., 2011). Although it may be difficult to distinguish between these two populations of NMDARs *in vivo*, further work in this direction can elucidate the mechanism that underlies the enhancement of synaptic NMDAR signaling in mouse models of CDD.

Taken together, our studies delineate the forebrain GABAergic origins of autistic-like features in CDKL5-deficient mice, showing for the first time that CDKL5 is required in this diverse population of neurons for proper neural development and function. At the synaptic level, we

reveal an enhancement of NMDAR signaling that contributes to circuit hyperexcitability. Finally, in a novel disease model of CDD, we show that acute reduction of NMDAR signaling can ameliorate behavioral deficits, highlighting a potentially important mechanism for CDD-related phenotypes in mice and supporting a novel therapeutic avenue for the treatment of these symptoms in CDD patients.

Materials and Methods

Mouse strains. The *Cdkl5* floxed mouse line with Cre-dependent excision of exon 6 was used for the generation of conditional knockout mice (Tang et al., 2017). *Dlx5/6-Cre*, a mouse line expressing Cre in forebrain inhibitory neurons, was obtained from Jackson Laboratories and maintained in the C59BL/6J background (Stock No. 008199) (Monory et al., 2006). The CDKL5 R59X knock-in line was generated as follows: a targeting vector was designed to insert a frt-flanked neomycin resistance (neo) cassette downstream of exon 5, and a single-nucleotide change of C to T, leading to a nonsense mutation at arginine 59 (R59X) of the *Cdkl5* gene. The construct was electroporated into C57BL/6N embryonic stem (ES) cells. Correctly targeted ES cells were injected into BALB/c blastocysts and resulting chimeric mice were bred with B6.Cg-Tg(ACTFLPe)9205Dym/J (Jackson Laboratories, Stock No. 005703) to remove the neo cassette. Resulting offspring were bred to C57BL/6J mice (Jackson Laboratories, Stock No. 000664) for at least ten generations. The R59X knock-in mouse line has been deposited at Jackson Laboratories (Stock No. 028856).

Mouse husbandry. Experiments were conducted in accordance with the ethical guidelines of the National Institutes of Health and with the approval of the Institutional Animal Care and Use Committee of the University of Pennsylvania. *Cdkl5^{fllox}* and R59X mice were backcrossed to C57BL/6 for at least ten generations before breeding for experiments. Mouse lines were genotyped using a PCR-based strategy, with their respective primer sequences and other details found on the Jackson Laboratories website under the appropriate stock numbers listed above.

Mice were group-housed in cages of three to five in a 12-h light/dark cycle with food and water provided *ad libitum*.

For breeding of Dlx-cKO and wild-type control mice, each breeding cage consisted of two homozygous female mice (genotype: *Cdkl5^{flox}/Cdkl5^{flox}*) and one male mouse (genotype: *Dlx5/6-Cre/+*). Male littermates (genotypes: *Cdkl5^{flox/y}; +/+* and *Cdkl5^{flox/y}; Dlx5/6-Cre*) were weaned at 3 weeks of age and housed together, with all experiments performed on age-matched adult mice between 9 and 12 weeks of age. For behavioral experiments, wild-type control mice (genotype: *Cdkl5^{flox/y}; +/+*) from Nex-cKO breedings¹⁴ were pooled with wild-type control mice from Dlx-cKO breedings (genotype: *Cdkl5^{flox/y}; +/+*). Nex-cKO mice were generated using a similar strategy as described previously. For breeding of R59X and wild-type control mice, each breeding cage consistent of two heterozygous female mice (genotype: *R59X/+*) and one male mouse (genotype: *+/y*). Male littermates (genotypes: *R59X/y* and *+/y*) were weaned at 3 weeks of age and housed together, with all experiments performed on age-matched adult mice between 9-12 weeks of age.

Behavioral assays. All animal behavioral studies were carried out blinded to genotype. Mice were allowed to habituate to the testing room for at least 1 h before the test, and testing was performed at the same time of day. All animal behaviors were performed on adult male mice at 9–12 weeks of age, and the analysis of behavioral data was carried out by a researcher blinded to genotype.

Elevated zero maze. The elevated zero maze (Stoelting, Illinois, USA) consists of a circular-shaped platform elevated above the floor. Two opposite quadrants of the maze are enclosed (wall height, 12 inches), whereas the other two are open (wall height, 0.5 inches). Mice were placed in one of the closed quadrants and their movement traced over the course of 5 min. Analysis, including the quantification of percent of time spent in open arms and the number of entries, was performed manually using a stopwatch. An entry was defined as a transition from a closed to open arm, or vice versa, that involves all four paws.

Three-chambered social approach assay. The social approach assay was performed as previously described (Fairless et al., 2013; Sankoorikal, Kaercher, Boon, Lee, & Brodtkin, 2006). The social choice test was carried out in a three-chambered apparatus that consisted of a center chamber and two end chambers. Before the start of the test and in a counter-balanced sequence, one end chamber was designated the social chamber, into which a stimulus mouse would be introduced, and the other end chamber was designated the nonsocial chamber. Two identical, clear Plexiglas cylinders with multiple holes to allow for air exchange were placed in each end chamber. In the habituation phase of the test, the test mouse was placed in the center chamber and allowed to explore all three chambers for 10 min. During this acclimation period, baseline measurements of how much time the mouse spent in each of the three chambers and the distance traveled by the test mouse were collected. In the social choice phase of the test, a stimulus mouse (adult gonadectomized A/J mice; The Jackson Laboratory) was placed in the cylinder in the social chamber while a novel object was simultaneously placed into the other cylinder in the nonsocial chamber. During the 5-min social choice period, chamber times and numbers of transitions among chambers were again recorded. In the direct social interaction test, the cylinders were removed simultaneously following the social choice test, and the amount of time test and stimulus mice spent in direct contact (sniffing, allogrooming) was measured. If fighting persisted for more than several seconds, the mice were removed from the apparatus and excluded from the study.

Y-maze. Spontaneous alternation behavior was measured on a Y-maze apparatus (San Diego Instruments, California, USA), composed of three arms (Arm A: 8in. x 5in. x 3in.; Arms B and C: 6in. x 5in. x 3in.). For habituation, the test mouse was placed in each of the three arms, facing the center, and allowed to make one choice to enter another arm. For testing, the mouse was placed in Arm C, facing the center, and allowed to freely explore the maze for 5 min. A spontaneous alternation was defined an entry into the arm less recently explored. Percent spontaneous alternation was calculated as the number of spontaneous alternations over the total number of

entries. For example, the sequence C,B,A,B,C,B,A,C (starting in arm C) resulted in a percent spontaneous alternation of $4/6 = 67\%$.

Barnes maze. Hippocampal-dependent memory was assessed on a Barnes Maze apparatus (San Diego Instruments, California, USA), a circular platform with 36-inch diameter and 20 equally spaced escape holes along the perimeter, one of which leads to a “target” escape box. Bright lighting was used as stimulus to complete the task. The assay consisted of five phases: adaptation, forward acquisition training, forward probe trials, reversal training, and reversal probe trials. For adaptation, each mouse was placed in a dark start chamber in the middle of the maze for 10 s, then uncovered and guided gently to the escape box. Forward acquisition training consisted of two trials per day for 4 days, with each mouse starting in the dark start chamber in the middle of the maze and subsequently allowed to explore the maze for 3 min. The trial ends when the mouse enters the target escape hole or after 3 min have elapsed, after which the mouse is guided gently to the escape hole. After reaching the escape hole, the mouse is allowed to remain there for 1 min. Forward probe trials were conducted on day 5, 24 h after the last training day. During the probe trial, the maze is in the same position as the training days, and the target hole is closed. Each trial lasted 90 s, during which the number of errors (pokes into non-target holes) made prior to reaching the target hole is quantified. Days 6–10 consisted of reversal training, conducted using a similar protocol as forward acquisition training, except that the target was a stable escape hole moved 180° from its location during forward acquisition training. Reversal probe trials were conducted on day 11 and identically to forward probe trials. In addition to quantifying the number of total errors, the number of perseverations, defined as pokes into the previous target hole during forward acquisition training, was counted.

Locomotor assay. Locomotor activity was measured by beam breaks in a photobeam frame (Med Associates, Vermont, USA). Mice were individually placed into a clean home-cage like environment lined with bedding and resting within a photobeam frame. The number of beam breaks as a measure of locomotor activity was quantified over 30 min in 5-min bins.

Accelerating Rotarod assay. Mice were placed on an accelerating Rotarod apparatus (Med Associates) for 16 trials (four trials a day for 4 consecutive days) with at least 15 min of rest between the trials. Each trial lasted for a maximum of 5 min, during which the rod accelerated linearly from 4 to 40 rpm. The amount of time for each mouse to fall from the rod was recorded for each trial.

Olfaction. Mice were tested for whether they could detect and differentiate odors in a habituation–dishabituation protocol modified from Yang and Crawley. Mice were presented with cotton-tipped wooden applicators dipped in water, vanilla, or swiped across the bottom of an unfamiliar social cage. Each stimulus was presented for 2 min with a 1-min inter-trial interval. Time spent sniffing was defined as when the animal was oriented with its nose 2 cm or closer toward the cotton tip.

Repetitive behavior. Mice were individually placed into a clean home-cage like environment lined with bedding. After allowing 5 min for habituation, 10 min of activity was videotaped for each mouse. The duration of repetitive behavior, defined as grooming or digging, was scored manually using a stopwatch.

Nesting. Nesting behavior was scored in accordance with the standard protocol and rating scale originally described by Deacon (Deacon, 2006). Four- to five-week old mice were assessed for amount of cotton material used after 20 h and for the height and shape of the nest. Rating scale as follows: (1) nestlet not noticeably touched (>90% intact); (2) nestlet partially torn (50–90% remaining intact); (3) nestlet mostly shredded but often no identifiable nest site: <50% of the Nestlet remains intact, but <90% is within a quarter of the cage floor area; (4) an identifiable but flat nest: >90% of the Nestlet is torn and the material is gathered into a nest within a quarter of the cage floor area, but the nest is flat, with walls higher than mouse body height (of a mouse curled up on its side) for <50% of its circumference; (5) a (near) perfect nest: >90% of the Nestlet is torn and the nest is a crater, with walls higher than mouse body height for >50% of its circumference.

Dyadic interaction. The dyadic interaction test is an abbreviated version of the three-chambered assay to quantitatively assess the duration of direct social interaction in two freely behaving mice.

One week prior to the assay, male R59X and wild-type control mice were singly housed to increase the motivation for social interaction and reduce aggression. Age-matched, novel, wild-type male stimulus mice were group-housed. On the day of the test, test and stimulus mice were acclimated to the room for 1 h prior to the start of the assay. Following this period, each test mouse is placed individually in a clear, round Plexiglass cage (Pinnacle Technology, Lawrence, Kansas, USA) measuring 8 inches tall and 9.5 inches in diameter, with a thin layer of bedding. Following 30 min of habituation in the cage, a novel, age-matched stimulus mouse was placed into the cage, and the mice were allowed to freely interact under video monitoring for 10 min. The total duration of social interaction initiated by the test mouse in the first 2 min was scored, and this included oro-genital sniffing, oro-facial sniffing, close following, placing one or both paws on the stimulus mouse, or allogrooming of the stimulus mouse. “Co-tested pairs” refer to side-by-side tests involving two littermate R59X and wild-type control mice, each interacting with a novel stimulus mouse in a separate cage.

Drug administration. Mice were acclimated to daily intraperitoneal (i.p.) injections of vehicle (saline) for 3 days prior to each set of behavioral assays. For each behavioral cohort, the entire cohort was administered either vehicle or drug, with the experimenter blinded to the genotypes of mice throughout. All animal behaviors were performed on adult male mice at 9–12 weeks of age, and the analysis of behavioral data was carried out by a researcher blinded to genotype. Vehicle and drug (memantine hydrochloride, Tocris Biosciences, United Kingdom) were diluted in saline at 10 μ L per gram mouse body weight for administration. Vehicle or drug was administered 1 h prior to the start of each behavioral assay, and during this period, mice were allowed to habituate in the room where the assay would be carried out. Notably, we used doses of memantine similar to those from studies in other mouse models of neurodevelopmental disorders, which are expected to result in reversible blockade of a relatively small fraction of synaptic NMDA receptors (Chung et al., 2015; Figueiredo et al., 2013).

Ex vivo slice preparation. All steps of electrophysiological experiments, including data collection and analysis, were performed by a researcher blinded to genotype. Acute hippocampal slices were prepared from mice 9 to 12 weeks of age. Animals were anesthetized with isoflurane and transcardially perfused with ice-cold oxygenated (95% O₂, 5% CO₂) cutting artificial cerebrospinal fluid (aCSF) solution (comprised of (mM): 2.5 KCl, 1.25 NaH₂PO₄, 5 MgSO₄, 0.5 CaCl₂, 200 sucrose, 25 NaHCO₃, 25 glucose, ~300 mOsm, 7.2–7.4 pH). After decapitation, brains were removed for sectioning in the same ice-cold cutting aCSF using a Vibratome (Leica Microsystems 1200 s). For whole-cell patch-clamp recordings of mE/IPSCs and the measurement of intrinsic membrane properties, 350- μ m transverse hippocampal sections were prepared. For all voltage-sensitive dye experiments, 400- μ m transverse hippocampal sections were prepared. Slices were recovered in the same cutting aCSF solution at 32 °C for 30 min and transferred to an oxygenated room-temperature solution composed of 50% cutting aCSF and 50% regular aCSF (comprised of (mM): 125 NaCl, 2.5 KCl, 1.25 NaH₂PO₄, 10 glucose, 26 NaHCO₃, 2 CaCl₂, 1 MgCl₂, ~300 mOsm, 7.2–7.4 pH) for 30 min. Subsequently, slices were transferred to 100% regular aCSF at room temperature for an additional 30 min before recording. All recordings were performed at 34 °C.

Miniature spontaneous excitatory postsynaptic currents (mEPSCs). A pipette internal solution comprised of (mM): 140 KCH₃OSO₃, 5 KCl, 0.5 EGTA, 1 MgCl₂, 10 HEPES, 5 MgATP, 0.25 NaGTP, ~292 mOsm, ECl = -78.8 mV was used. Pipettes 4–6 M Ω in resistance were pulled from borosilicate glass capillaries (World Precision Instruments, 1B150F-4) on a Sutter Instruments P-1000 pipette puller. Voltage-clamp traces 5 min in duration were recorded at a holding potential of -70 mV in the presence of 1 μ M tetrodotoxin (Tocris). All recordings were conducted with access resistance of <20 M Ω , leak current of <100 pA, and an applied series resistance compensation of 80%. Cells that did not maintain these parameters for the duration of the recording were eliminated. Analysis of mEPSCs was performed using pCLAMP10 (Axon Instruments, Molecular Devices) using a variable-amplitude template method, generated from a

stable recording of at least 50 mEPSC events. Each trace was first low-pass filtered at 1 kHz, and negative-going mEPSCs were detected using a template match threshold of 4, without fitting.

Miniature spontaneous inhibitory postsynaptic currents (mIPSCs). In order to record mIPSCs while maintaining a hyperpolarized membrane voltage, a high-chloride pipette internal solution (comprised of (mM): 100 CsCH₃O₃S, 50 CsCl, 10 HEPES, 0.2 BAPTA, 3 KCl, 1 MgCl₂, 0.25 GTP-Tris, 2.5 creatine phosphate disodium, 2 MgATP, ~296 mOsm, ECl = -23.7 mV) was used. Pipettes 4–6 MΩ in resistance were pulled from borosilicate glass capillaries (World Precision Instruments, 1B150F-4) on a Sutter Instruments P-1000 pipette puller. Voltage-clamp traces 3 min in duration were recorded at a holding potential of -70 mV in the presence of 1 μM tetrodotoxin (Tocris) and 2 mM kynurenic acid (Sigma Aldrich). All recordings were conducted with access resistance of <20 MΩ, leak current of <100 pA, and an applied series resistance compensation of 80%. Cells that did not maintain these parameters for the duration of the recording were eliminated. Analysis of mIPSCs was performed using pCLAMP10 (Axon Instruments, Molecular Devices) using a variable-amplitude template method, generated from a stable recording of at least 50 mIPSC events. Each trace was first low-pass filtered at 1 kHz, and negative-going mIPSCs were detected using a template match threshold of 4, without fitting.

Voltage-sensitive dye imaging. Following recovery, each slice was bulk-loaded with 100 μL of a solution containing the voltage-sensitive dye di-2-ANEPEQ_{49,50} (JPW1114, Molecular Probes) diluted at 0.05 mg/mL in aCSF (Antic & Zecevic, 1995; Habib-E-Rasul Mullah et al., 2013). Each slice was stained for 14 min, washed with aCSF, and imaged in an interface chamber using an 80 x 80 CCD camera recording with a 1 kHz frame rate (NeuroCCD; RedShirt Imaging). Illumination was provided by a 530 nm Green LED (Thor Labs, M530L3-C2). A filter set (Chroma Technologies 11007v2 wide Green) was used to allow excitation at 510–560 nm and collection of emitted fluorescence at a wavelength > 592 nm.

A concentric bipolar tungsten microelectrode was used for stimulation of the perforant path. Two successive stimuli were applied with an inter-stimulus interval of 200 ms. Two stimulation intensities (200 μ A and 400 μ A) were used. Imaging trials lasted a total of 1000 ms each, with a 20 s inter-trial interval. Interleaved trials without stimulation allowed for background subtraction.

All data analysis was performed in IGOR (Wavemetrics) on the average of 12 trials. Data were displayed as the change in fluorescence divided by the resting fluorescence ($\Delta F/F$). Regions of interest (ROIs) were drawn for the molecular layer of the dentate gyrus, the dentate granule cell layer, and the hilus. Like other dyes of the ANEPP family, di-2-ANEPEQ decreases in fluorescence upon membrane depolarization. To be consistent with electrophysiological conventions, depolarizing $\Delta F/F$ signals were displayed as upward signals (warmer colors) and hyperpolarization $\Delta F/F$ signals were displayed as downward signals (colder colors). Snapshots of VSDI represent an 80 \times 80 pixel window, corresponding to an $\sim 1.7 \times 1.7$ mm field of view.

Postsynaptic density protein purification. We adapted a widely used protocol for the preparation of PSD fractions (Bermejo, Milenkovic, Salahpour, & Ramsey, 2014). Mice were sacrificed via cervical dislocation, and their brains quickly extracted. Forebrain cortical tissues were microdissected and Dounce-homogenized in 10 mL of homogenization buffer (0.32 M sucrose, 4 mM HEPES, pH 7.4 with protease inhibitors). The homogenate was centrifuged at 1000 \times g for 10 min at 4 $^{\circ}$ C to pellet cellular debris and nuclei (P1), and the subsequent supernatant (S1) was centrifuged for another 15 min at 10,000 \times g at 4 $^{\circ}$ C. The resulting pellet (P2, "crude" synaptosomes) was resuspended in another 10 mL of homogenization buffer and centrifuged at 10,000 \times g for 15 min at 4 $^{\circ}$ C. The supernatant was discarded, and the resulting pellet (P2') was resuspended in 10 mL of 4 mM HEPES (pH 7.4) then homogenized on ice. The lysate was incubated at 4 $^{\circ}$ C for 30 min while shaking to hypo-osmotically lyse the synaptosomes, and then centrifuged for 20 min at 25,000 \times g at 4 $^{\circ}$ C. The pellet (LP1) was resuspended in 1 mL of homogenization buffer and layered on top of a discontinuous sucrose gradient (bottom to top: 1.5 mL of 1.2 M sucrose, 1 mL of 1.0 M sucrose, and 1 mL of 0.8 M sucrose). The gradient was

ultracentrifuged at $150,000 \times g$ for 1.5 h at 4°C . The turbid layer between the 1.0/1.2 M sucrose interphase containing the synaptic plasma membranes (~ 1 mL) was collected and resuspended in 5 mL of 4 mM HEPES to dilute out the sucrose. This fraction was ultracentrifuged again at $200,000 \times g$ for 30 min at 4°C . The resulting pellet was resuspended in 1 mL of 50 mM HEPES with 2 mM EDTA (pH 7.4), and the membrane proteins extracted by adding Triton X-100 at a final concentration of 0.5% and incubating at 4°C while rotating for 15 min. The proteins were centrifuged at $32,000 \times g$ for 20 min at 4°C , and the resulting pellet resuspended in 75 μL of 50 mM HEPES with 2 mM EDTA.

Brain microdissection. To assess CDKL5 protein expression in various brain regions, adult male mice were sacrificed by cervical dislocation. After decapitation, brains were removed and sectioned into 1 mm coronal slices using a mouse brain matrix. Tissue was dissected from the somatosensory cortex, striatum, hippocampus, and cerebellum and homogenized in lysis buffer containing 1% NP-40, pH 8.0.

Western blot. Protein concentration was measured using a Bradford assay. Purified synaptic density membrane proteins or protein lysates were prepared for gel electrophoresis by adding 4X LDS Sample Buffer (NuPAGE, NP0008) to a final concentration of 1x and β -mercaptoethanol to a final concentration of 5%. Samples were heat-denatured at 75°C for 20 min, and 7.5 μg of protein was loaded into each well of a 4–12% Bis-Tris gradient gel (Invitrogen 10-well, 1.5 mm; NP0335). Protein gels were run for 2 h at 125 V at room temperature on a ThermoFisher XCell SureLock mini-cell electrophoresis box (EI001) using BioRad PowerPac HC High-Current Power Supply (1645052), then transferred onto a nitrocellulose membrane (0.45 μm pore-size; Biorad 162–0115) for 1 h and 10 min at 27 V at room temperature. The resulting membrane was blocked with a 1:1 solution of LI-COR Odyssey blocking buffer (927–40100) and 1x PBS for 1 h at room temperature.

Primary antibodies used for CDKL5 detection are anti-N-terminal CDKL54 (in house; diluted 1:500), anti-GAPDH (MA5–15738, Invitrogen; RRID: AB_10977387; diluted 1:1000), anti-EB2 (AB45767, Abcam, diluted 1:1000). Secondary antibodies (Licor) are goat anti-rabbit IRDye 800CW and donkey anti-rabbit IRDye 680RD at dilutions of 1:10,000. Standard protocols were used for the Odyssey Infrared Imaging System for visualization and quantification.

For postsynaptic density studies, the primary antibodies used were anti-N-terminal CDKL5, anti-GluN1 (ThermoFisher, OMA1–04010; diluted 1:1000), anti-GluN2A (Frontier Institute, AB_2571605; diluted 1:200), anti-GluN2B (Frontier Institute AB_2571761; diluted 1:200), anti-GluA1 (Abcam, ab31232; diluted 1:1000), anti-GluA2 (Abcam, ab133477; diluted 1:2000), and anti- β -Actin (Abcam, ab8226; diluted 1:10,000). Secondary antibodies (LI-COR) were goat anti-rabbit IgG IRDye800CW and goat anti-mouse IgG IRDye680LT at dilutions of 1:10,000, and incubated for 1 h at room temperature. Standard protocols were used for the Odyssey Infrared Imaging System (LI-COR) for visualization and quantification.

Statistical analyses. For behavioral assays involving *Dlx-cKO* mice, we chose similar sample sizes for all behavioral experiments based on previous published studies of *Cdkl5* constitutive knockout mice and *Cdkl5* glutamatergic conditional knockout mice (Tang et al., 2017; I. T. Wang et al., 2012). For behavioral assays involving drug administration, we used pilot behavioral cohorts to estimate effect sizes required for detecting significant wild-type-mutant differences and used similar sample sizes for saline- and drug-administered cohorts. Importantly, the number of mice used were pre-determined prior to the start of each experiment.

For behavioral assays, statistical analyses were performed using Prism (GraphPad). All data sets were analyzed using the Shapiro-Wilk test for normality. For one-sample comparisons, data sets with normal distributions were analyzed for significance using the one-sample t-test, whereas data sets with non-normal distributions were analyzed using the Wilcoxon signed-rank test. For two-sample comparisons, data sets with normal distributions were analyzed for significance using the unpaired Student's t-test, whereas data sets with non-normal distributions

were analyzed using the Mann–Whitney test. Two-way repeated measures ANOVA or the Kruskal–Wallis test was conducted for the appropriate data sets with Holm-Sidak’s multiple-comparison test. All one-sample, two-sample, and multiple-comparison tests were two-tailed.

All other assays that involved sub-sampling of animals were analyzed using R (The R Project for Statistical Computing). Each data set was analyzed using a linear mixed effect model, where *Genotype* was modeled as a fixed effect term and *Animal* was modeled as a random effect term. This model accounts for both between-animal and between-cell variation. For each assay, null and alternative models were constructed using the *lmer* function in the lme4 package⁵² in the following format (Bates, Machler, Bolker, & Walker, 2015):

```
m0=lmer(Outcome~(1|Animal),REML=TRUE)
m1=lmer(Outcome~Genotype+(1|Animal),REML=TRUE)
```

For data sets involving a third term (e.g., cumulative frequency bin), the following null and alternative models were constructed, in order to test the significance of an interaction between Genotype and the third term:

```
m0=lmer(Outcome~Bin+Genotype+(1|Animal),REML=TRUE)
m1=lmer(Outcome~Bin*Genotype+(1|Animal),REML=TRUE)
```

To make statistical comparisons, the *KRmodcomp* function from the pbkrtest package (Halekoh and Højsgaard, 2014) was used:

```
KRmodcomp (m0,m1)
```

The *KRmodcomp* function reports a modified F-test statistic based on the Kenward and Roger approximation, which accounts for the small sample sizes in our study, modified numerator and denominator degrees of freedom, and a p-value. The estimated effect of Genotype is obtained from the alternative model constructed using the *lmer* function from lme4.

Post-hoc testing for linear mixed effect models (e.g., at cumulative frequency bins) was performed using the least-squares means method for multiple comparisons. The *lsmeans* package was used⁵³ on the alternative model generated by *lmer*(Lenth, 2016):

```
lsmeans(m1, pairwise ~ Genotype | Bin, mode = 'kenward-roger')
```

For the analysis of cumulative distributions (mEPSC and mIPSC inter-event intervals and amplitudes), all samples from each individual cell was sorted, binned, and averaged at percent intervals, effectively generating a binned cumulative distribution curve for each cell. Data from all cells of a given genotype were plotted at these distinct binned percent intervals with the mean and error bars indicating s.e.m. The results were analyzed using linear mixed effect models, incorporating a third term, cumulative frequency bin.

All graphs are plotted using Prism (GraphPad). Boxplot limits indicate the minimum and maximum, and boxplot center line indicates the median. In our figures, p-values between 0.05 and 0.1 are shown explicitly, * is used to denote all $0.01 < p < 0.05$, ** for $0.001 < p < 0.01$, *** for $0.0001 < p < 0.001$, and **** for $p < 0.0001$.

Figures

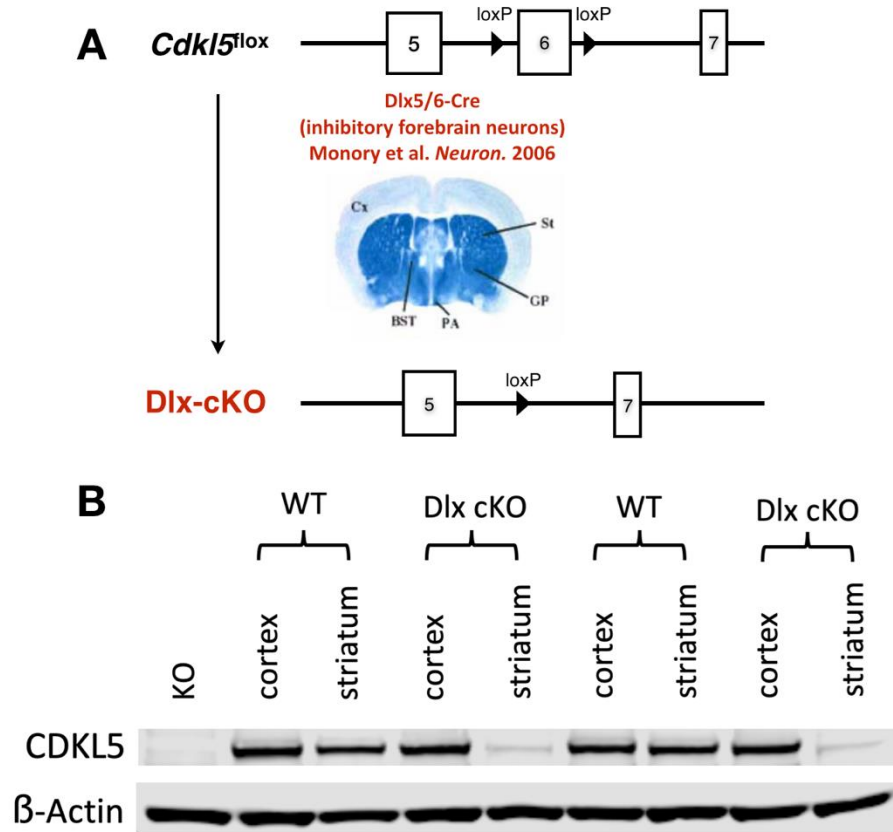


Figure 1. Generation and validation of mice lacking CDKL5 selectively in forebrain GABAergic neurons (Dlx-cKO).

(A) Schematic representing the generation of Dlx-cKO mice using a conditional *Cdkl5* exon 6-floxed *Cdkl5* mouse line (Tang et al., 2017) and the *Dlx5/6-Cre* driver (Monory et al., 2006). (B) Validation of the cell type-specificity of CDKL5 protein knockout using microdissected brain tissue. Two pairs of WT and Dlx-cKO littermates were used. In the cortex, a region enriched for glutamatergic neurons, Dlx-cKO mice show comparable amounts of CDKL5 protein to WT. In the striatum, a region enriched for GABAergic neurons, Dlx-cKO mice show reduced CDKL5 protein in comparison to WT. The residual CDKL5 protein likely originates from non-GABAergic cells in this brain region.

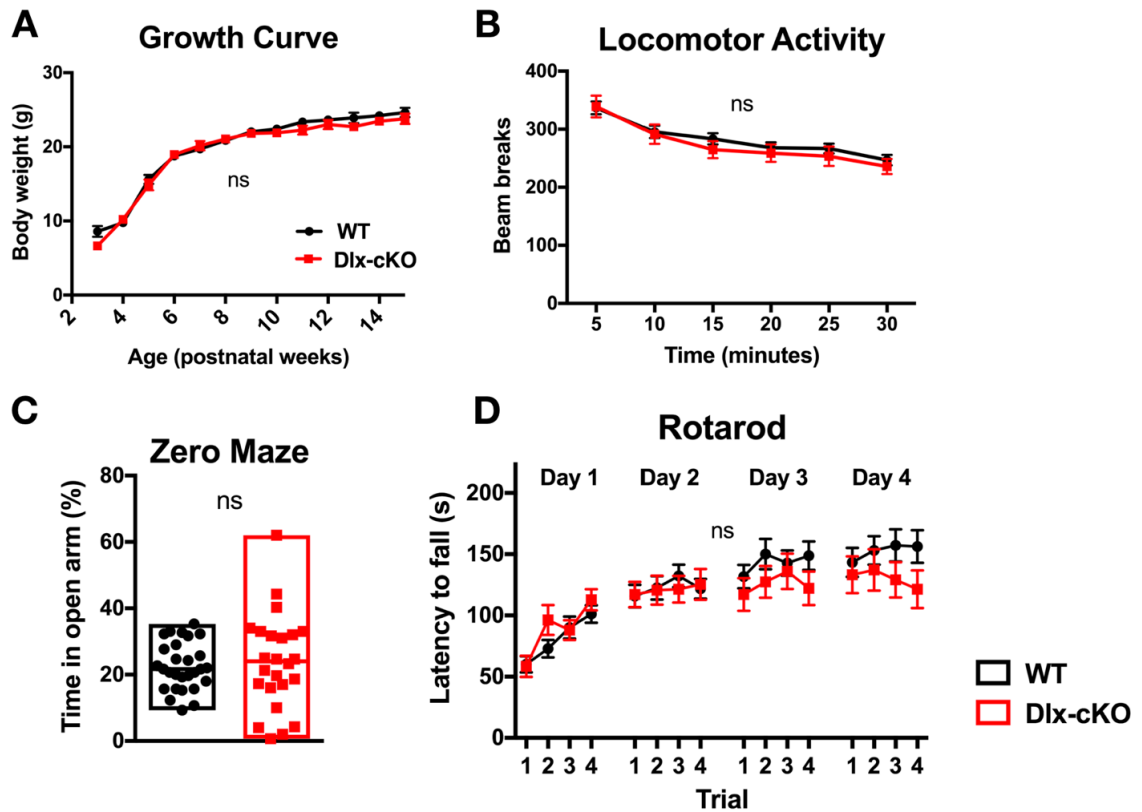


Figure 2. Dlx-cKO mice show unaltered growth, locomotion, anxiety-related behavior, and motor coordination.

(A) Unaltered body weight of Dlx-cKO mice at various ages (WT, n = 4-36 mice / time point; Dlx-cKO, 14-29 mice / time point; unpaired t-tests with Holm-Sidak's correction for multiple comparisons). (B) Dlx-cKO mice show unaltered home-cage locomotion on the beam break assay (WT, n = 43, Dlx-cKO, n = 32; one-way repeated-measures ANOVA). (C) Dlx-cKO mice, show unaltered anxiety-related behavior, as assessed by the percent time spent in open arms, on the elevated zero maze assay (WT, n = 28, Dlx-cKO, n = 24; unpaired t-test). (D) Dlx-cKO mice show unaltered motor coordination and learning on the Rotarod assay (WT, n = 39, Dlx-cKO, n = 23; one-way repeated-measures ANOVA).

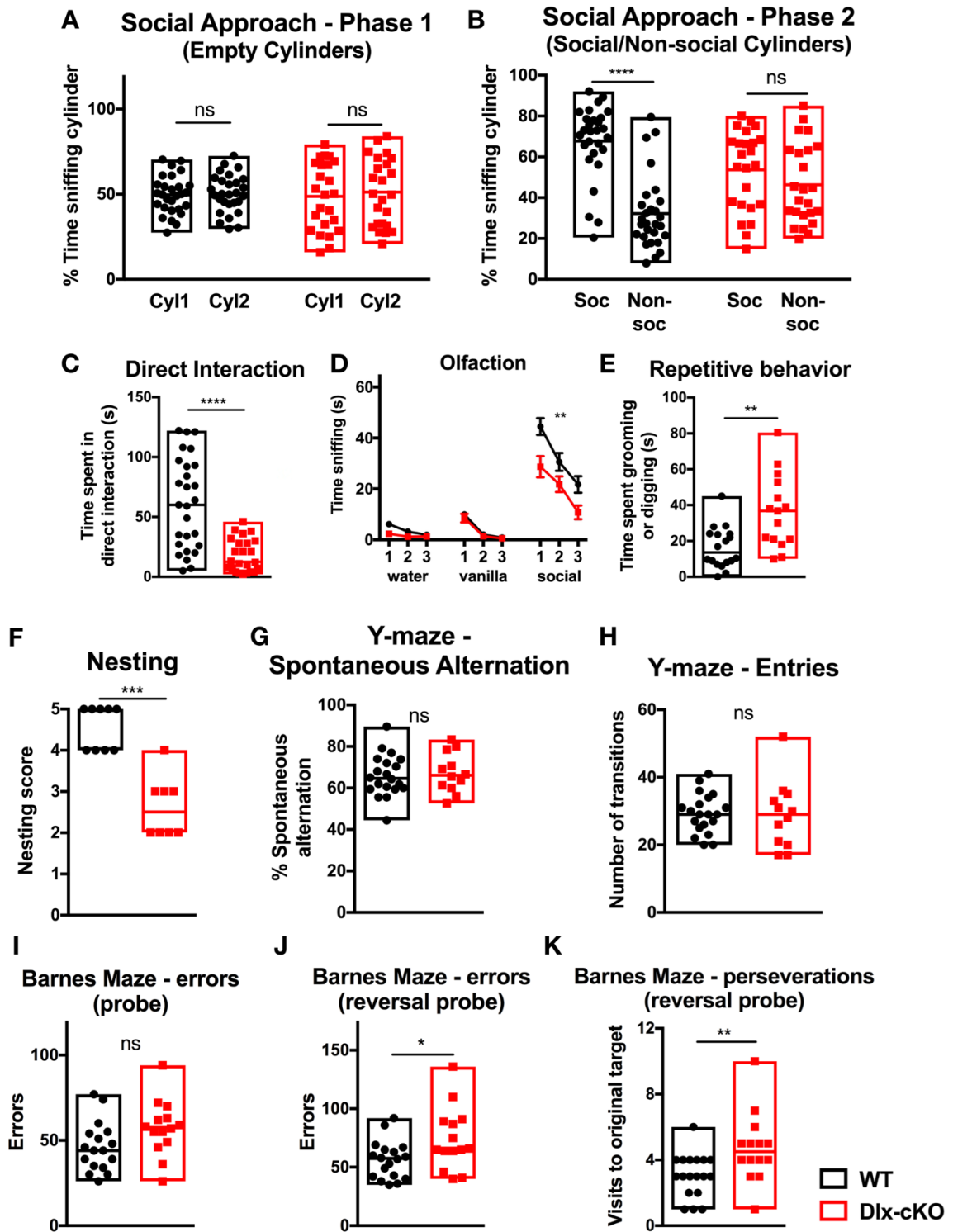


Figure 3. Dlx-cKO mice exhibit an autistic-like phenotype.

(A) Dlx-cKO mice showed similar times spent interacting with empty cylinders during the habituation phase of the three-chambered social assay. Cyl1/Cyl2: empty cylinders 1 and 2. Soc: social cylinder containing a stimulus mouse. Non-soc: non-social cylinder containing an object. (WT, n = 28; Dlx-cKO, n = 26; paired t-test). (B) Wild-type mice showed a significant preference for interacting with the cylinder containing a social stimulus, but Dlx-cKO mice did not show a significant difference in time spent sniffing the social and non-social cylinders (paired t-test). (C) Dlx-cKO mice also spent significantly reduced time initiating social contact during the direct interaction phase (unpaired t-test). (D) Dlx-cKO mice showed unaltered ability to discriminate between odors and habituation to the same odor upon repeated presentation. However, Dlx-cKO mice show a reduced time sniffing a social scent compared to WT (WT, n = 20; Dlx-cKO, n = 14; two-way ANOVA with Holm-Sidak's multiple comparisons test; error bars demonstrate s.e.m.). (E) Dlx-cKO mice spent significantly more time engaging in repetitive behaviors, including grooming and digging, within a 10-minute period in a home cage-like environment (WT, n = 18; Dlx-cKO, n = 16; unpaired t-test). (F) Dlx-cKO mice show significantly reduced nesting scores on the nesting assay (WT, n = 9; Dlx-cKO, n = 8; Mann-Whitney test). (G) Dlx-cKO mice show unaltered spontaneous alternation percentage in comparison to WT mice (WT, n = 20; Dlx-cKO: n = 12; unpaired t-test). (H) The total number of entries made were not significantly different between Dlx-cKO and WT mice (unpaired t-test). (I) Dlx-cKO mice did not show a significant difference in the total number of errors made on forward probe trials of the Barnes maze (WT, n = 18; Dlx-cKO: n = 14; unpaired t-test). (J) Dlx-cKO mice made significantly more errors on the reversal probe trials of the Barnes maze (unpaired t-test). (K) On the reversal probe trials, Dlx-cKO mice also made significantly more perseverations, or visits to the original target hole location (Mann-Whitney test). *p<0.05, **p<0.01, ***p<0.001, and ****p<0.0001.

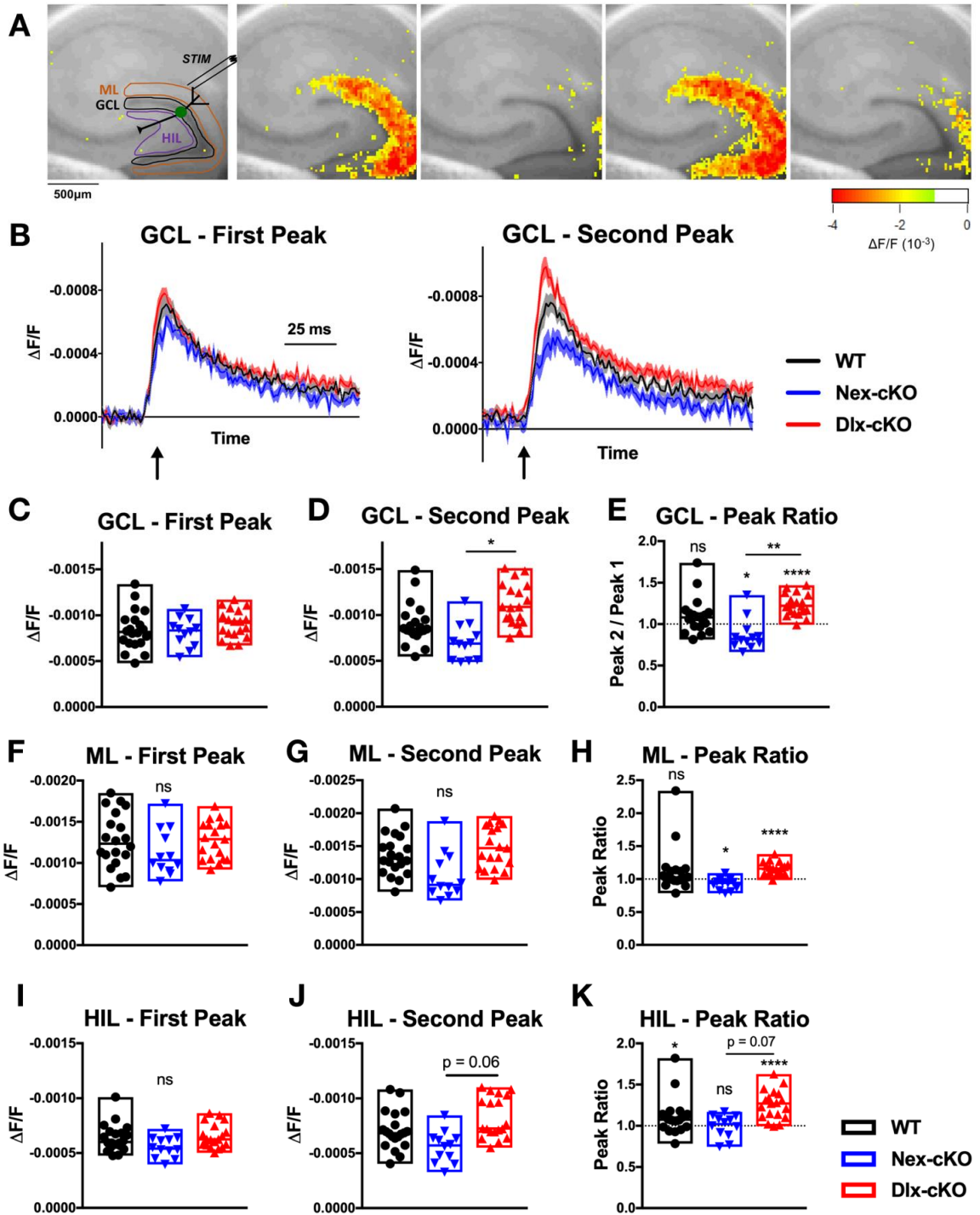


Figure 4. Dlx-cKO mice show aberrant paired-pulse facilitation.

(A) Schematic of voltage-sensitive dye imaging (VSDI) showing the site of stimulation at the perforant path and regions of interest used for quantitative analysis (GCL, granule cell layer; ML, molecular layer; HIL, hilus). Snapshots of VSDI responses in a wild-type slice, from left to right: baseline, peak response to first stimulus, baseline immediately prior to second stimulus, peak response to second stimulus, 100 ms after second peak response (200 μ A x 2 stimuli, with 200 ms inter-stimulus interval). (B) Averaged VSDI responses ($\Delta F/F$) in the GCL for WT, Nex-cKO, and Dlx-cKO mice in response to each of the two stimuli. Depolarization (decrease in $\Delta F/F$) is displayed as an upward signal, while hyperpolarization (increase in $\Delta F/F$) is displayed as a downward signal. Error envelopes represent mean \pm s.e.m. (C) Peak amplitudes of the GCL response to the first stimulus were not different between WT, Nex-cKO, and Dlx-cKO mice (linear mixed effect analysis). (D) Peak amplitudes of the GCL response to the second stimulus were significantly different between Nex-cKO and Dlx-cKO mice (linear mixed effect analysis with Tukey's correction for multiple comparisons). (E) Ratios of peak responses in the GCL. Nex-cKO slices showed significant paired-pulse depression, whereas Dlx-cKO slices showed significant paired-pulse facilitation (one-sample t-tests for each of WT, Nex-cKO, and Dlx-cKO, two-tailed). Dlx-cKO also showed significantly increased paired-pulse ratio in comparison to Nex-cKO (linear mixed effect analysis with Tukey's correction for multiple comparisons). (F-K) Averaged VSDI responses ($\Delta F/F$) in the ML and HIL for WT, Nex-cKO, and Dlx-cKO mice in response to each of the two stimuli (linear mixed effect analysis). (H) Peak ratios in ML (one-sample t-test or Wilcoxon signed-rank test, two-tailed). (K) Peak ratios in HIL (one-sample t-test or Wilcoxon signed-rank test, two-tailed). For all experiments, n=20 slices/5 mice for WT, n=12 slices / 4 mice for Nex-cKO, and n=19 slices/5 mice for Dlx-cKO. *p<0.05, ****p<0.0001.

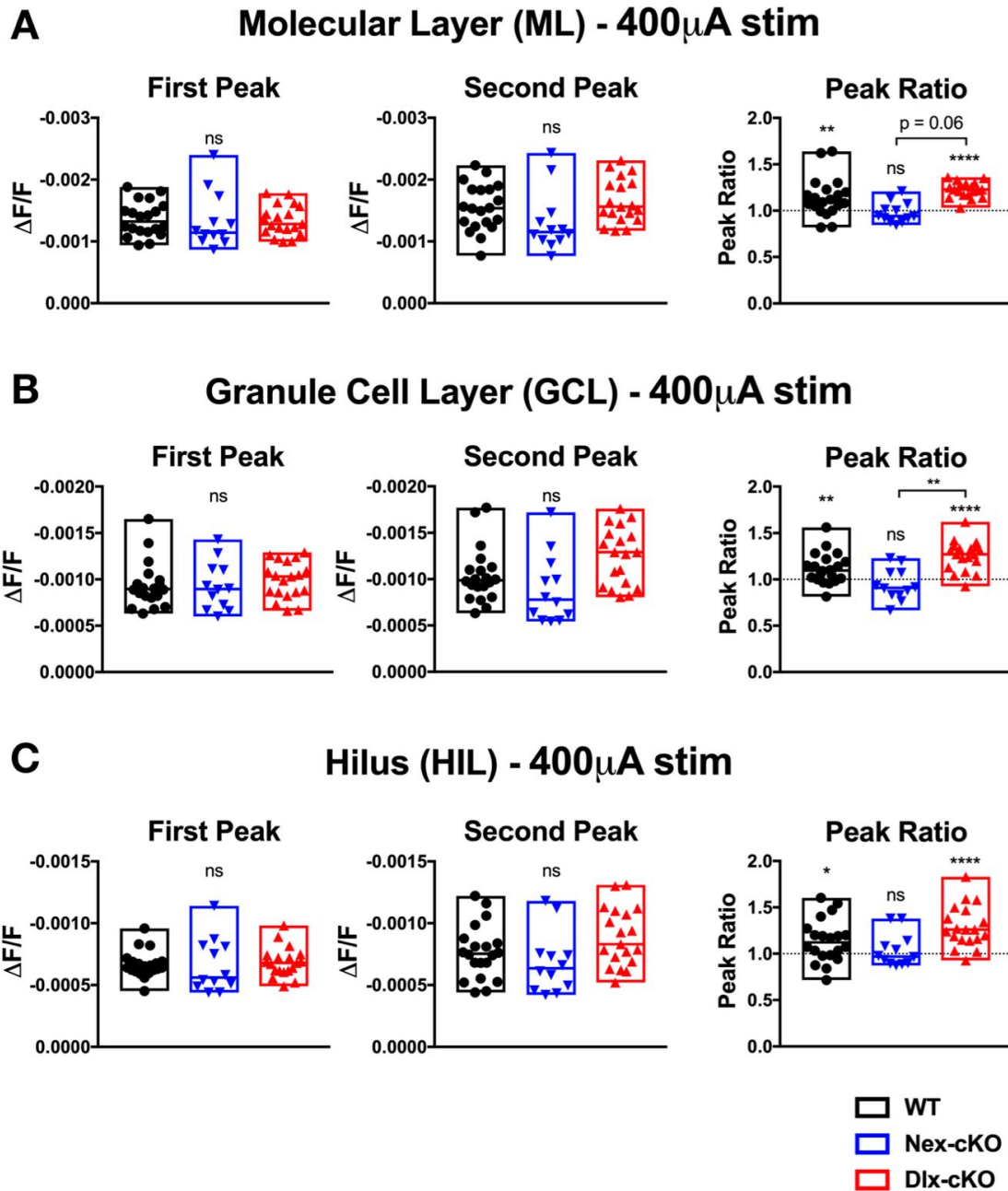


Figure 5. VSDI responses in regions of the dentate gyrus at 400 μ A stimulation intensity.

(A-C) Peak responses are not significantly different between WT, Nex-cKO, and Dlx-cKO (linear mixed effect analysis). In all three regions (ML, GCL, and HIL) at this higher stimulation intensity, Dlx-cKO show significantly increased facilitation, whereas Nex-cKO shows no significant facilitation or depression (one-sample t-test or Wilcoxon signed-rank test, two-tailed). In the GCL, Dlx-cKO also showed significantly increased paired-pulse ratio in comparison to Nex-cKO (linear mixed effect analysis with Tukey's correction for multiple comparisons). * $p < 0.05$, ** $p < 0.01$, *** $p < 0.001$, and **** $p < 0.0001$.

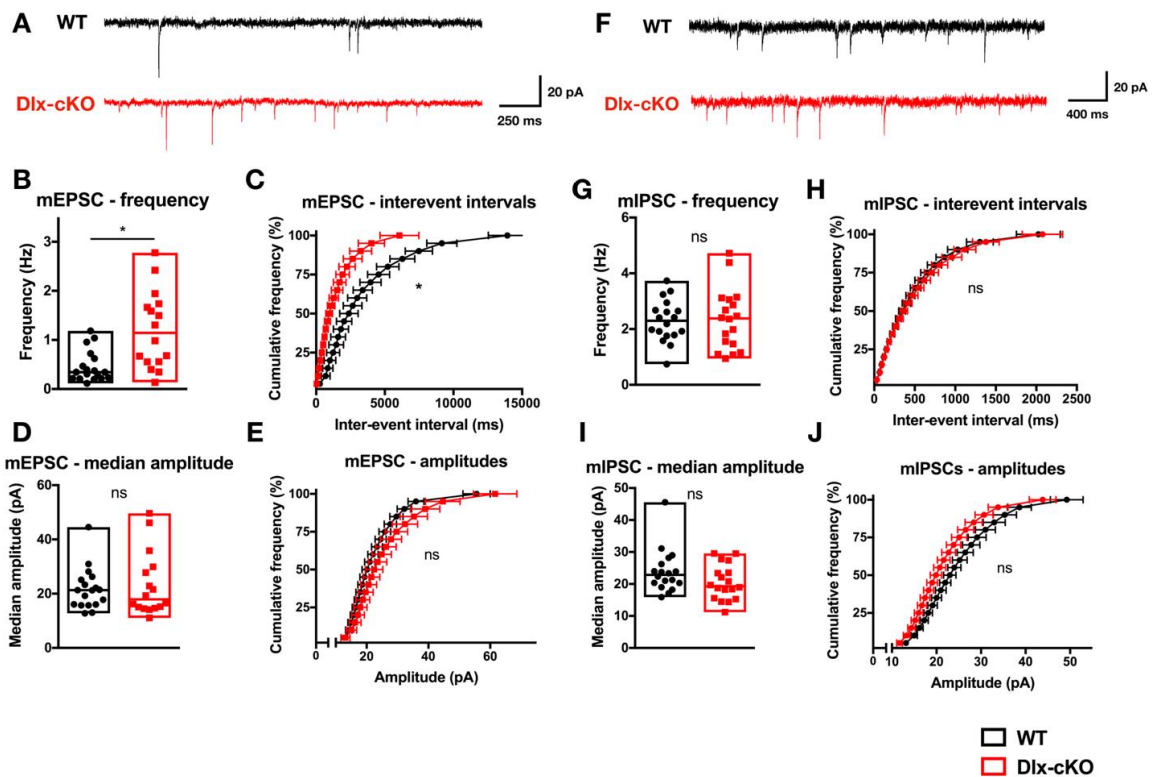


Figure 6. Enhanced excitatory synaptic transmission but unaltered inhibitory synaptic transmission in Dlx-cKO mice.

(A) Representative mEPSC traces for cells from WT and Dlx-cKO mice. (B) Dlx-cKO mice show significantly enhanced mEPSC frequency at CA1 pyramidal neurons (linear mixed effect analysis). (C) The cumulative frequency distribution of mEPSC inter-event intervals is also significantly shifted in Dlx-cKO mice (linear mixed effect analysis with least-square means post-hoc testing). (D) The mEPSC median amplitude is unaltered in Dlx-cKO mice (linear mixed effect analysis). (E) The cumulative frequency distributions of mEPSC amplitudes are not significantly different between Dlx-cKO and WT mice (linear mixed effect analysis). (F) Representative mIPSC traces for cells from WT and Dlx-cKO mice. (G) Dlx-cKO mice show unaltered mIPSC frequency at CA1 pyramidal neurons (linear mixed effect analysis). (H) The cumulative frequency distributions of mIPSC inter-event intervals were not significantly different between Dlx-cKO and WT mice (linear mixed effect analysis). (I) The median amplitude of mIPSCs is not significantly different between Dlx-cKO and WT mice (linear mixed effect analysis). (J) The cumulative frequency distributions of mIPSC amplitudes are not significantly different between Dlx-cKO and WT mice (linear mixed effect analysis). For mEPSCs: WT, $n = 18$ cells / 3 mice; Dlx-cKO, $n = 16$ cells / 3 mice; for mIPSCs: WT, $n = 18$ cells / 3 mice; Dlx-cKO, $n = 18$ cells / 3 mice. * $p < 0.05$. Error bars s.e.m.

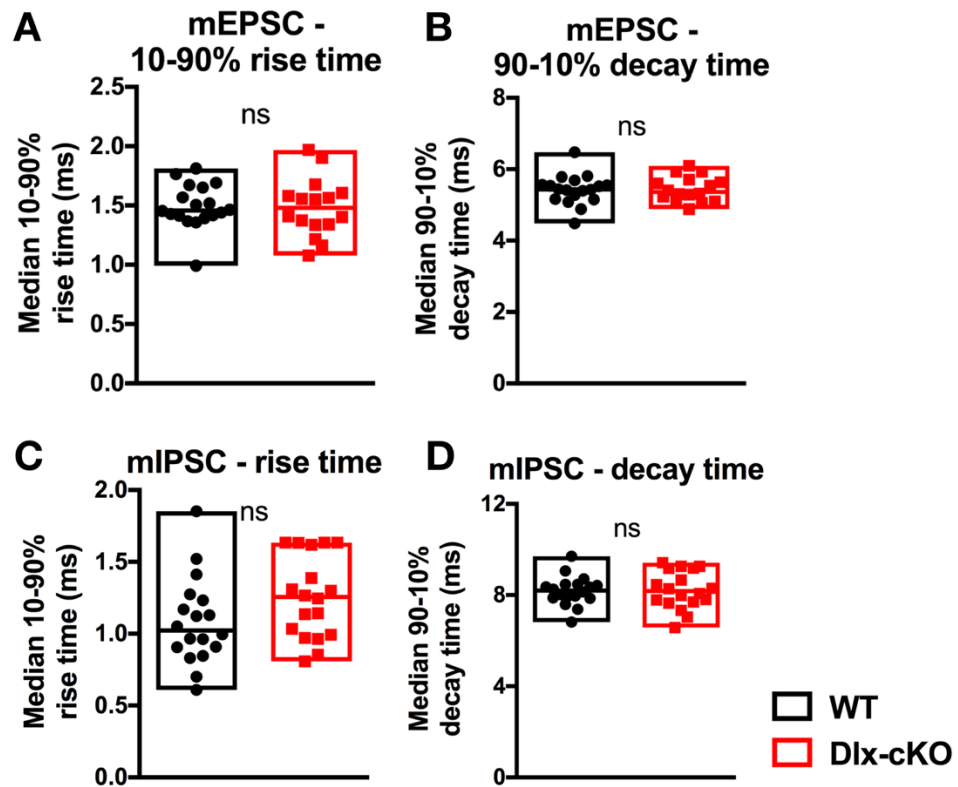


Figure 7. Unaltered mEPSC and mIPSC kinetics in Dlx-cKO mice.

(A) The median 10-90% rise time of mEPSCs is unaltered in Dlx-cKO mice (linear mixed effect analysis). (B) The median 90-10% decay times of mEPSCs is unaltered in Dlx-cKO mice (linear mixed effect analysis). (C) The median 10-90% rise time of mIPSCs is unaltered in Dlx-cKO mice (linear mixed effect analysis). (D) The median 90-10% decay times of mIPSCs is unaltered in Dlx-cKO mice (linear mixed effect analysis).

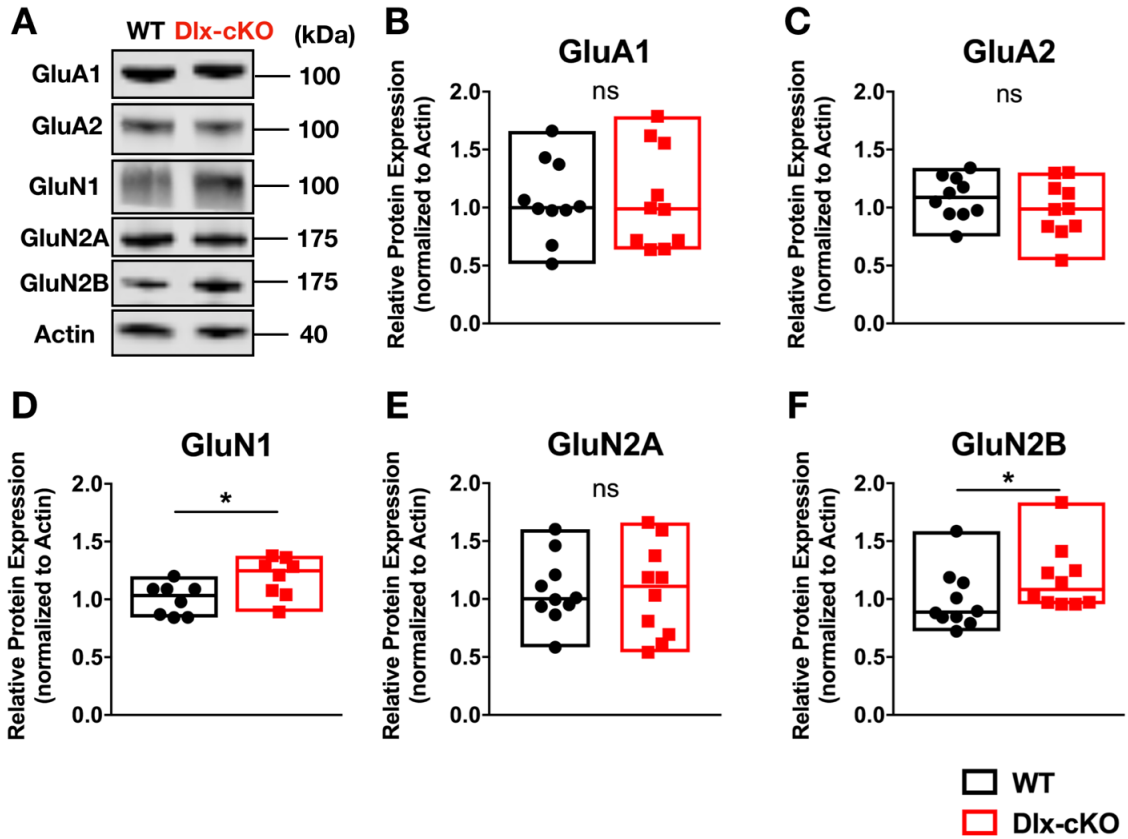


Figure 8. Dlx-cKO mice have an upregulation of NMDA receptors at the postsynaptic membrane.

(A) Representative western blot results for several major ionotropic glutamate receptor subunits from postsynaptic density membrane fractions. Samples are from pairs of WT and Dlx-cKO littermates. (B-F) Dlx-cKO mice show a selective increase in levels of GluN1 and GluN2B, two of the major subunits that compose the NMDA receptor (WT, n = 10 mice; Dlx-cKO, n = 10 mice; unpaired *t*-test or Mann-Whitney test). **p*<0.05.

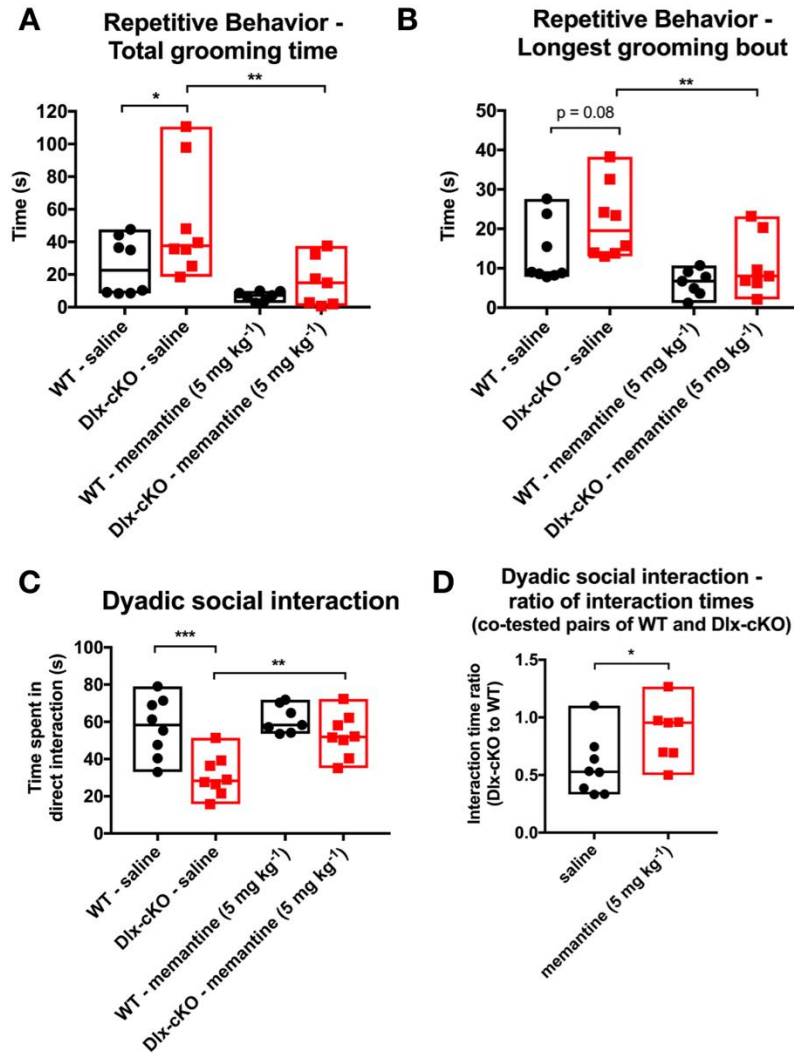


Figure 9. Acute NMDAR blockade ameliorates autistic-like features in Dlx-cKO mice.

(A) Total grooming in a home cage-like environment is significantly increased in saline-treated Dlx-cKO mice in comparison to WT, and memantine at 5 mg kg⁻¹ significantly rescued the increased grooming phenotype in Dlx-cKO mice ($n = 8$ for saline groups; $n = 7$ for memantine groups; one-way ANOVA with Holm-Sidak's multiple comparisons test). (B) Memantine significantly reduces the duration of the longest grooming bout in Dlx-cKO mice. (C) On the dyadic social assay, saline-treated Dlx-cKO mice spend significantly less time initiating social interaction with a novel stimulus mouse in comparison to WT. Memantine at 5 mg kg⁻¹ resulted in a significant increase in time spent in social interaction ($n = 8$ for saline groups; $n = 7$ for WT - memantine; $n = 8$ for Dlx-cKO - memantine; one-way ANOVA with Holm-Sidak's multiple comparisons test). (D) For co-tested pairs of Dlx-cKO and WT mice, the ratio of time spent in direct interaction was significantly reduced in saline-treated mice. Memantine normalized this ratio, indicating a differential effect of this drug on social interaction in WT and Dlx-cKO mice ($n = 7$ for all groups; unpaired t-test). * $p < 0.05$, ** $p < 0.01$, and *** $p < 0.001$.

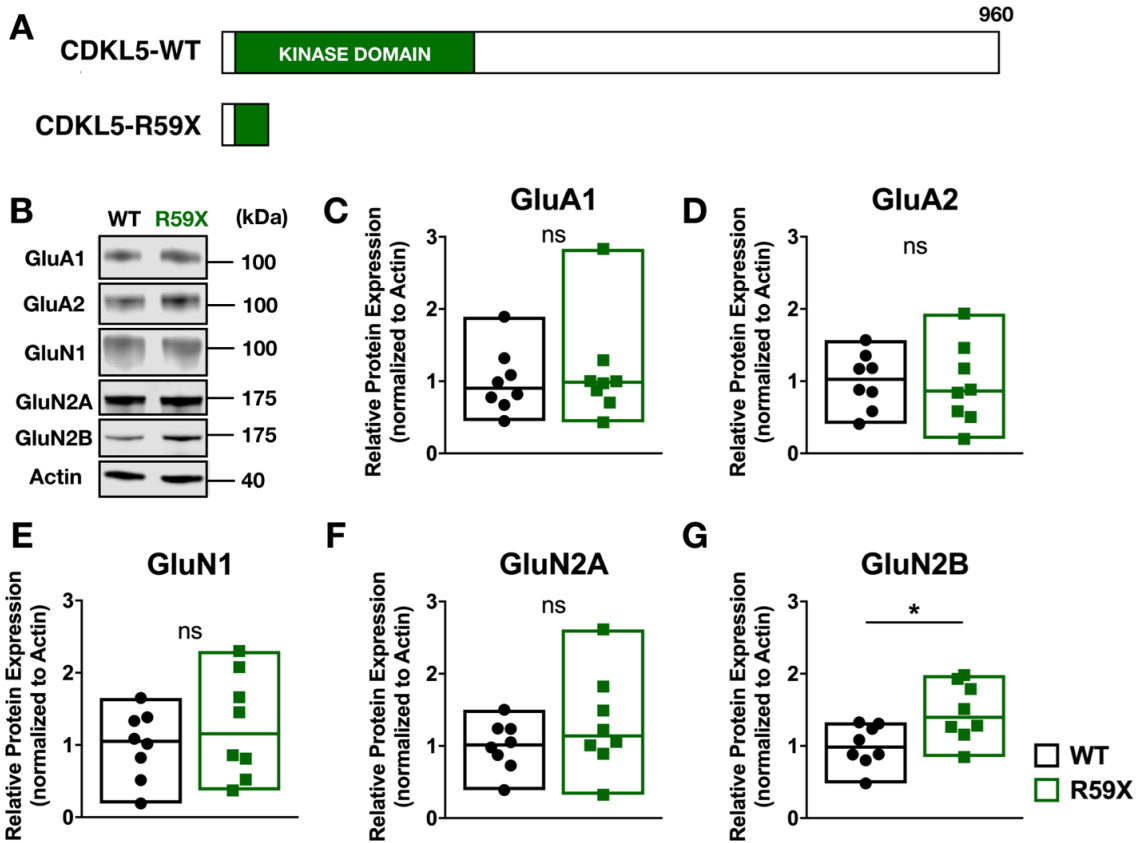


Figure 10. R59X mice have an upregulation of NMDA receptors at the postsynaptic membrane.

(A) Schematic of the R59X non-sense mutation at arginine 59, which results in early truncation of the catalytic domain of CDKL5. (B) Representative western blot results for several major ionotropic glutamate receptor subunits from postsynaptic density membrane fractions. Samples are from pairs of WT and R59X littermates. (C-G) R59X mice show a selective increase in level of GluN2B, a major subunit of the NMDA receptor (WT, n = 8 mice; R59X, n = 8 mice; unpaired *t*-test or Mann-Whitney test). **p*<0.05

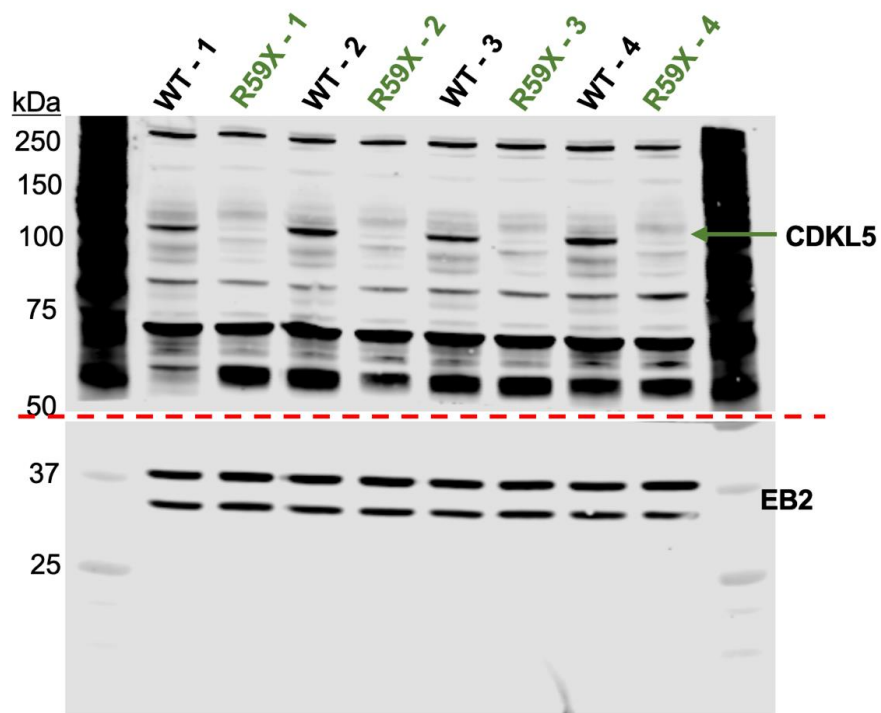


Figure 11. Loss of full-length CDKL5 protein in R59X knock-in mice.

Loss of full-length CDKL5 protein in R59X mice, shown with western blots of dissected whole cortex lysate in four pairs of WT and R59X littermates. Green arrow indicates band corresponding to CDKL5 (note a non-specific band running at approximately the same size). Total EB2 protein was used as a loading control.

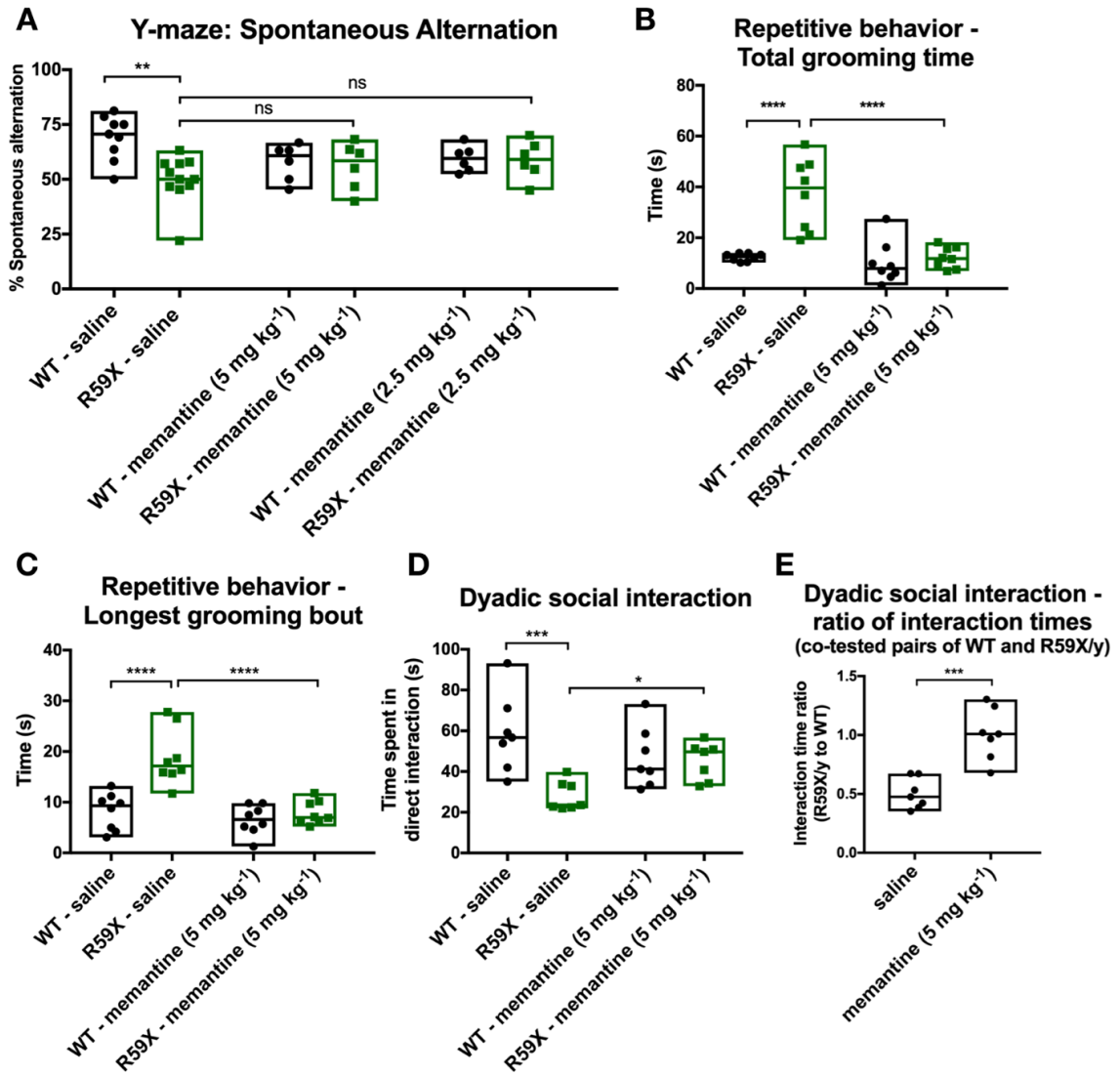


Figure 12. Acute NMDAR blockade ameliorates autistic-like features, but not learning and memory, in CDKL5-deficient mice.

(A) Spontaneous alternation percentage is significantly reduced in saline-treated R59X mice in comparison to WT mice. However, acute memantine administration at either 2.5 or 5 mg kg⁻¹ doses did not significantly rescue the spontaneous alternation deficit (WT-saline, n = 9; R59X-saline, n = 11; WT-memantine (5 mg kg⁻¹), n = 6; R59X-memantine (5 mg kg⁻¹), n = 6; WT-memantine (2.5 mg kg⁻¹), n = 6; R59X-memantine (2.5 mg kg⁻¹), n = 6; Kruskal-Wallis test with Dunn's multiple comparisons test). (B) Total grooming in a home cage-like environment is significantly increased in saline-treated R59X mice in comparison to WT, and memantine at 5 mg kg⁻¹ significantly ameliorated the increased grooming phenotype in R59X mice (n = 8 for all

groups; one-way ANOVA with Holm-Sidak's multiple comparisons test). (C) The duration of the longest grooming bout is significantly increased in saline-treated R59X mice in comparison to WT, and memantine also ameliorated this aspect of repetitive behavior (n = 8 for all groups; one-way ANOVA with Holm-Sidak's multiple comparisons test). (D) On the dyadic social assay, saline-treated R59X mice spend significantly less time initiating social interaction with a novel stimulus mouse in comparison to WT. Memantine at 5 mg kg⁻¹ resulted in a significant increase in time spent in social interaction (n = 7 for all groups; one-way ANOVA with Holm-Sidak's multiple comparisons test). (E) For co-tested pairs of R59X and WT mice, the ratio of time spent in direct interaction was significantly reduced in saline-treated mice. Memantine normalized this ratio, indicating a differential effect of this drug on social interaction in WT and R59X mice (n=7 for all groups; unpaired t-test). *p<0.05, **p<0.01, ***p<0.001, and ****p<0.0001.

CHAPTER 3 – CDKL5 IS ESSENTIAL IN THE POST-DEVELOPED BRAIN TO MAINTAIN MULTIPLE BEHAVIORAL DOMAINS, HIPPOCAMPAL CIRCUIT COMMUNICATION, AND SYNAPTIC MORPHOLOGY

Contributions: Barbara Terzic led this study with help from Sheng Tang and Yu-Ting Liu for cellular morphology experiments, and Zhaolan Zhou for the review and interpretation of data. Yue Cui managed all mouse husbandry, genotyping, and breeding. Barbara Terzic wrote this chapter with input from all authors.

Abstract

CDKL5 deficiency disorder (CDD) is an early-onset, neurodevelopmental syndrome characterized by intractable seizures, intellectual disability, hypotonia, and autistic features. It is associated with pathogenic variants in the gene encoding cyclin-dependent kinase-like 5 (CDKL5), but the specific action of CDKL5 in neuronal development and maintenance remains unclear. Although CDD is an early-onset disorder, from both a basic science and therapeutic perspective it will be imperative to understand whether CDKL5 also serves a critical role in the nervous system after development. In this study, we address this uncertainty by employing a conditional adult knockout of *Cdkl5* in mice to examine the post-developmental requirement of CDKL5. We present, for the first time, that CDKL5 function is required in adult mice to maintain proper performance within several behavioral domains, hippocampal circuit communication, and dendritic spine morphology. We also demonstrate that CDKL5 continuously regulates phosphorylation of the microtubule-associate protein EB2, highlighting disrupted microtubule networks as a potential node in CDD pathogenesis. Collectively, these results demonstrate that adult neural function requires CDKL5, and expand upon our current understanding of CDKL5 in regulating neurological function. Importantly, our results also suggest that chronic treatment may be needed for effective mitigation of CDD.

Introduction

Mutations in the X-linked gene encoding cyclin-dependent kinase-like 5 (CDKL5) are associated with a devastating neurodevelopmental syndrome known as CDKL5 deficiency disorder (CDD)(Fehr et al., 2013; Kalscheuer et al., 2003; Tao et al., 2004; Weaving et al., 2004). CDD is characterized by a constellation of phenotypes including intractable seizures, severe neurodevelopmental delay, intellectual disability, hypotonia, and autistic features(S. T. Demarest et al., 2019; H. E. Olson et al., 2019). The disorder predominantly afflicts young females heterozygous for mutations in *CDKL5*, but hemizygous male cases have also been reported (albeit at a significantly lower prevalence)(S. T. Demarest et al., 2019; Liang, Huang, Wang, & Lu, 2019). With an overall incidence of one per forty-two thousand live births, mutations in *CDKL5* currently comprise one of the most common genetic causes of epilepsy in children(Symonds et al., 2019). Despite this strong genetic link, the pathogenesis of CDD remains unclear. Presently, there is no cure, and the limited treatment options available have focused on mitigating seizure burden using a variety of non-specific anticonvulsants(H. E. Olson et al., 2019).

In 2012, the first knockout mouse model of CDD was generated and found to recapitulate several of the cardinal phenotypes of the human disease including learning and memory impairments, motor deficits, and autistic-like behaviors(I. T. Wang et al., 2012). This line carries a deletion of *Cdkl5* exon 6, mimicking a reported CDD patient splice site mutation resulting in exon 6 skipping and loss of full-length protein(Archer et al., 2006). Several additional knockout and knock-in lines have since been generated with similar behavioral deficits, highlighting the reproducibility of CDD-related phenotypes in mice(Amendola et al., 2014; Okuda et al., 2018; Tang et al., 2019). Despite the multitude of CDD models, the time course of CDD pathogenesis, specific roles for CDKL5 in nervous system development versus maintenance, and reversibility of CDD-related phenotypes remain undetermined.

CDKL5 is a serine-threonine kinase most highly expressed in forebrain neurons and enriched at the neuronal post-synaptic density(Kilstrup-Nielsen et al., 2012; Ricciardi et al., 2012; Zhu et al., 2013). Recent work has identified microtubule-associated proteins as targets of the

kinase, revealing a potential role for CDKL5 in regulating the microtubule network and morphology of neurons(Lucas L. Baltussen et al., 2018; Muñoz et al., 2018). Indeed, previous studies have reported that shRNA-mediated knockdown of CDKL5 leads to an increased density of filipodia-like, or immature, spine protrusions, consistent with observed reductions in the frequency of miniature excitatory postsynaptic currents (mEPSCs) in cultured hippocampal neurons(Ricciardi et al., 2012). Loss of CDKL5 *in vivo* in mice results in reduced dendritic spine stability and density in somatosensory cortex and visual cortex, but increased spine density in the hippocampus. Conditional knockout of CDKL5 selectively from forebrain excitatory neurons also results in an increased spine density and frequency of mEPSCs within the hippocampal CA1(Della Sala et al., 2016; Lupori L, 2019; Okuda et al., 2018; Tang et al., 2017). Conflicting results on these cellular phenotypes are likely due to regional differences within the brain as well as *in vitro* versus *in vivo* variability on neuronal activity and spine dynamics. Furthermore, the cell-autonomous versus non cell-autonomous effects of CDKL5 loss on these reported phenotypes, particularly in light of developmental compensation that may occur with germline or cell type-specific *Cdkl5* deletion, remain unaddressed.

Clinical reports illustrating the early, postnatal onset of CDD symptomology support a critical role for CDKL5 in the developing nervous system(H. E. Olson et al., 2019; Y. C. Zhu & Z. Q. Xiong, 2019). However, from a treatment perspective, it will be important to determine whether CDKL5 is also required for the maintenance of neurological function after development. Would transient treatment of CDKL5-related functional pathways during early postnatal life be sufficient to permanently mitigate disease? With recent advances in precision medicine highlighting promising treatment options for CDD patients in the future, it is imperative to establish the temporal role of CDKL5 in neuronal development versus maintenance in order to inform treatment time windows.

To address these questions, we have employed a genetic strategy to ablate *Cdkl5* expression in adult mice and evaluate the functional significance of CDKL5 in the mature brain. We find that post-developmental deletion of *Cdkl5* results in behavioral and circuit deficits in adult

mice similar to germline knockout mice, suggesting that CDKL5 is indispensable in adulthood. We also demonstrate that adult loss of CDKL5 alters neuronal dendritic spine morphology, but not dendrite complexity, in a cell autonomous manner, highlighting a critical role for this kinase in synaptic maintenance. These findings are the first to delineate a post-developmental requirement for CDKL5, providing critical insight into the endogenous requirements of CDKL5 and informing future therapeutic efforts aimed towards the treatment of CDD.

Results

Post-developmental loss of CDKL5 results in behavioral deficits similar to germline knockout mice

Several groups have previously reported on the early-developmental expression of CDKL5 across different tissues, demonstrating it to be mostly highly enriched in forebrain neurons (Kilstrup-Nielsen et al., 2012; Y. C. Zhu & Z. Q. Xiong, 2019). We extended these studies by quantifying CDKL5 protein expression in the forebrain at different developmental timepoints, using knockout littermates to corroborate antibody specificity. We found that CDKL5 protein was detectable in forebrain tissues at postnatal day (P)0, followed by a gradual increase and peak in expression around P14 (Figure 1a). After this postnatal peak, CDKL5 remained stably expressed in the forebrain throughout adulthood, suggesting that its function may not be exclusively limited to developmental processes (Figure 1a). This prompted us to investigate the necessity of CDKL5 in the maintenance of proper neurological function after development.

We crossed our previously-reported *Cdkl5* floxed mouse line (*Cdkl5^{fllox}*) to transgenic mice expressing a Cre-ERT2 fusion gene under the control of the human ubiquitin C promoter (UBC-Cre-ERT2, hereafter referred to as CreER) (Tang et al., 2017). This line drives ubiquitous Cre-ER expression, and thereby allows for temporal control of gene deletion using tamoxifen (Ruzankina et al., 2007). We delivered tamoxifen via oral gavage (0.3mg·kg⁻¹ every other day for a total of 5 doses) to mice beginning at P42, the end of adolescence in C57BL/6 mice and well after the closure of developmental critical periods in the mouse brain (Hensch,

2004). This regimen resulted in successful ablation of CDKL5 protein expression to <5% of wild-type levels one week after tamoxifen delivery (Figure 2). We then waited approximately two months before beginning a battery of behavioral assessments, similar to those examined in germline knockout animals, to determine the functional impact of adult loss of CDKL5 (I. T. Wang et al., 2012). All experiments were performed on the following three groups: *Cdkl5^{fllox/y}; +/+* (Flx), *Cdkl5^{+/y}; CreER/+* (Cre), and *Cdkl5^{fllox/y}; CreER/+* (AKO) where all genotypes received tamoxifen in order to minimize potential variability introduced upon tamoxifen administration. Post-hoc CDKL5 protein quantification in all experimental mice confirmed a nearly complete loss of CDKL5 protein in the brains of AKO animals but not Flx or Cre littermate controls (Figure 1b).

We found that AKO mice exhibit motor and anxiety-related impairments similar to *Cdkl5* germline knockout animals. AKO mice spent significantly more time in the open arm of the elevated zero-maze suggestive of decreased anxiety-related behaviors (Figure 1c, Figure 3a), and displayed hyperactivity during an open field test (Figure 1d, Figure 3b). They also recapitulate several of the autistic-like features observed in germline knockout models of CDD, namely, reduced time sniffing and directly interacting with a novel stimulus mouse in the 3-chambered social choice test (Figure 1e-f, Figure 3f-g) as well as increased repetitive grooming and digging behaviors (Figure 1g) when compared to littermate Flx and Cre controls. Moreover, AKO mice displayed significantly impaired contextual- and cue-dependent memory in a Pavlovian fear conditioning paradigm when compared to Flx and Cre controls, though working memory measured by the Y-Maze assay appeared unaffected (Figure 1h, Figure 3c-e). Interestingly, AKO mice show enhanced motor coordination on the rotarod assay, with a significantly increased latency to fall from an accelerating, rotating rod, and show no hindlimb claspings when compared to Flx and Cre controls (Figure 1i, Figure 3h). This is contrary to *Cdkl5* germline knockout mice that exhibit significantly impaired motor coordination and a penetrant hindlimb claspings phenotype. Importantly, we did not find any significant differences across all examined behavioral domains between Flx and Cre controls, suggesting that the presence of the Cre allele alone does not induce any abnormal phenotypes. In summary, although two documented germline knockout

phenotypes were not recapitulated in AKO mice, our results highlight several major behavioral domains disrupted upon adult loss of CDKL5, supporting an indispensable role for CDKL5 in the post-developed brain.

Adult loss of CDKL5 disrupts hippocampal, low-frequency event-related neuronal oscillations similar to germline knockout mice

Auditory or visual event-related potentials (ERPs) have been increasingly leveraged as a biomarker for sensory information processing deficits in both patients and animal models of various neurodevelopmental disorders (Saby, Peters, Roberts, Nelson, & Marsh, 2020). We previously reported that germline loss of CDKL5 resulted in disrupted auditory-evoked ERPs recorded from the hippocampus, reflecting an impairment in neural circuit activity (I. T. Wang et al., 2012). We thus measured sensory-evoked ERPs in the hippocampus of AKO mice in response to an auditory cue. These assessments were performed on nonanesthetized, freely mobile mice and are not confounded by the motor and cognitive deficits observed in our CDD models. We found that AKO animals displayed an aberrant ERP waveform with a significantly decreased amplitude of the canonical N1 (negative) and P2 (positive) polarity peaks as well as a significantly increased latency in the P2 polarity peak, similar to *Cdkl5* germline knockout animals (Figure 4a). The amplitude and latency of these ERP polarity peaks are thought to reflect the strength and timing of cognitive processes, thereby suggesting that adult loss of CDKL5 also impairs sensory information processing in conjunction with compromised behavioral functions.

Time-frequency analysis of these ERPs in the hippocampus also demonstrated reduced oscillatory strength specifically in the low-frequency delta (δ , 2-4Hz), theta (θ , 4-8Hz), and alpha (α , 8-12Hz) oscillations, but no differences in the high-frequency beta (β , 12-30Hz), low gamma (γ_{low} , 30-50Hz), and high gamma (γ_{high} , 70-140Hz) oscillations in AKO mice relative to Flx littermate controls (Figure 4b-c). Similarly, event-related phase locking (measured by the phase-locking factor, PLF), which reflects the reliability and sensitivity of the circuit communication, was also significantly decreased in AKO mice compared to Flx littermate controls but selectively in the

low-frequency δ and θ (Figure 4b-c). Notably, EEG studies in ASD children have reported selective deficits in low-frequency δ , θ , and α oscillations, suggesting similar neural network defects in CDD and related syndromic ASDs (Saby et al., 2020). Together, these results indicate that adult loss of CDKL5 leads to similar hippocampal network alterations as reported in germline knockout animals, and that CDKL5 is required for the maintenance of proper signaling within this circuit throughout life.

Germline, but not adult, loss of CDKL5 disrupts dendritic complexity of hippocampal CA1 pyramidal neurons

We next sought to investigate any cellular deficits that may be underlying the circuit and behavioral abnormalities that emerge upon loss of CDKL5. In culture models, shRNA knockdown of CDKL5 impairs neurite outgrowth in rat primary hippocampal neurons, and several *Cdkl5* knockout mice have been reported to display reduced dendritic complexity in the hippocampus (Amendola et al., 2014; Chen et al., 2010; Okuda et al., 2018; Tang et al., 2017). However, the direct impact of CDKL5 loss on pyramidal neuron morphology remains undetermined. Ablating CDKL5 selectively in adulthood provided us with a unique opportunity to examine the consequences of CDKL5 loss independent of developmental confounds or any homeostatic compensatory mechanisms that may be occurring. Our present EEG recordings, as well as previous studies in various mouse models of CDD, have repeatedly revealed hippocampal circuit abnormalities coupled to deficits in hippocampal-dependent learning and memory (Okuda et al., 2017; Tang et al., 2019; Tang et al., 2017; I. T. Wang et al., 2012). These data, along with the fact that CDKL5 is highly enriched in excitatory cells of this circuit, directed our initial studies to pyramidal neurons of the hippocampal CA1 (Zeisel et al., 2015).

We initially examined the effects of germline loss of CDKL5 on dendritic complexity of hippocampal pyramidal neurons by crossing *Cdkl5* constitutive knock-in mice (*Cdkl5*^{R59X}, which results in early truncation and loss of protein) to *Thy1-GFPm* transgenic mice. This reporter allele allows for *in vivo* visualization of pyramidal neurons in their entirety, and subsequent analysis of

dendritic arborization and complexity (Feng et al., 2000). In comparison to wild-type littermate controls (*Cdkl5*^{+/y}; Thy1-GFPm/+), WT, germline knockout mice (*Cdkl5*^{R59X/y}; Thy1-GFPm/+), KO, displayed a significant decrease in the complexity of both the basal and proximal apical dendrites of their CA1 pyramidal neurons as shown by Sholl analysis (Figure 5a & 5c). These data are in line with previous studies describing the effects of CDKL5 knockdown and knockout *in vitro* and *in vivo*. Furthermore, both basal and proximal apical dendrite length were significantly reduced in germline knockout mice in comparison to wild-type littermates (Figure 5b & 5d).

We next wanted to evaluate whether similar morphological deficits might be recapitulated upon adult loss of CDKL5. We crossed our AKO mice (*Cdkl5*^{fllox/y}; CreER/+) and Flx littermate controls (*Cdkl5*^{fllox/y}; +/+) to mice carrying the Thy1-GFPm reporter allele and delivered tamoxifen to all animals at the previously described dosage and regiment beginning at P42. We then evaluated cellular morphology at the same age we had previously assessed behavioral impairments in AKO mice (P120). Interestingly, dendritic complexity at either the proximal apical or basal dendritic tree, measured via Sholl analysis, was not altered between *Cdkl5*^{fllox/y}; CreER/+; Thy1-GFPm/+ (AKO) mice and *Cdkl5*^{fllox/y}; +/+; Thy1-GFPm/+ (Flx) littermates at this age (Figure 5e & 5g). In fact, there were very subtle but significant increases in basal dendrite complexity at the 120-150µm distances from the soma. These minor morphological shifts were in stark contrast to the reduction in dendrite complexity seen in germline knockout animals. We also saw no significant differences in average basal or apical dendrite length (Figure 5f & 5h). These findings argue that germline, but not adult, loss of CDKL5 is capable of modulating pyramidal neuron dendrite complexity and length in the hippocampal CA1, and suggest a specific developmental window for the emergence of this phenotype.

CDKL5 is required for the maintenance of dendritic spine morphology on hippocampal CA1 pyramidal neurons

Previous studies have also reported that loss of CDKL5 leads to aberrant dendritic spine stability/morphology and perturbed miniature excitatory post-synaptic currents (mEPSCs),

suggesting an important role for CDKL5 in neuronal synapse maturation(Della Sala et al., 2016; Lupori L, 2019; Okuda et al., 2018; Ricciardi et al., 2012; Tang et al., 2017; Zhu et al., 2013). The extent to which CDKL5 regulates the formation and/or maintenance of these highly dynamic compartments, however, remains inconclusive.

We examined the effects of germline and adult loss of CDKL5 on dendritic spines of pyramidal neurons in the hippocampal CA1 by utilizing the same Thy1-GFPm reporter line described above, allowing us to evaluate dendritic spine density and morphology *in vivo*. We found that dendritic spine density was not significantly altered on either basal or proximal apical dendritic trees of CA1 pyramidal neurons between germline knockout (*Cdkl5*^{R59X/y}; Thy1-GFPm/+) and wild-type littermate (*Cdkl5*^{+/y}; Thy1-GFPm/+) animals, or between AKO (*Cdkl5*^{flx/y}; CreER/+; Thy1-GFPm/+) mice and Flx littermate controls (*Cdkl5*^{flx/y}; +/+; Thy1-GFPm/+). These results argue that loss of CDKL5 during either germline or adulthood does not significantly alter dendritic spine density in the hippocampal CA1 (Figure 6).

Aside from spine density and turnover, previous work in cultured neurons and *Cdkl5* knockout animals has also proposed an altered spine morphology in CDD models(Della Sala et al., 2016; Lupori L, 2019; Okuda et al., 2018; Ricciardi et al., 2012; Tang et al., 2017). We thus evaluated various components of dendritic spine morphology in an *in vivo* setting using reconstruction and analysis of the three-dimensional confocal image stacks taken for spine density quantifications. We found that, on average, spine length was significantly increased on both basal and apical dendrites of pyramidal CA1 neurons of AKO mice compared to Flx controls (Figure 7a,d). This phenotype, coupled to a trending decrease in spine head diameter, is reflective of a filipodia-like state typically associated with immature spines(Harris KM, 1989). Given that the total density of dendritic spines remained unchanged, these findings suggest a significantly increased representation of morphologically immature spines on both apical and basal trees of CA1 pyramidal neurons in AKO mice, resembling similar findings seen upon loss of CDKL5 in cultured hippocampal neurons(Ricciardi et al., 2012).

Our adult knockout allows for an evaluation of neuronal morphological deficits resulting from CDKL5 loss *in vivo* independent of developmental confounds, yet, it remained uncertain whether this spine phenotype was indeed a cell autonomous effect of CDKL5 loss or a compensatory phenotype due to ablation of CDKL5 in every cell. Sparse, conditional deletion isolates the single-neuron consequences of CDKL5 loss while also bypassing pre- versus post-synaptic effects of mutant cells on spine dynamics. We therefore performed a conditional, sparse deletion of CDKL5 in adult mice by crossing *Cdkl5* floxed mice to SLICK transgenic mice. The Single-neuron Labeling with Inducible Cre-mediate Knockout technique (or SLICK) utilizes two copies of the Thy1 promoter to simultaneously drive sparse expression CreER and yellow fluorescent protein (YFP), thereby allowing for conditional knockout and simultaneous labeling of individual neurons to assess cell autonomous-driven morphology (Young et al., 2008). *Cdkl5*^{fllox/y}; SLICK/+ mice and wild-type controls (*Cdkl5*^{+/y}; SLICK/+) received tamoxifen beginning at P42, and their spine morphology was subsequently analyzed at P70. We found that sparse, conditional deletion of CDKL5 in adulthood amplified the increased spine length of both apical and basal dendritic spines on CA1 pyramidal neurons seen in AKO animals (Figure 8b & 8f). Remarkably, we also observed a significantly decreased spine head diameter and decreased spine volume, on average, of basal and apical CA1 dendritic spines on knockout neurons in comparison to wild-type control neurons (Figure 8c-d, 8g-h). Again, there was no change in spine density on both apical and basal dendritic arbors between *Cdkl5* sparse knockout and wild-type control neurons (Figure 8a & 8e).

Taken together, these results demonstrate an increased proportion of filipodia-like, or morphologically immature, dendritic spines on CA1 pyramidal neurons of the hippocampus with loss of *Cdkl5*, and highlight a key role for CDKL5 in the maintenance of dendritic spine morphology in a cell autonomous manner.

CDKL5 continuously regulates phosphorylation of the microtubule end-binding 2 protein

Previous work in *Cdkl5* knockout mice has reported disruptions of AKT–mTOR signaling with reduced phosphorylation of AKT Ser473 and mTOR Ser2448, specifically, but no concomitant alteration in total AKT or mTOR protein levels (I. T. Wang et al., 2012). Phosphorylation of these residues normally promotes AKT activation and mTOR complex 1 (mTORC1) assembly, respectively, likely reflecting decreased AKT and mTORC1 activity upon *Cdkl5* loss-of-function (Bhaskar & Hay, 2007; Rosner, Siegel, Valli, Fuchs, & Hengstschläger, 2010). To profile whether similar molecular signaling disruptions were also occurring upon post-developmental deletion of CDKL5, we harvested forebrain cortical tissues from AKO mice and FLX littermate controls and evaluated the phosphorylation of key AKT pathway members, including AKT, mTOR, S6, GSK-3 β , and β -catenin. In contrast to what is reported in germline *Cdkl5* knockout mice, adult loss of CDKL5 did not lead to any significant changes in the phosphorylation of pAKT Ser473, pmTOR Ser2448, pS6 Ser240/244, pGSK-3 β Ser9, and β -catenin compared to their respective total protein levels (Figure 9). These results raise the possibility that loss of CDKL5 may indirectly disrupt these cell growth/proliferation transduction cascades during a critical time window in development, or that they are simply a compensatory by-product of germline loss of CDKL5. Regardless, our findings highlight the potential for CDKL5 loss-of-function behavioral, circuit, and cellular phenotypes to emerge without a concomitant disruption of AKT/mTOR signaling.

Notably, recent studies have suggested a role for CDKL5 in microtubule dynamics through its direct phosphorylation of microtubule-associated proteins such as end-binding 2 (EB2) protein (Lucas L. Baltussen et al., 2018; Muñoz et al., 2018). Interestingly, we found that phosphorylation of endogenous EB2 Ser222 (pS222) was significantly reduced in forebrain tissues of AKO mice to a similar magnitude as observed in germline knockout mice (Figure 10). This suggests that this microtubule-associated substrate remains modulated by CDKL5 in adulthood, and highlights that similar microtubule network disruptions may occur upon post-

developmental loss of CDKL5. Given the expression pattern of CDKL5 is developmentally regulated (Figure 1a), it will be informative to determine whether EB2 phosphorylation is also dynamically regulated with CDKL5 throughout critical periods of brain development.

To investigate this, we harvested forebrain cortical tissues from wild-type mice at various developmental and adult ages: postnatal day (P)0, P7, P14, P21, P30, and P60 and subsequently examined the protein levels of CDKL5, phospho-EB2 (Ser22), and total EB2. CDKL5 protein expression was developmentally regulated as previously shown (Figure 1a), with a postnatal peak in expression ~P14 (Figure 11a-b). Interestingly, we found pEB2 Ser222 levels to also be developmentally regulated and correlating with CDKL5, with phosphorylation levels peaking ~P14 and subsequently declining into adult ages (>P21) (Figure 11a, c). Total levels of EB2 protein remained unchanged throughout the time points examined, and CDKL5 and pEB Ser222 levels were significantly ablated in *Cdkl5* knockout brain tissues (Figure 11a). These findings suggest that phosphorylation of EB2 at Ser222 correlates with the expression levels of CDKL5.

We next profiled CDKL5, phospho-EB2 (Ser22), and total EB2 protein levels across the same ages in *Cdkl5* knockout forebrain cortical tissues (P0-P60). As expected, CDKL5 protein levels were undetectable at every age in *Cdkl5* knockout cortices, however, phosphorylation of EB2 Ser22 was still detectable at each age (Figure 11a, d). We examined the relative developmental progression of EB2 phosphorylation in *Cdkl5* knockout brain tissues across various ages. Intriguingly, pEB2 Ser222 levels still reflected a developmental regulation: peaking early postnatally and subsequently declining into adulthood (Figure 11a, d). However, the peak pEB2 level occurred at P7, rather than at P14 as observed in *Cdkl5* wild-type animals (Figure 11a, e). A comparison of EB2 phosphorylation across all ages between *Cdkl5* wild-type and *Cdkl5* knockout brains reflects an overall reduction in pEB2 as previously shown (Figure 10), but also demonstrates this shift in the peak levels of pEB2 Ser222 to an earlier age (Figure 11e). These results highlight that CDKL5 dynamically regulates phosphorylation of EB2 throughout development and adulthood, and perhaps plays a role in continuously regulating microtubule dynamics via its regulation of microtubule-associated proteins such as EB2. The synaptic

morphological deficits reported in our AKO, coupled with an impaired regulation of EB2, represent a potential cellular basis for the behavioral and circuit phenotypes exhibited by AKO animals.

Discussion

Several mouse models of CDD have been characterized to date, and although they recapitulate many of the hallmark phenotypes of the human disorder, it remains unclear whether these deficits are solely a consequence of detrimental changes occurring in the developing nervous system or also due to loss of CDKL5 function in mature neurons (Amendola et al., 2014; Okuda et al., 2018; I. T. Wang et al., 2012; Yennawar et al., 2019). Furthermore, from a therapeutic perspective, it will be imperative to delineate the temporal requirement of CDKL5 action needed to establish as well as maintain proper neurological function. Prior to this study, it was uncertain if providing CDKL5 function, or abrogating kinase pathway dysfunction, exclusively during critical periods of development would be sufficient to significantly mitigate disease pathology for life or whether chronic treatment would be required in CDD. Along this line, our adult knockout experiments comprise a seminal foundation for future studies aiming to dissect the temporal requirement of CDKL5 in various circuits and behavioral domains, informing future therapeutic endeavors aimed at treating CDD.

Adult neural function requires CDKL5

Our results demonstrate that multiple features of disease-associated behavioral and circuit phenotypes in mouse models of CDD can be recapitulated following adult deletion of *Cdkl5*. Since *Cdkl5* germline knockout mice have been reported to present with a constellation of behavioral deficits, we began by testing various behavioral domains in our adult knockout animals. We found that adult loss of CDKL5 resulted in similar deficits in anxiety-related behaviors, locomotion, sociability, repetitive behaviors, and context- and cue-dependent fear conditioning as previously reported in germline knockout mice (I. T. Wang et al., 2012). Adult knockout of *Cdkl5* also resulted in perturbation of auditory-evoked ERPs recorded from the

hippocampus, reflective of gross circuit abnormalities that can arise even upon post-developmental CDKL5 loss. Specifically, auditory-evoked ERP recordings in the hippocampus of these AKO mice displayed significant decreases in amplitude and increases in latency of the canonically-elicited polarity peaks, suggesting perturbed sensory processing in these animals (a hallmark feature of several ASDs in both humans and mouse models)(Gandal et al., 2010; Jeste & Nelson, 2009; Riva et al., 2018; Roberts et al., 2010). Furthermore, our expression data reflect a peak in CDKL5 protein levels during the critical period of synaptogenesis for several brain regions followed by stable expression throughout adulthood, further highlighting that the kinase's functional roles are likely not sequestered to developmental processes. Collectively, these results demonstrate that adult neural function still requires CDKL5, and suggest that early postnatal expression of the kinase, or transient, early-developmental treatments, would offer little protection against the disease. Rather, our findings argue that either chronic treatment of CDD or gene-replacement therapy will comprise viable avenues(Gao et al., 2020). These data also contend that many of the phenotypes associated with CDD may be unrelated to any stage-restricted functions of CDKL5, at least in mice. Notably, similar results have been highlighted with loss of MECP2 in Rett syndrome as well as postnatal deletion of various synaptic proteins, and may reflect a unifying theme for synaptopathies and related ASDs(Chabbert et al., 2019; Djuricic, Brott, Saw, Shamloo, & Shatz, 2018; Huang et al., 2019; McGraw, Samaco, & Zoghbi, 2011; Spratt et al., 2019; X. Wang et al., 2016).

Interestingly, working memory (measured via spontaneous alternations in a Y-Maze assay) was not significantly affected by adult loss of CDKL5. This effect could be governed by specific circuits that, after proper establishment, are resilient to later loss of CDKL5 or carry the ability to more readily compensate to kinase loss at these later ages. The dorsolateral prefrontal cortex plays a known role in working memory functions thought to be executed by the basal ganglia. The fact that working memory was not affected in AKO mice in spite of concomitant motor and anxiety-related deficits suggests that the working memory impairment reported in germline *Cdkl5* knockout animals is not simply a byproduct of other phenotypic confounds.

Rather, loss of CDKL5 may directly modulate this circuitry during a critical time window in development. In contrast, context- and cue-dependent memory retrieval were both sensitive to adult loss of CDKL5, further emphasizing these hippocampal-mediated memory domains as distinct in their circuit-origins from working memory. Furthermore, the sensitivity of hippocampal-mediated behaviors and hippocampal circuit function to loss of CDKL5 at both ages reflects a likely critical maintenance role for the kinase in this brain region throughout life. In the future, it will be interesting to dissect the temporal role of CDKL5 in the various circuits that underlie these behavioral domains, and to perhaps delineate a critical time window of CDKL5 action in regulating these behaviors.

Surprisingly, adult knockout of *Cdkl5* resulted in a significantly enhanced motor coordination phenotype in contrast to the deficit in motor coordination typically reported in germline knockout animals and severe hypotonia reported in CDD patients (S. Demarest et al., 2019). It is unlikely that the concomitant hyperactivity or repetitive behavior phenotypes present in AKO animals influence this enhanced motor coordination given germline knockout mice mirror similar deficits yet still carry impaired motor coordination. Although motor coordination and learning are strongly associated with proper cerebellar functioning, CDKL5 is minimally expressed in this brain region suggesting additional circuitry may drive this phenotype (Lein et al., 2007; I. T. Wang et al., 2012). Furthermore, a recent, pilot gene therapy study in *Cdkl5* knockout mice utilizing AAV-CDKL5 vectors revealed only partial rescue of motor coordination deficits on the rotarod assay. This is likely due to the fact that vector expression was mostly limited to the hindbrain regions of treated mice (including cerebellum) but not forebrain or midbrain regions where CDKL5 is most highly expressed (Gao et al., 2020). This incomplete rescue further highlights the importance of additional, extra-cerebellar circuitry to the motor phenotypes regulated by CDKL5. Notably, the basal ganglia (where CDKL5 is highly expressed) also play a known role in motor control and learning, and have been highlighted as common node for ASD pathophysiology (Fuccillo, 2016). We previously reported that loss of CDKL5 exclusively from forebrain GABAergic neurons (including the striatum) selectively recapitulates the autistic-like

features present in *Cdkl5* constitutive knockout models, including aberrant repetitive behaviors. However, this conditional deletion of CDKL5 from forebrain inhibitory neurons did not elicit any changes in locomotor activity, anxiety-related behaviors, or motor coordination (Tang et al., 2019). This may suggest that aberrant striatal circuitry does not autonomously drive the motor coordination phenotypes seen across CDD mouse models, including our AKO mice, yet it is important to highlight that the *Dlx5/6* Cre driver used in this study does not encompass the entirety of basal ganglia circuitry. Namely, the midbrain and subthalamic nuclei of the diencephalon are not targeted in this conditional knockout (Monory et al., 2006). Thus, loss of CDKL5 may still be affecting proper motor output of this circuitry via 1) a critical function in basal ganglia subregions not affected upon *Dlx5/6* conditional knockout or 2) the synergistic action of CDKL5 across the basal ganglia and additional forebrain circuits not modeled by conditional deletion. Alternatively, CDKL5 may regulate motor coordination and learning through a different circuit or mechanism including contributions from the spinal cord (where CDKL5 expression is detectable). How loss of CDKL5 in adulthood leads to improved motor coordination and learning remains uncertain, but represents an interesting future avenue to investigate temporally-distinct influences of CDKL5 loss of the same behavioral output.

Loss of CDKL5 influences dendritic arborization of CA1 pyramidal neurons during a critical time window in development

Impaired dendritic arborization and complexity, particularly within the hippocampus, has been reported across multiple *Cdkl5* knockout models (Amendola et al., 2014; Okuda et al., 2018; Tang et al., 2017). These morphological deficits were initially postulated to contribute to the impaired hippocampal-dependent memory phenotypes robustly seen in various CDD mouse models. Thus, we were surprised when we saw no significant alterations in dendrite length or complexity with post-developmental deletion of *Cdkl5*, yet observed similar behavioral phenotypes such as impaired context-dependent memory retrieval. These findings suggest that impaired dendrite arborization or outgrowth of hippocampal CA1 neurons is not necessary for the

impaired learning and memory phenotypes seen with CDKL5 loss. In fact, the majority of behavioral impairments reported for germline *Cdkl5* knockout animals were recapitulated upon post-developmental deletion of CDKL5, highlighting alternative cellular mechanisms as likely driving loss-of-function behavioral impairments.

Our findings argue that CDKL5 either modulates dendritic complexity during a specific time window during development, or that this phenotype is a compensatory mechanism in response to loss of CDKL5. For example, the reduction in dendritic complexity reported in germline *Cdkl5* knockout models could be a secondary, homeostatic response to altered spine morphology and synaptic activity. Activity-dependent dendritic retraction is known to occur both *in vivo* and *in vitro*, and elevated GSK-3 activity, which is associated with activity-dependent shrinkage of dendrites, has been reported in mouse models of CDKL5 deficiency (Fuchs et al., 2014; Krey et al., 2013; Rui et al., 2013; Wong & Ghosh, 2002). Alternatively, CDKL5 may simply regulate dendrite and synapse formation through distinct mechanisms at distinct periods of development. This idea is consistent with recent findings in which neuronal activity in immature neurons leads to the induction of CDKL5 protein levels, whereas neuronal activity in mature neurons leads to the degradation of CDKL5 (P. La Montanara et al., 2015). CDKL5 may therefore have distinct functions during stages of development that uniquely affects the processes of dendrite growth, spine generation, and activity-dependent pruning. One such example of a family of kinases that serve two contrasting cellular functions is the doublecortin-like kinases (DLCKs), which promote dendrite growth but suppress synapse maturation (Shin et al., 2013).

Concomitant with a significant reduction of dendritic arborization and length of pyramidal neurons, germline *Cdkl5* knockout mouse models also have reported AKT/mTOR/GSK-3 β signaling disruptions (Amendola et al., 2014; I. T. Wang et al., 2012). These findings aligned with the known importance of mTOR as a regulator of cell growth, proliferation, and neuronal plasticity, and motivated a subsequent study to administer IGF-1 to juvenile *Cdkl5* knockout mice as a treatment for dendritic spine instability (Della Sala et al., 2016). However, the efficacy of this

therapy in CDD patients remains uncertain, especially since these signaling changes may be an indirect effect of *Cdkl5* loss (Costales & Kolevzon, 2016).

Surprisingly, adult loss of CDKL5 did not lead to significant disruption of AKT-mTOR signaling in spite of recapitulated germline knockout behavioral, circuit, and synaptic deficits. These data suggest that disrupted AKT-mTOR signaling is not required for the emergence of several CDD-related phenotypes, but may be a compensatory, or developmentally-specific outcome of CDKL5 loss. The two, germline knockout-specific phenotypes highlighted in this chapter (dendritic arborization and AKT/mTOR signaling) may be regulated by a developmental-specific function of CDKL5 on neuronal outgrowth and arborization, and align with the known importance of AKT/mTOR signaling in cell growth and proliferation.

CDKL5 is required for the maintenance of hippocampal dendritic spine morphology

The direct impact of CDKL5 loss on pyramidal neuron morphology has been contentious, likely due to context-dependent variability. In our initial findings, we observed no significant differences in dendritic spine density upon CDKL5 loss on either the basal or apical dendritic arbors of hippocampal CA1 pyramidal neurons. This is in contrast to previous studies that have reported either increased dendritic spine density with CDKL5 shRNA-mediated knockdown *in vitro*, or decreased dendritic spine density in somatosensory and visual cortex of *Cdkl5* knockout mice (Della Sala et al., 2016; Ricciardi et al., 2012). These discrepancies are likely due to *in vitro* versus *in vivo* circuit differences that can alter spine signaling and dynamics, as well as potential regional differences of CDKL5 action across different circuits. We sought to overcome these confounds by harnessing an adult deletion of CDKL5 to observe more direct effects of kinase loss. However, adult knockout of CDKL5 did not result in significant changes in dendritic spine density on pyramidal cells within the hippocampal CA1. Taken together, we suggest that there are likely not significant effects on dendritic spine density within the hippocampal CA1 with loss of CDKL5.

Interestingly, however, we did notice significant morphological changes for the dendritic spines we imaged upon adult deletion of *Cdkl5*. Overall, dendritic spines on both the apical and basal dendritic trees of hippocampal CA1 pyramidal neurons were significantly longer upon adult knockout of *Cdkl5*. We found that sparse, conditional deletion of CDKL5 in adulthood recapitulated this increased spine length phenotype we saw in our constitutive AKO, and also resulted in a significantly decreased head diameter and decreased total volume of analyzed spines. Taken together, these filipodia-like structures are suggestive of a more morphologically immature spine state that, when combined with no change in overall spine density, reflect a greater proportion of morphologically immature spines on hippocampal CA1 pyramidal neurons (Arellano, 2007). Collectively, these results suggest that CDKL5 is required for the maintenance of dendritic spine maturation or morphology within the hippocampal CA1, and align with the deficits in hippocampal-dependent behavioral domains and hippocampal circuit communication presented in our AKO model. Future work will aim to dissect the causal role of these spine phenotypes in relation to the hippocampal behavioral and circuit abnormalities resulting from CDKL5 loss. It will also be relevant to examine whether CDKL5 plays a similar spine maintenance role across various brain regions, particularly those implicated in the behavioral domains disrupted in our AKO mice.

Our sparse, conditional deletion addresses the cell-autonomous effects of CDKL5 loss on pyramidal neuron spines, however, it is still possible that these results are a compensatory or secondary effect of CDKL5 loss within excitatory neurons of the hippocampus. We show that CDKL5 is capable of regulating EB2 phosphorylation, a member of the end-binding protein family, even during adulthood. End-binding proteins are plus-end-tracking proteins that accumulate at the growing microtubule end, and play pivotal roles in microtubule dynamics that mediate cellular architecture, cargo trafficking, and spine stability. Thus, it is appealing to hypothesize that CDKL5 may play a role in continuously regulating microtubule dynamics, particularly those related to receptor trafficking at the post-synaptic density, via its continuous regulation of microtubule-associated proteins such as EB2 (Baltussen, Rosianu, & Ulanir, 2018; Barbiero, De Rosa, &

Kilstrup-Nielsen, 2019; Jaworski et al., 2009; Merriam et al., 2013). However, the extent to which CDKL5 regulation of EB2 activity, specifically, can affect cellular morphology and synaptic maturation remains uncertain. This target's well-characterized family member, EB3, has previously been implicated in regulating dendritic spine morphology within hippocampal neurons, but whether EB2 itself is essential for similar functions remains undetermined (Leterrier et al., 2011; Pchitskaya et al., 2017; Straube & Merdes, 2007). In our future work, we are focused on delineating the specific role of CDKL5 in regulating synaptic turnover and maturation through the microtubule network.

Materials and Methods

Regulatory approval. Experiments were conducted in accordance with the ethical guidelines of the National Institutes of Health and with the approval of the Institutional Animal Care and Use Committee of the University of Pennsylvania. Mice were group-housed in cages of two to five in a twelve-hour light/dark cycle with food and water provided *ad libitum*.

Mouse strains and genotyping. The *Cdkl5* conditional (*Cdkl5^{fllox}*) and R59X knock-in (*Cdkl5^{R59X}*) lines were generated as previously described, and are available from the Jackson Laboratories (*Cdkl5^{fllox}*: Stock No. 030523; R59X: Stock No. 028856) (Tang et al., 2019; Tang et al., 2017). UBC-CreER (Stock No. 007001), Thy1-GFP line M (Thy1-GFPm; Stock No. 007788), and SLICK (Stock No. 007610) mice were all obtained from the Jackson Laboratories. All lines have been maintained in the C57BL/6J background.

Experimental cohorts were all weaned at 3 weeks of age and littermates housed together. *Cdkl5^{fllox}*, *Cdkl5^{R59X}*, and Thy1-GFPm mice were genotyped using previously-reported PCR-based strategy or with qPCR by Transnetyx, Inc. For genotyping of UBC-CreER and SLICK transgenics, primers and genotyping strategy were identical to that used by Jackson Laboratories.

Tamoxifen preparation and administration. Tamoxifen (Sigma, T5648) was dissolved in corn oil (Sigma, C8267) at a concentration of $20\text{mg}\cdot\text{ml}^{-1}$ by vortexing and slowly heating the solution at 40°C for approximately one hour. Freshly prepared tamoxifen was protected from light by aluminum foil and stored at 4°C for a maximum of one week. Animal feeding needles from Roboz Surgical Store (20 gauge, 1.5" length, curved; FN-7910) were used for oral gavage delivery of $0.3\text{mg}\cdot\text{kg}^{-1}$ of tamoxifen every other day for a total of five doses. All genotypes received tamoxifen within each experimental cohort.

Behavioral assessments. All animal behavioral studies were carried out blinded to genotype. Mice were allowed to habituate to the testing room for at least 1 hr before the test, and testing was performed at the same time of day. All animal behaviors were performed on adult male mice between postnatal days 120-160, and the analysis of behavioral data was carried out by a researcher blinded to genotype.

Elevated zero-maze. The elevated zero-maze (San Diego Instruments; California, USA) consists of a circular-shaped platform elevated 3 feet above the floor. Two opposite quadrants of the maze are enclosed (wall height, 12 inches), whereas the other two are open (wall height, 0.5 inches). Mice were placed in one of the closed quadrants and their movement traced over the course of 5 min. Analysis, including the quantification of percent of time spent in open arms and the number of entries, was performed manually using a stopwatch. An entry was defined as a transition from a closed to open arm, or vice versa, that involves all four paws. Total distance traveled over the entire assay was measured by a ceiling-mounted camera coupled to a video-tracking software (SmartScan 3.0), allowing for real-time analysis of all movements.

Open-field test. Locomotor activity was measured via an open-field test where mice were individually placed into, and allowed to explore, a 15" x 15" arena for a total of 60 min. A ceiling-mounted camera allowed for a video-tracking software (SmartScan 3.0) to real-time analyze the total distance traveled as well as the percent time spent in the center of the arena (defined as the central 25% of the total area).

Y-maze. Spontaneous alternation behavior was measured on a Y-maze apparatus (San Diego Instruments; California, USA), composed of three arms (Arm A: 8in. x 5in. x 3in.; Arms B and C: 6in. x 5in. x 3in.). For testing, the mouse was placed in Arm C, facing the center, and allowed to freely explore the maze for 5 min. A spontaneous alternation was defined an entry into the arm less recently explored. Percent spontaneous alternation was calculated as the number of spontaneous alternations over the total number of entries. For example, the sequence C,B,A,B,C,B,A,C (starting in arm C) resulted in a percent spontaneous alternation of $4/6 = 67\%$.

Three-chambered social approach assay. The social choice test was carried out in a three-chambered apparatus that consisted of a center chamber and two end chambers. Before the start of the test and in a counter-balanced sequence, one end chamber was designated the social chamber, into which a stimulus mouse would be introduced, and the other end chamber was designed the nonsocial chamber. Two identical, clear Plexiglas cylinders with multiple holes to allow for air exchange were placed in each end chamber. In the habituation phase of the test (Phase I), the test mouse was placed in the center chamber and allowed to explore all three chambers for 10 min. During this acclimation period, baseline measurements of how much time the mouse spent in each of the three chambers and the distance traveled by the test mouse were collected. In the social choice phase of the test (Phase II), an age-matched stimulus mouse (adult, gonadectomized A/J mice) was placed in the cylinder in the social chamber while a novel object was simultaneously placed into the other cylinder in the nonsocial chamber. During the subsequent 10 min social choice period, chamber times and numbers of transitions among chambers were again recorded as well as the percent time spent sniffing the social cylinder. In the direct social interaction test, the cylinders were removed simultaneously following the social choice test, and the amount of time test and stimulus mice spent in direct contact (sniffing, allogrooming) was measured for a total of 5 min. If fighting persisted for more than several seconds, the mice were removed from the apparatus and excluded from the study.

Accelerating rotarod assay. Mice were placed on an accelerating rotarod apparatus (Harvard Apparatus) for 16 trials (four trials a day for four consecutive days) with at least 15 min of rest

between the trials. Each trial lasted for a maximum of 5 min, during which the rod accelerated linearly from 4 to 40 rpm. The amount of time for each mouse to fall from the rod was recorded for each trial.

Context- and cue-dependent fear conditioning. For the training day, mice were placed in individual chambers (Med Associates) for 2 min followed by a loud tone (85 dB, 2 kHz) lasting 30 s that coterminated with a 2-s, 1.25-mA foot shock. Mice were left undisturbed for an additional 30 s in the chamber and then immediately placed back into their home cage. Freezing behavior, defined as no movement except for respiration, was determined before and after the tone-shock pairings and scored by FreezeScan NI version 2.00. To test for context-dependent learning, we placed mice back into the same testing boxes 24 hr later for a total of 5 min without any tone or shock, and again measured the total time spent freezing. After 4 hrs, we tested for cue-dependent fear memory by placing the mice into a novel chamber consisting of altered flooring, wall-panel inserts, and vanilla scent. After 2 min in the chamber, the cue tone (85 dB, 2 kHz) was played for a total of 3 min, and the total time spent freezing during the presentation of this cue tone was recorded.

Olfaction. Mice were tested for whether they could detect and differentiate odors in a habituation-dishabituation protocol modified from Yang and Crawley (Yang & Crawley, 2009). Mice were presented with cotton-tipped wooden applicators dipped in either water, vanilla, or swiped across the bottom of an unfamiliar social cage. Each stimulus was presented for 2 min with a 1-min inter-trial interval. Time spent sniffing was defined as when the animal was oriented with its nose 2 cm or closer toward the cotton tip.

Repetitive behavior. Mice were individually placed into a clean, home-cage like environment lined with bedding. After allowing 5 min for habituation, 10 min of activity was videotaped for each mouse. The duration of repetitive behavior, defined as grooming or digging, was scored manually using a stopwatch.

Hindlimb clasping. Mice were suspended by the base of their tail at least 6 inches above a flat surface for up to 1 min. If the hindlimbs were consistently splayed outward, away from the

abdomen, the mouse was assigned a score of 0. If one hindlimb was retracted towards the abdomen for more than 50% of the time, the score was 1. If both hindlimbs were partially retracted for greater than 50% of the time, the score was 2. Finally, if both hindlimbs were entirely retracted and touching the abdomen for more than 50% of the time suspended, the mouse received a score of 3.

Event-related potentials. ERP surgeries, recordings, and analyses were performed as previously described (Goffin et al., 2012; I. T. Wang et al., 2012).

Surgery. Mice underwent stereotaxic implantation of tripolar electrode assemblies (PlasticsOne) for nonanesthetized recording of auditory ERPs. Mice were anesthetized with isoflurane (4% for induction (vol/vol), 1.5-2% for surgery with 1 L·min⁻¹ O₂). Three stainless steel electrodes, mounted in a single pedestal were aligned to the sagittal axis of the skull. A stainless steel recording electrode was placed 2.0 mm posterior, 2.0 mm left lateral relative to bregma, and at -1.8 mm depth. Ground and reference electrodes were placed posterior of the hippocampal electrode at 1.0 mm and 2.0 mm distances, respectively. The electrode pedestal was secured to the skull with ethyl cyanoacrylate and dental cement. Postoperative analgesia was supplied using the opioid analgesic, buprenorphine (buprenex, subcutaneous, 0.1 µg · gram⁻¹ of body weight). Mice were allowed to recover for 7 days before EEG recordings.

Recordings. EEG recordings were performed on freely mobile, nonanesthetized mice in their home cage environment after a 20 min acclimation to the recording room. Recordings were performed using Spike2 software connected to a Power 1401 II interface module (CED) and high impedance differential AC amplifier (A-M Systems). Signals were acquired at 1,667 Hz and band-pass filtered between 1 and 500 Hz with a 60-Hz notch filter and gain of 1,000.

Event-related potentials (ERPs) were recorded by presentation of auditory stimuli consisting of a series of 250 white-noise clicks of 10 ms duration, 85 dB sound pressure, and 4 s interstimulus intervals. Stimuli were presented through speakers on the recording chamber ceiling (model 19-318A, 700-10,000 Hz frequency response; Radio Shack) connected to a digital audio

amplifier (RCA model STAV3870; Radio Shack). ERP traces were generated by averaging across single trial epochs centered at $t = 0 \pm 2$ s. Single trials were baseline corrected by subtracting the temporal mean at $t = -1$ s to $t = 0.5$ s. Altering the baseline closer to sound presentation had no effect on the results shown. The mean ERP amplitudes were subsequently calculated across 250 trials.

Time-frequency analysis of EEG. For each recording in which mice were presented with 250 white-noise clicks (10 ms duration, 85 dB sound pressure, 4 s interstimulus intervals), we computed event-related power and phase as a function of frequency and time. Time-frequency calculations were performed as previously described (Goffin et al., 2012; I. T. Wang et al., 2012).

Brain microdissection. To assess CDKL5 protein expression in various brain regions, adult male mice were sacrificed by cervical dislocation. After decapitation, brains were removed and sectioned into 1mm coronal slices using a mouse brain matrix. Tissue was dissected from the somatosensory cortex, striatum, hippocampus, and cerebellum and homogenized in RIPA lysis buffer (150mM NaCl, 1% Triton X-100, 0.5% sodium deoxycholate [DOC], 0.1% sodium dodecyl sulfate [SDS], 25mM Tris [pH7.4] with protease inhibitors [Roche, cOmplete, EDTA-free protease inhibitor cocktail tablets; 5056489001]). To prepare protein extracts, homogenized lysates were incubated on ice for 15 min, and then centrifuged at 21,000 x g for 15min at 4°C. The supernatant fraction was removed and sonicated using a Biorupter for 3 alternating session at max frequency for 15 sec, each followed by a 60 sec cooldown period. The lysate was then centrifuged at 21,000 x g for 15min at 4°C, and the top aqueous layer carefully removed and collected as the total protein fraction.

Western blot. Protein concentration was measured using a Bradford assay. Purified synaptic density membrane proteins or protein lysates were prepared for gel electrophoresis by adding 4X LDS Sample Buffer (NuPAGE, NP0008) to a final concentration of 1X and β -mercaptoethanol to a final concentration of 5%. Samples were heat-denatured at 75°C for 20 min, and 25 μ g of

protein was loaded into each well of a 4–12% Bis-Tris gradient gel (Invitrogen, 10-well, 1.5mm; NP0335) for brain lysate quantification, respectively. Protein gels were run for 2hr at 125V at room temperature on a XCell SureLock mini-cell electrophoresis box (ThermoFisher; EI001) using a PowerPac HC High-Current Power Supply (BioRad; 1645052), then transferred onto a polyvinylidene fluoride (PVDF) membrane (0.45µm pore-size; Biorad 162–0115) at 27V for 1hr and 10min at room temperature. The resulting membrane was blocked with a 1:1 solution of Odyssey blocking buffer (LICOR; 927-40100) and 1X PBS for 1hr at room temperature.

Primary antibodies used were rabbit anti-N-terminal CDKL5 (in house; diluted 1:500), mouse anti-β-Actin (Abcam; ab8226; diluted 1:10,000), rat anti-EB2[K52] (Abcam, ab45767; diluted 1:10,000), and rabbit anti-phospho-EB2[S222] (generously shared by Dr. Sila Ultanir at the Francis Crick Institute; London, UK; diluted 1:1000). For AKT/mTOR signaling studies, the primary antibodies used were rabbit anti-AKT (CST4691P), rabbit anti-pAKT S473 (CST4060), rabbit anti-mTOR (CST2983), rabbit anti-p-mTOR S2448 (ab109268), rabbit anti-S6 (CST2217), rabbit anti-pS6 S240/244 (CST5364), rabbit anti-GSK-3β (CST9315), rabbit anti-pGSK-3β S9 (CST5558), rabbit anti-β-Catenin (CST9562), and anti-β-Actin. Secondary antibodies (LI-COR) used were goat anti-rabbit IgG IRDye800CW, rabbit anti-mouse IgG IRDye680LT, and goat anti-rat IRDye680LT, all incubated for 50min at room temperature at dilutions of 1:10,000. Standard protocols were used for the Odyssey Infrared Imaging System (LI-COR) for protein visualization and quantification.

Dendritic branching and dendritic spine analysis. All steps of sectioning, imaging, and data analysis were performed by a researcher blinded to genotype. Adult male mice at postnatal day 120 (*Cdkl5^{R59X/y}*; Thy1-GFPm/+ versus *Cdkl5^{R59X/y}*; +/+ or *Cdkl5^{fllox/y}*; +/+ ; Thy1-GFPm/+ versus *Cdkl5^{fllox/y}*; UBC-CreER; Thy1-GFPm/+ or *Cdkl5^{fllox/y}*; SLICK/+ versus *Cdkl5^{+/y}*; SLICK/+) were transcardially perfused with 4% paraformaldehyde. Brains were extracted and postfixed additionally for 1hr (for dendritic branching analysis) or overnight at 4°C (for dendritic spine analysis). For dendritic branching analysis, brains were embedded in 2% agar and sectioned

coronally at 200 μ m on a Leica VT1000S vibratome. For dendritic spine analysis, brains were cryoprotected upon overnight fixation by sinking in 15% sucrose and subsequently 30% sucrose in PBS, and then frozen in OCT (Sakura Finetek). Frozen brains were sectioned coronally at 50 μ m on a Leica CM3050S cryostat. For both dendrite and spine imaging, unstained sections were mounted with ProLong™ Glass Antifade Mountant (Thermo Fisher; P36982).

GFP-positive pyramidal neurons located in the hippocampal CA1 region (approximately between bregma coordinates -1.34 to -1.94) with well-preserved morphology were chosen for imaging. For dendritic branching, confocal image stacks were taken on a laser scanning confocal microscope (Leica TCS SP8, 488 laser) with a 20X/0.75 NA immersion objective at 1X zoom. Each neuron was oriented diagonally and centered in a field of view with dimensions 553.57 X 553.57 μ m, with a step size of 0.5 μ m. For dendritic spines, secondary and tertiary dendritic branches of basal and proximal apical dendrites, excluding the apical tuft, of CA1 pyramidal neurons were imaged. Image stacks were taken with a 63X/ 1.40 NA oil-immersion objective at 4X zoom. Each dendritic segment was centered in a field of view with dimensions 43.93 X 10.95 μ m, with a step size of 0.22 μ m and total depth spanning a depth of <7 μ m.

All image analysis was performed by a researcher blinded to genotype. For dendritic branching analysis, the dendrites of each neuron were traced in a supervised manner using Imaris FilamentTracer (Bitplane; RRID: SCR_007366). Each branch was individually traced using a combination of the Autopath and Autodepth functions, with the center of the soma designated as the dendrite beginning point. The basal and apical dendritic trees were separately traced. Sholl analysis was automatically performed by Imaris, and the statistics were exported for analysis.

For spine analysis, three-dimensional blind deconvolution was first performed on confocal image stacks with an iterative constrained Tikhonov-Miller algorithm (DeconvolutionLab, ImageJ) using a pointspread function generated from the imaging parameters (PSF Generator, ImageJ). The deconvolved image stack was imported into Imaris and analyzed. The dendritic backbone of each segment was first traced using the Autopath function and a cone-type dendrite diameter was built using a contrast threshold of 0.2 and dendrite maximum diameter of 1 μ m.

Spines were manually traced on each dendrite using the Autopath function, with a cutoff of a maximum distance of 3 μm from the dendritic backbone. Automated spine reconstruction of manually-traced spines was performed using the Imaris Bitplane Wizard builder. Imaris performed automated computation of spine density and estimation of morphometric parameters for individual spines, including spine length, terminal point (head) diameter, and volume.

Statistical Analysis. For behavioral assays, we chose similar sample sizes for all behavioral experiments based on previous published studies of *Cdk15* constitutive knockout mice and *Cdk15* conditional knockout mice (Tang et al., 2019; Tang et al., 2017; I. T. Wang et al., 2012). Importantly, the number of mice used was pre-determined prior to the start of each experiment. Statistical analyses were performed using Prism (GraphPad). All data sets were analyzed using the Shapiro-Wilk test for normality. For one-sample comparisons, data sets with normal distributions were analyzed for significance using the one-sample *t*-test, whereas data sets with non-normal distributions were analyzed using the Wilcoxon signed-rank test. For two-sample comparisons, data sets with normal distributions were analyzed for significance using the unpaired Student's *t*-test, whereas data sets with non-normal distributions were analyzed using the Mann-Whitney test. Two-way repeated measures ANOVA or the Kruskal-Wallis test was conducted for the appropriate data sets with *post hoc* Sidak's or Dunn's multiple-comparisons tests. All one-sample, two-sample, and multiple-comparison tests were two-tailed.

All other assays that involved sub-sampling of animals were analyzed using R (The R Project for Statistical Computing). Each data set was analyzed using a linear mixed effect model, where *Genotype* was modeled as a fixed effect term and *Animal* was modeled as a random effect term. This model accounts for both between-animal and between-cell variation. For each assay, null and alternative models were constructed using the *lmer* function in the *lme4* package in the following format:

$$m0 = \text{lmer}(\text{Outcome} \sim (1|\text{Animal}), \text{REML} = \text{TRUE})$$
$$m1 = \text{lmer}(\text{Outcome} \sim \text{Genotype} + (1|\text{Animal}), \text{REML} = \text{TRUE})$$

To make statistical comparisons, the *KRmodcomp* function from the *pbkrtest* package (Halekoh and Højsgaard, 2014) was used:

`KRmodcomp(m0, m1)`

The *KRmodcomp* function reports a modified *F*-test statistic based on the Kenward and Roger approximation, which accounts for the small sample sizes in our study, modified numerator and denominator degrees of freedom, and a *p*-value. The estimated effect of *Genotype* is obtained from the alternative model constructed using the *lmer* function from *lme4*.

All graphs are plotted using Prism (GraphPad). Bolded center lines reflect the mean, and all error bars indicate s.e.m. For boxplots, the limits indicate the minimum and maximum with boxplot center line indicating the median. In our figures, *p*-values between 0.05 and 0.1 are shown explicitly, * is used to denote all $0.01 < p < 0.05$, ** for $0.001 < p < 0.01$, *** for $0.0001 < p < 0.001$, and **** for $p < 0.0001$.

Figures

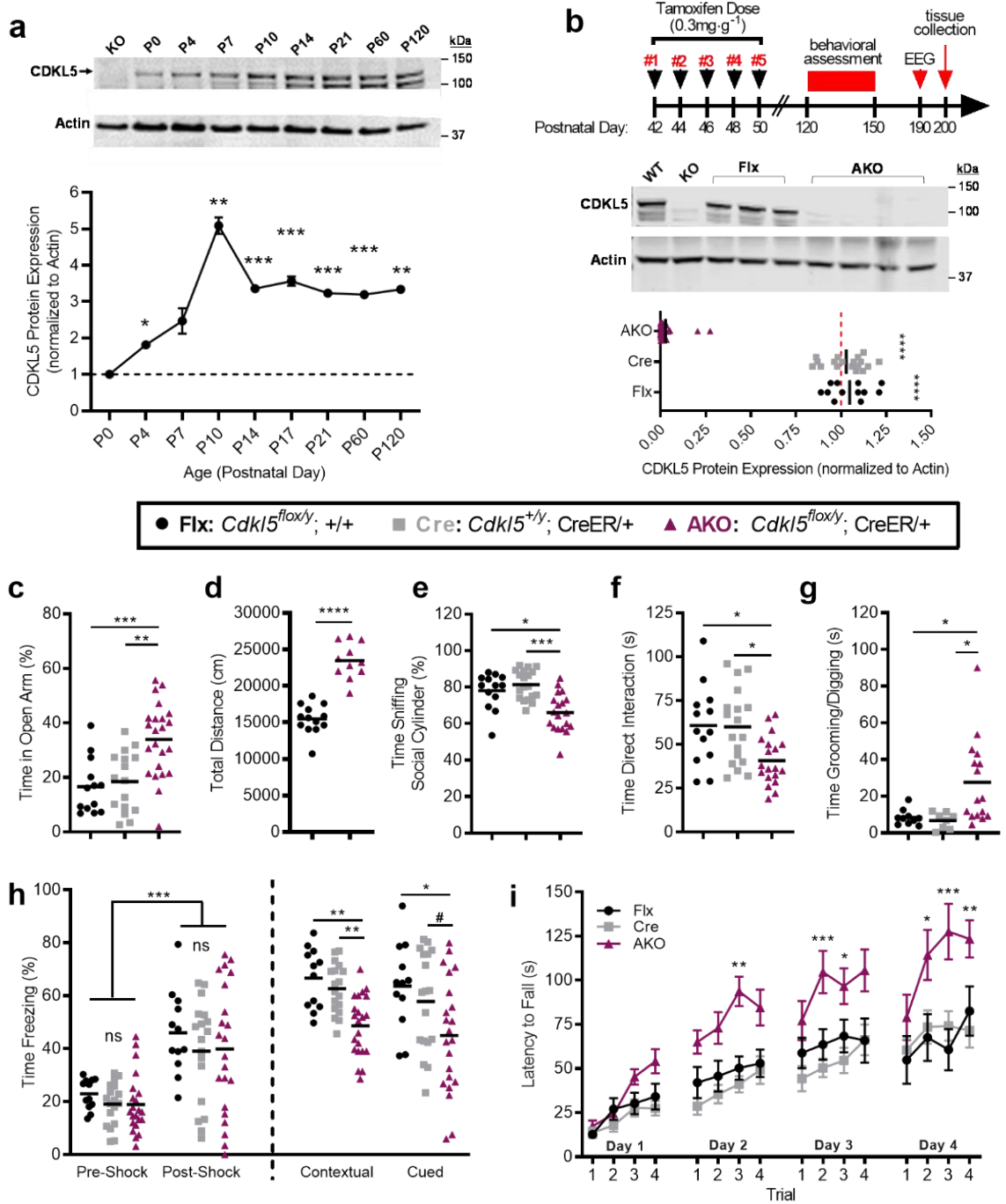


Figure 1: Post-developmental loss of CDKL5 disrupts multiple behavioral domains in mice

(a) Top: Representative western blot showing CDKL5 protein expression from forebrain tissues of wild-type mice across multiple ages (Postnatal Day (P)0, P4, P7, P10, P14, P21, P60, P120) with Actin protein as a loading control and forebrain tissue from *Cdkl5* knockout mice as a reference for antibody specificity; Bottom: Quantification of western blot results for CDKL5 protein expression across multiple ages demonstrates a postnatal increase in CDKL5 forebrain expression and peak ~P14, with stable expression detectable into adulthood. Normalized to Actin loading control and plotted relative to P0 levels (n=4). **(b)** Top: Tamoxifen administration scheme and experimental schedule; Bottom: Representative western blot and quantification for CDKL5 protein expression in all experimental mice demonstrates significant reduction of CDKL5 protein in AKO over Flx and Cre forebrain tissues collected after undergoing behavioral evaluation. Actin protein served as a loading control, and *Cdkl5* knockout and wild-type brain tissues were used as a reference for antibody specificity with all values normalized to Cre-only control CDKL5 levels. **(c)** AKO mice spent significantly more time in the open arm of the elevated Zero-maze assay over Flx and Cre littermate controls suggestive of decreased anxiety. **(d)** AKO mice travel significantly more distance than Flx littermates in the open-field assay suggesting hyperactivity. **(e)** AKO mice spent significantly less time than Flx and Cre littermates sniffing and **(f)** directly interacting with a novel stimulus mouse during the 3-chambered social choice test, suggestive of decreased sociability. **(g)** AKO mice carry aberrant repetitive behaviors demonstrated by increased time spent grooming or digging in a homecage-like environment when compared to Flx and Cre littermates. **(h)** AKO mice freeze in response to a mild footshock similarly to Flx and Cre littermates, but show decreased percent time freezing compared to Flx and Cre littermates when returned to the testing chamber (contextual) and upon hearing the testing tone (cue), demonstrating impaired learning and memory. **(i)** AKO mice take significantly more time to fall from an accelerating, rotating rod than Flx and Cre littermates, indicating enhanced motor coordination. For all panels: Flx, n=13; Cre, n=19; AKO, n=23 where all genotypes received tamoxifen; Kruskal-Wallis test with Dunn's multiple comparisons test (except Open-field: Mann-Whitney test & Rotarod: 2-way repeated measures ANOVA with Sidak's multiple comparisons test). *p<0.05, **p<0.01, ***p<0.001, ****p<0.0001. Bars represent mean ± SEM.

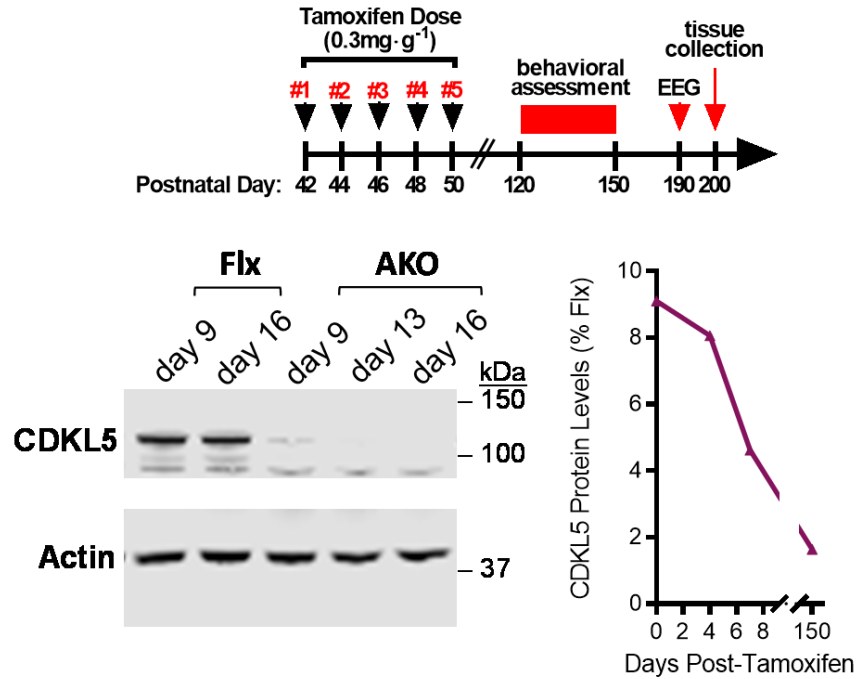


Figure 2. Timecourse of CDKL5 protein knockdown with tamoxifen

Top: tamoxifen administration scheme and experimental schedule; Bottom: representative western blot results and quantification demonstrating significant reduction in CDKL5 protein in forebrain tissues of *Cdkl5^{fllox/y}; CreER/+* (AKO) mice compared to *Cdkl5^{fllox/y}; +/+* (Flx) littermate controls after tamoxifen administration. Forebrain tissues were collected and analyzed for CDKL5 protein 9, 13 and 16 days after the first tamoxifen dose, and all experimental mice were sacrificed after behavioral assessment for post-hoc protein quantification. Actin protein was a loading control, and AKO CDKL5 protein was normalized to Flx levels.

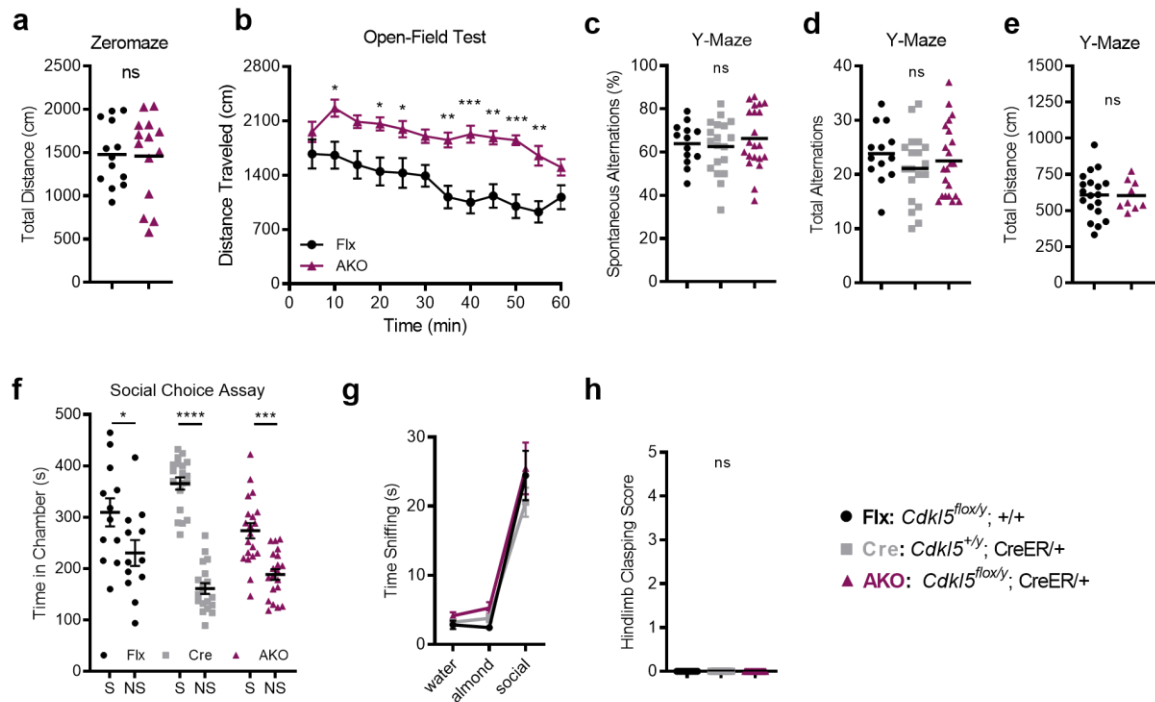


Figure 3. Additional behavioral domains analyzed upon adult deletion of *Cdk15*

(a) Total distance traveled in the elevated Zeromaze assay was similar between AKO and Flx mice (Mann-Whitney test). (b) AKO mice traveled significantly more in an open-field assay relative to Flx littermates over the course of one hour (distance traveled binned in 5min intervals; two-way, repeated measures ANOVA with Sidak's multiple comparisons test). (c) AKO mice showed no difference in percentage of spontaneous alternations in a Y-Maze assay, and no difference in the (d) total number of alternations or (e) total distance traveled when compared to Flx and Cre littermate controls (Kruskal-Wallis test). (f) Flx, Cre, and AKO mice all spent significantly more time in the chamber containing a social stimulus (S; novel mouse) over a non-social stimulus (NS; rock) during the 3-chambered social choice test (paired t test). (g) Flx, Cre, and AKO mice all spent significantly more time sniffing a social scent over either water or almond scents, with no significant difference detected between genotypes (two-way ANOVA with Dunnett's multiple comparisons test). (h) No Flx, Cre, or AKO animals displayed any hindlimb clasping phenotypes (Kruskal-Wallis test). For all panels: Flx, n=13; Cre, n=19; AKO, n=23 where all genotypes received tamoxifen; *p<0.05, **p<0.01, ***p<0.001, ****p<0.0001. Bars represent mean \pm SEM.

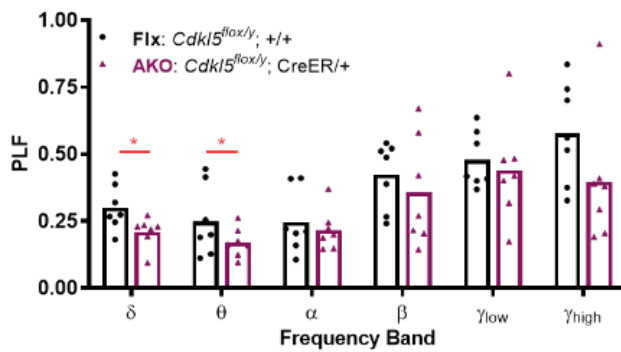
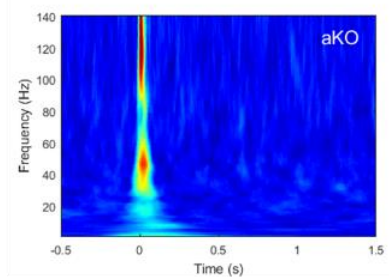
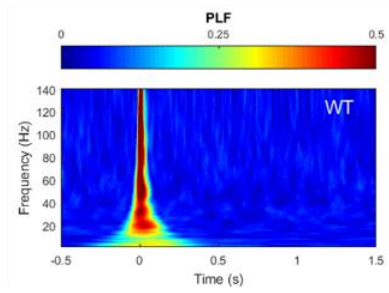
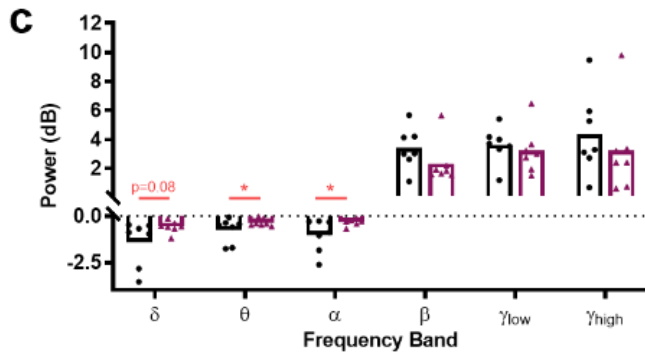
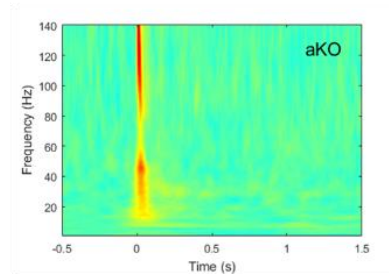
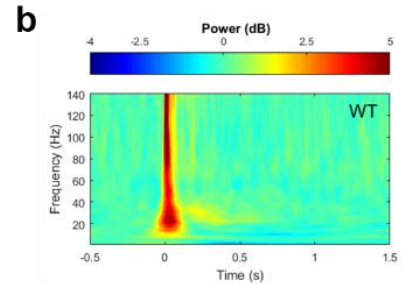
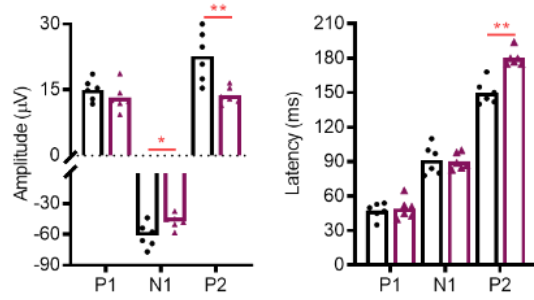
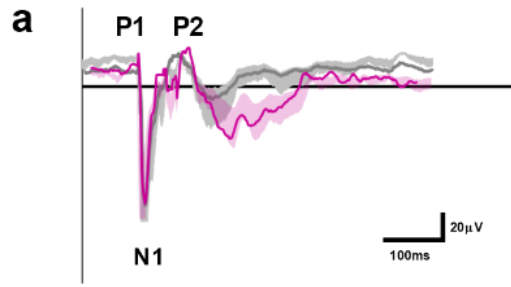
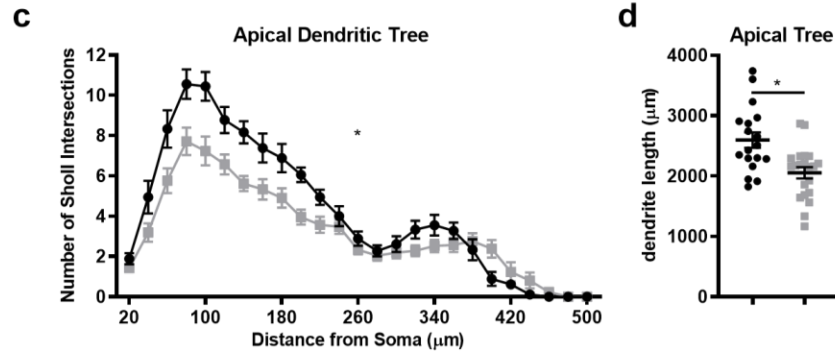
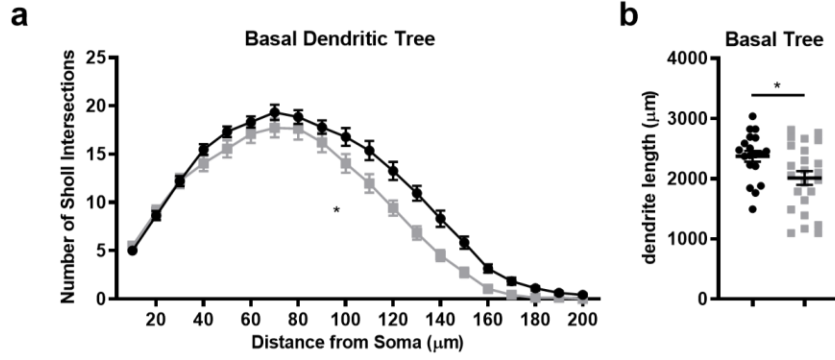
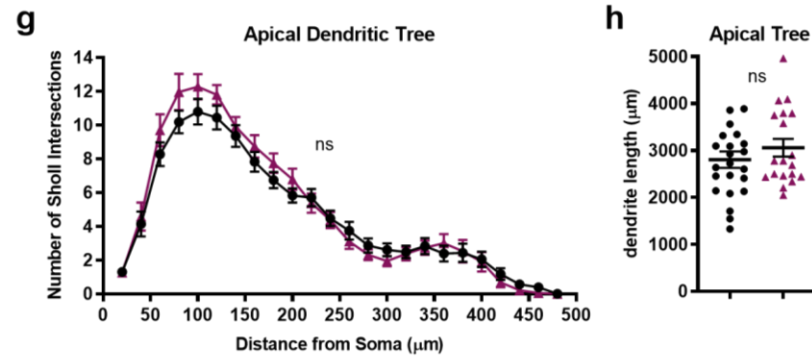
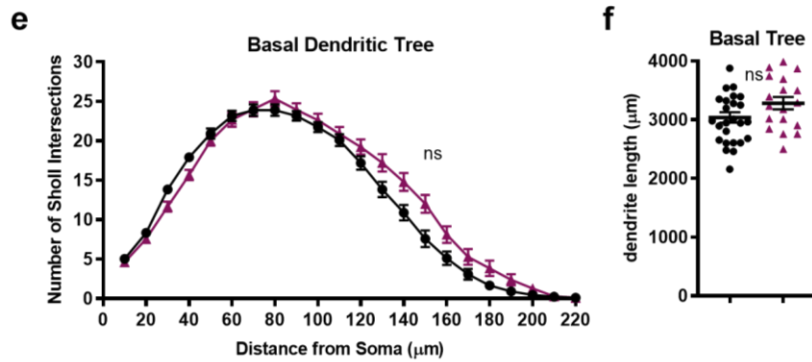


Figure 4: Post-developmental loss of *Cdk15* disrupts hippocampal event-related potentials.

(a) Top: grand-average hippocampal CA1 ERP waveform following presentation of auditory stimuli in *Cdk15^{fllox/y}; +/+* (Flx) and *Cdk15^{fllox/y}; CreER/+* (AKO) mice demonstrates abnormal ERP waveform in AKO mice. Traces represent mean amplitude \pm SEM. Characteristic polarity peaks P1, N1, and P2 in Flx control are labeled (scale bar: 100ms [horizontal] and 20mV [vertical]); Bottom: quantification of the amplitude and latency of ERP peaks shows significantly decreased amplitude of the canonical N1 and P2 peaks and increased latency in the P2 polarity peak (unpaired, two-tailed *t* test). **(b)** Time-frequency plots showing changes in event-related power (top) and phase-locking factor (PLF; bottom) following auditory stimulus. Color represents mean power/PLF, where warmer colors correspond to increased power/PLF and cooler colors correspond to decreased power/PLF relative to prestimulus baseline. **(c)** Changes in event-related mean power (top) and PLF (bottom) averaged across δ (2-4Hz), θ (4-8Hz), α (8-12Hz), β (12-30Hz), γ_{low} (30-50Hz), and γ_{high} (70-140Hz) oscillation frequencies demonstrate a selective disruption of power and phase-locking in the low-frequency oscillations in AKO mice over Flx littermate controls (unpaired, two-tailed *t* test). Bars represent mean \pm SEM; n=7 Flx and n=7 AKO for all ERP experiments.



● WT: *Cdk15*^{+y}; Thy1-GFPm ■ KO: *Cdk15*^{R59X/y}; Thy1-GFPm



● Flx: *Cdk15*^{fllox/y}; +/+; Thy1-GFP ▲ AKO: *Cdk15*^{fllox/y}; CreER/+; Thy1-GFP

Figure 5: Germline, but not adult, loss of *Cdkl5* results in decreased dendrite length and complexity of CA1 pyramidal neurons.

(a) Reduced complexity of the basal dendritic tree of hippocampal CA1 neurons in *Cdkl5*^{R59X/y}; Thy1-GFPm (KO) mice compared to *Cdkl5*^{+/y}; Thy1-GFPm (WT) littermate control mice measured via Sholl analysis. **(b)** Total basal dendrite length is significantly decreased in KO animal CA1 neurons compared to WT neurons. **(c)** Reduced complexity of the apical dendritic tree of hippocampal CA1 neurons in KO mice compared to WT littermate control mice measured via Sholl analysis. **(d)** Total apical dendrite length is significantly decreased in KO animal CA1 neurons compared to WT neurons. (n=18 cells/3 mice for WT; n=21 cells/3 mice for KO). **(e)** There was no significant difference in basal tree dendritic complexity of hippocampal CA1 neurons between *Cdkl5*^{flx/y}; CreER/+; Thy1-GFPm (AKO) mice and *Cdkl5*^{flx/y}; +/+; Thy1-GFPm (Flx) littermate control mice measured via Sholl analysis. **(f)** Total basal dendrite length was unchanged in AKO animal neurons compared to Flx littermate controls. **(g)** There was no significant difference in apical tree dendritic complexity of hippocampal CA1 neurons between AKO mice and Flx littermate control mice measured via Sholl analysis. **(h)** Total apical dendrite length was unchanged in AKO animal neurons compared to Flx littermate controls. Basal: n= 24 cells/6 mice for WT, n= 40 cells/8 mice for cKO; Apical: n=23 cells/6 mice for WT, n=26 cells/8 mice for AKO. Linear mixed effects analysis, *p<0.05.

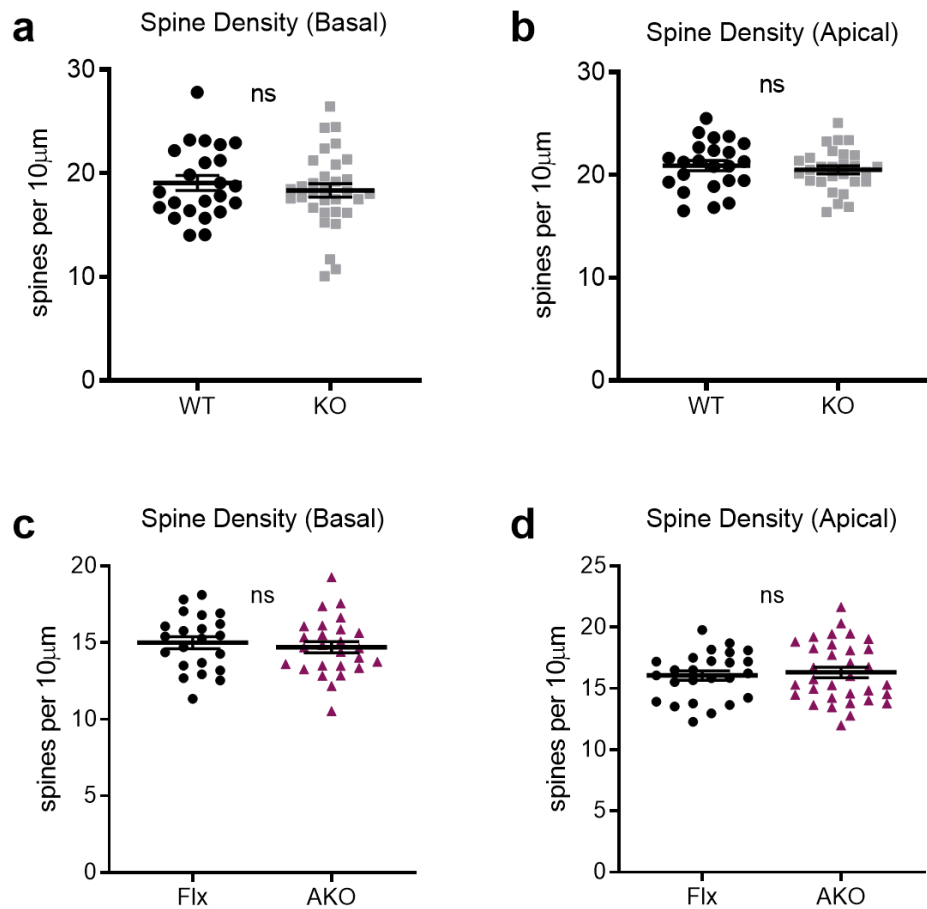


Figure 6. Germline or post-developmental deletion of *Cdk15* does not alter dendritic spine density on hippocampal CA1 neurons.

(a) *Cdk15* germline knock-in mice (*Cdk15^{R59X/y}*; Thy1-GFPm/+), KO, show no significant difference in spine density compared to wild-type littermate controls (*Cdk15^{+/y}*; Thy1-GFPm/+), WT, on either basal or **(b)** apical dendritic arbors of hippocampal CA1 pyramidal neurons (Basal: n=23 cells/5 mice for WT; n=32 cells/5 mice for KO. Apical: n=23 cells/5 mice for WT; n=28 cells/5 mice for KO). **(c)** *Cdk15^{flox/y}*; CreER/+; Thy1-GFPm/+ (AKO) mice similarly show no significant change in spine density compared to *Cdk15^{flox/y}*; +/+; Thy1-GFPm/+ (Flx) littermate controls on either basal or **(d)** apical dendritic arbors of hippocampal CA1 pyramidal neurons (Basal: n= 22 cells/8 mice for Flx, n= 30 cells/7 mice for AKO. Apical: n=25 cells/8 mice for Flx; n=36 cells/7 mice for AKO). Linear mixed effects analysis.

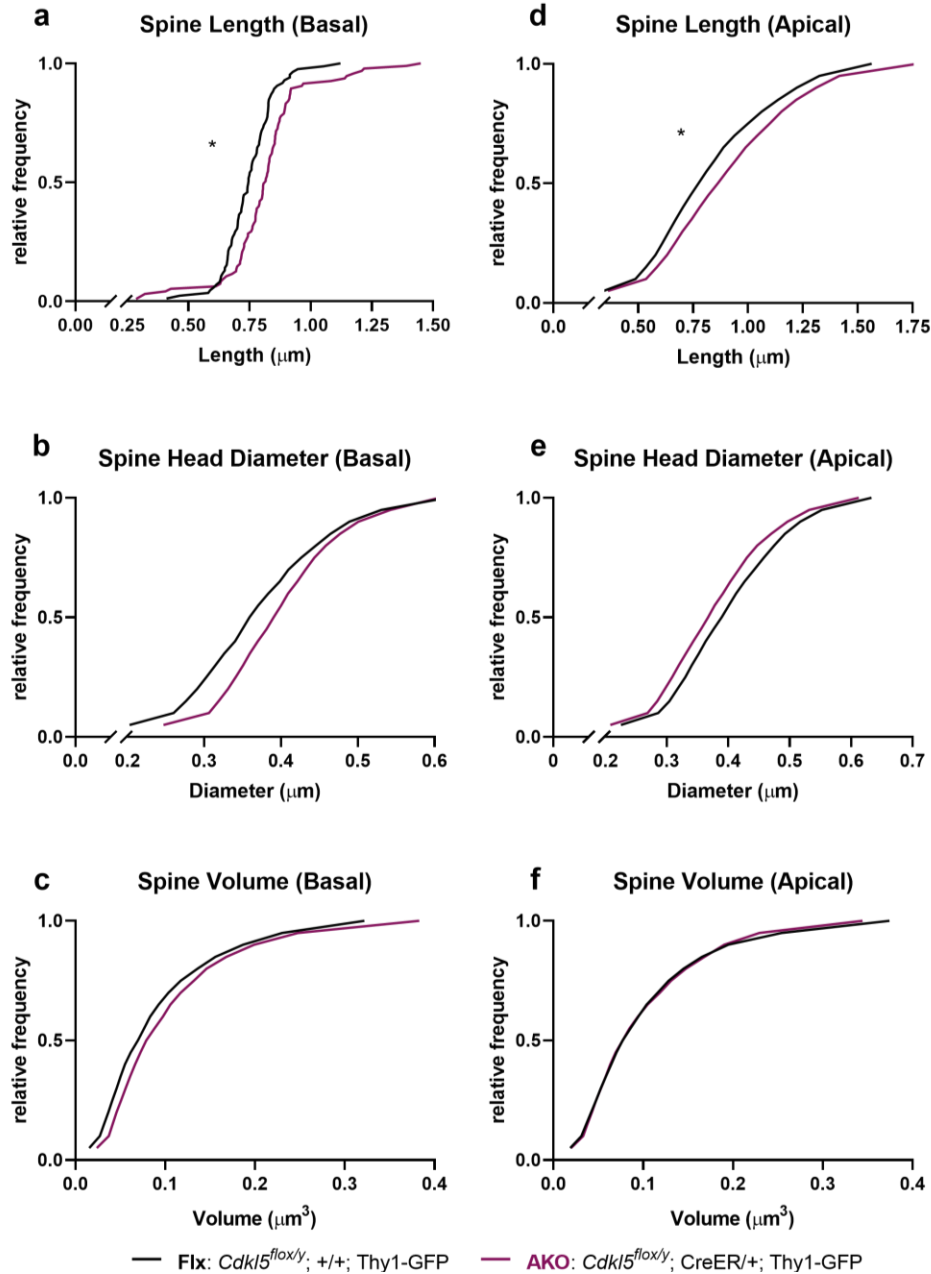


Figure 7. Post-developmental deletion of *Cdk15* disrupts hippocampal CA1 dendritic spine morphology.

(a) *Cdk15^{flx/y}; CreER/+; Thy1-GFPm/+* (AKO) neurons have increased spine length compared to *Cdk15^{flx/y}; +/+; Thy1-GFPm/+* (Flx) littermate control neurons on both basal and **(d)** apical dendritic arbors. Spine head diameter [**(b)** basal; **(e)** apical] and spine volume [**(c)** basal; **(f)** apical] were not significantly different between AKO neurons and Flx neurons. For all spine analyses: Basal: n= 22 cells/8 mice for Flx; n= 30 cells/7 mice for AKO. Apical: n=25 cells/8 mice for Flx; n=36 cells/7 mice for AKO. Linear mixed effects analysis, *p<0.05.

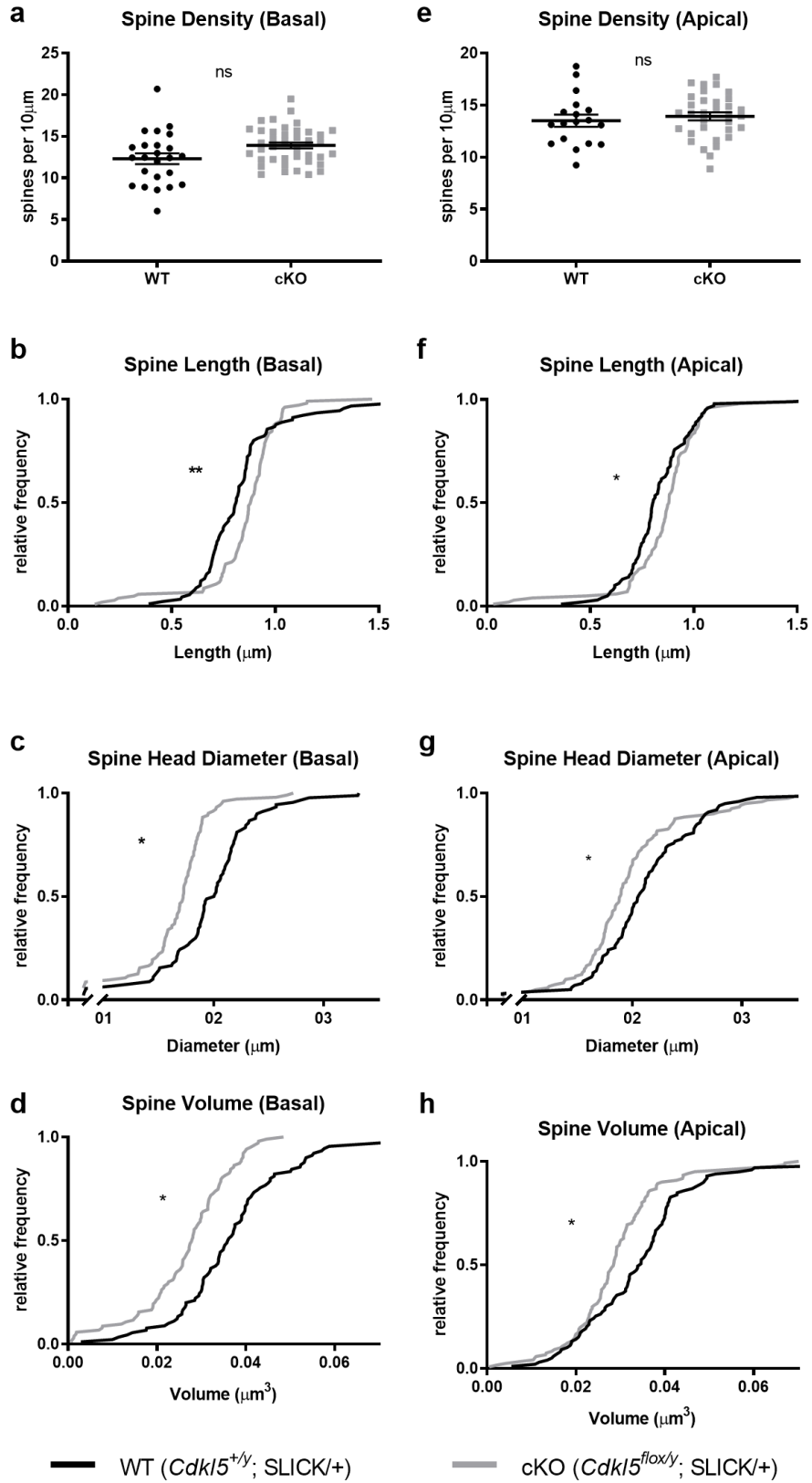


Figure 8: Post-developmental loss of *Cdk15* results in cell-autonomous disruption of dendritic spine morphology on CA1 pyramidal neurons.

(a) *Cdk15^{flx/y}*; SLICK/+ (cKO) mice show no significant change in spine density on (a) basal or **(e)** apical dendritic arbors of CA1 pyramidal neurons compared to *Cdk15^{+/y}*; SLICK/+ (WT) littermate control neurons. cKO neurons have increased spine length compared to WT controls on both **(b)** basal and **(f)** apical dendritic arbors as well as significantly reduced head diameter [**(c)** basal; **(g)** apical] and reduced volume [**(d)** basal; **(h)** apical]. Basal: n= 24 cells/6 mice for WT, n= 40 cells/8 mice for cKO; Apical: n=19 cells/6 mice for WT, n=33 cells/8 mice for cKO. Linear mixed effects analysis. *p<0.05, **p<0.01.

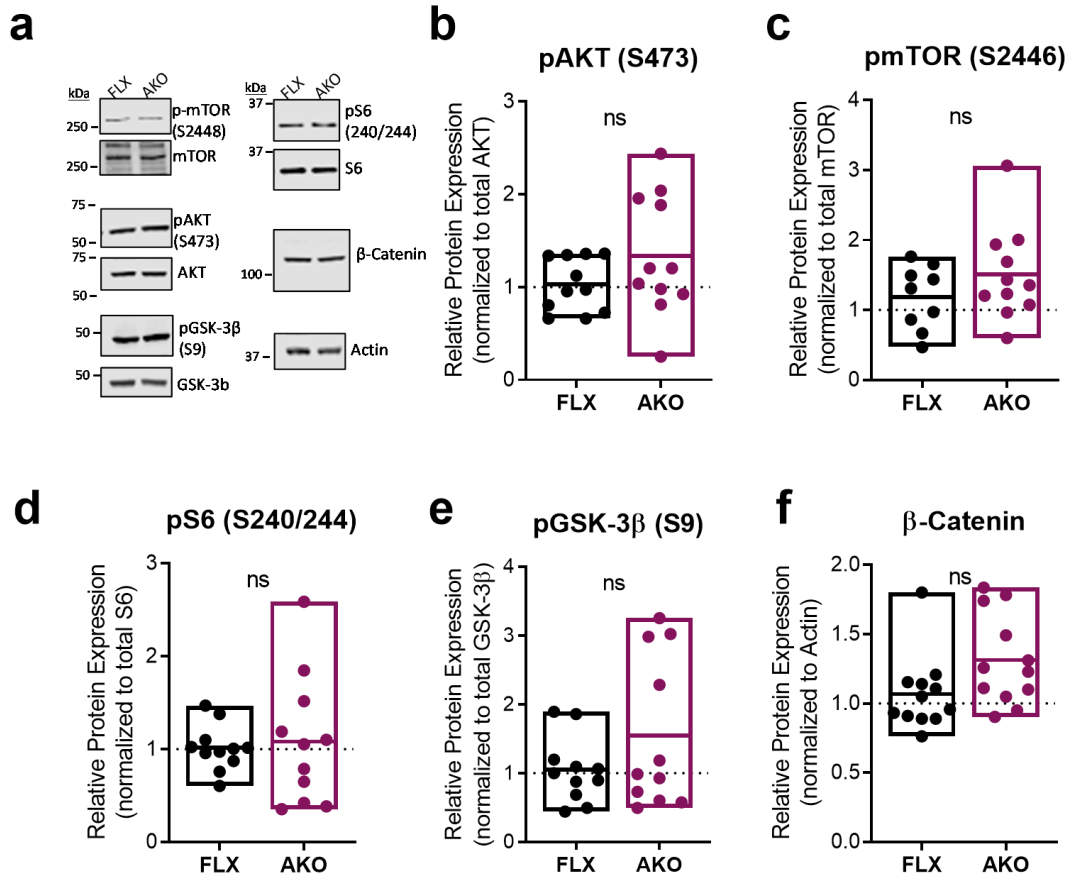


Figure 9. AKO mice do not demonstrate disrupted AKT-mTOR pathway signaling

(a) Representative western blot results for several major proteins within the AKT-mTOR signal cascade including phospho-protein levels and total protein levels for each. Samples are from pairs of *Cdk15^{flox/y}; +/+* (FLX) and *Cdk15^{flox/y}; CreER/+* (AKO) littermates. **(b-f)** AKO mice do not show significant changes in levels of pAKT S473, p-mTOR S2446, pS6 S240/244, and pGSK-3β S9 over respective total protein levels, or changes in total levels of β-catenin compared to FLX littermate controls. (FLX, n = 10 mice; AKO, n = 10 mice; unpaired Mann-Whitney test).

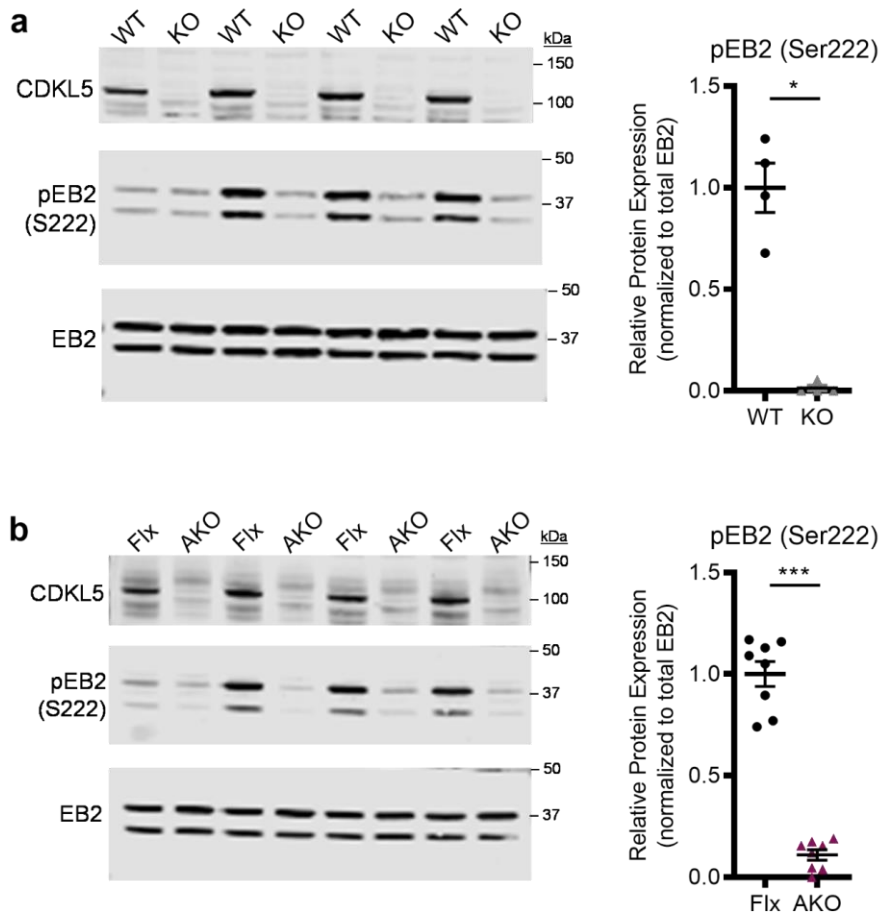


Figure 10. Germline and post-developmental deletion of *Cdkl5* abrogate EB2 phosphorylation.

(a) Left: representative western blot demonstrating CDKL5, phospho-EB2 (S222), and total EB2 protein levels in wild-type (WT) versus *Cdkl5* germline knock-in (*Cdkl5^{R59X/y}*; KO) forebrain tissues. Two bands present for EB2 represent two isoforms detectable in brain tissue (both containing Ser222); Right: quantification of phospho-EB2 (S222) western blot results demonstrates a nearly total loss of EB2 phosphorylation at Ser222 in KO forebrains compared to WT, normalized to total EB2 protein levels (n=4 per genotype). **(b)** Left: representative western blot demonstrating CDKL5, phospho-EB2 (S222), and total EB2 protein levels in *Cdkl5^{fllox/y}*; +/- (Flx) versus *Cdkl5^{fllox/y}*; CreER/+ (AKO) forebrain tissues (both genotypes receiving tamoxifen); Right: quantification of phospho-EB2 (S222) western blot results demonstrates a nearly total loss of EB2 phosphorylation at Ser222 in AKO forebrains compared to Flx, normalized to total EB2 protein levels (n=8 per genotype). For all panels: Mann-Whitney test; *p<0.05, **p<0.01, ***p<0.001.

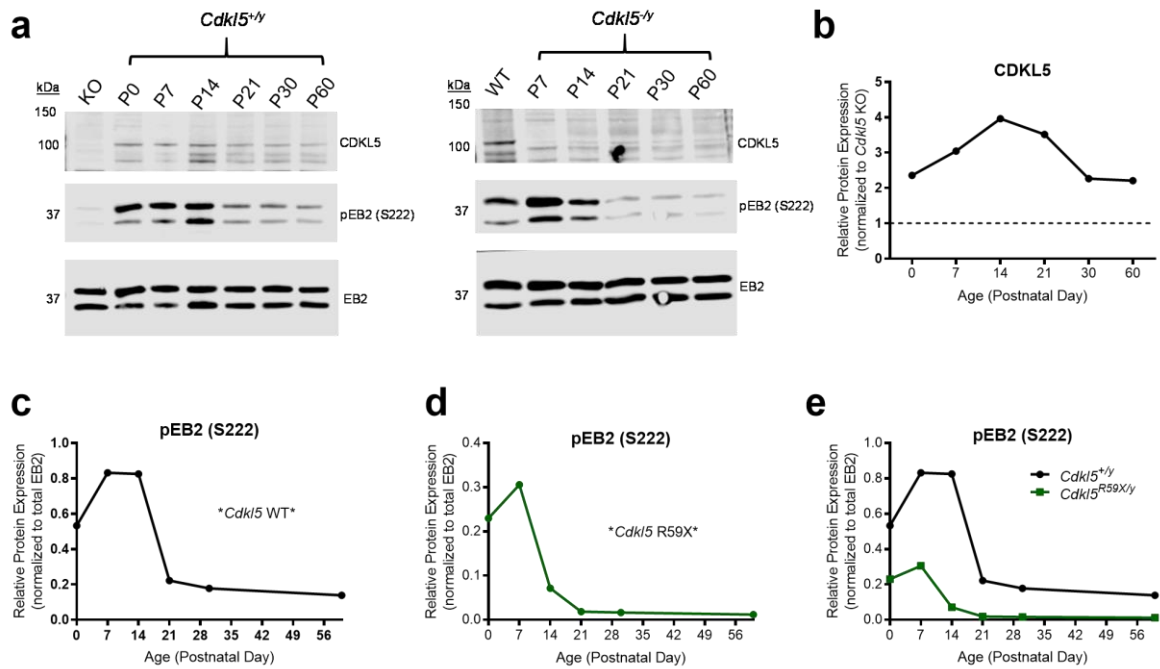


Figure 11. EB2 phosphorylation is developmentally regulated and correlates with CDKL5.

(a) Representative western blot results for CDKL5, pEB2 Ser222, and total EB2 protein levels from forebrain cortices of *Cdkl5* wild-type (left) and *Cdkl5* knockout (right) mice at various ages (Postnatal Day (P)0, P7, P14, P21, P30, P60). Two bands present for EB2 represent two isoforms detectable in brain tissue (both containing Ser222). **(b)** Quantification of total CDKL5 protein levels in wild-type mice across various ages, normalized to *Cdkl5* knockout, demonstrates a postnatal increase and expression peak ~P14. **(c)** Quantification of phospho-EB2 Ser222 levels, normalized to total EB2 levels, in *Cdkl5* wild-type mice across various ages demonstrate a developmental regulation that correlates with CDKL5 expression, including a peak ~P14. **(d)** Quantification of phospho-EB2 Ser222 levels, normalized to total EB2 levels, in *Cdkl5* knockout mice across various ages reflects a shift in the peak phosphorylation levels of EB2 from P14 to P7. **(e)** Overlay of pEB2 Ser222 protein quantifications from *Cdkl5* wild-type and knockout mice demonstrates the overall reduction in EB2 phosphorylation in knockout mice at each timepoint, and highlights the shifted peak phosphorylation age.

CHAPTER 4 – LATE RESTORATION OF CDKL5 EXPRESSION IS SUFFICIENT TO RESCUE CDD-RELATED BEHAVIORAL IMPAIRMENTS AND ABBERANT NMDA-RECEPTOR SIGNALING

Contributions: Barbara Terzic led this study with help from M. Felicia Davatolhagh for electrophysiological experiments, Joshua Ross for data analysis, and Marc V. Fuccillo and Zhaolan Zhou for the review and interpretation of data. Yue Cui and Erin Nugent managed all mouse husbandry, genotyping, and breeding. Barbara Terzic wrote this chapter with input from all authors.

Abstract

CDKL5 deficiency disorder (CDD) is an early-onset, neurodevelopmental syndrome associated with pathogenic variants in the gene encoding cyclin-dependent kinase-like 5 (CDKL5). CDKL5 has been implicated in neuronal synapse maturation and NMDA receptor subunit trafficking at the post-synaptic membrane, however, the reversibility of these and other CDD-associated impairments remain unknown. We genetically manipulated endogenous *Cdkl5* expression in mice, and found adult restoration of CDKL5 in hemizygous male knockout mice significantly ameliorates CDD-related behavioral impairments, NMDA-induced seizure susceptibility, and aberrant NMDA receptor signaling. We have further extended these findings into a novel, independent conditional rescue line to corroborate that late rescue of CDKL5 also reverses several behavioral deficits in heterozygous female models of CDD. These findings underscore the potential for disease reversal in both male and female CDD patients, and suggest a broad therapeutic time window exists for numerous CDD-related deficits.

Introduction

Mutations in the X-linked gene encoding cyclin-dependent kinase-like 5 (CDKL5) are associated with a devastating neurodevelopmental syndrome known as CDKL5 deficiency disorder (CDD)(Fehr et al., 2013; Kalscheuer et al., 2003; Tao et al., 2004; Weaving et al., 2004). CDD is characterized by a constellation of phenotypes including intractable seizures, severe neurodevelopmental delay, intellectual disability, hypotonia, and autistic features(S. T. Demarest et al., 2019; H. E. Olson et al., 2019). The disorder predominantly afflicts young females heterozygous for mutations in *CDKL5*, but hemizygous male cases have also been reported (albeit at a significantly lower prevalence)(S. T. Demarest et al., 2019; Liang et al., 2019). Despite this strong genetic link, the pathogenesis and treatability of CDD remains unclear. Presently, there is no cure, and the limited treatment options available have focused on mitigating seizure burden using a variety of non-specific anticonvulsants(H. E. Olson et al., 2019).

In 2012, the first knockout mouse model of CDD was generated and found to recapitulate several of the cardinal phenotypes of the human disease including learning and memory impairments, motor deficits, and autistic-like behaviors(I. T. Wang et al., 2012). Several additional knockout and knock-in lines have since been generated with similar behavioral deficits, highlighting the reproducibility of CDD-related phenotypes in mice(Amendola et al., 2014; Okuda et al., 2018; Yennawar et al., 2019). Intriguingly, *Cdkl5* knockout mouse models have also demonstrated a robust sensitivity to NMDA-induced seizures concomitant with an increased postsynaptic localization of NMDA receptors (NMDARs), specifically GluN2B-containing NMDARs(Okuda et al., 2017). These results were supported by our recent study which demonstrated that acute, NMDAR blockade was capable of selectively ameliorating autistic-like phenotypes in CDKL5-deficient mice (see Chapter 2)(Tang et al., 2019). Despite these multitude of CDD models, however, the extent of reversibility of the remaining heterogeneous constellation of CDD-related phenotypes, particularly at later ages, remains undetermined.

Clinical reports illustrating the early, postnatal onset of CDD symptomology support a critical role for CDKL5 in the developing nervous system(H. E. Olson et al., 2019; Y. C. Zhu & Z.

Q. Xiong, 2019). However, it remains unknown whether restoration of the kinase after critical periods of brain development can reverse any CDD-related deficits. With recent advances in precision medicine highlighting promising treatment options for CDD patients in the future, it is imperative to establish the temporal role of CDKL5 in neuronal development versus maintenance, and the potential for symptom amelioration in patients who may have already passed a specific developmental time window (Benke & Kind, 2020).

To address these questions, we have employed a genetic strategy to investigate the reversibility of CDD-associated symptoms by generating conditional rescue mice enabling temporal control of *Cdkl5* re-expression at its endogenous locus. We find that the majority of CDD-related behavioral deficits, as well as aberrant NMDA receptor signaling, are significantly mitigated with late restoration of CDKL5 expression. We corroborate these findings an independent conditional rescue model, demonstrating that several CDD-related behavioral impairments are also reversible in heterozygous female *Cdkl5* knockout mice with late *Cdkl5* re-expression. These findings, in conjunction with our adult knockout studies highlighted in Chapter 3, are the first to delineate a post-developmental requirement for CDKL5, and the first to demonstrate the potential for disease reversal in CDD. Importantly, our results also uncover a broad therapeutic time window for numerous CDD-related deficits, supporting future therapeutic efforts aimed towards the treatment of CDD.

Results

Adult restoration of CDKL5 rescues numerous CDD-related behavioral deficits in hemizygous male knockout mice

Our previous findings support that post-developmental loss of CDKL5 induces similar phenotypes as germline knockout (see Chapter 3). However, the reversibility of CDD-associated symptoms remains a long-standing question in the field, especially since the disorder presents very early in life. Given that CDD patients do not normally experience neurodegeneration, the viability of mutant neurons in CDD patients opens up the prospect that re-expression of CDKL5

(or therapeutic intervention) may restore CDKL5-dependent signaling pathways and thereby alleviate some of the disorder phenotypes (H. E. Olson et al., 2019). If a critical time window of CDKL5 function does exist, then delayed treatment (or gene replacement) may have little effect or even contravening outcomes in a system that has partially compensated for its loss.

To address this, we created a mouse line in which the endogenous *Cdkl5* gene is conditionally silenced by the insertion of a *loxP*-flanked transcriptional STOP cassette, and where physiological levels of *Cdkl5* expression can be restored upon Cre-mediated cassette deletion (*Cdkl5^{STOP}*, hereafter referred to as STOP; Figure 1a). This is particularly relevant as human genetic studies have reported that duplication of *CDKL5* is associated with neurological impairments (Szafranski et al., 2015). A preliminary characterization of STOP mice demonstrated that they do not express detectable levels of CDKL5 protein and display similar phenotypes to *Cdkl5* germline knockout mice by P42 when we began tamoxifen administration (Figure 2). We delivered tamoxifen to four experimental groups of mice: *Cdkl5^{+y}; +/+* (WT), *Cdkl5^{+y}; CreER/+* (Cre), *Cdkl5^{STOP/y}; +/+* (STOP), and *Cdkl5^{STOP/y}; CreER/+* (rescue, Res) beginning at P42 using the same regimen applied in our adult knockout experiments (0.3mg·kg⁻¹ every other day for a total of 5 doses). We observed significant restoration of CDKL5 protein expression in forebrain tissues of Res mice, but not STOP mice, that was comparable to WT and Cre-only littermate controls within two weeks of tamoxifen delivery. Unexpectedly, however, we noticed significant lethality at this dosage selectively in Res mice, but not WT, Cre, or STOP animals (Figure 3a). These findings suggest there may be toxicity associated with rapid *Cdkl5* reactivation, even at endogenous levels of CDKL5 expression. We therefore optimized our tamoxifen administration protocol and found that a more gradual *Cdkl5* re-expression (1 tamoxifen dose of 0.3mg·kg⁻¹ every week for a total of 3 weeks, followed by 2 booster treatments) was able to eliminate this toxicity while restoring CDKL5 expression to nearly WT levels (Figure 1b, Figure 3b). Consequently, we adhered to this gradual *Cdkl5* activation protocol for subsequent rescue experiments. Remarkably, phosphorylation of EB2 Ser222 was also restored to control levels

upon adult reversal of *Cdkl5* expression, highlighting that CDKL5-dependent signaling pathways are likely rescued with *Cdkl5* re-expression (Figure 1b).

Using this gradual gene reversal strategy, we next examined the extent to which late restoration of CDKL5 expression could mitigate CDD-related behavioral deficits. We again administered tamoxifen to a cohort of Cre, STOP, and Res littermates beginning at P42 (the age at which most behavioral deficits have arisen in STOP mice, Figure 2) and then beginning at P140 evaluated multiple behavioral domains known to be disrupted in *Cdkl5* germline and adult knockout animals. We found that Res animals showed significant improvement over STOP littermates in hyperactivity and anxiety-related behaviors. STOP mice spent significantly more time exploring the open arm of the elevated zero-maze in comparison to Cre-only controls, suggestive of decreased anxiety (Figure 1c). However, adult restoration of *Cdkl5* resulted in a significant decrease in open-arm time compared to STOP mice, with Res animals behaving comparable to Cre controls (Figure 1c, Figure 4a). STOP mice also moved significantly more over the course of one hour in an open field test when compared to Cre-only controls, whereas Res mice exhibited activity levels closer to Cre control littermates (Figure 1d, Figure 4b). Adult restoration of CDKL5 also ameliorated several of the autistic-like phenotypes frequently reported upon *Cdkl5* deletion. During the three-chambered social choice assay, Res animals spent similar amounts of time to Cre-only controls sniffing the social cylinder and directly interacting with a novel stimulus mouse, while STOP mice spent significantly less time sniffing the social cylinder and directly interacting with a novel stimulus mouse, suggestive of decreased sociability (Figure 1e-f, Figure 4f-h). STOP mice also exhibited aberrant repetitive behaviors, illustrated by an increased time spent grooming/digging in a home cage-like environment when compared to Cre controls, whereas Res mice displayed control-level grooming/digging behaviors (Figure 1g).

Similar to other *Cdkl5* knockout models, STOP mice recapitulate impaired motor learning on the rotarod assay, as demonstrated by a decreased latency to fall from an accelerating, rotating rod as well as a penetrant hindlimb clasp phenotype. Adult rescue of CDKL5 significantly ameliorated these motor deficits, with Res mice performance on the rotarod assay

comparable to littermate Cre-only controls and no hindlimb claspings present in any of the 17 Res animals tested (Figure 1h-i). Finally, normal context- and cue-dependent learning and memory were also restored to nearly control levels in Res animals, while STOP mice displayed significant impairment in both of these memory domains (Figure 1j). Interestingly, working memory, as measured by spontaneous alternations during the Y-Maze assay, was not significantly improved in Res animals when compared to STOP-only littermate mice (Figure 4c). However, total activity during the Y-Maze assay (measured by the total number of alternations) was significantly restored to Cre control levels in Res animals which aligns with the ameliorated hyperactivity phenotype illustrated by the open field test (Figure 4d-e). Collectively, these findings support that adult restoration of CDKL5 is sufficient to reverse or ameliorate the majority of loss-of-function behavioral impairments; namely, the hyperactivity, anxiety-related phenotypes, autistic-like behaviors, motor impairments, and learning and memory deficits appear to remain amenable to post-developmental restoration of CDKL5 expression. Additionally, post-hoc examination of CDKL5 restoration revealed that several rescue mice showed only 20-50% of wild-type protein expression (Figure 5). The rescue of numerous behavioral domains in these mice underscores the potential that even partial restoration of CDKL5 expression may show notable therapeutic benefit, at least in mice.

Adult restoration of CDKL5 abrogates NMDA-induced hyperexcitability and aberrant NMDAR-mediated synaptic responses

The significant rescue of behavioral phenotypes upon re-expression of endogenous *Cdkl5* in adult mice raises the possibility that the molecular and cellular deficits caused by loss of CDKL5 are also reversible. To investigate this, we focused on the aberrant NMDA receptor (NMDAR) signaling phenotypes previously found to be altered in *Cdkl5* knockout and knock-in mice. Specifically, CDD mouse models display an increase in the ratio of NMDA-mediated to AMPA-mediated synaptic responses (NMDA/AMPA EPSC ratio) in the CA1 region of the hippocampus that correlates with an increased susceptibility to NMDA-induced seizures (Okuda et

al., 2017; Tang et al., 2019). The NMDA-mediated synaptic responses in CDD mouse models also display significantly larger decay times, suggestive of a higher contribution of GluN2B-containing NMDARs.

Consistent with our previous studies in *Cdkl5* knockout and knock-in models, we found that the levels of membrane-associated GluN2B in postsynaptic density fractions purified from STOP mice were significantly elevated compared to littermate controls, but detected no change in several other major ionotropic glutamate receptor subunits such as GluA1, GluA2, and GluN2A (Figure 6a-e). Correspondingly, STOP mice also recapitulated the enhanced susceptibility to NMDA-induced seizures as shown in other *Cdkl5* knockout lines (Figure 6f)(Okuda et al., 2017; Tang et al., 2019). These phenotypes were further supported by an increase in the NMDA/AMPA ratio onto CA1 pyramidal neurons of the hippocampus. Additionally, the NMDA-mediated currents displayed a significantly larger decay time constant, highlighting that our STOP mice carry similar NMDAR signaling deficits to other CDD models (Figure 6g-i)(Okuda et al., 2017). Remarkably, we found that late restoration of *Cdkl5* expression was able to reverse these NMDAR synaptic phenotypes. Adult reversal of *Cdkl5* expression, using our established tamoxifen regiment beginning at P42, restored GluN2B expression to Cre-only levels, and consistently attenuated the enhanced susceptibility to NMDA-induced seizures exhibited by STOP-only mice (Figure 6a-f). Furthermore, the ratio of NMDA/AMPA currents and NMDAR-current kinetics were rescued as a result of restoring *Cdkl5*, suggesting reestablishment of control-level NMDAR subunit composition (Figure 6g-i). Together, these findings demonstrate that late restoration of CDKL5 expression attenuates the aberrant NMDAR signaling deficits in the hippocampus that result from CDKL5 loss, underscoring the reversibility of molecular and synaptic signaling deficits present in CDD models.

Adult restoration of *Cdkl5* expression ameliorates CDD-related behavioral deficits in heterozygous female mouse models of CDD

Given the variability introduced from X-chromosome inactivation and mosaic *Cdkl5* expression in females, we confined our initial experiments to hemizygous male knockout animals. However, the majority of carriers for this X-linked disorder are heterozygous females (H. E. Olson et al., 2019). Thus, we expanded upon our initial findings to also examine the reversibility of CDD-related deficits in adult, heterozygous female mouse models of CDD. We generated an independent conditional rescue line, *Cdkl5^{FLEX}*, that, similar to our *Cdkl5^{STOP}* animals allows for temporal control of *Cdkl5* re-expression at its endogenous locus upon Cre-mediated recombination. *Cdkl5^{FLEX}* mice carry an inverted *Cdkl5* exon 4 flanked by two pairs of *loxP* sites that allow for proper cassette re-orientation and gene expression upon tamoxifen delivery (Figure 7a). We crossed this novel conditional rescue line to a second, inducible Cre allele, CAG-CreER. We next delivered tamoxifen to three experimental groups of mice: *Cdkl5^{+/+}; CreER/+* (Cre), *Cdkl5^{FLEX/+}; +/+* (FLEX), and *Cdkl5^{FLEX/+}; CreER/+* (rescue, Res) beginning at P90 using the same regiment applied in our adult knockout experiments (0.3mg·kg⁻¹ every other day for a total of 5 doses). We subsequently assayed a similar battery of behavioral test as in our male rescue studies 3 months later.

An open-field test demonstrated significant hyperactivity of FLEX heterozygous knockouts compared to Cre littermate controls, similar to what is reported for hemizygous *Cdkl5* knockout male mice (Figure 7b). Interestingly, although Res females appeared to also be slightly hyperactive, there was no significant activity change between Cre-only controls and Res mice, suggesting reduced hyperactivity with late *Cdkl5* re-expression (Figure 7b). We also examined sociability behaviors, known to be disrupted in *Cdkl5* knockout male mice, using a 3-chambered social choice test. FLEX female mice spent significantly less time sniffing and directly interacting with a novel stimulus mouse compared to Cre littermate controls, reflecting impaired sociability upon heterozygous *Cdkl5* loss similar to male knockouts (Figure 7c-d). In contrast, Res mice

spent similar amounts of time sniffing and directly interacting with a stimulus mouse as their Cre littermate controls, demonstrating rescued sociability with late *Cdkl5* restoration (Figure 7c-d). FLEX heterozygous females also carry impaired context-dependent memory retrieval in a Pavlovian fear-conditioning paradigm highlighted by reduced time spent freezing upon return to the foot-shock chamber (Figure 7e). Res mice show significantly increased time freezing compared to FLEX knockouts, suggesting improved contextual memory retrieval (Figure 7e). These results suggest that the hyperactivity, sociability, and learning and memory deficits exhibited by hemizygous *Cdkl5* knockout male mice are also recapitulated upon heterozygous loss of *Cdkl5*. More importantly, we demonstrate that these domains appear to be amenable to late kinase rescue in female models of CDD, similar to what we report for hemizygous male mice.

Discussion

Adult restoration of CDKL5 ameliorates several loss-of-function deficits

Several models have been putatively proposed for CDKL5's role in nervous system function, including neuronal signaling, PSD stability, and microtubule dynamics (Lucas L. Baltussen et al., 2018; Fuchs et al., 2014; Ricciardi et al., 2012). However, the absence of a unifying hypothesis likely explains the scarcity of effective therapeutics currently available to reverse or ameliorate CDD. Therefore, gene replacement has been recently explored as a viable strategy for treatment (Gao et al., 2020). A key question along this avenue, however, is whether later restoration of CDKL5 is sufficient to restore normal neurological function or if the absence of CDKL5 results in irreversible abnormalities. If a critical time window of CDKL5 does exist, then later treatment (or gene replacement) may have little effect or even contravening outcomes in a system that has partially compensated for its loss.

Our adult rescue study of CDKL5 highlights the capability of late reversal of *Cdkl5* expression in ameliorating several loss-of-function deficits in mice. Namely, we see significant rescue of anxiety-related behaviors, hyperactivity, autistic-related phenotypes, motor

coordination, hindlimb claspings, and learning and memory impairments, suggesting that the underlying circuitry essential for these behavioral domains is amenable to later kinase restoration. Notably, working memory was not rescued with adult restoration of CDKL5, which aligns with our adult knockout study (Chapter 3) where we accordingly saw no impairment of this behavior upon adult loss of CDKL5. This further reinforces that this behavioral domain and its underlying circuitry may be modulated by CDKL5 during a critical developmental time window in development. Importantly, rescue mice exhibited working memory deficits in spite of their ameliorated hyperactivity phenotype (demonstrated both by the open-field test and total number of alternations on the Y-Maze assay), again suggesting that this behavioral domain is impaired upon loss of CDKL5 independent of motor confounds. These findings also suggest that the reported working memory phenotypes in germline *Cdkl5* knockout animals likely exist independent of any motor activity confounds. Regardless, the promise of late restoration of CDKL5 mitigating several CDD-associated deficits in patients represents an exciting development for the field.

In 2016, IGF-1 treatment in juvenile *Cdkl5* knockout mice was shown to partially rescue dendritic spine instability, and although preliminary clinical trials have demonstrated some success for this therapy in Rett syndrome, its efficacy in CDD patients remains undetermined (Costales & Kolevzon, 2016). CDKL5 protein substitution therapy in knockout mice was also reported to rescue neurological phenotypes, but only with continuous administration. Furthermore, this study exclusively reported on short-term outcomes, and, analogous to IGF-1 therapies, its feasibility and efficacy in CDD patients is untested (Trazzi et al., 2018). Finally, as the majority of these studies were performed in juvenile animals, the reversibility of CDKL5 loss-of-function phenotypes at later ages remains to be addressed. These results, combined with the monogenetic nature of CDD, highlight the pertinence of gene replacement therapy for viable treatment in this highly heterogeneous disease. Previous studies have applied the concept of late gene reversal in rodents to attempt phenotypic rescue in various disease models (Chandran et al., 2017; Guy, Gan, Selfridge, Cobb, & Bird, 2007; James et al., 2012; Y. Mei et al., 2016). Notably, late restoration of *Mecp2* expression in knockout mouse models has been reported to alleviate

impairments associated with Rett syndrome, and adult restoration of *Shank3* is capable of rescuing selective autistic-like phenotypes (Guy et al., 2007; Y. Mei et al., 2016). However, no study to date in rodent models of neurodevelopmental disorders other than CDD has reported rescue of autistic phenotypes using AAV gene therapy (Gadalla et al., 2017; Garg et al., 2013; Gholizadeh, Arsenault, Xuan, Pacey, & Hampson, 2014). This pernicious lack of effective gene therapy treatments for neurodevelopmental syndromes highlights the potential for gene replacement in CDD to set the stage for future attempts at widespread CNS delivery of gene vectors to treat the heterogeneous assortment of symptoms associated with these disorders. As mentioned, a preliminary gene therapy study in *Cdkl5* knockout mice achieved successful AAV-*hCDKL5* development and expression of CDKL5, but only in hindbrain regions (Gao et al., 2020). Although this was capable of partially restoring some motor coordination deficits in this model, further work is needed to improve upon forebrain and CNS-wide delivery of *CDKL5*. Nevertheless this study, together with our findings, highlights the promise of late gene restoration in successfully alleviating CDD-associated impairments.

CDKL5 and NMDA receptor signaling

Our results suggest that loss of CDKL5 is capable of regulating post-synaptic localization of NMDA receptor subunits, namely GluN2B, with resultant behavioral effects on NMDA-induced hyperexcitability. During development, the canonical switch from predominantly GluN2B-containing to GluN2A-containing NMDA receptors across the CNS is thought to be a regulatory mechanism involved in shaping circuit plasticity during the critical period of synaptogenesis for several brain regions (Paoletti, Bellone, & Zhou, 2013). Interestingly, the peak expression of CDKL5 in mouse forebrain appears to coincide with this subunit composition switch during a time window also associated with circuit refinement and acquisition of learning abilities (Shipton & Paulsen, 2014). Our results in STOP mice are unable to demonstrate whether this phenotype is a result of a failed switch from GluN2B to GluN2A early in development, or a continual role of CDKL5 in maintaining receptor subunit composition at the post-synaptic membrane. Our gene

reversal study demonstrates that this aberrant GluN2B expression and NMDA hyperexcitability phenotype is reversible upon late restoration of CDKL5, arguing that CDKL5 may continuously regulate NMDA receptor composition rather than carry a specific function early in development. However, the direct role of the kinase within this domain remains to be dissected. Interestingly, CDKL5 has been reported to target EB2 pS222 via an NMDAR-dependent mechanism, providing a potential link between disrupted NMDAR signaling, microtubule dynamics, and CDKL5 loss-of-function phenotypes (Lucas L. Baltussen et al., 2018). While we see a significant reduction in EB2 phosphorylation at Ser222 in STOP mice, this reduction is restored to nearly Cre control levels upon adult rescue of CDKL5. Still, a more mechanistic examination of the role of EB2 phosphorylation, and its effects on synaptic maturation, is needed before a direct role for CDKL5 in this pathway can be corroborated.

Modeling and treating CDD-related phenotypes in heterozygous female mice

The final component of this study demonstrates that several behavioral domains disrupted in hemizygous knockout mouse models of CDD are also impaired in heterozygous females of our second, novel knockout line (*Cdkl5^{FLEx}*). These findings further confirm that heterozygous *Cdkl5* knockout female mice can serve as a viable pre-clinical model for CDD. Importantly, we also demonstrate that late restoration of *Cdkl5* expression in these females ameliorates several CDD-related deficits, similar to what we reported in hemizygous male rescue mice. Our future work aims to provide a more in-depth analysis on the reversibility of additional CDKL5 loss-of-function phenotypes in this female model, however, these initial results provide promising evidence that the findings of our hemizygous male studies may also extend to female CDD models.

In contrast to the pervasive epilepsy in CDD patients, the absence of an overt seizure phenotype in *Cdkl5* knockout male mice could contribute to the success of phenotypic reversibility found in this study. This is particularly pertinent given that in the subsequent chapter (Chapter 5), we report the occurrence of spontaneous and disturbance-associated seizures exclusively in

heterozygous *Cdkl5* knockout female mice. This epilepsy phenotype appears to increase in frequency and severity with age, with a median age of onset around 28-30 weeks. Although our behavioral testing was confined to heterozygous females within 21-25 weeks of age (prior to seizure development), we cannot exclude the fact that an altered seizure susceptibility or circuit hyperexcitability may affect the reversibility of certain deficits in heterozygous female models, particularly after seizure onset. In the future, it will be necessary to extend these experiments to aged (seizing), heterozygous female mouse models of CDD, determine the minimum and maximum levels of CDKL5 expression required for safe phenotypic reversal, and define the latest time window allowable for rescue, at least in mouse models. In the subsequent chapter, we expand upon this analysis of heterozygous female models of CDD, and provide promising insights into the treatability of these seizure-like phenotypes specifically.

Materials and Methods

Regulatory approval. Experiments were conducted in accordance with the ethical guidelines of the National Institutes of Health and with the approval of the Institutional Animal Care and Use Committee of the University of Pennsylvania. Mice were group-housed in cages of two to five in a twelve-hour light/dark cycle with food and water provided *ad libitum*.

Mouse strains and genotyping. *Cdkl5*^{STOP} mice were generated in collaboration with Biocytogen using CRISPR-mediated genomic editing techniques. A selected gRNA (TGCAACTACAGCATTAGCTCTGG) was chosen upon screening of 12 candidates for targeting specificity and efficacy at intron 3 of the *Cdkl5* locus. The DNA repairing template constituted a *loxP*-flanked transcriptional STOP cassette, flanked by 817bp of DNA as the 5' homologous arm and 1453bp of DNA as the 3' homologous arm. Synthesized gRNA, purified and linearized DNA repairing template, as well as Cas9 mRNA were co-injected into a one-cell zygote of C57BL/6 background to allow for homology-directed repair, followed by implantation. PCR primers specific to the 5' and 3' integration sites flanking the gRNA sequence at *Cdkl5* intron 3 were used to

screen for positively targeted pups. Southern blotting was finally conducted to confirm the correct targeting of the F1 generation, followed by establishment a *Cdkl5* floxed-STOP (STOP) colony in a C57BL/6J genetic background.

Cdkl5^{FLEX} mice were generated in collaboration with Biocytogen using CRISPR-mediated genomic editing techniques. A pair of gRNAs (TGCAACTACAGCATTAGCTCTGG & TTTCACAGTAGGTTACCCAGGGG) were chosen upon screening of 22 candidates for targeting specificity and efficacy at introns 3 and 4 of the *Cdkl5* locus. The DNA repairing template constituted the endogenous *Cdkl5* exon 4 flanked by a pair of *mloxP* and *loxP* sites, all flanked by 888bp of DNA as the 5' homologous arm and 1800bp of DNA as the 3' homologous arm. Synthesized gRNA, purified and linearized DNA repairing template, as well as Cas9 mRNA were co-injected into a one-cell zygote of C57BL/6 background to allow for homology-directed repair, followed by implantation. PCR primers specific to the 5' and 3' integration sites flanking the gRNA sequence at *Cdkl5* exon 4 were used to screen for positively targeted pups. Southern blotting was finally conducted to confirm the correct targeting of the F1 generation, followed by establishment a *Cdkl5* FLEX (FLEX) colony in a C57BL/6J genetic background.

UBC-CreER (Stock No. 007001) mice and CAG-CreER (Stock No. 004682) mice were obtained from the Jackson Laboratories. All lines have been maintained in the C57BL/6J background.

Experimental cohorts were all weaned at 3 weeks of age and littermates housed together. For genotyping of UBC-CreER and CAG-CreER transgenics, primers and genotyping strategy were identical to that used by Jackson Laboratories. *Cdkl5*^{STOP} and *Cdkl5*^{FLEX} mice were genotyped using a qPCR based strategy optimized by Transnetyx to detect the presence of a *loxP*-flanked STOP cassette within intron 3 of the endogenous *Cdkl5* gene and the inversion of exon 4 of the endogenous *Cdkl5* gene, respectively.

Tamoxifen preparation and administration. Tamoxifen (Sigma, T5648) was dissolved in corn oil (Sigma, C8267) at a concentration of 20mg·ml⁻¹ by vortexing and slowly heating the solution at

40°C for approximately one hour. Freshly prepared tamoxifen was protected from light by aluminum foil and stored at 4°C for a maximum of one week. Animal feeding needles from Roboz Surgical Store (20 gauge, 1.5" length, curved; FN-7910) were used for oral gavage delivery of 0.3mg·kg⁻¹ of tamoxifen every other day for a total of five doses. For adult restoration of *Cdkl5*, a slower dosage timeline was introduced to avoid the lethality associated with rapid reintroduction of CDKL5: *Cdkl5*^{+/y}; CreER/+, *Cdkl5*^{STOP/y}; +/+, and *Cdkl5*^{STOP/y}; CreER/+ cohorts all received 0.3mg·kg⁻¹ of tamoxifen once a week for a total of three weeks, and then two subsequent booster deliveries every other day after the third dose (total of 5 doses). See schematic in Figure 3a for details. All genotypes received tamoxifen within each experimental cohort.

Behavioral assessments. All animal behavioral studies were carried out blinded to genotype. Mice were allowed to habituate to the testing room for at least 1 hr before the test, and testing was performed at the same time of day. All animal behaviors were performed on adult male and female mice between postnatal days 120-160, and the analysis of behavioral data was carried out by a researcher blinded to genotype.

Elevated zero-maze. The elevated zero-maze (San Diego Instruments; California, USA) consists of a circular-shaped platform elevated 3 feet above the floor. Two opposite quadrants of the maze are enclosed (wall height, 12 inches), whereas the other two are open (wall height, 0.5 inches). Mice were placed in one of the closed quadrants and their movement traced over the course of 5 min. Analysis, including the quantification of percent of time spent in open arms and the number of entries, was performed manually using a stopwatch. An entry was defined as a transition from a closed to open arm, or vice versa, that involves all four paws. Total distance traveled over the entire assay was measured by a ceiling-mounted camera coupled to a video-tracking software (SmartScan 3.0), allowing for real-time analysis of all movements.

Open-field test. Locomotor activity was measured via an open-field test where mice were individually placed into, and allowed to explore, a 15" x 15" arena for a total of 60 min. A ceiling-mounted camera allowed for a video-tracking software (SmartScan 3.0) to real-time analyze the

total distance traveled as well as the percent time spent in the center of the arena (defined as the central 25% of the total area).

Y-maze. Spontaneous alternation behavior was measured on a Y-maze apparatus (San Diego Instruments; California, USA), composed of three arms (Arm A: 8in. x 5in. x 3in.; Arms B and C: 6in. x 5in. x 3in.). For testing, the mouse was placed in Arm C, facing the center, and allowed to freely explore the maze for 5 min. A spontaneous alternation was defined an entry into the arm less recently explored. Percent spontaneous alternation was calculated as the number of spontaneous alternations over the total number of entries. For example, the sequence C,B,A,B,C,B,A,C (starting in arm C) resulted in a percent spontaneous alternation of $4/6 = 67\%$.

Three-chambered social approach assay. The social choice test was carried out in a three-chambered apparatus that consisted of a center chamber and two end chambers. Before the start of the test and in a counter-balanced sequence, one end chamber was designated the social chamber, into which a stimulus mouse would be introduced, and the other end chamber was designed the nonsocial chamber. Two identical, clear Plexiglas cylinders with multiple holes to allow for air exchange were placed in each end chamber. In the habituation phase of the test (Phase I), the test mouse was placed in the center chamber and allowed to explore all three chambers for 10 min. During this acclimation period, baseline measurements of how much time the mouse spent in each of the three chambers and the distance traveled by the test mouse were collected. In the social choice phase of the test (Phase II), an age-matched stimulus mouse (adult, gonadectomized A/J mice) was placed in the cylinder in the social chamber while a novel object was simultaneously placed into the other cylinder in the nonsocial chamber. During the subsequent 10 min social choice period, chamber times and numbers of transitions among chambers were again recorded as well as the percent time spent sniffing the social cylinder. In the direct social interaction test, the cylinders were removed simultaneously following the social choice test, and the amount of time test and stimulus mice spent in direct contact (sniffing, allogrooming) was measured for a total of 5 min. If fighting persisted for more than several seconds, the mice were removed from the apparatus and excluded from the study.

Accelerating rotarod assay. Mice were placed on an accelerating rotarod apparatus (Harvard Apparatus) for 16 trials (four trials a day for four consecutive days) with at least 15 min of rest between the trials. Each trial lasted for a maximum of 5 min, during which the rod accelerated linearly from 4 to 40 rpm. The amount of time for each mouse to fall from the rod was recorded for each trial.

Context- and cue-dependent fear conditioning. For the training day, mice were placed in individual chambers (Med Associates) for 2 min followed by a loud tone (85 dB, 2 kHz) lasting 30 s that coterminated with a 2-s, 1.25-mA foot shock. Mice were left undisturbed for an additional 30 s in the chamber and then immediately placed back into their home cage. Freezing behavior, defined as no movement except for respiration, was determined before and after the tone-shock pairings and scored by FreezeScan NI version 2.00. To test for context-dependent learning, we placed mice back into the same testing boxes 24 hr later for a total of 5 min without any tone or shock, and again measured the total time spent freezing. After 4 hrs, we tested for cue-dependent fear memory by placing the mice into a novel chamber consisting of altered flooring, wall-panel inserts, and vanilla scent. After 2 min in the chamber, the cue tone (85 dB, 2 kHz) was played for a total of 3 min, and the total time spent freezing during the presentation of this cue tone was recorded.

Olfaction. Mice were tested for whether they could detect and differentiate odors in a habituation-dishabituation protocol modified from Yang and Crawley (Yang & Crawley, 2009). Mice were presented with cotton-tipped wooden applicators dipped in either water, vanilla, or swiped across the bottom of an unfamiliar social cage. Each stimulus was presented for 2 min with a 1-min inter-trial interval. Time spent sniffing was defined as when the animal was oriented with its nose 2 cm or closer toward the cotton tip.

Repetitive behavior. Mice were individually placed into a clean, home-cage like environment lined with bedding. After allowing 5 min for habituation, 10 min of activity was videotaped for each mouse. The duration of repetitive behavior, defined as grooming or digging, was scored manually using a stopwatch.

Hindlimb clasping. Mice were suspended by the base of their tail at least 6 inches above a flat surface for up to 1 min. If the hindlimbs were consistently splayed outward, away from the abdomen, the mouse was assigned a score of 0. If one hindlimb was retracted towards the abdomen for more than 50% of the time, the score was 1. If both hindlimbs were partially retracted for greater than 50% of the time, the score was 2. Finally, if both hindlimbs were entirely retracted and touching the abdomen for more than 50% of the time suspended, the mouse received a score of 3.

Brain microdissection. To assess CDKL5 protein expression in various brain regions, adult male mice were sacrificed by cervical dislocation. After decapitation, brains were removed and sectioned into 1mm coronal slices using a mouse brain matrix. Tissue was dissected from the somatosensory cortex, striatum, hippocampus, and cerebellum and homogenized in RIPA lysis buffer (150mM NaCl, 1% Triton X-100, 0.5% sodium deoxycholate [DOC], 0.1% sodium dodecyl sulfate [SDS], 25mM Tris [pH7.4] with protease inhibitors [Roche, cOmplete, EDTA-free protease inhibitor cocktail tablets; 5056489001]). To prepare protein extracts, homogenized lysates were incubated on ice for 15 min, and then centrifuged at 21,000 x g for 15min at 4°C. The supernatant fraction was removed and sonicated using a Biorupter for 3 alternating session at max frequency for 15 sec, each followed by a 60 sec cooldown period. The lysate was then centrifuged at 21,000 x g for 15min at 4°C, and the top aqueous layer carefully removed and collected as the total protein fraction.

Postsynaptic density protein purification. We adapted a widely used protocol for the preparation of PSD fractions that we previously reported on (Bermejo et al., 2014; Tang et al., 2019). Mice were sacrificed via cervical dislocation, and their brains quickly extracted. Forebrain cortical tissues were microdissected and Dounce-homogenized in 10mL of homogenization buffer (0.32M sucrose, 4mM HEPES, pH 7.4 with protease inhibitors [Roche, cOmplete, EDTA-free protease inhibitor cocktail tablets; 5056489001]). The homogenate was centrifuged at 1000 x g

for 10 min at 4°C to pellet cellular debris and nuclei (P1), and the subsequent supernatant (S1) was centrifuged for another 15 min at 10,000 × g at 4°C. The resulting pellet (P2, “crude” synaptosomes) was re-suspended in another 10mL of homogenization buffer and centrifuged at 10,000 × g for 15 min at 4°C. The supernatant was discarded, and the resulting pellet (P2’) was re-suspended in 10mL of 4mM HEPES (pH 7.4) then homogenized on ice. The lysate was incubated at 4°C for 30 min while shaking to hypo-osmotically lyse the synaptosomes, and then centrifuged for 20 min at 25,000 × g at 4°C. The resultant pellet (LP1) was re-suspended in 1 mL of homogenization buffer and layered on top of a discontinuous sucrose gradient (bottom to top: 1.5mL of 1.2M sucrose, 1mL of 1.0M sucrose, and 1mL of 0.8M sucrose). The gradient was ultracentrifuged at 150,000 × g for 1.5hr at 4 °C. The turbid layer between the 1.0/1.2 M sucrose interphase containing the synaptic plasma membranes (~1mL) was collected and re-suspended in 5mL of 4mM HEPES to dilute out the sucrose. This fraction was ultracentrifuged again at 200,000 × g for 30 min at 4°C. The resulting pellet was re-suspended in 1mL of 50mM HEPES with 2mM EDTA (pH 7.4), and the membrane proteins extracted by adding Triton X-100 at a final concentration of 0.5% and incubating at 4°C while rotating for 15 min. The proteins were centrifuged at 32,000 × g for 20 min at 4°C, and the resulting pellet re-suspended in 75µL of 50mM HEPES with 2 mM EDTA.

Western blot. Protein concentration was measured using a Bradford assay. Purified synaptic density membrane proteins or protein lysates were prepared for gel electrophoresis by adding 4X LDS Sample Buffer (NuPAGE, NP0008) to a final concentration of 1X and β-mercaptoethanol to a final concentration of 5%. Samples were heat-denatured at 75°C for 20 min, and 7.5µg or 25 µg of protein was loaded into each well of a 4–12% Bis-Tris gradient gel (Invitrogen, 10-well, 1.5mm; NP0335) for PSD protein or brain lysate quantification, respectively. Protein gels were run for 2hr at 125V at room temperature on a XCell SureLock mini-cell electrophoresis box (ThermoFisher; EI001) using a PowerPac HC High-Current Power Supply (BioRad; 1645052), then transferred onto a polyvinylidene fluoride (PVDF) membrane (0.45µm pore-size; Biorad 162–0115) at 27V for

1hr and 10min at room temperature. The resulting membrane was blocked with a 1:1 solution of Odyssey blocking buffer (LICOR; 927-40100) and 1X PBS for 1hr at room temperature.

Primary antibodies used were rabbit anti-N-terminal CDKL5 (in house; diluted 1:500), mouse anti- β -Actin (Abcam; ab8226; diluted 1:10,000), rat anti-EB2[K52] (Abcam, ab45767; diluted 1:10,000), and rabbit anti-phospho-EB2[S222] (generously shared by Dr. Sila Ultanir at the Francis Crick Institute; London, UK; diluted 1:1000). For postsynaptic density studies, the primary antibodies used were rabbit anti-N-terminal CDKL5, mouse anti-GluN1 (ThermoFisher, OMA1-04010; diluted 1:1000), rabbit anti-GluN2A (Frontier Institute, AB_2571605; diluted 1:200), rabbit anti-GluN2B (Frontier Institute AB_2571761; diluted 1:200), rabbit anti-GluA1 (Abcam, ab31232; diluted 1:5000), rabbit anti-GluA2 (Abcam, ab133477; diluted 1:5000), and anti- β -Actin. Secondary antibodies (LI-COR) used were goat anti-rabbit IgG IRDye800CW, rabbit anti-mouse IgG IRDye680LT, and goat anti-rat IRDye680LT, all incubated for 50min at room temperature at dilutions of 1:10,000. Standard protocols were used for the Odyssey Infrared Imaging System (LI-COR) for protein visualization and quantification.

NMDA-induced seizure scoring. Seizures were induced in postnatal day 180 mice by intraperitoneal administration of 90 mg·kg⁻¹ NMDA (Sigma-Aldrich; M3262) in sterilize, 0.9% PBS. Seizure progression was scored using a modified Racine scale as previously described: (0) no abnormality; (1) exploring, sniffing, and grooming ceased, animal becomes motionless; (2) forelimb and/or tail extension, appearance of rigid posture; (3) myoclonic jerks of the head and neck, with brief twitching movement, or repetitive movements with head bobbing or “wet-dog shakes”; (4) forelimb clonus and partial rearing, or rearing and falling; (5) forelimb clonus, continuous rearing and falling; (6) tonic-clonic movements with loss of posture tone, often resulting in death(Okuda et al., 2017). After drug injection, max seizure scores were recorded within a 30 min observation period.

Electrophysiology recordings. Mice were deeply anesthetized using isoflurane and perfused transcardially with ice-cold ACSF (pH 7.3 – 7.4) containing (in mM): 124 NaCl, 2.5 KCl, 1.2 NaH₂PO₄, 24 NaHCO₃, 5 HEPES, 12.5 glucose, 1.3 MgSO₄, 7H₂O, 2.5 CaCl₂. The brain was rapidly removed, and transverse sections (400 μ M) were cut on a vibratome (VT 1200s, Leica). Slices were incubated in a holding chamber for 12-15 minutes at 32-34°C in a NMDG-based recovery solution (pH 7.3-7.4, pH adjusted with HCl) (in mM): 92 NMDG, 2.5 KCl, 1.2 NaH₂PO₄, 30 NaHCO₃, 20 HEPES, 25 glucose, 5 sodium ascorbate, 2 thiourea, 3 sodium pyruvate, 10 MgSO₄, 7H₂O, 0.5 CaCl₂. Osmolarity for the NMDG-based solution and ACSF was kept between 300-310 mOsm. Following incubation, slices were moved to a second holding chamber containing ACSF at room temperature (20-22°C) for at least 1 hr. prior to recording. For recording, slices are transferred to the recording chamber (Scientifica) fully submerged in oxygenated (95% O₂, 5% CO₂) ACSF at a perfusion rate of 1.4-1.6 mL/min, bath temperature of 29-30°C, and secured using a slice anchor (Warner Instruments). Electrophysiology data were acquired using custom-built Recording Artist software version (Rick Gerkin), Igor Pro 6.37 (Wavemetrics). All recordings were sampled at 20kHz, filtered at 2.8kHz.

Evoked AMPA/NMDA currents. CA1 pyramidal neurons were visualized using differential interference contrast (DIC) video microscopy on an upright microscope (Olympus, BX51). Somatic whole-cell recordings were performed using borosilicate glass (World Precision Instruments, TW150-3) that had a tip resistance of 3-5 M Ω , filled with cesium-based internal for voltage-clamp recordings (in mM): 115 CsMeSO₃, 20 CsCl, 10 HEPES, 0.6 EGTA, 2.5 MgCl, 10 Na-Phosphocreatine, 4 Na-ATP, 4 Na-GTP, 0.1 Spermine, 1 QX-314 (pH adjusted to 7.3-7.4 with CsOH). A bipolar theta glass electrode backfilled with ACSF was positioned in the Schaffer collaterals for electrical stimulation. Stimulation intensity was adjusted to evoke single component EPSCs with a frequency of 0.1Hz. Voltage-clamp traces were recorded at a holding potential of -70 mV (for AMPA-EPSCs) or +40 mV (for NMDA-EPSCs) in the presence of 100 μ M picrotoxin (Sigma-Aldrich). For each cell, at least 15 traces were averaged to obtain a representative

response at each holding potential. The peak EPSC amplitude at -70 mV was taken as the magnitude of the AMPA-EPSCs. To isolate the NMDA-mediated current, 10 μ M NBQX (Abcam) was bath-applied and blockade of AMPA-mediated currents was confirmed at -70mV. To calculate the NMDA/AMPA ratio, the amplitude taken at +40mV in the presence of NBQX was divided by the peak amplitude of the AMPA-EPSC at -70mV. The access resistance was monitored throughout the experiment and data was excluded if access resistance increased above 20 M Ω . The decay time constant of NMDAR-mediated EPSCs was calculated with a single-exponential fit in Igor 7.

Statistical Analysis. For behavioral assays, we chose similar sample sizes for all behavioral experiments based on previous published studies of *Cdk15* constitutive knockout mice and *Cdk15* conditional knockout mice (Tang et al., 2019; Tang et al., 2017; I. T. Wang et al., 2012). Importantly, the number of mice used was pre-determined prior to the start of each experiment. Statistical analyses were performed using Prism (GraphPad). All data sets were analyzed using the Shapiro-Wilk test for normality. For one-sample comparisons, data sets with normal distributions were analyzed for significance using the one-sample *t*-test, whereas data sets with non-normal distributions were analyzed using the Wilcoxon signed-rank test. For two-sample comparisons, data sets with normal distributions were analyzed for significance using the unpaired Student's *t*-test, whereas data sets with non-normal distributions were analyzed using the Mann-Whitney test. Two-way repeated measures ANOVA or the Kruskal-Wallis test was conducted for the appropriate data sets with *post hoc* Sidak's or Dunn's multiple-comparisons tests. All one-sample, two-sample, and multiple-comparison tests were two-tailed.

For NMDA seizure induction experiments, we tested a pilot cohort of wild-type and *Cdk15* knockout animals at various doses of NMDA to establish an effect size in our own hands on this reported phenotype. This enabled proper power analysis to determine the appropriate sample size for our experimental cohorts (n=10 at 90 mg·kg⁻¹). Max seizure scores were statistically analyzed using the Kruskal-Wallis test and *post hoc* Dunn's multiple comparisons test for

significance. Similarly, we referenced reported effect sizes for NMDA/AMPA ratio phenotypes reported in mouse models of CDD and related models of neurodevelopmental disorders in order to determine proper sample sizes for our physiology experiments. To analyze significance, we conducted One-way ANOVA with *post hoc* Tukey's multiple-comparisons test.

All graphs are plotted using Prism (GraphPad). Bolded center lines reflect the mean, and all error bars indicate s.e.m. For boxplots, the limits indicate the minimum and maximum with boxplot center line indicating the median. In our figures, *p*-values between 0.05 and 0.1 are shown explicitly, * is used to denote all $0.01 < p < 0.05$, ** for $0.001 < p < 0.01$, *** for $0.0001 < p < 0.001$, and **** for $p < 0.0001$.

Figures

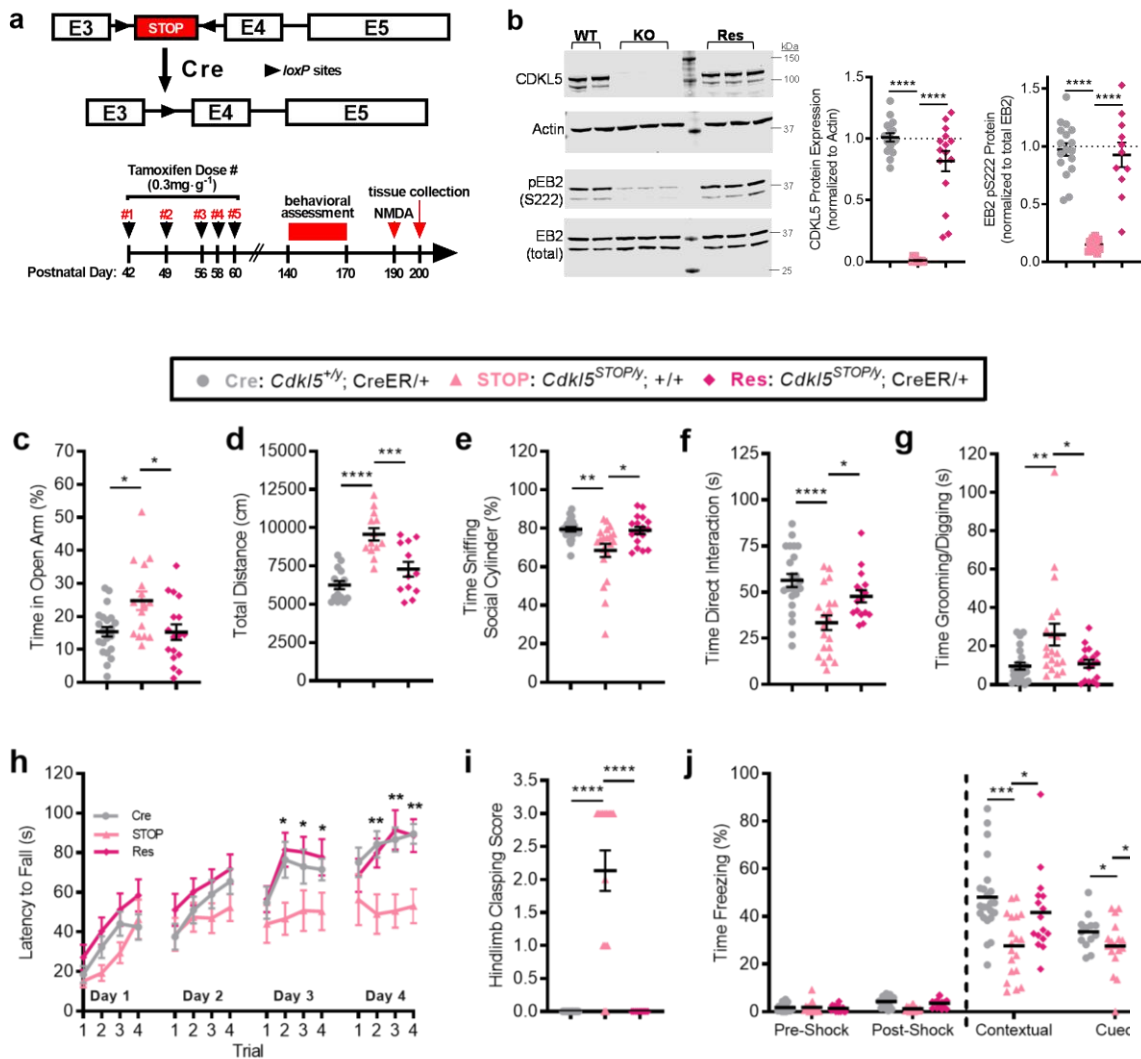


Figure 1: Adult restoration of *Cdkl5* expression rescues CDD-associated behavioral deficits.

(a) Top: schematic of conditional rescue approach in *Cdkl5^{STOP}* mice where a *loxP*-flanked transcriptional STOP cassette can be removed in the presence of Cre; Bottom: tamoxifen administration scheme and experimental schedule. **(b)** Left: representative western blot demonstrating restored CDKL5 protein expression in *Cdkl5^{STOP/+}*; CreER/+ (Res) mice, but not *Cdkl5^{STOP/+}*; +/+ (STOP) mice, to nearly *Cdkl5^{+/-}*; CreER/+ (Cre) levels with tamoxifen administration concomitant with significant rescue of phosphorylation of EB2 at Ser222 but no change in total EB2 levels; Right: quantification of CDKL5 and EB2 pSer222 protein levels in forebrain tissues of all genotypes demonstrates significant rescue of both in Res mice upon

tamoxifen administration. **(c)** STOP mice, but not Res mice, spend significantly more time than Cre littermates in the open arm of the elevated zero-maze assay suggestive of decreased anxiety that is rescued in Res animals. **(d)** STOP mice travel significantly more distance in the open-field assay than Cre and Res littermates, demonstrating rescued hyperactivity in Res animals. **(e)** STOP mice spent significantly less time sniffing and **(f)** directly interacting with a stimulus mouse during the 3-chambered social choice test compared to Cre and Res littermates, highlighting rescued sociability phenotypes in Res animals. **(g)** STOP mice, but not Res mice, spend significantly more time grooming and digging in a home cage-like environment, demonstrating aberrant repetitive behaviors that are rescued in Res animals. **(h)** STOP mice take significantly less time to fall from an accelerating, rotating rod, suggestive of impaired motor coordination, whereas Res mice fall at a similar latency to Cre littermate controls demonstrating rescue of motor coordination. **(i)** STOP mice present with hindlimb clasping behaviors, whereas no Cre or Res mice were observed to carry hindlimb clasping phenotypes. **(j)** STOP and Res mice freeze in response to a mild footshock similarly to Cre littermates, but STOP mice show decreased percent time freezing compared to Cre and Res littermates when returned to the testing chamber (contextual) and upon hearing the testing tone (cue), demonstrating impaired learning and memory selectively in STOP mice that is restored in Res mice. For all panels: Cre, n=23; STOP, n=20; Res, n=17 where all genotypes received tamoxifen; Kruskal-Wallis test with Dunn's multiple comparisons test (except Rotarod: 2-way repeated measures ANOVA with Sidak's multiple comparisons test). *p<0.05, **p<0.01, ***p<0.001, ****p<0.0001. Bars represent mean ± SEM.

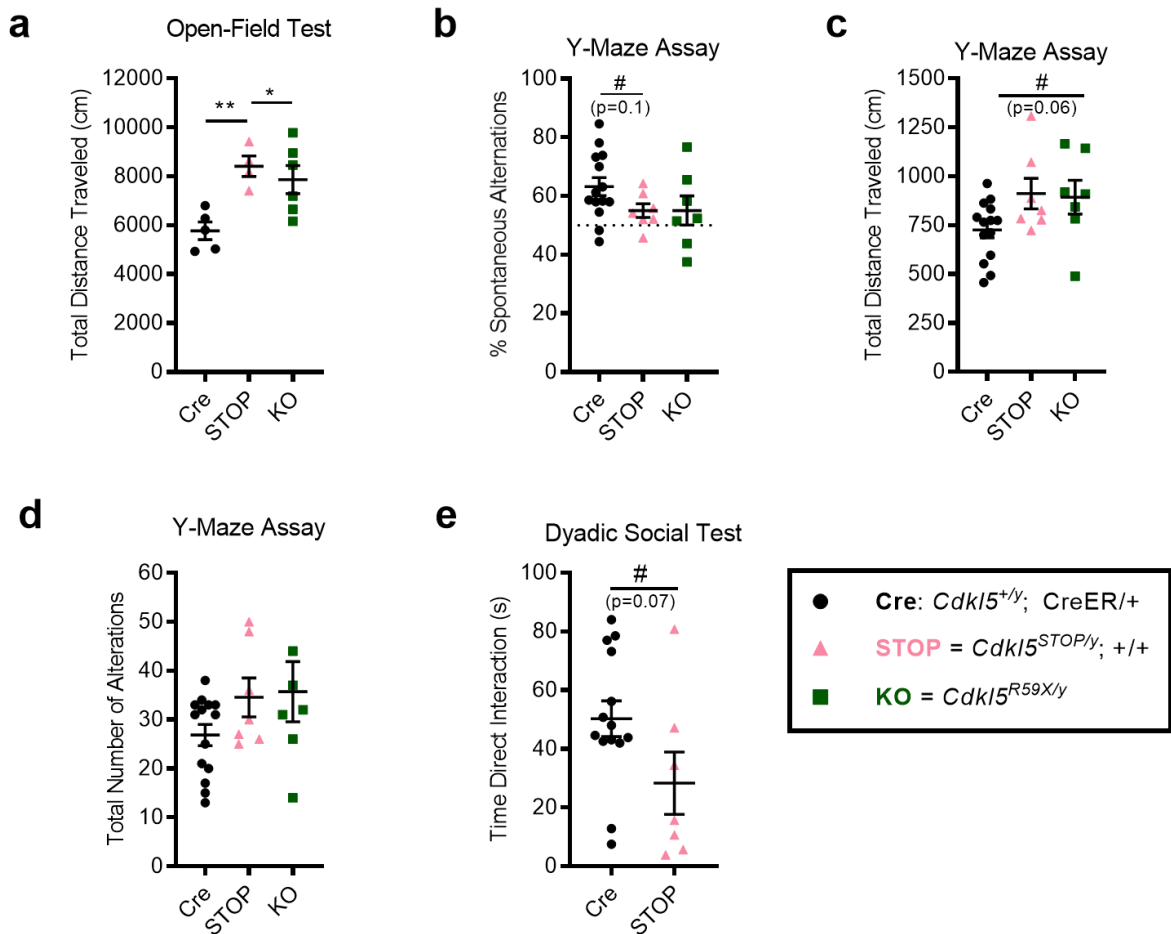


Figure 2. STOP mice are behaviorally similar to *Cdk15* germline knock-in mice by postnatal day 42.

(a) STOP and KO mice move significantly more in the open-field test compared to Cre controls suggestive of hyperactivity. **(b)** STOP and KO mice show a trending decrease in percentage of spontaneous alternations during the Y-Maze assay compared to Cre controls suggestive of impaired working memory. STOP and KO mice also **(c)** travel significantly more and **(d)** make more total alternations compared to Cre controls in the Y-Maze assay. **(e)** STOP mice spend less time directly interacting with a novel stimulus mouse during a dyadic social test, demonstrating decreased sociability as reported for other *Cdk15* knockout and knock-in lines. For all panels: n=14 Cre (*Cdk15*^{+/-}; CreER/+); n=7 STOP (*Cdk15*^{STOP/+}; +/+); n=7 KO (*Cdk15*^{R59X/+}) all at postnatal day 42. Kruskal-Wallis test with Dunn's multiple comparisons test (except dyadic social: Mann-Whitney test); *p<0.05, **p<0.01. Bars represent mean ± SEM.

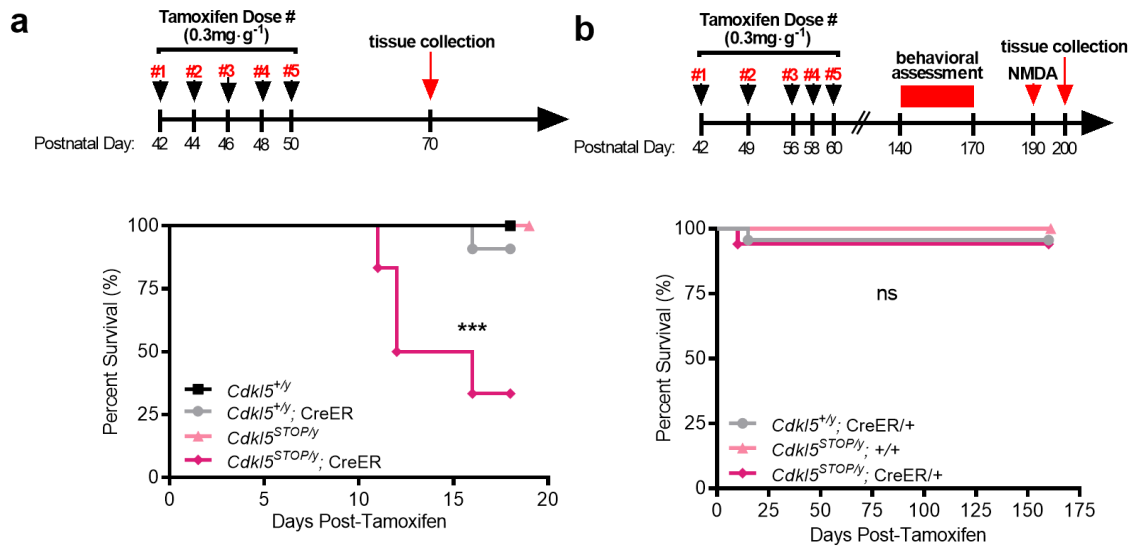


Figure 3. Rapid, but not gradual, reversal of *Cdkl5* expression is associated with significant lethality.

(a) Top: tamoxifen administration schematic (rapid); Bottom: survival curve demonstrating significant lethality in $Cdkl5^{STOP/y}; CreER/+$ mice, exclusively, with tamoxifen delivery suggesting rapid *Cdkl5* reintroduction could be detrimental (n=8 $Cdkl5^{+/y}; +/+$; n=11 $Cdkl5^{+/y}; CreER/+$; n=8 $Cdkl5^{STOP/y}; +/+$; n=6 $Cdkl5^{STOP/y}; CreER/+$). **(b)** Top: tamoxifen administration schematic (gradual); Bottom: survival curve demonstrating no significant difference in lethality between $Cdkl5^{STOP/y}; CreER/+$ mice and other genotypes with tamoxifen delivery, suggesting that gradual *Cdkl5* reintroduction mitigates lethality associated with its re-expression (n=23 $Cdkl5^{+/y}; CreER/+$; n=20 $Cdkl5^{STOP/y}; +/+$; n=17 $Cdkl5^{STOP/y}; CreER/+$). For all panels: all genotypes received tamoxifen; Mantel-Cox (log-rank) test; *p<0.05, **p<0.01, ***p<0.001.

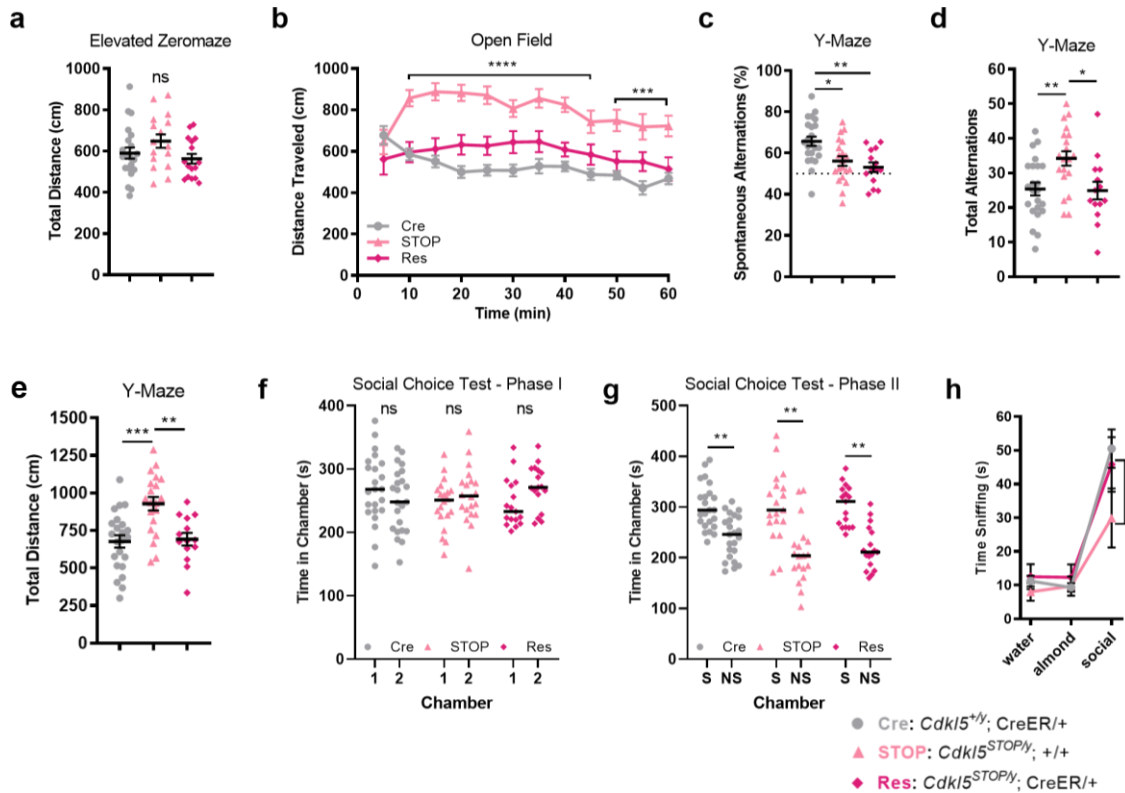


Figure 4. Additional behavioral domains analyzed upon adult rescue of *Cdk15*.

(a) Total distance traveled during the elevated Zero-maze assay was similar between Cre, STOP, and Res mice. (b) STOP, but not Res, mice traveled significantly more in an open-field assay relative to Cre littermates over the course of one hour (distance traveled binned in 5min intervals) suggestive of rescued hyperactivity in Res mice. (c) STOP and Res mice show a significant decrease in percentage of spontaneous alternations in a Y-Maze assay compared to Cre littermates, suggestive of impaired working memory. (d) STOP, but not Res, mice make significantly more total number of alternations and (e) travel more distance during the Y-Maze when compared to Cre littermate controls further highlighting rescued hyperactivity in Res animals. (f) Cre, STOP, and Res mice all spent equal time exploring chamber 1 and chamber 2 during Phase I of the 3-chambered social choice test (prior to any social/non-social stimulus presentation). (g) Cre, STOP, and Res mice all spent significantly more time in the chamber containing a social stimulus (S; novel mouse) over a non-social stimulus (NS; rock) during Phase II of the 3-chambered social choice test. (h) Cre, STOP, and Res mice all spent significantly more time sniffing a social scent over either water or almond scents, with STOP mice spending significantly less time than Cre or Res animals sniffing the social scent. For all panels: Cre, n=23; STOP, n=20; Res, n=17 where all genotypes received tamoxifen; Kruskal-Wallis test with Dunn's multiple comparisons test (except open field & olfaction: two-way, repeated measures ANOVA with Dunnett's multiple comparisons test & social choice test: paired t test); *p<0.05, **p<0.01, ***p<0.001, ****p<0.0001. Bars represent mean \pm SEM.

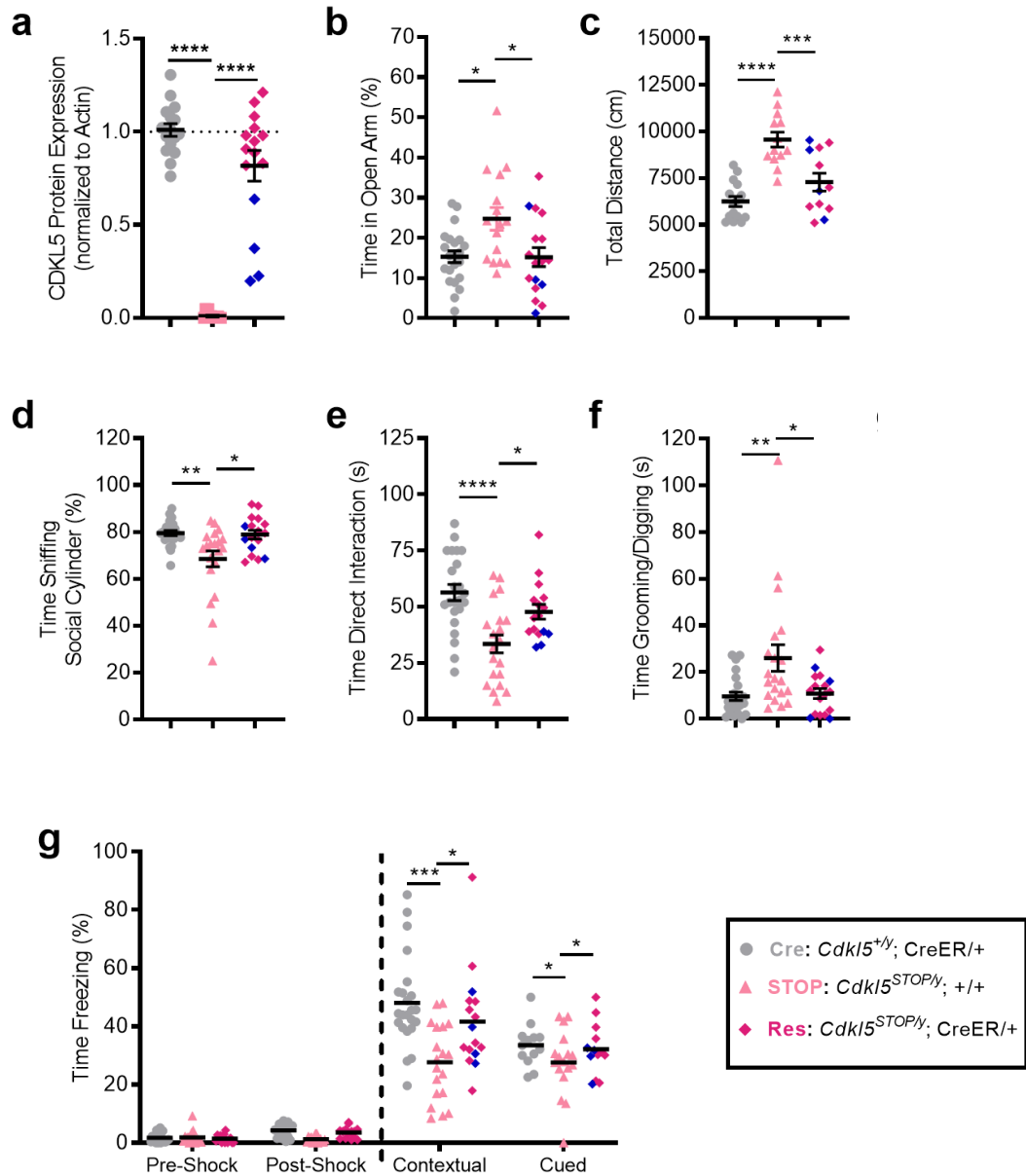


Figure 5. Partial restoration of CDKL5 protein is capable of rescuing multiple behavioral domains.

All panels reference data from Figure 1 with four partial rescue (Res) animals highlighted in blue. **(a)** Quantification of western blot results for CDKL5 protein levels in forebrain tissues of all genotypes demonstrates significant rescue of CDKL5 protein to nearly Cre-only levels in most Res, but not STOP, mice upon tamoxifen administration except for four animals (highlighted in blue) demonstrating between 20-60% CDKL5 protein restoration. Results from the **(b)** elevated zero-maze assay, **(c)** open-field assay, **(d-e)** 3-chambered social choice test, **(f)** repetitive

behavior assay, and **(g)** fear conditioning paradigm highlight that the four Res animals not showing full CDKL5 protein restoration (blue diamond) still cluster with the remaining Res animals versus STOP mice, demonstrating rescue on most behavioral domains evaluated. For all panels: Cre, n=23; STOP, n=20; Res, n=17; partial rescue Res, n=4 where all genotypes received tamoxifen; Kruskal-Wallis test with Dunn's multiple comparisons test; *p<0.05, **p<0.01, ***p<0.001, ****p<0.0001. Bars represent mean \pm SEM.

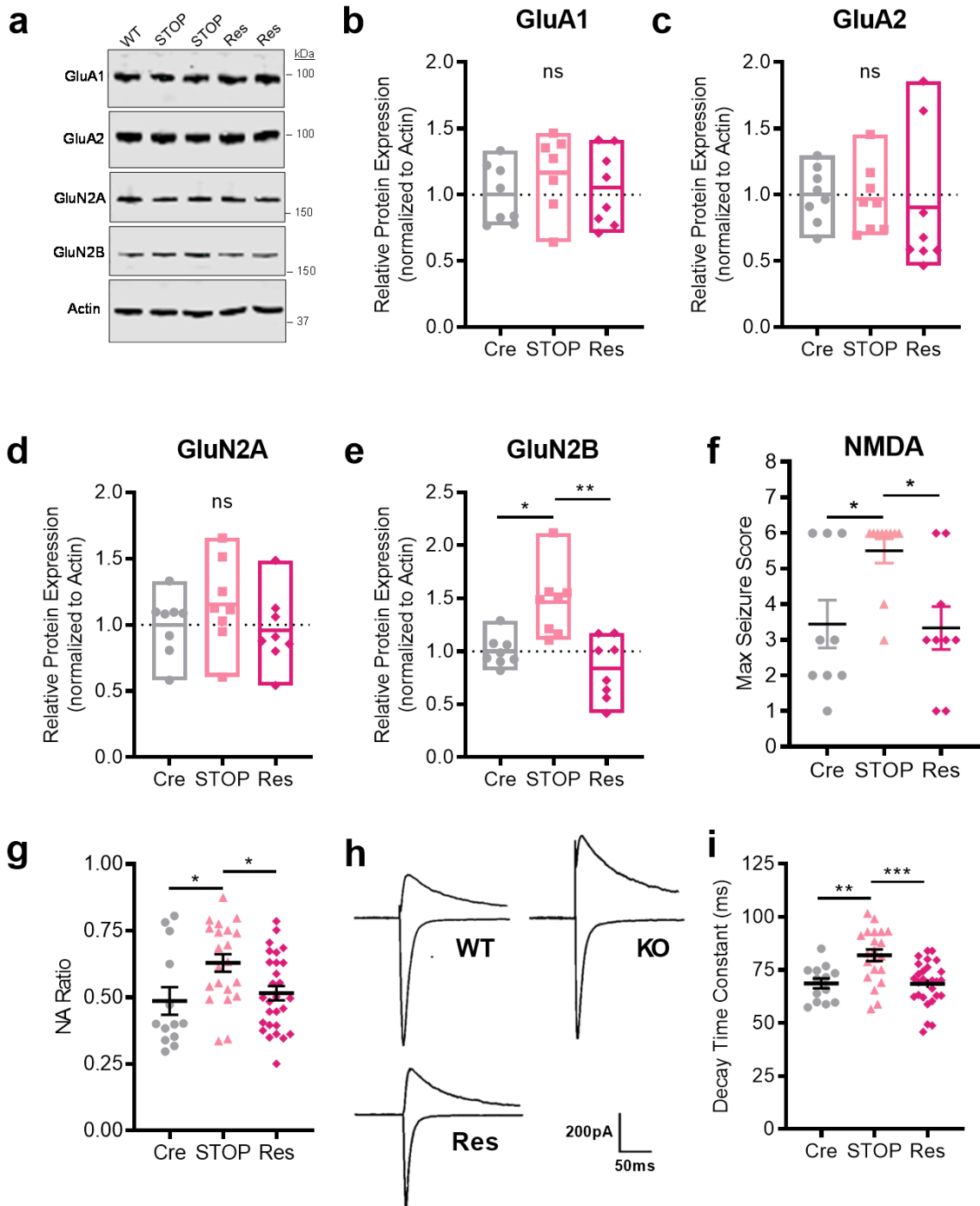


Figure 6: Adult restoration of CDKL5 abrogates aberrant NMDAR-mediated synaptic responses.

(a) Representative western blots showing several major ionotropic glutamate receptor subunits from postsynaptic density membrane fractions in Cre, STOP, and Res mice. **(b-e)** STOP, but not Res, mice show a selective increase in levels of GluN2B, a major subunit of the NMDA receptor compared to Cre littermate controls (n=8 per genotype). **(f)** STOP, but not Res, mice show a significantly increased susceptibility to NMDA-induced seizures compared to Cre littermate controls (Cre, n=9; STOP, n=10; Res, n=9). **(g-i)** STOP, but not Res, mice show an increased ratio of NMDA-mediated to AMPA-mediated synaptic responses in the hippocampal CA1 (g) concomitant with a significantly larger decay time constant of NMDAR-mediated EPSCs (i), suggestive of a higher contribution of GluN2B-containing NMDARs (representative traces shown in (h)) and demonstrating an attenuation of aberrant NMDAR signaling deficits in Res mice. For all panels: Kruskal-Wallis test with Dunn's multiple comparisons test (except for (g) and (i): one-way ANOVA with Tukey's multiple comparisons test). *p<0.05, **p<0.01, ***p<0.001. Bars represent mean \pm SEM.

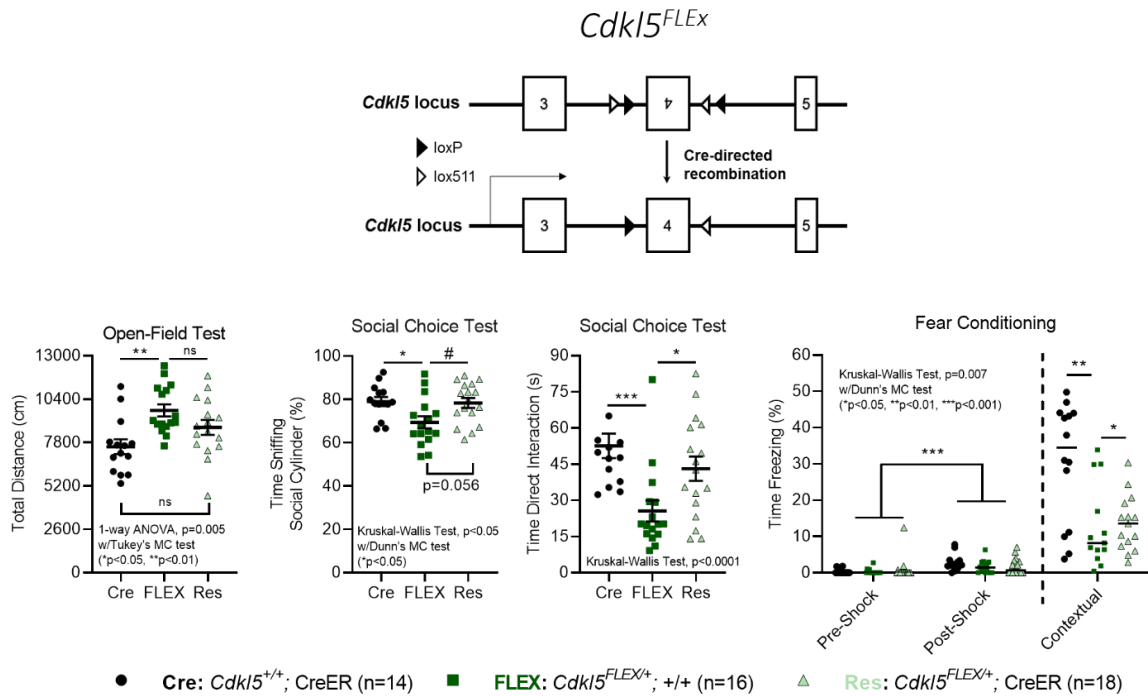


Figure 7: Adult restoration of *Cdk15* expression ameliorates several CDD-associated behavioral deficits in heterozygous female CDD mice

(a) *Cdk15^{FLEX}* mice carry an inverted exon 4 of the endogenous *Cdk15* locus, flanked by two pairs of *loxP* sites that allow for proper cassette re-orientation and gene expression upon tamoxifen delivery. All female mice received tamoxifen beginning at postnatal day 90, and behavioral analysis was performed 3 months later. **(b)** Open-field test demonstrating significant hyperactivity in heterozygous female *Cdk15* knockout mice (*Cdk15^{FLEX/+}*; +/+, or FLEX), but no significant activity change between Cre-only controls (*Cdk15^{+/+}*; CreER, or Cre) and rescue mice (*Cdk15^{FLEX/+}*; CreER, or Res) suggesting reduced hyperactivity. **(c)** Examination of sociability behaviors during a 3-chambered social choice test demonstrates reduced sociability in FLEX females mice compared to Cre littermate controls indicated by reduced (c) time spent sniffing and **(d)** directly interacting with a novel stimulus mouse. Res mice spent similar amounts of time sniffing and directly interacting with a stimulus mouse as their Cre littermate controls, demonstrating rescued sociability. **(e)** FLEX heterozygous females carry impaired context-dependent memory retrieval in a Pavlovian fear-conditioning paradigm highlighted by reduced time spent freezing upon return to the foot-shock chamber. Res mice show significantly increased time freezing compared to FLEX, suggesting improved memory retrieval. Relevant statistical details are embedded in each graph.

CHAPTER 5 – X-LINKED CELLULAR MOSAICISM UNDERLIES AGE-DEPENDENT SEIZURE OCCURRENCE IN MOUSE MODELS OF CDKL5 DEFICIENCY DISORDER

Contributions: Barbara Terzic, Yolanda Cui, and Andrew C. Edmondson co-led this study with help from Nicolas Sarmiento and Dasha Zaitseva for data analysis, Erin Nugent for seizure monitoring, and Zhaolan Zhou for the review and interpretation of data. Yue Cui and Erin Nugent managed all mouse husbandry, genotyping, and breeding. Barbara Terzic wrote this chapter with input from all authors.

Abstract

CDKL5 Deficiency Disorder (CDD) is an infantile epileptic encephalopathy presenting with early-onset seizures, intellectual disability, motor impairment, and autistic features. The disorder has been linked to mutations in the X-linked *CDKL5*, and mouse models of the disease recapitulate several aspects of CDD symptomatology including learning and memory impairments, motor deficits, and autistic-like features, but not spontaneous seizures. Here, we report the first observation of disturbance-associated and spontaneous seizure-like events in heterozygous female mice across two independent mouse models of CDD: *Cdkl5* knockout mice and CDKL5 R59X knock-in mice. We find that both the prevalence and severity of this phenotype increase with aging, with a median onset around 28 weeks of age. Similar seizure-like events are not observed in hemizygous knockout male or homozygous knockout female littermates, suggesting that X-linked cellular mosaicism is a driving factor underlying these epileptic events. Furthermore, we successfully demonstrate significant prevention of seizure activity upon early (pre-epilepsy) *Cdkl5* expression restoration, and a significant abatement of seizure activity upon late (post-epilepsy) *Cdkl5* expression restoration across 2 independent, conditional rescue mouse lines. Together, these findings not only contribute to our understanding of the effects of CDKL5 loss on seizure susceptibility, but also strengthen the face validity of current CDD mouse models for future therapeutic development.

Introduction

Pathogenic variants in the X-linked gene encoding cyclin-dependent kinase-like 5 (CDKL5) have been associated with the severe childhood epileptic encephalopathy known as CDKL5 Deficiency Disorder (CDD)(Bahi-Buisson & Bienvenu, 2012; Fehr et al., 2013; Kalscheuer et al., 2003; Tao et al., 2004; Weaving et al., 2004). CDD is characterized by a heterogeneous array of clinical symptoms including early-onset seizures, marked hypotonia, autistic features, and severe neurodevelopmental impairment(S. Demarest et al., 2019; H. E. Olson et al., 2019). The disorder predominantly affects young females heterozygous for mutations in the X-linked *CDKL5*, with an overall incidence of one per forty-two thousand live births, making it one of the most common genetic causes of epilepsy in children(S. Demarest et al., 2019; Symonds et al., 2019). Despite the constellation of phenotypes presented in CDD, the severe, early-onset seizures in particular drastically impact quality of life, with ninety percent of patients displaying seizures by three months of age. Eighty percent of children with CDD have daily seizures, and fewer than half report more than two months of seizure freedom(H. E. Olson et al., 2019). Furthermore, children with epilepsy that presents before 3 years of age have been shown to carry a high burden of behavioral and cognitive comorbidities, and this risk increases with increased seizure incidence(Berg et al., 2008; Berg, Zelko, Levy, & Testa, 2012). This high burden of refractory seizures in CDD make it a particularly debilitating aspect of the disorder for both patients and their families, highlighting the pressing need to develop effective therapeutics for seizure management.

Several mouse models of CDD have been established and exhibit many of the cardinal phenotypes of the disorder, including autistic-like behaviors, impaired motor control, and poor learning and memory(Zhou, Han, & Zhou, 2017; Y.-C. Zhu & Z.-Q. Xiong, 2019). The first *Cdkl5* knockout mouse was generated and characterized in 2012, mimicking a reported CDD splice-site mutation resulting in skipping of exon 6 and loss of CDKL5 function(Archer et al., 2006; I. T. Wang et al., 2012). Although hippocampal electroencephalographic (EEG) recordings in postnatal

day (P) 70-90 male mice of this line demonstrated disruptions in event-related neuronal oscillations in response to auditory stimuli, chronic video-EEG recordings revealed no spontaneous seizure activity. Furthermore, basal EEG patterns and power distribution across various oscillation frequencies were unchanged in hemizygous knockout male mice compared to littermate controls. In 2014, Amendola et al. developed and characterized another *Cdkl5* knockout mouse (exon 4 deletion) in which EEG recordings also revealed no spontaneous epileptiform activity in hemizygous male knockouts (Amendola et al., 2014). More recently, an exon 2 deletion mouse of *Cdkl5* as well as the CDKL5 R59X knock-in, mimicking a CDD-associated nonsense mutation resulting in loss of CDKL5 function, were created. Although these animals display an increased sensitivity to NMDA-induced seizures, no overt spontaneous seizure activity was initially reported (Okuda et al., 2017; Tang et al., 2019). Recently, aged heterozygous female mice from the first *Cdkl5* knockout (exon 6 deletion) and CDKL5 R59X knock-in mouse lines were reported to exhibit spontaneous epileptic spasms (Mulcahey, et al. 2020)

The lack of a robust seizure phenotype in CDD mouse models has so far been attributed to neural network differences between human and mouse brains (Zhou et al., 2017). EEG recordings in loss-of-function models of CDD have not revealed spontaneous seizures, but the majority of these studies have been limited to hemizygous male mice (Amendola et al., 2014; I. T. Wang et al., 2012). Despite the lack of overt, behavioral seizures in animal models of CDD reported to date, several groups have observed synaptic and circuit-level hyperexcitability in various brain regions as well as altered sensitivity to specific chemoconvulsants. CDKL5 is most highly expressed in neurons of the forebrain, and selective loss of CDKL5 from forebrain excitatory neurons results in increased frequency of miniature excitatory post-synaptic currents (mEPSC) in the hippocampal CA1 region (Tang et al., 2017). Interestingly, selective loss from GABAergic forebrain neurons also recapitulates this increased mEPSC frequency coupled with circuit hyperexcitability in the form of aberrant paired-pulse facilitation (Tang et al., 2019). In this same region, loss of CDKL5 was found to result in enhanced long-term potentiation by a

misregulation of postsynaptic GluN2B-containing NMDA receptor localization, and in line with this, knockout mice exhibit significant hyperexcitability to NMDA (Okuda et al., 2017; Tang et al., 2019). Although high-dose kainic acid induces overt seizures in *Cdkl5* hemizygous knockout males at similar latency to wild-type littermates, the mean duration of the resultant epileptic EEG bursts is reported to be longer (Amendola et al., 2014). *Cdkl5* knockout mice have also been reported to display decreased latency to the first stages of seizure progression upon low-dose pentylenetetrazol administration (Yennawar et al., 2019). These findings suggest that seizure susceptibility may in fact be altered in the absence of CDKL5, but perhaps only under certain environmental conditions or specific periods of development and aging.

Here, we report the occurrence of overt, myoclonic and tonic-clonic behavioral seizure-like events in two distinct mouse models of CDD: a *Cdkl5* knockout carrying a deletion of exon 6 and the CDKL5 R59X knock-in, both resulting in loss of CDKL5 function. These events are specific to female mice heterozygous for mutations in *Cdkl5*, and not seen in hemizygous knockout males, homozygous knockout females, or wild-type littermates. Both the frequency and severity of this seizure-like activity increased with aging, with a median age of onset around 28 weeks of age. The lack of overt similar seizure-like events in hemizygous male knockout and homozygous female knockout mice suggests that X-linked mosaicism of *Cdkl5* deficiency likely drives the seizure phenotype in mouse models of CDD. Importantly, we demonstrate for the first time that these seizure-like events in CDD mouse models are preventable and reversible with restoration of *Cdkl5* expression, providing a positive outlook for seizure management and treatment in CDD patients.

Results

Female mice heterozygous for mutations in *Cdkl5* exhibit seizure-like events in an age-dependent manner

The severity and prevalence of seizures in patients with CDD has motivated numerous efforts to model and examine seizure-related phenotypes in *Cdkl5*-deficient mice (Amendola et al.,

2014; Okuda et al., 2018; Tang et al., 2019; Tang et al., 2017; I. T. Wang et al., 2012; Yennawar et al., 2019). Initial reports in several mouse models of CDD failed to recapitulate the spontaneous seizure phenotype commonly presented in CDD patients. However the majority of these studies, including our own, have focused on hemizygous knockout male mice. Furthermore, the majority of these behavioral or functional assays have been confined to young adult mice (postnatal days (P) 50-90).

Given that *Cdkl5* is X-linked, we maintain and generate experimental mice by crossing wild-type males to females heterozygous for *Cdkl5* mutations (e.g., R59X). In the process of breeding R59X heterozygous females (*Cdkl5*^{R59X/+} or R59X/+), we observed that numerous aged (>P200) females displayed abnormal movements following cage opening/disturbance. Upon observing these abnormal movements, which we felt resembled seizure-like behaviors, we sought to establish a methodology to consistently and quantitatively score these events. We modified the Racine scale widely used to describe the progress and severity of chemoconvulsant-induced seizures (Table 1), and set up a process of regular monitoring (3 minutes per cage, 2-3 times a week) and seizure scoring along this scale for our R59X/+ breeder and non-breeder females as well as wild-type littermate controls (Velíšková, Velíšek, Mareš, & Rokyta, 1990). Over the span of fourteen months, upon cage opening or handling, we have documented behavioral events that we believe resemble seizures beginning as early as 17 weeks of age.

The most frequent seizure-like events observed consisted of myoclonic jerks involving sudden and repetitive movement of the head and neck with or without tail stiffening (Racine Stage 1, Supplementary Video 1A, 1B, 1C). Tonic-clonic seizures with an initial appearance of wild running followed by loss of the righting reflex (Racine Stage 4, Supplementary Video 4A, 4B, 4C) were the second most frequent seizure type observed. On rare occasions, the tonic-clonic seizures would progress into extension of fore- and hind-limbs, reaching Racine Stage 5 (Supplementary Video 5). Clonic seizures with forelimb clonus and rearing were also relatively rare (Racine Stage 3, Supplementary Video 3A, 3B, 3C). To streamline data collection, analysis, and presentation, all seizures ranging from Racine stages 1 to 2 were termed 'myoclonic

seizures-like events' and events resembling Racine stages 3 to 5 were grouped as 'severe seizure-like events.' Mice were defined as being epileptic only after a second seizure-like event had been observed (typically Racine Stage 1). By 20 weeks of age, we found that 12% of R59X/+ females had displayed a second seizure-like event, and this increased to 70% of R59X/+ females exhibiting at least 2 seizures-like events by 40 weeks of age. We never observed similar events (or similar behaviors of any type) in wild-type (+/+) females, hemizygous knockout male mice (R59X/y), or wild-type male mice (+/y) across any of the age groups (Figure 1A).

As no laboratory had previously documented seizures in any CDD mouse model at the time, we attempted to confirm our findings in an independent *Cdkl5* knockout line lacking *Cdkl5* exon 6 (hereafter referred to as KO). Indeed, by 12 weeks of age we had observed at least two of these similar events in 8.7% of KO/+ females, and this increased to 65% of KO/+ females by 40 weeks of age. Again, no seizure-like activity was observed in wild-type (+/+) females, hemizygous knockout male mice (KO/y), or wild-type male mice (+/y) across any of the age groups (Figure 1B).

To rule out the possibility that this epilepsy phenotype is exclusive to the CDKL5 colonies we have maintained in our laboratory, we obtained additional R59X/+ females (Stock No. 028856) and KO/KO females (Stock No. 003724) from the Jackson Laboratory, crossed them to newly obtained C57BL/6J males (Stock No. 000664), and subsequently monitored their progeny twice a week for seizure-like events as described above. 10 out of 13 R59X/+ females (77%), but no +/+ female or R59X/y male littermates, were observed to have at least one seizure-like event by 30 weeks of age. Similarly, KO/+ females, but no +/+ female or KO/y male littermates, displayed seizure-like events by 30 weeks of age. We therefore concluded that the phenotype we had detected was indeed due to loss of *Cdkl5* function.

Seizure-like event frequency and severity in *Cdkl5* heterozygous females increases with age with a concomitant reduced life span

While monitoring R59X/+ female mice, we observed that several mice reaching Racine Stage 5 seizures would die after reaching the tonic phase of the seizure. We found that on average, R59X/+ females have a significantly decreased lifespan compared to their wild-type littermate (+/+) females with significantly more R59X/+ females dying between 40-50 weeks of age (Figure 1C), possibly as a result of infrequent but lethal seizures. In contrast, no significant change in life span was found between R59X/y males and their wild-type (+/y) littermates (Figure 1D). These results suggest that the seizure-like events occurring in R59X/+ females may decrease life span.

Of the R59X/+ females observed starting at 12 weeks of age, the median age of onset of a second observed myoclonic seizure-like event (Racine Stages 1 to 2) was 28 weeks. More severe seizure-like events (Racine Stages 3 to 5) also occurred more frequently with increasing age, with a median onset of 47 weeks of age (Figure 2A). In addition to this increasing seizure-like event severity, the frequency of all observed seizure-like events also increased with age (Figure 2B).

It should be noted that there is significant individual variability within R59X/+ females for both the onset and the frequency of these seizure-like events. During our observations, some females displayed their first disturbance-associated seizure-like event as early as 17 weeks of age while others did not display an overt seizure-like event until 49 weeks of age or ever. For some R59X/+ mice, disturbance-associated seizure-like events occurred every week for a time span of a few months, while for other mice no events were observed after two initial seizure-like events. A summary of 20 R59X/+ females monitored from 12 to 45 weeks of age for all seizure-like events demonstrates this trend of age-dependency and variability (Figure 2C).

We similarly tracked the age-dependent development of seizure-like events in our second *Cdkl5* knockout line to validate our findings. In KO/+ females, the median age of onset of a

second observed myoclonic seizure-like event (Racine Stages 1 to 2) was 32 weeks, with a first seizure-like event observed as early as 16 weeks of age in some mice. More severe seizure-like events (Racine Stages 3 to 5) occurred in KO/+ females with a median age of onset of 57 weeks (Figure 3A). Similar to the R59X/+ females, the likelihood of both myoclonic seizure-like events and a severe seizure-like events in KO/+ females increased with age (Figure 3B). We monitored 17 KO/+ females from 12 weeks until 42-45 weeks of age and recorded all seizure-like events, and found similar individual variability in both age-of-onset and seizure frequency as reported above for R59X/+ (Figure 3C).

We recognize that this variability may also be a result of our sampling method of only observing seizure-like events 2-3 times a week upon cage disturbance, and that our incomplete reported penetrance of ~70% may not accurately reflect the actual incidence of seizure-like events amongst heterozygous female carriers of *Cdkl5* mutations. To investigate whether the seizure-like events we were observing only occur with cage opening/disturbance, we continuously video recorded R59X/+ female mice that had previously displayed a disturbance-associated seizure-like event for >72 hours to determine whether events can also occur spontaneously. Both myoclonic seizure-like events (Supplementary Video 6A, 6B) and tonic-clonic seizure-like events (Supplementary Video 7) were observed during this recording session. These events occurred spontaneously without any disturbances or environmental changes, suggesting that loss of CDKL5 leads to spontaneous seizure-like events as well as the disturbance-associated seizure-like events we reported above.

In an attempt to capture EEG correlates of these seizure-like events, we performed EEG implantation surgery utilizing 2 cortical surface electrode and video monitoring in R59X/+ female mice as described in the methods section (n=13). Mice under EEG surveillance with time-locked video were mildly disturbed by a gentle touch of the hand at varying times and intervals throughout the monitoring period to mimic the seizure monitoring interactions. No Racine stage 4 or 5 handling-provoked generalized tonic-clonic seizures were evoked. We also watched the

recorded video and analyzed the EEG tracing using integrated seizure detection software without observing any unprovoked Racine stage 4 or 5 seizures. Over 1,574 hours of video-EEG data across 13 R59X/+ female mice (roughly 121 hours/mouse) we were only able to observe one female displaying a stage 1 handling-associated seizure-like event (Supplemental Videos 8A, 8B), characterized by brief movements involving neck extension and body stiffening temporally associated with bilaterally synchronous slow-wave discharges on EEG. We also recorded over 145 hours of video-EEG data across 4 wild-type female and wild-type male mice without detection of similar seizure-like events as reported prior to surgery and implantation. Using this technique, we did detect epileptic spasms as recently described in the same mouse lines (Mulcahey et al., 2020).

Given the concern that inability to observe these seizure-like behaviors could be due to a possible blunting effect from the surgery itself, we utilized a different EEG implantation technique with 2 cortical surface electrodes and a double-depth electrode in right hippocampus in 7 R59X/+ and 9 KO/+ heterozygous female mice, as well as 8 wild-type female mice. Each mouse underwent video-EEG recording for at least 11 days as described in the methods. Over the entire duration of over 2,300 hours of video-EEG monitoring for all 24 mice, the technicians who handled the mice observed no Racine stage 4 or 5 handling-provoked generalized tonic-clonic seizures. We also utilized a third EEG implantation technique with 8 electrodes (hippocampal, bilateral parietal, bilateral motor, bilateral visual electrodes) and failed to detect any Racine stage 4 or 5 handling-provoked generalized tonic-clonic seizures while working with these mice. Interestingly, a recent publication reported spontaneous epileptic spasms, associated with generalized, slow-wave activity on EEG, in identical strains of KO/+ and R59X/+ female mice at similar ages (Mulcahey et al., 2020). Our findings of disturbance-associated myoclonic and tonic-clonic seizure-like events, therefore, complement the previous findings and suggest that multiple seizure semiologies exist in mouse models of CDD.

Heterozygous mosaic, but not homozygous or hemizygous, loss of CDKL5 underlies spontaneous seizure development

We were intrigued by the sex-specificity of our observed seizure-like phenotype and wanted to dissect the contributing factors that may underlie this segregation of seizure presentation to R59X/+ and KO/+ females but not R59X/y or KO/y hemizygous male knockouts. Since sex hormones are well known to affect the seizure threshold of both epileptic humans and mice, we examined whether estrous cycle or androgen hormones may be contributing to the sex-specificity of this phenotype (Tauboll, Sveberg, & Svalheim, 2015). We collected vaginal lavage samples from R59X/+ and KO/+ females immediately upon observing disturbance-associated seizure-like events in order to test for estrous cycle stage at the time of seizure occurrence. We identified seizing females in all four stages of the mouse estrous cycle (Figure 4A), suggesting that the levels of sex hormones or estrous cycle stage are unlikely to be triggering factors for the seizure-like events we observed. We also compared the median age of seizure onset between breeder and nulligravid R59X/+ females and did not observe any significant differences (Figure 4B).

An additional factor that differs between our seizing heterozygous knockout females and hemizygous males is the X-linked mosaicism exclusively present in heterozygous female knockouts. To investigate whether mosaicism may be underlying the seizure-like phenotype segregation between our male and female CDD mice, we have been generating a cohort of mice by breeding R59X/+ females to +/y and R59X/y males. To date, we have monitored 14 homozygous knockout females (R59X/R59X) together with 16 heterozygous knockout females (R59X/+) and 9 wild-type (+/+) littermate controls beginning at 12 weeks of age. 12 out of 16 (75%) R59X/+ females have been observed to display at least two disturbance-associated seizure-like events with a median age-of-onset of 32 weeks, while no seizure-like events have been seen in +/+ littermate controls and only one seizure-like event being observed in a single R59X/R59X female littermate (Figure 4C). This supports the idea that X-linked mosaicism of

Cdkl5 deficiency may be a driving factor of the disturbance-associated and spontaneous seizure-like events observed in female models of CDD.

Restoration of *Cdkl5* expression prevents and reverses the evolution of seizure-like events in heterozygous female models of CDD

Our unexpected seizure phenotype finding provoked a unique insight into genetic models of CDD, and led us to examine the reversibility of this epileptic phenotype in our *Cdkl5*^{STOP} and *Cdkl5*^{FLEX} heterozygous female mice. We began by examining *Cdkl5*^{STOP} heterozygous females (*Cdkl5*^{STOP/+}, hereafter referred to as STOP/+) for the occurrence of any seizure-like events similar to what we reported in R59X/+ and KO/+ females. STOP/+ females developed age-dependent seizure-like events by a median age of 31 weeks, confirming our seizure phenotype in an independent *Cdkl5* knockout model (Figure 5). Similar events were not detected in UB-CreER-only control littermates (*Cdkl5*^{+/+}, CreER/+). We first tested the potential for prevention or mitigation of this epilepsy phenotype with early *Cdkl5* expression restoration (i.e. prior to epilepsy onset).

We subsequently raised up a cohort of STOP/+; +/+ and STOP/+; CreER/+ female littermates, and administered tamoxifen to all genotypes beginning at P90 (13 weeks of age) using the same regiment applied in our conditional knockout experiments in Chapter 3 (0.3mg·kg⁻¹ every other day for a total of 5 doses). This regiment restores *Cdkl5* expression in STOP/+; CreER/+ mice, but not STOP/+ mice, prior to the onset of any seizure phenotype. Using the same bi-weekly-monitoring method as described in previous sections, we noticed that STOP/+; but not STOP/+; CreER/+ mice, developed seizure-like behaviors by 31 weeks of age. These results demonstrate a successful prevention (or at least significant mitigation) of seizure-like events with early *Cdkl5* restoration (Figure 5), and align with our previous behavioral rescue studies in females (Chapter 4, Figure 7).

We next tested whether late *Cdkl5* expression restoration (i.e. after epilepsy onset) was also capable of mitigating the occurrence of seizure-like events in heterozygous *Cdkl5* knockout female models. In an independent cohort, we report that STOP/+ mice and their STOP/+; CreER/+ littermates all develop seizure-like events by a median age of 28.5 weeks (Figure 6). We subsequently delivered tamoxifen ($0.3\text{mg}\cdot\text{kg}^{-1}$ every other day for a total of 5 doses) to all animals beginning at 33 weeks of age in order to test the reversibility of this epileptic phenotype. While STOP/+ mice continued to present with seizure-like events even after tamoxifen administration, no subsequent seizure-like events were detected in STOP/+; CreER/+ littermates (Figure 6). These results suggest that *Cdkl5* expression restoration can reverse or significantly mitigate the occurrence of seizure-like events even in mice that were previously seizing. Importantly, we corroborated these findings in our independent conditional rescue line, the *Cdkl5*^{FLEX/+} (FLEX/+) crossed to a distinct inducible Cre (CAG-CreER). We demonstrate that FLEX/+ females and their FLEX/+; CreER/+ littermates all develop seizure-like events at a median age of onset of 37 and 28.5 weeks, respectively (Figure 7). Importantly, late *Cdkl5* expression restoration (33 weeks of age) using our same tamoxifen regiment successfully mitigated the occurrence of seizure-like events in FLEX/+; CreER/+ females, but not FLEX/+ littermates (Figure 7). Together, these results demonstrate the potential for seizure prevention and reversal in heterozygous female mouse models of CDD.

Discussion

Despite the presence of multiple behavioral and neurophysiological impairments, the spontaneous seizures that are a hallmark feature of CDD have not been reported across four independent *Cdkl5* knockout mouse models (Amendola et al., 2014; Okuda et al., 2018; I. T. Wang et al., 2012; Yennawar et al., 2019). It is therefore imperative to establish animal models with stronger face validity in order to dissect the mechanisms underlying the epilepsy associated with mutations in *CDKL5* as well as to facilitate future development of targeted therapeutics. This

is the first report of disturbance-associated and spontaneous seizure-like phenotypes in mouse models of CDD. Both the disturbance-associated and spontaneous seizure-like activity appear to be specific to female mice heterozygous for mutations in *Cdkl5*, with no hemizygous male knockout, homozygous female knockout, or wild-type littermate control mice displaying epileptic activity to our knowledge. In contrast to humans with CDD, we find that our female CDD mice display a delayed seizure phenotype onset, at a median age around 30 weeks (averaged across our two independent loss-of-function lines). We speculate that this delayed-onset as well as the variable presentation between individual animals (Figures 2C and 3C) may account for the absence of previous reports of seizures across various heterozygous female models of CDD.

Our initial observations in R59X/+ females led us to investigate and validate our seizure-like findings across three additional, independent *Cdkl5* knockout lines (KO/+, STOP/+, and FLEX/+) with similar age-of-onset and incidence, suggesting that this phenotype is indeed linked to mutations in *Cdkl5* and will likely be shared across additional mouse models of CDD. Myoclonic seizures, as well as generalized tonic-clonic seizures, have been widely described in CDD patients, reflecting a potential similarity between human CDD epilepsy and the events we observe in our mice (H. E. Olson et al., 2019). Furthermore, we find that the segregation of this seizure-like phenotype exclusively to heterozygous female knockouts (and not hemizygous males or homozygous females) highlights X-linked mosaicism as a potential driving factor for seizure presentation in mouse models of CDD.

Late-onset of epilepsy phenotype in female CDD mouse models

The delayed onset of seizure-like events in our CDD mice reflects a key distinction between the human CDD patient seizure phenotype and that of our models. The median age of onset for a second observed seizure-like event in our R59X/+ and KO/+ females was 28 weeks and 32 weeks of age, respectively; considered well into the middle-aged stage of the lifespan of C57BL/6 mice (Flurkey et al., 2007). In contrast, CDD patients display early-onset seizures with a median age of onset at six weeks of age and with 90% developing seizures by three months of

age(Fehr et al., 2013; H. E. Olson et al., 2019). As previously discussed, one factor that could be underlying this variability between human and mouse CDD seizure onset in this study is the behavioral method of observation for seizure-like events. By sampling events in our mouse models 2-3 times a week, it is possible we may have missed any spontaneous seizure-like events occurring at earlier ages, especially given the frequency of seizure-like events appears to increase with age. It is also plausible that earlier-occurring seizures in our mice may not have had recognizable behavioral correlates. The prevalence, frequency, and semiology of spontaneous epileptic spasms are characterized in a recent publication using chronic video-EEG recording in aged, *Cdk15* mutant mice(Mulcahey et al., 2020). In future studies, a more detailed characterization of seizure progression and onset in younger animals via chronic, video-EEG will allow for a more fine dissection of the temporal progression of this seizure phenotype.

In CDD patients, typical seizure progression appears to follow a pattern progressing from early onset and at times pharmacoresponsive seizures (Stage I; onset 1-10 weeks), to epileptic encephalopathy with infantile spasms (Stage II; onset 6 months to 3 years), and subsequently refractory, multifocal and myoclonic epilepsy (Stage III; onset 5-7 years)(Bahi-Buisson, Kaminska, et al., 2008). This final stage of refractory epilepsy appears to continue long-term in most patients, highlighting an increasing seizure severity with age that human CDD patients also appear to display. Developmental differences between human and mouse brains may underlie these phenotypic differences in age of onset. As such, a more in-depth focal analysis of the cell type or circuit of origin for these epileptic events in the future will provide clarity on the nature of this delayed-onset phenotype in mice. Our findings of a second seizure type in addition to the recently described epileptic spasms complements the previous findings and suggest that similar to CDD patients, mouse models of CDD exhibit multiple seizure semiologies(Mulcahey et al., 2020).

Disturbance-associated nature of CDD mouse seizure phenotypes

Seizures are known to be precipitated by a myriad of factors including stress, menses, photic stimulation, etc.(Engel Jr., 2012). Our initial observations of seizure-like events in our aging CDD female mice occurred upon cage opening or disturbance, suggesting that specific environmental triggers may precipitate seizure presentation in our model. Although mice were often gently separated by hand for easier observation, disturbance by touching was not required for seizure-like events to occur. These events may have been invoked by the movement of the cage during transfer to the changing station, sound from the ventilation of the changing station hood, brighter light, exposure to human odor, or a combination of multiple of the above factors. Even though it remains unclear what aspects of cage disturbance specifically trigger the associated seizure-like events we observed in our R59X/+ and KO/+ females, it is important to note that we have also observed spontaneous seizure-like events during chronic video monitoring, in the absence of any discernible external stimuli (Supplementary Videos 7A, 7B, 7C, 8), highlighting that this environmental disturbance is not required for seizure onset. Interestingly, some CDD patients have been reported to have reflex seizures, or seizures that are predictably triggered by specific stimuli, suggesting a precedence for this phenotype in humans(Peikes, Hartley, Mhanni, Greenberg, & Appendino, 2019; Solazzi et al., 2018). While we are convinced these observed events are seizures, we were unfortunately unable to electrographically capture these events despite using three different EEG implantation techniques since the nature of the behavioral phenotype changed upon EEG electrode implantation. Failing to capture these events could be due to the rarity and unpredictability of the events in individual mice, a possible blunting effect from the surgery itself, altered semiology of seizure-like events, or inability to replicate a more consistent environmental trigger while in our video-EEG system. The unpredictability of seizure events in chronic epilepsy is cited as a major factor affecting quality of life, thus, further work into the potential triggering factors for CDD-associated seizures could provide valuable insight into environmental influences on seizure development and potential avenues for

mitigation(Devinsky et al., 1995). Our findings, together with those of Mulcahey et al., suggest that multiple seizure semiologies likely exist in mouse models of CDD(Mulcahey et al., 2020).

Mosaic loss of CDKL5 drives the overt presentation of spontaneous seizures

CDD affects both male and female patients, albeit at varying frequencies, and hemizygous male *Cdkl5* knockout mice have been able to recapitulate several of the cardinal phenotypes presented in CDD patients(Akamine et al., 2018; Amendola et al., 2014; Liang et al., 2019; Mirzaa et al., 2013; Okuda et al., 2018; Sartori et al., 2009; Szafranski et al., 2015; Van Esch, Jansen, Bauters, Froyen, & Fryns, 2007; I. T. Wang et al., 2012; Yennawar et al., 2019). However, in our study, no overt seizure-like activity was observed in either R59X/y or KO/y male mice, at least at the ages we focused on, and previously reports in various hemizygous CDD knockout males have also not observed spontaneous seizures(Amendola et al., 2014; Okuda et al., 2018; I. T. Wang et al., 2012; Yennawar et al., 2019). Both of our loss-of-function CDD lines (*Cdkl5*^{R59X} and *Cdkl5* knockout) have been generated and maintained in the C57BL/6 strain for at least 10 generations – an inbred strain of mouse known to confer increased seizure resistance, thus potentially occluding the presentation of spontaneous seizures in other *Cdkl5* knockout mice(Ferraro et al., 2010; McKhann, Wenzel, Robbins, Sosunov, & Schwartzkroin, 2003). Despite this, previous attempts by our group and others at backcrossing our *Cdkl5* lines to less seizure-resistant strains (e.g., DBA/2J, FVB, 129) have not precipitated the manifestation of any spontaneous seizure events in hemizygous *Cdkl5* knockout males (data not shown)(Amendola et al., 2014). This suggests that genetic background is likely not causal to the lack of overt behavioral seizures in hemizygous male CDD models.

We propose the differences we observe between hemizygous male and heterozygous female mouse models of CDD may be due to the mosaicism of CDKL5 loss caused by X-chromosome inactivation in R59X/+ and KO/+. This hypothesis is supported by the lack of an overt seizure-like phenotype in either hemizygous male knockout (R59X/y; KO/y) or homozygous female knockout (R59X/R59X; KO/KO) mice. Furthermore, estrous cycle and androgen hormone

levels appear to be unrelated to event incidence across seizing female mice. Interestingly, another epileptic encephalopathy, caused by mutations in the X-linked *PCDH19*, is well known for causing seizures predominantly in heterozygous females and mosaic males (Kolc et al., 2019). The mechanism underlying *PCDH19*-related epilepsy has been traced to abnormalities in cellular adhesion and consequent cell sorting in animal models (Bartnik et al., 2011; Pederick et al., 2018). While it remains unclear whether epilepsy in CDD is definitively related to mosaicism, mosaic exon deletions and mosaic *de novo* point mutations have been reported in both male and female CDD patients and may be an underappreciated phenomenon (Stosser et al., 2018).

Seizure treatment in mouse models of CDD

Collectively, our gene rescue findings successfully demonstrated significant prevention of seizure activity upon early (pre-epilepsy; Figure 5) *Cdkl5* expression restoration and a significant abatement of seizure activity upon late (post-epilepsy; Figure 6 & Figure 7) *Cdkl5* expression restoration across 2 independent rescue lines. These results highlight the potential not only for inhibition of CDD-associated seizure onset with early gene replacement or treatment, but also demonstrate the reversibility of seizure occurrence with late *Cdkl5* restoration. Again, due to a possible blunting effect from the surgery itself, altered semiology of seizure-like events, or inability to replicate a more consistent environmental trigger while in our video-EEG system, the nature of this seizure-like phenotype changes upon EEG implantation, making it difficult to electrographically capture these events. However, as mentioned, a recent study in collaboration with our group also identified epileptic spasms that were associated with generalized slow-wave activity on EEG specific to heterozygous female CDD mice (Mulcahey et al., 2020). Our current endeavors include attempting to capture correlates of these distinct epileptic spasms using video-EEG in *STOP/+* and *FLEX/+* mice, and subsequently evaluating their evolution upon early and late *Cdkl5* restoration. Early-onset epilepsy is a cardinal phenotype within CDD, therefore, these seminal results are a critical development for future examinations into the reversibility, treatment, and pathogenesis of epilepsy associated with CDD. Our results also highlight the potential for

mouse models of CDD, especially our novel, conditional reversal line, to serve as a valuable tool to dissect the circuit and EEG progression of childhood epilepsy more generally.

Together, our findings demonstrate the first report of overt, disturbance-associated and spontaneous seizure-like events in *Cdkl5* deficient mice, a second, distinct seizure phenotype, and provide the community with newfound face validity for existing CDD models. Although we were not able to capture the events described in this study on video-EEG, our video records suggest that they closely resemble the spectrum of behavioral seizure phenotypes described by the Racine scale. Our current and future work aim to more extensively dissect both the focal circuits (or multi-focality) and continuum of severity underlying seizures presented in these CDD mouse models as well as the mechanism of seizure reversal with late gene restoration. Investigating the circuit origin/nature of this epilepsy phenotype in mice will continue to highlight mechanisms by which loss of CDKL5 drives network imbalance and circuit hyperexcitability, and will provide the CDD community with crucial insights towards the development of seizure therapeutics.

Materials and Methods

Mouse strains. The CDKL5 R59X knock-in(Tang et al., 2019) and *Cdkl5* knockout(I. T. Wang et al., 2012) lines were generated as previously described, and have since been deposited at Jackson Laboratories (R59X: Stock No. 028856; *Cdkl5* KO: Stock No. 021967). UBC-CreER (Stock No. 007001) mice and CAG-CreER (Stock No. 004682) mice were obtained from the Jackson Laboratories. *Cdkl5*^{STOP} and *Cdkl5*^{FLEX} mice were generated as described in Chapter 4 ('Materials and Methods'). All lines have been maintained in the C57BL/6J background.

Animal husbandry. Experiments were conducted in accordance with the ethical guidelines of the National Institutes of Health and with the approval of the Institutional Animal Care and Use Committee of the University of Pennsylvania. Mice were group-housed in cages of two to five in a

twelve-hour light/dark cycle with food and water provided *ad libitum*. Each breeding cage contains one male (C57BL/6J or *Cdkl5^{R59X/y}*, R59X/y) and one to two females (*Cdkl5^{R59X/+}*, R59X/+, or *Cdkl5^{KO/+}*, KO/+). All progeny were genotyped either with the previously reported PCR strategies or with qPCR by Transnetyx, Inc (Tang et al., 2019; I. T. Wang et al., 2012). Male littermates (*Cdkl5^{R59X/y}* with *Cdkl5^{+/y}*; *Cdkl5^{KO/y}* with *Cdkl5^{+/y}*) and female littermates (*Cdkl5^{+/+}* and/or *Cdkl5^{R59X/R59X}* with *Cdkl5^{R59X/+}*; *Cdkl5^{KO/+}* with *Cdkl5^{+/+}*) were weaned at 3 weeks of age and housed together.

Seizure monitoring. Mice were monitored for disturbance-associated seizures two to three times over the course of each week (every other day), during varying times between 8AM to 7PM. Times of day with no extra disturbances occurring (such as cage changing) were chosen. Cages were swiftly and gently pulled out of the rack and moved onto the cage changing station, one cage at a time. Cage lids were immediately removed and mice were mildly disturbed by a gentle touch of the hand. Mice in the cage were then closely observed for 3 minutes for the occurrence of any seizure events and scored according to the modified Racine scale (see Table 1, adapted from Velíšková et al., 1990). Stage 0: no changes in behavior; Stage 1: myoclonic jerks with sudden and repetitive movement of the head and neck with or without tail stiffening; Stage 2: atypical (unilateral or incomplete) clonic seizure; Stage 3: clonic seizure with forelimb clonus and rearing; Stage 4: tonic-clonic seizure with an initial wild run and subsequent loss of righting reflex; Stage 5: tonic-clonic seizure with full extension of fore- and hind-limbs. To streamline data collection, analysis, and presentation, all seizures ranging from Racine stages 1 to 2 were termed ‘myoclonic seizures’ and events resembling Racine stages 3 to 5 were grouped as ‘severe seizures.’

Determination of estrous cycle stage. Mice observed having disturbance-associated seizures underwent vaginal lavage immediately after they resumed normal activities to check for estrous cycle stage. Each mouse was picked up by the base of the tail and 20ul of saline was gently

expelled into the vaginal cavity using a pipette, aspirated back five times, and then dispensed onto a microscopic slide. Dry smears were then evaluated under the microscope and scored for the estrous cycle stage according to the presence/absence and percentage of neutrophils, nucleated epithelial cells and cornified epithelial cells (Caligioni, 2009). Proestrus stage: predominance of nucleated epithelial cells; Estrus stage: predominance of cornified epithelial cells; Metestrus stage: predominance of leucocytes with a small amount of nucleated and/or cornified epithelial cells; Diestrus stage: predominance of leucocytes.

Two-Channel EEG implantation surgery. Experiments were conducted in accordance with the approval of the Institutional Animal Care and Use Committee of the University of Pennsylvania. Mice were stereotaxically implanted with an electrode assembly under continuous isoflurane anesthesia. The electrode assembly consisted of 4 leads: 2 surface electrodes attached to miniature skull screws placed over the left and right frontal cortices (from Bregma: A/P + 1.0 mm, M/L \pm 1.5 mm); and a reference and a ground electrode also attached to miniature skull screws directly behind Lambda on either side of midline (from Bregma: A/P - 5.2 mm, M/L \pm 1.5 mm); Silver wires (0.13 mm diameter) were attached to each electrode and connected to an 8-pin headmount (Pinnacle Technology Inc, Lawrence, KS). The entire assembly was secured on the skull with dental cement (Ortho-Jet, Lang Dental, Wheeling, IL). Mice were given at least 72 hours post-surgery to recover prior to being placed in a Plexiglas recording cage (Pinnacle Technology Inc, Lawrence, KS). EEG waveform was amplified by a preamplifier with a gain of 10 μ V (Pinnacle Technology Inc, Lawrence, KS) at the head of the animal before being passed through a low-torque commutator to the Sirenia Acquisition system (Pinnacle Technology Inc, Lawrence, KS) for final-stage amplification and filtering. EEG was sampled at 2000 Hz in a 12-hour light/dark cycle with food and water provided ad libitum. Mice in the monitoring cages were mildly disturbed by a gentle touch of the hand at varying times and intervals throughout the monitoring period to mimic the seizure monitoring interactions as described above. Video was watched by a reviewer familiar with the appearance of the disturbance-associated seizures. EEG

traces were also processed with the application of a 1 Hz high-pass filter, 500 Hz low-pass filter, and 60 Hz notch filter and analyzed within Serenia Basic (Pinnacle Technology Inc, Lawrence, KS) using amplitude and line length individually to identify potential seizure event. For each potential seizure event, time-locked video was used to assess for the presence of motor behavior typical of disturbance-associated seizures.

Four-Channel EEG implantation surgery. EEG recordings were performed as previously described in Mulcahey et al. (Mulcahey et al., 2020). All experiments were conducted in accordance with the approval of the Institutional Animal Care and Use Committee of the Children's Hospital of Philadelphia. Mice were stereotaxically implanted with an electrode assembly under continuous isoflurane anesthesia. The electrode assembly consisted of 6 leads: 2 surface electrodes attached to miniature skull screws placed over the left and right frontal cortices (from Bregma: A/P -1.2 mm, M/L ± 1.1 mm); a double-depth electrode in right hippocampus (A/P -2.2 mm, M/L $+1.2$ mm, D/V -1.3 mm); and finally a reference and a ground electrode directly behind Lambda on either side of midline. Teflon-coated silver wires (0.13 mm diameter) were attached to each electrode and connected to a 6-pin pedestal (Plastics One, Roanoke, VA). The entire assembly was secured on the skull with dental cement (Ortho-Jet, Lang Dental, Wheeling, IL). All surgeries were performed by an experimenter blinded to genotype.

Video-EEG recording. Video-EEG recording was conducted as previously described in Mulcahey et al. (Mulcahey et al., 2020). A flexible cable connected each animal's headcap assembly to a commutator thus allowing the mouse to move freely during the recordings. Mice were given at least 72 hours post-surgery to recover prior to being placed in a recording cage and were acclimatized for at least 72 hours before recording initiation. Video-monitored EEG recordings of awake and behaving mice were performed in custom-made Plexiglas cages using a Stellate Harmonie acquisition interface (Natus Medical, Pleasanton, CA) and sampled at 200 Hz in a 12-hour light/dark cycle with food and water provided *ad libitum*. As previously described

(Mulcahey et al.), each mouse underwent video-EEG recording for at least 11 days across 8 wild type mice, 7 R59X/+ mice, and 9 KO/+ mice. During this period, each mouse underwent a routine cage cleaning each week at approximately 9:00-11:00 AM (lights out at 1:00 PM). Cage cleanings alternated between “deep” cleans (mouse is removed from recording cage while recording cage is cleaned) and “quick” cleans (mouse is lifted, a temporary floor is placed in the recording cage, a clean floor and clean bedding are placed in the cage). In addition to cage cleanings, veterinary staff checked each recording cage each morning before 11:00 AM. Veterinary staff only opened the cages (1) if the mouse needed food or water or (2) if the mouse appeared unhealthy. At the conclusion of video-EEG recording, the mice were removed from the recording apparatus.

Eight-channel EEG implantation surgery. Electroencephalographic mouse studies were performed as previously described using 8 electrodes (hippocampal, bilateral parietal, bilateral motor, bilateral visual electrodes) using the following coordinates (from Bregma – Bilateral motor: 0.5 mm Anterior-Posterior (A-P) and 1.0 mm medial-lateral (M-L); bilateral parietal: -0.7 mm A-P, 3.0 mm M-L; bilateral visual -3.5 A-P, 2.0 mm M-L; hippocampus: -2.2 mm A-P, 2.0 mm M-L, and 1.7 mm ventral). (Marsh et al., 2009; Simonet et al., 2015). All experiments were conducted in accordance with the approval of the Institutional Animal Care and Use Committee of the Children’s Hospital of Philadelphia. After 24–48 h of recovery in their home cage the animals were transferred to the monitoring cage and recorded using a 32- channel Intan extracellular amplifier (RHD2000 USB Interface Board, Intan Technologies) using either DataWave software or importing the raw data into Matlab. The recordings were sampled at 2000 Hz, with no on-line filtering. Electrode impedances were tested prior to all recordings. All animals were recorded for at least 72 h. Other than when being placed in the chambers or removed, mice were not handled during the monitoring.

Statistical analyses. Similar sample sizes for all seizure monitoring across genotypes was chosen. Statistical analyses were performed using Prism (GraphPad). All data sets were

analyzed using the Shapiro-Wilk test for normality. All survival curves were compared using a log-rank (Mantel-Cox) test to test for significance. All graphs are plotted using Prism (GraphPad). In our figures, * is used to denote all $0.01 < p < 0.05$, ** for $0.001 < p < 0.01$, *** for $0.0001 < p < 0.001$, and **** for $p < 0.0001$.

Figures

Table 1. Modified Racine scale used for behavioral seizure scoring			
Seizure Stage	Behavioral Expression	Grouping for analysis	Video Example
0	No changes in behavior		
1	Myoclonic jerks with sudden and repetitive movement of the head and neck with or without tail stiffening	Myoclonic	Suppl Video 1A-C, 6A-B, 8
2	Atypical (unilateral or incomplete) clonic seizure	Myoclonic	Suppl Video 2
3	Clonic seizure with forelimb clonus and rearing	Severe	Suppl Video 3A-C
4	Tonic-clonic seizure with an initial wild run and subsequent loss of righting reflex	Severe	Suppl Video 4A-C, 7
5	Tonic-clonic seizure with full extension of fore- and hind-limbs	Severe	Suppl Video 5

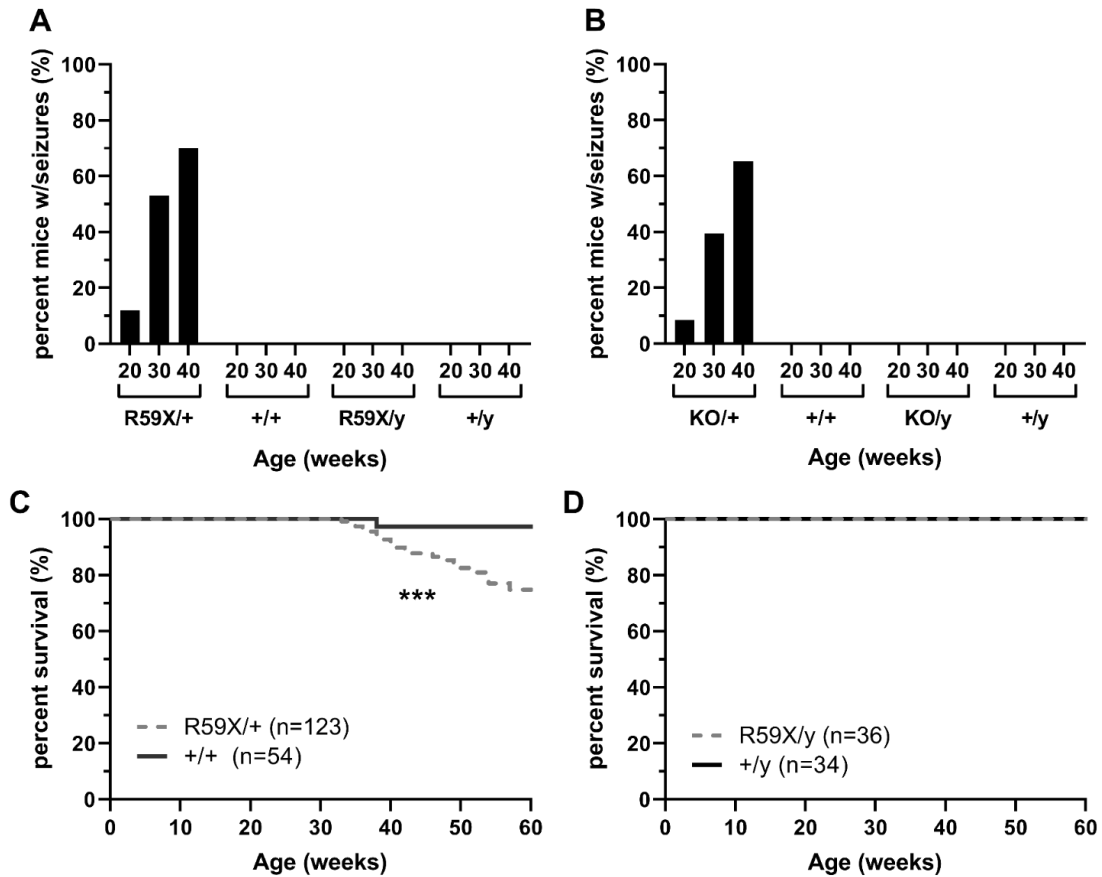


Figure 1. Disturbance-associated seizure-like events in heterozygous CDD female mice.

(A) Percentage of *Cdkl5*^{R59X} (R59X) mice and littermates demonstrating seizure-like events at 20, 30, and 40 weeks of age. *Cdkl5*^{R59X/+} (R59X/+): 12% at 20 weeks (n=31); 53% at 30 weeks (n=28); 70% at 40 weeks (n=20). *Cdkl5*^{+/+} (+/+): 0% at 20 weeks (n=21); 0% at 30 weeks (n=19); 0% at 40 weeks (n=12). *Cdkl5*^{R59X/y} (R59X/y): 0% at 20 weeks (n=33); 0% at 30 weeks (n=24); 0% at 40 weeks (n=10). *Cdkl5*^{+/y} (+/y): 0% at 20 weeks (n=34); 0% at 30 weeks (n=22); 0% at 40 weeks (n=10). (B) Percentage of *Cdkl5*^{KO} (KO) mice and littermates displaying seizure-like events at 20, 30, and 40 weeks of age. *Cdkl5*^{KO/+} (KO/+): 8.57% at 20 weeks (n=35); 39.39% at 30 weeks (n=33); 65.22% at 40 weeks (n=23). *Cdkl5*^{+/+} (+/+): 0% at 20 weeks (n=34); 0% at 30 weeks (n=9); 0% at 40 weeks (n=5). *Cdkl5*^{KO/y} (KO/y): 0% at 20 weeks (n=18); 0% at 30 weeks (n=8); 0% at 40 weeks (n=5). *Cdkl5*^{+/y} (+/y): 0% at 20 weeks (n=20); 0% at 30 weeks (n=8); 0% at 40 weeks (n=7). (C) Longevity of R59X/+ (gray, dotted line; n=123) and +/+ (black, solid line; n=54) females. Mantel-Cox (log-rank) test, p=0.0007. (D) Longevity of R59X/y (gray, dotted line; n=36) and +/y (black, dotted line; n=34) males. Mantel-Cox (log-rank) test, ns. *p<0.05, **p<0.01, ***p<0.001, and ****p<0.0001.

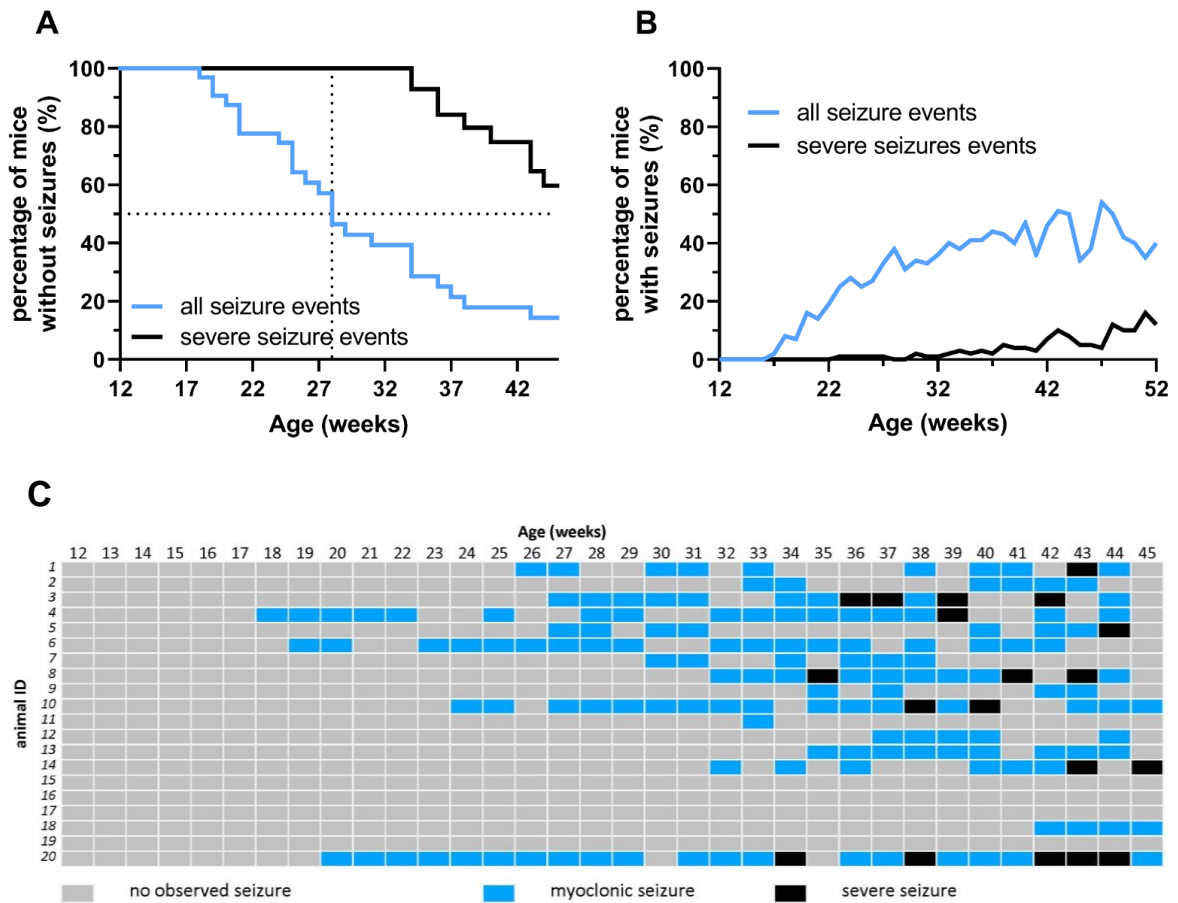


Figure 2. Prevalence and severity of disturbance-associated seizure-like events in R59X/+ females increases with age.

(A) Percentage of *Cdk15*^{R59X/+} (R59X/+) females presenting with any seizure-like event (Racine Stages 1 to 5; black line) and percentage of R59X/+ females presenting with at least one severe seizure-like event (Racine Stages 3 to 5; blue line) between 12 weeks to 45 weeks of age (n=20). Median age of onset for second observed seizure-like event was 28 weeks; median age of onset for severe seizure-like events was 47 weeks of age. (B) Percentage of R59X/+ females observed having at least one seizure-like event (Racine Stages 1 to 5; black line) and percentage of R59X/+ females observed having at least one severe seizure-like event (Racine Stages 3 to 5; blue line) any given week between 12 to 52 weeks of age (n=25).

(C) Event record of 20 *Cdk15*^{R59X/+} females observed from 12 weeks to 45 weeks of age. Gray: no seizure-like events observed during that week. Blue: at least one myoclonic seizure-like event (Racine Stages 1 to 2), but no severe seizure-like event, observed during that week. Black: at least one severe seizure-like event (Racine Stages 3 to 5) observed during that week.

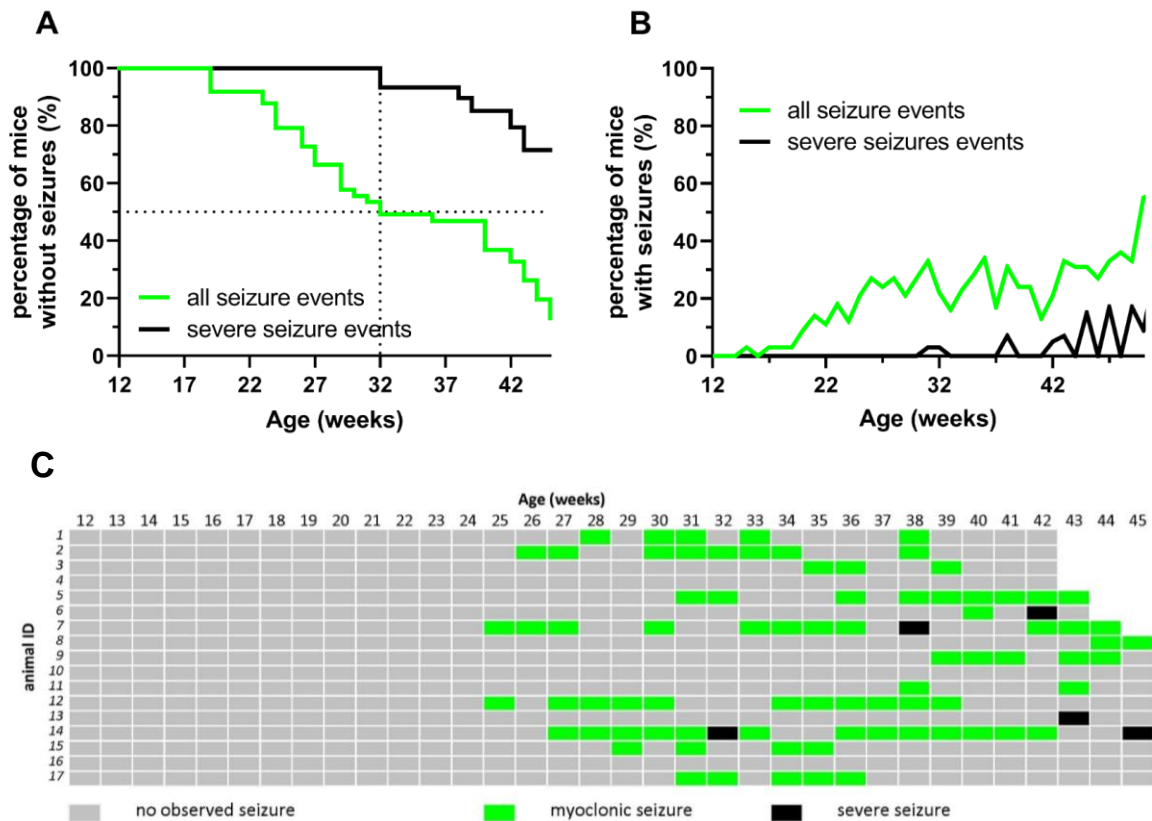


Figure 3. Prevalence and severity of disturbance-associated seizure-like events in $KO/+$ females increases with age.

(A) Percentage of $Cdk15^{KO/+}$ ($KO/+$) females presenting with any seizure-like event (Racine Stages 1 to 5; black line) and percentage of $KO/+$ females presenting with at least one severe seizure-like event (Racine Stages 3 to 5; green line) between 12 weeks to 45 weeks of age ($n=10$). (B) Percentage of $KO/+$ females observed having at least one seizure-like event (Racine Stages 1 to 5; black line) and percentage of $KO/+$ females observed having at least one severe seizure-like event (Racine Stages 3 to 5; green line) any given week between 12 to 50 weeks of age ($n \geq 10$ at any given time point). Median age of onset for second observed seizure-like event was 32 weeks; median age of onset for severe seizure-like events was 57 weeks of age. (C) Event record of 17 $KO/+$ females observed from 12 weeks to 45 weeks of age. Gray: no seizure-like event observed during that week. Green: at least one myoclonic seizure-like event (Racine Stages 1 to 2), but no severe seizure-like event, observed during that week. Black: at least one severe seizure-like event (Racine Stages 3 to 5) observed during that week.

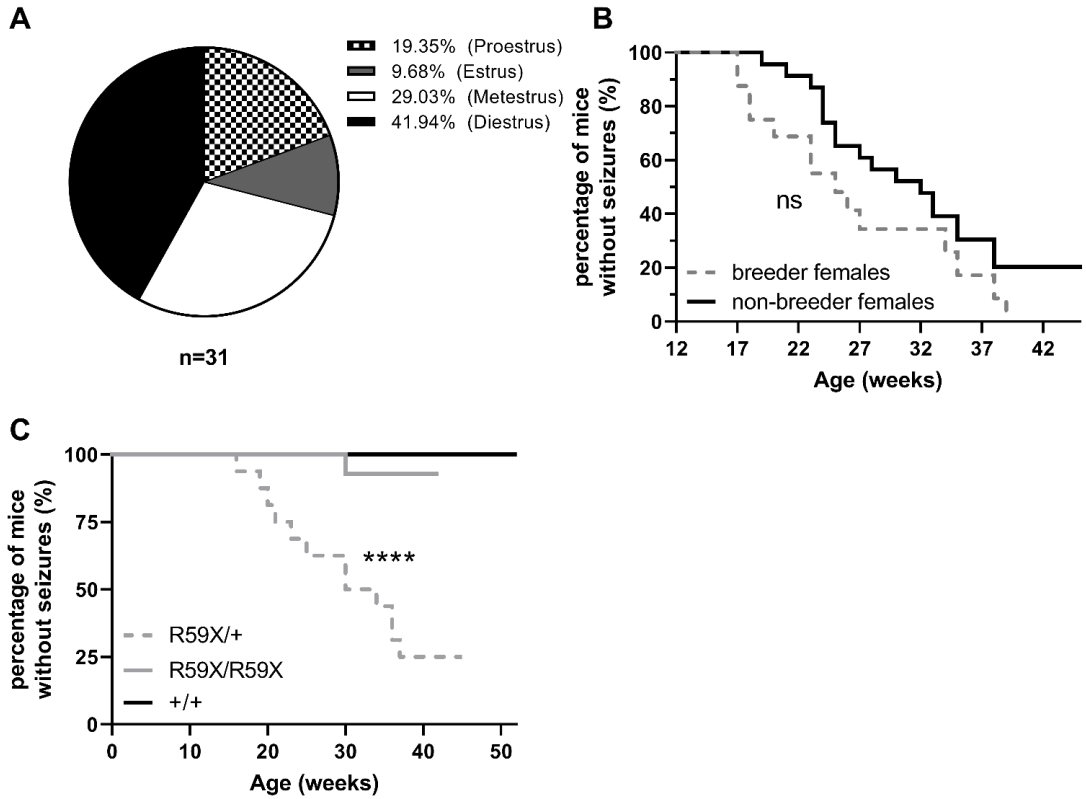


Figure 4. Seizure-like events are confined to *Cdk15* heterozygous female knockout mice and are independent of estrous cycle and parity.

(A) Estrous cycle stages of females displaying disturbance-associated seizures. Proestrus: 19.35% (n=6); estrus: 9.68% (n=3); metestrus: 29.03% (n=9); diestrus: 41.94% (n=13). (B) Percentage of breeder (gray, dotted line; n=16) and nulligravid (black, solid line; n=23) R59X/+ females not exhibiting seizure-like events between 12 to 45 weeks of age. Mantel-Cox (log-rank test), ns. (C) Percentage of R59X/+ females (gray, dotted line; n=16), R59X/R59X females (gray, solid line; n=14), and +/+ females (black line; n=9) not exhibiting seizure-like events between 12 to 42 weeks of age. Mantel-Cox (log-rank) test, $p < 0.0001$. * $p < 0.05$, ** $p < 0.01$, *** $p < 0.001$, and **** $p < 0.0001$.

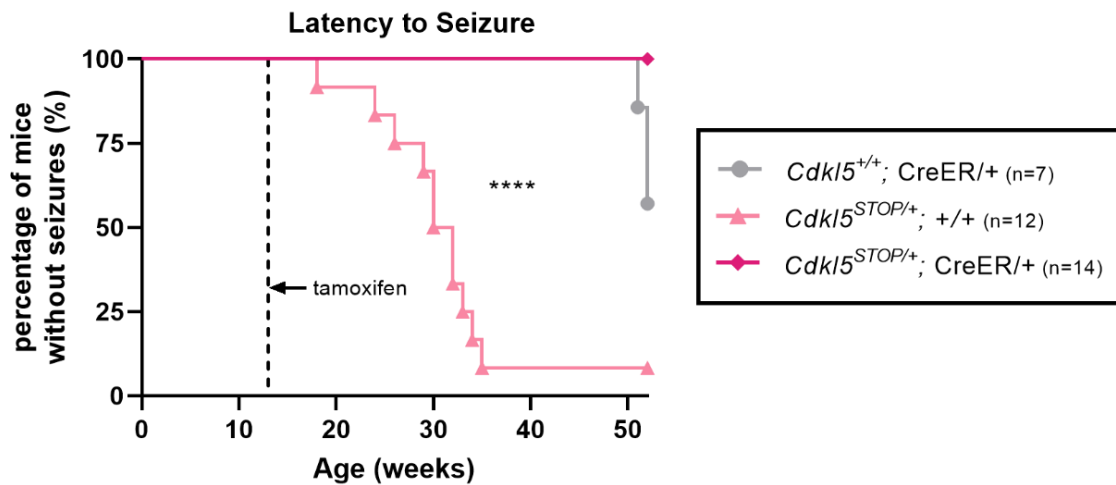


Figure 5: Prevention of seizure phenotype in heterozygous *Cdkl5* knockout female mice with early gene restoration.

Survival curve demonstrating the latency to a second seizure-like event in all mice monitored, plotted as percentage of mice without seizures. *Cdkl5*^{STOP/+} (STOP/+) heterozygous female mice exhibit seizure-like events at a median age of 31 weeks. Tamoxifen delivery (and *Cdkl5* expression restoration) at 12 weeks of age (before seizure onset) prevented the development of seizure-like events in STOP/+; CreER/+ females, but not STOP/+; +/+ littermate controls. Cre-only littermate controls exhibit no similar seizure-like events. This demonstrates the potential for seizure prevention with early *Cdkl5* expression restoration. n=7 CreER/+, n=12 STOP/+, n=14 STOP/+; CreER/+ where all mice received tamoxifen. Mantel-cox (log-rank) test, ****p<0.0001.

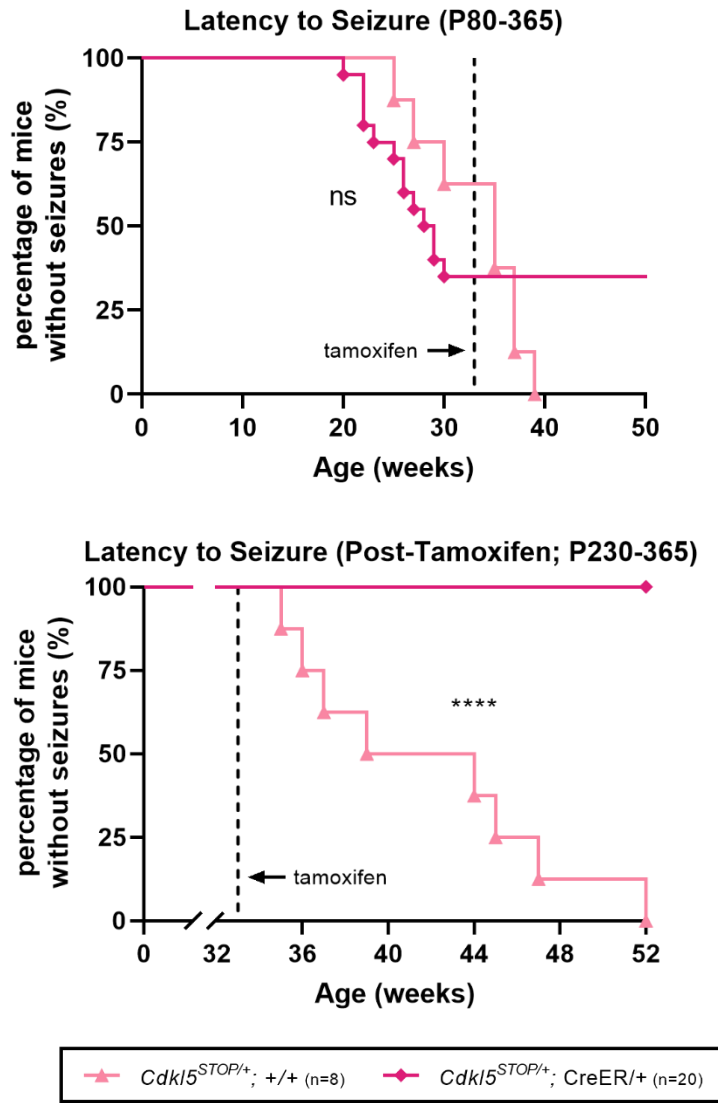


Figure 6: Reversal of seizure phenotype in heterozygous *Cdkl5* knockout female mice with late gene restoration.

Cdkl5^{STOP/+} (STOP/+) and STOP/+; CreER/+ heterozygous female mice exhibit seizure-like events by a median age of 28.5 weeks (prior to tamoxifen delivery). Tamoxifen delivery (and *Cdkl5* expression restoration) at 33 weeks of age (after seizure onset) abrogates the occurrence of any subsequent seizure-like events in STOP/+; CreER/+ females, but not STOP/+; +/+ littermate controls, suggesting a rescued seizure phenotype. Top: survival curve demonstrating latency to a second seizure-like event in all observed mice between 10-52 weeks of age. Bottom: survival curve demonstrating latency to a second seizure-like event in all observed mice after tamoxifen administration (33-52 weeks of age). This demonstrates the potential for seizure phenotype rescue with *Cdkl5* expression restoration even in mice that were previously displaying seizures. n=8 STOP/+; n=20 STOP/+; CreER/+ where all mice received tamoxifen. Mantel-cox (log-rank) test, ****p<0.0001.

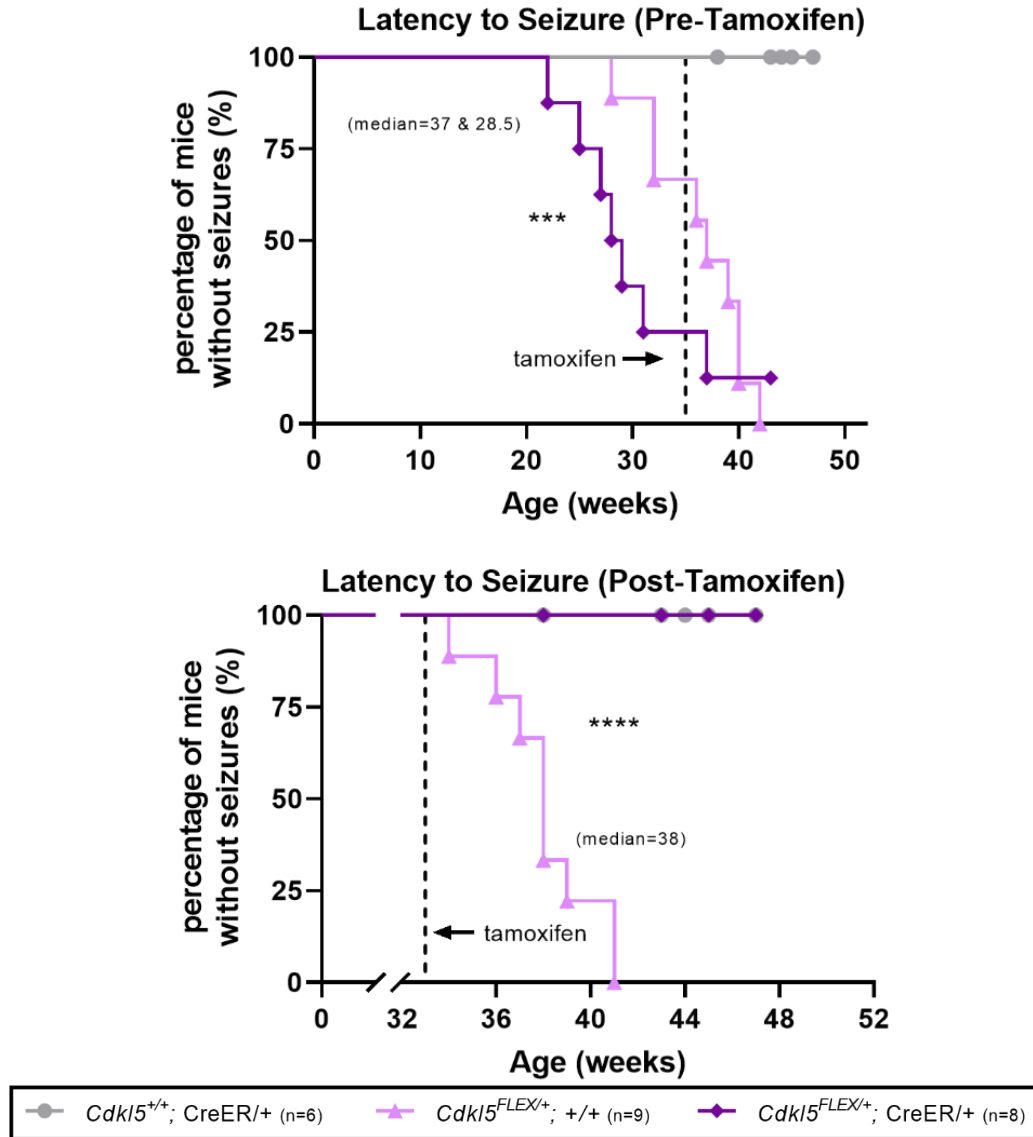


Figure 7: Reversal of seizure phenotype in heterozygous females of an independent *Cdk15* knockout mouse line with late gene restoration.

Cdk15^{FLEX/+} (FLEX/+) and FLEX/+; CreER/+ heterozygous female mice exhibit seizure-like events by a median age of 37 and 28.5 weeks, respectively (prior to tamoxifen delivery). Tamoxifen delivery (and *Cdk15* expression restoration) at 33 weeks of age (after seizure onset) abrogates the occurrence of any subsequent seizure-like events in FLEX/+; CreER/+ females, but not FLEX/+; +/+ littermate controls, suggesting a rescued seizure phenotype. Top: survival curve demonstrating latency to a second seizure-like event in all observed mice between 10-52 weeks of age. Bottom: survival curve demonstrating latency to a second seizure-like event in all observed mice after tamoxifen administration (33-52 weeks of age). This demonstrates the potential for seizure phenotype rescue with *Cdk15* expression restoration in an independent conditional rescue line, even in mice that were previously displaying seizures. n=6 CreER/+, n=9 FLEX/+, n=8 FLEX/+; CreER/+. All mice received TAM. Mantel-cox (log-rank) test, ****p<0.0001.

Supplemental Videos

Supplemental Video 1. Disturbance-associated seizure-like events of Racine stage 1 in *Cdk15^{R59X/+}*

- (a) *Cdk15^{R59X/+}* female at 70 weeks of age displaying a seizure-like event of Racine stage 1.
- (b) *Cdk15^{R59X/+}* female at 59 weeks of age displaying a seizure-like event of Racine stage 1.
- (c) *Cdk15^{R59X/+}* female at 26 weeks of age displaying a seizure-like event of Racine stage 1.

Supplemental Video 2. Disturbance-associated seizure-like event of Racine stage 2 in *Cdk15^{R59X/+}*

Cdk15^{R59X/+} female at 56 weeks of age displaying a seizure-like event of Racine stage 2.

Supplemental Video 3. Disturbance-associated seizure-like events of Racine stage 3 in *Cdk15^{R59X/+}*

- (a) *Cdk15^{R59X/+}* female at 71 weeks of age displaying a seizure-like event of Racine stage 3.
- (b) *Cdk15^{R59X/+}* female at 63 weeks of age displaying a seizure-like event of Racine stage 3.
- (c) *Cdk15^{R59X/+}* female at 50 weeks of age displaying a seizure-like event of Racine stage 3.

Supplemental Video 4. Disturbance-associated seizure-like events of Racine stage 4 in *Cdk15^{R59X/+}*

- (a) *Cdk15^{R59X/+}* female at 60 weeks of age displaying a seizure-like event of Racine stage 4.
- (b) *Cdk15^{R59X/+}* female at 71 weeks of age displaying a seizure-like event of Racine stage 4.
- (c) *Cdk15^{R59X/+}* female at 58 weeks of age displaying a seizure-like event of Racine stage 4.

Supplemental Video 5. Disturbance-associated seizure-like event of Racine stage 5 in *Cdk15^{R59X/+}*

Cdk15^{R59X/+} female at 26 weeks of age displaying a seizure-like event of Racine stage 5.

Supplemental Video 6. Spontaneous seizure-like events of Racine stage 1 in *Cdk15^{R59X/+}* females

- (a) *Cdk15^{R59X/+}* female at 31 weeks of age with a Racine stage 1 seizure-like event.
- (b) *Cdk15^{R59X/+}* female at 31 weeks of age with a Racine stage 1 seizure-like event.

Supplemental Video 7. Spontaneous seizure-like event of Racine stage 4 in *Cdk15^{R59X/+}* female

Cdk15^{R59X/+} female at 43 weeks of age with a Racine stage 4 seizure-like event starting at 8:02:52 PM

Supplemental Video 8. Video-EEG recording of disturbance-associated seizure in *Cdk15^{R59X/+}*

- (a) *Cdk15^{R59X/+}* female at 75 weeks of age displaying a Racine stage 1 seizure. Real-time playback of a video-EEG recording clip demonstrating myoclonic jerks with time-locked EEG.
- (b) Manual frame-by-frame viewing of the corresponding myoclonic event captured on video-EEG in Supplemental Video 8A. Note that the onset of the behavioral spasm occurs immediately after the onset of spike-wave activity.

CHAPTER 6 – EXTENDED DISCUSSION AND FUTURE DIRECTIONS

Cellular Origins of CDKL5 Deficiency Disorder-Related Phenotypes

The findings presented in Chapter 2 on *Cdkl5* conditional knockout mice (Dlx-cKO) complement a previous report characterizing behavioral and circuit phenotypes in Nex-cKO animals (Tang et al., 2017). Together, these results demonstrate the behavioral segregation of *Cdkl5* constitutive knockout phenotypes between forebrain glutamatergic (Nex-cKO) and GABAergic (Dlx-cKO) *Cdkl5* conditional knockout mice, where impaired learning and memory is selectively recapitulated in Nex-cKO mice and autistic-like features are selectively recapitulated in Dlx-cKO mice. This suggests that CDKL5 is necessary in each of these forebrain neuronal populations in order to development and/or maintain proper learning and memory and social behaviors, respectively.

Interestingly, the anxiety-related behaviors, hyperactivity, and motor coordination deficits reported in germline *Cdkl5* knockout mice were not impaired in either Dlx- or Nex-cKO mouse line (Tang et al., 2019; Tang et al., 2017). These phenotypes may be regulated by CDKL5 action in cell types and/or brain regions not targeted by either NEX-Cre or Dlx5/6-Cre drivers. Alternatively, their disruption may arise via a synergistic disruption across multiple cell types and circuits upon loss of CDKL5 that cannot be modeled by conditional knockout. Either way, these results present an interesting future avenue to further dissect the cell types and circuits underlying these specific CDD-related phenotypes.

We also highlight aberrant NMDAR signaling as contributing to the autistic-like features of Dlx-cKO animals, and selectively rescue these aberrant behaviors in constitutive knockout mice using a competitive NMDAR antagonist, memantine (Tang et al., 2019). Together, these findings emphasize the importance of further dissecting cell-type-specific functions of CDKL5 within the heterogeneous brain, especially in regards to targeted therapies for the constellation of phenotypes comorbid in CDD.

Given that CDKL5 is a kinase, the identification of CDKL5 substrates and interacting proteins remains key to illuminating the etiology of CDD. However, CDKL5 is expressed across multiple heterogeneous circuits and cell-types, confounding the identification of reliable targets *in vivo* (Zeisel et al., 2015). Furthermore, the difficulty to date in generating a specific antibody for CDKL5 has impeded the visualization and sub-cellular localization of this kinase in the brain. To bypass these confounds, we generated genetically modified mice wherein CDKL5 can be labeled with biotin in a Cre-dependent manner for future molecular investigations into cell-type-specific signaling targets.

Generation of CDKL5-TAVI knock-in mice for the investigation of CDKL5 molecular targets and signaling pathways

As part of a future direction, we develop and characterize a novel genetic tool, CDKL5-TAVI, that allows for cell-type-specific biotin tagging of CDKL5 *in vivo*. We inserted a short affinity tag immediately upstream of the endogenous *Cdkl5* stop codon, termed TAVI, which comprises a TEV protease cleavage site and a 15 amino acid biotinylation consensus motif that can be post-translationally labeled with biotin by *Escherichia coli* biotin ligase BirA (Figure 1a). To control biotinylation of CDKL5 in a cell-type-specific manner, we crossed these mice to transgenic mice carrying a conditional BirA allele (*R26^{Cre}BirA*) that allows for Cre-dependent expression of BirA. Upon crossing these mice to mice carrying a cell-type-specific Cre allele (e.g., NEX-Cre), we are able to restrict BirA expression (and CDKL5 biotinylation) to select cell-types (Figure 1b).

We crossed our *Cdkl5^{TAVI}* (hereafter referred to as CDKL5-TAVI) mice to mice carrying the conditional BirA allele and NEX-Cre (*Cdkl5^{Tavi/y}; BirA/+; NEX^{Cre}*). These mice carry CDKL5-TAVI in every cell, but only NEX+ neurons will express Cre, and therefore have BirA-mediated biotinylation of CDKL5. We confirmed this result in forebrain cortices of *Cdkl5^{Tavi/y}; BirA/+; NEX^{Cre}* mice, demonstrating selective biotinylation of CDKL5, but no biotinylation of CDKL5-TAVI in *Cdkl5^{Tavi/y}; BirA/+; +/-* littermate controls or wild-type littermates (Figure 1c). The strong affinity between biotin and avidin/streptavidin can be harnessed to visualize a biotin-tagged protein (e.g.,

with streptavidin-conjugated antibodies), or to purify a biotin-tagged protein using streptavidin-conjugated beads (Deal & Henikoff, 2010). We attempted the latter in order to evaluate the extent to which our CDKL5-TAVI tool allowed for successful purification of CDKL5 *in vivo*. We subsequently optimized a condition to successfully enrich biotinylated CDKL5 protein from brain tissue extracts of *Cdkl5^{Tavi/y}; BirA/+; NEX^{Cre}* mice via immunoprecipitation with streptavidin-conjugated beads, but not *Cdkl5^{Tavi/y}; BirA/+; +/+* control littermate brain tissues (Figure 1d). The details of this immunoprecipitation protocol are outlined in the 'Materials and Methods' section below. In the future, this novel genetic tool can serve as an invaluable resource for cell-type-specific *in vivo* visualization of CDKL5, purification and identification of co-interactors, and sorting of biotin-labeled cells for further proteomic or transcriptomic analyses. This advancement provides the CDD and CDKL5 research community with a valuable tool for future dissection of cell-type-specific CDKL5 interactomes and signaling cascades throughout the brain. This will be particularly relevant when considering the cell-type-specific effects and overall efficacy of any CDD-targeting drugs or therapeutics.

Synaptic Convergence of CDKL5 Loss-of-Function Phenotypes

Several studies to date have highlighted disrupted neuronal arborization and/or dendritic spine stability with loss of CDKL5 (Amendola et al., 2014; Della Sala et al., 2016; Lupori L, 2019; Okuda et al., 2018; Ricciardi et al., 2012; Tang et al., 2017; Zhu et al., 2013). The direct impact of CDKL5 loss on pyramidal neuron morphology has been contentious, likely due to context-dependent variability and confounds of mixing cell and non-cell autonomous cellular effects. Interestingly, we find that adult deletion of *Cdkl5* can lead to similar behavioral deficits without concomitant effects on neuronal morphology or dendritic arborization, bringing into question the necessity of these reported arborization phenotypes to CDD-related behavioral deficits. Alternatively, we find that both post-developmental and sparse deletion of CDKL5 in mice increased dendritic filipodia-like structures suggestive of a morphologically immature spine state that, when combined with the absence of changes in overall spine density, reflects a greater

proportion of morphologically immature spines on hippocampal CA1 pyramidal neurons(Harris KM, 1989).

These findings are in line with the observation that CDKL5 is responsible for the phosphorylation of EB2, a member of the microtubule end-binding protein family. End-binding proteins are plus-end-tracking proteins that accumulate at the growing microtubule end, and play pivotal roles in microtubule dynamics that mediate cellular architecture, cargo trafficking, and spine stability(Akhmanova & Steinmetz, 2015; Komarova et al., 2009). In Chapter 3, we demonstrate that EB2 phosphorylation is developmentally regulated and correlates with the expression pattern of CDKL5. The known roles of end-binding proteins in microtubule dynamics align with the cellular and synaptic phenotypes we report upon loss of CDKL5 in mice (e.g., disrupted NMDA receptor subunit trafficking and spine morphology). Importantly, we also demonstrate that restoration of *Cdkl5* expression in adulthood is capable of restoring EB2 phosphorylation to wild-type levels (Chapter 4), highlighting the dynamic regulation by CDKL5 of this microtubule-associated substrate. Thus, CDKL5 may play a role in regulating microtubule dynamics, particularly those related to spine morphology and receptor trafficking at the post-synaptic density, via its continual regulation of microtubule-associated proteins such as EB2. An EB2-related family member, EB3, has previously been implicated in regulating dendritic spine morphology within hippocampal neurons(Leterrier et al., 2011). However, the extent to which CDKL5-mediated phosphorylation of EB2 may play similar roles remains undetermined. Interestingly, it has been reported that EB2 suppresses neurite outgrowth and attenuates the microtubule growth mediated by EB1 activity, but how phosphorylation of EB2 at Ser222 specifically modulates this action is untested(Laketa, Simpson, Bechtel, Wiemann, & Pepperkok, 2006).

We also demonstrate that CDKL5 plays a critical role in maintaining the post-synaptic composition of NMDA receptor subunits, namely GluN2B. During development, the canonical switch from predominantly GluN2B-containing to predominantly GluN2A-containing NMDA receptors across the CNS is thought to be a regulatory mechanism involved in shaping circuits

and constraining synaptic plasticity during the critical period of synaptogenesis for several brain regions(Paoletti et al., 2013). Interestingly, the peak expression of CDKL5 in mouse forebrain appears to coincide with this subunit composition switch during a time window also associated with circuit refinement and acquisition of learning abilities. Loss of CDKL5 may therefore result in an elongated or unconstrained critical period that ultimately leads to maladaptive plasticity across multiple neural circuits and the subsequent heterogeneous collection of symptomology associated with CDD(H. E. Olson et al., 2019). Surprisingly, post-developmental restoration of CDKL5 expression reverses this elevation of GluN2B expression and NMDA hyperexcitability phenotype observed in germline knockout mice, arguing that CDKL5 may persistently regulate NMDA receptor composition beyond the early stages of development. Interestingly, CDKL5 has been reported to target EB2 pS222 via an NMDAR-dependent mechanism, providing a potential link between disrupted NMDAR signaling, microtubule dynamics, and CDKL5 loss-of-function phenotypes(Lucas L. Baltussen et al., 2018). Nonetheless, the causal relationship among the molecular, cellular, and behavioral domains examined in this study requires further examination.

Temporal Dissection of CDKL5 Deficiency Disorder Pathophysiology

Several mouse models of CDD have been characterized to date, and although they recapitulate many of the hallmark phenotypes of the human disorder, it remained unclear whether these phenotypes were a consequence of detrimental changes exclusively accumulating in the developing nervous system or are similarly inducible upon loss of CDKL5 in mature neurons. Furthermore, from a therapeutic perspective, it remained imperative to determine the reversibility of CDD-related deficits particularly after the early stage of brain development, and to delineate the temporal requirement of CDKL5 action needed to establish as well as maintain proper neurological function. Prior to this dissertation, it remained unknown if CDD symptomology was treatable and whether a critical developmental time window was required for treatment. Our temporal knockout and temporal rescue experiments highlighted in Chapters 3-4 address these

questions, and constitute a seminal foundation for future endeavors to dissect the pathogenic origins and design effective therapeutic strategies for CDD.

Our findings demonstrate that multiple behavioral and circuit phenotypes in knockout mouse models of CDD are recapitulated following adult deletion of *Cdkl5*. In parallel, post-developmental restoration of *Cdkl5* expression ameliorates most of these loss-of-function deficits in mice, suggesting that the underlying circuitry critical for many of the behavioral domains disrupted upon loss of CDKL5 are amenable to later kinase restoration. Thus, CDKL5 appears to be required not only during development, but also in adulthood, suggesting that chronic, lifelong treatment of CDD will likely be required.

Notably, working memory, as measured via spontaneous alternations in a Y-Maze assay, was not significantly affected by adult loss or restoration of CDKL5 expression, demonstrating that CDKL5 does function critically in early development. It remains relevant to dissect the emergence of this working memory phenotype in developing animals, and to examine the circuit and cellular mechanisms that drive its perturbation early in life. In parallel, adult knockout of *Cdkl5* resulted in significantly enhanced motor learning in contrast to the impaired motor learning and coordination reported in germline knockout animals. How loss of CDKL5 in adulthood leads to improved motor coordination and learning remains uncertain, but also represents an interesting future avenue to investigate temporally-distinct influences of CDKL5 loss on the same behavioral output.

Through genetic manipulation of endogenous *Cdkl5* expression in a temporal manner, we uncover for the first time that CDKL5 is required to maintain proper spine morphology, sensory-information processing, and behavioral output in the adult brain. Consistent with this, post-developmental restoration of *Cdkl5* expression is sufficient to ameliorate NMDAR-related synaptic deficits, and leads to significant reversal of multiple behavioral domains related to CDD. Together, our findings highlight the promise of disease reversal in CDD across a broader than expected time window, and present an exciting and pressing development for therapeutic treatment of CDD.

Therapeutic Insights for CDKL5 Deficiency Disorder

Previous studies have applied the concept of late gene reversal in rodents to attempt phenotypic rescue in various models of neurodevelopmental disorders (Creson et al., 2019; Guy et al., 2007; Y. Mei et al., 2016). Late restoration of *Mecp2* expression in knockout mice has been reported to alleviate impairments associated with Rett syndrome, and adult restoration of *Shank3* is capable of rescuing selective autistic-like phenotypes (Guy et al., 2007; Y. Mei et al., 2016). Meanwhile, a recent finding reported that adult restoration of the SynGAP protein selectively improved electrophysiological measures of memory and seizures (Creson et al., 2019). CDD, however, is distinct from these and other autism spectrum and neurodevelopmental disorders in that it is characterized by early-onset features within the first few weeks after birth as opposed to a developmental regression after the first few years of life (Ozonoff, Heung, Byrd, Hansen, & Hertz-Picciotto, 2008; Zoghbi & Bear, 2012). Thus, our temporal reversal findings provide a novel development over these previous studies, and demonstrate the potential for treatment of neurological symptoms despite the lack of a relatively stable early-postnatal period. We also found that post-developmental restoration of *Cdkl5* expression significantly ameliorated multiple behavioral deficits related to CDD, rather than a few behavioral domains as was reported in previous reversal studies, arguing a uniquely critical role for CDKL5 in the maintenance of various neurological functions throughout life.

Surprisingly, we observed that a relatively rapid reversal of *Cdkl5* expression led to significant lethality in rescue mice, in line with previous findings from a *Mecp2* re-expression study (Guy et al., 2007). As with MeCP2, a gradual restoration of CDKL5 expression alleviated this lethality issue, and resulted in significant phenotypic reversal. Thus, the time course and dosage of CDKL5 re-introduction need to be carefully considered in future gene replacement trials to avoid contravening outcomes, particularly in a system that may have partially compensated for its loss (Benke & Kind, 2020). Additionally, post-hoc examination of CDKL5 restoration revealed that several rescue mice showed only 20-50% of wild-type protein expression. The rescue of numerous behavioral domains in these mice underscores the potential

that even partial restoration of CDKL5 expression may show notable therapeutic benefit, at least in mice.

We acknowledge that many of our findings are limited to studies in male mice in order to avoid potential confounding effects of mosaic *Cdkl5* expression in females from random X-chromosome inactivation. However, our preliminary behavioral rescue data in heterozygous *Cdkl5* knockout female mice (Chapter 4) presents a promising outlook for the reversal of additional CDD-related cellular and circuit deficits in female models. In the future, it will be necessary to extend these experiments to heterozygous female mouse models of CDD, determine the minimum and maximum levels of CDKL5 expression required for safe phenotypic reversal, and define the latest time window allowable for rescue, at least in mouse models (Benke & Kind, 2020). Finally, the potential for seizure mitigation with *Cdkl5* re-expression also highlights promising outcomes for seizure management and phenotypic reversal for the pervasive epilepsy in CDD.

Materials and Methods

Regulatory approval. Experiments were conducted in accordance with the ethical guidelines of the National Institutes of Health and with the approval of the Institutional Animal Care and Use Committee of the University of Pennsylvania. Mice were group-housed in cages of two to five in a twelve-hour light/dark cycle with food and water provided *ad libitum*.

Mouse strains and genotyping. *Cdkl5*^{TAVI} mice were generated using CRISPR-mediated genomic editing techniques. A specific gRNA was chosen upon screening for targeting specificity and efficacy just upstream of the *Cdkl5* stop codon. The DNA repairing template constituted a TAVI sequence containing a TEV protease cleavage site and a 15 amino acid biotinylation consensus sequence (ENLYFQGLNDIFEAQKIEWHE), flanked by 100bp of DNA as the 5' homologous arm and 100bp of DNA as the 3' homologous arm. Synthesized gRNA, single strand DNA repairing template, as well as Cas9 mRNA were co-injected into a one-cell zygote of

C57BL/6 background to allow for homology-directed repair, followed by implantation. PCR primers specific to the 5' and 3' integration sites flanking the gRNA sequence at the 3' end of the *Cdkl5* locus were used to screen for positively targeted pups. Southern blotting was finally conducted to confirm the correct targeting of the F1 generation, followed by establishment a CDKL5-TAVI colony in a C57BL/6J genetic background.

R26^{cre} (BirA) mice were generated as previously described, and Nex-Cre mice (RRID: MGI: 4429523), generously shared by Klaus-Armin Nave (Max Planck Institute of Experimental Medicine, Göttingen, Germany) and Lazzarini Denchi (The Scripps Research Institute)(Goebbels et al., 2006; Johnson et al., 2017). All lines have been maintained in the C57BL/6J background.

Experimental cohorts were all weaned at 3 weeks of age and littermates housed together. Mice were genotyped using a qPCR based strategy optimized by Transnetyx.

Brain microdissection. To assess protein expression in various brain regions, adult male mice were sacrificed by cervical dislocation. After decapitation, brains were removed and sectioned into 1mm coronal slices using a mouse brain matrix. Tissue was dissected from the somatosensory cortex, striatum, hippocampus, and cerebellum and homogenized in RIPA lysis buffer (150mM NaCl, 1% Triton X-100, 0.5% sodium deoxycholate [DOC], 0.1% sodium dodecyl sulfate [SDS], 25mM Tris [pH7.4] with protease inhibitors [Roche, cOmplete, EDTA-free protease inhibitor cocktail tablets; 5056489001]). To prepare protein extracts, homogenized lysates were incubated on ice for 15 min, and then centrifuged at 21,000 x g for 15min at 4°C. The supernatant fraction was removed and sonicated using a Biorupter for 3 alternating session at max frequency for 15 sec, each followed by a 60 sec cooldown period. The lysate was then centrifuged at 21,000 x g for 15min at 4°C, and the top aqueous layer carefully removed and collected as the total protein fraction.

Streptavidin-Mediated Pull-Down. Brain tissue lysates were prepared as described above. 500µg of protein lysate was utilized for each pull-down reaction, with 10% of the lysate collected

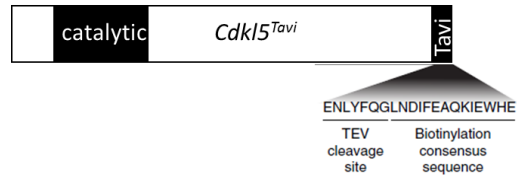
prior to streptavidin treatment as an “input” loading control. Protein lysates were incubated with 70µL streptavidin-conjugated magnetic beads (Dynabeads M-280 Streptavidin; Invitrogen 11205D) for 1hr at 4°C while rotating. Magnetic beads were separated away from the remaining lysate using a DynaMag-2™ rack (Invitrogen; 12321D), and 20µL of remaining lysate collected as “flow-through.” The lysate was then discarded and the beads subsequently washed 4X with 1% NP-40 in 150mM NaCl wash buffer. Beads were resuspended in the appropriate amount of LDS Sample buffer and β-mercaptoethanol, and then heat denatured at 90°C for 15min.

Western blot. Protein concentration was measured using a Bradford assay. Purified synaptic density membrane proteins or protein lysates were prepared for gel electrophoresis by adding 4X LDS Sample Buffer (NuPAGE, NP0008) to a final concentration of 1X and β-mercaptoethanol to a final concentration of 5%. Samples were heat-denatured at 75°C for 20 min, and 7.5µg or 25 µg of protein was loaded into each well of a 4–12% Bis-Tris gradient gel (Invitrogen, 10-well, 1.5mm; NP0335) for PSD protein or brain lysate quantification, respectively. Protein gels were run for 2hr at 125V at room temperature on a XCell SureLock mini-cell electrophoresis box (ThermoFisher; EI001) using a PowerPac HC High-Current Power Supply (BioRad; 1645052), then transferred onto a polyvinylidene fluoride (PVDF) membrane (0.45µm pore-size; Biorad 162–0115) at 27V for 1hr and 10min at room temperature. The resulting membrane was blocked with a 1:1 solution of Odyssey blocking buffer (LICOR; 927-40100) and 1X PBS for 1hr at room temperature.

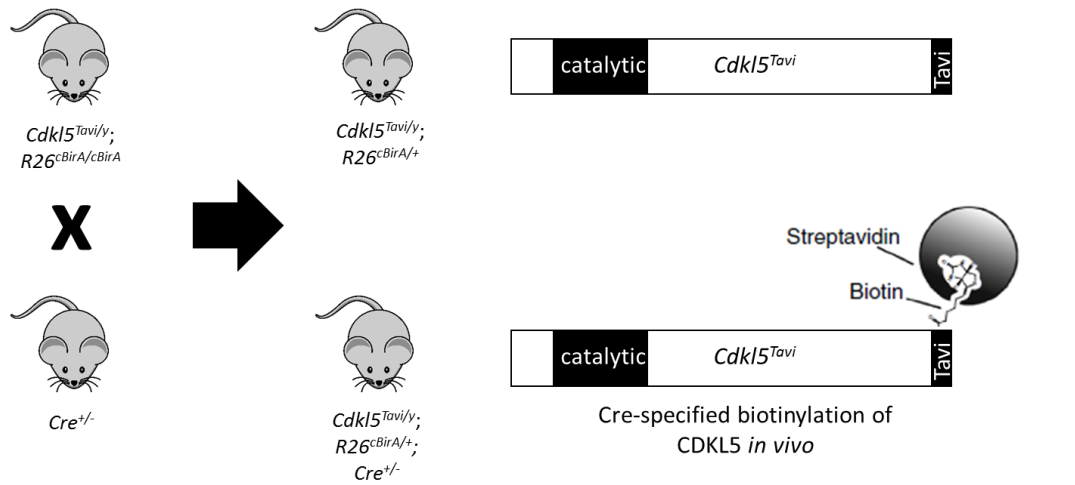
Primary antibodies used were rabbit anti-N-terminal CDKL5 (in house; diluted 1:500), rabbit anti-BirA consensus sequence (Abcam; ab1400; diluted 1:1,000), and mouse anti-β-Actin (Abcam; ab8226; diluted 1:10,000). A streptavidin-conjugated fluorophore, IRDye 680RD Streptavidin (LI-COR; 926-68079; diluted 1:1,000), was utilized for visualization of biotinylated proteins. Secondary antibodies (LI-COR) used were goat anti-rabbit IgG IRDye800CW and rabbit anti-mouse IgG IRDye680LT, all incubated for 50min at room temperature at dilutions of 1:10,000. Standard protocols were used for the Odyssey Infrared Imaging System (LI-COR) for protein visualization and quantification.

Figures

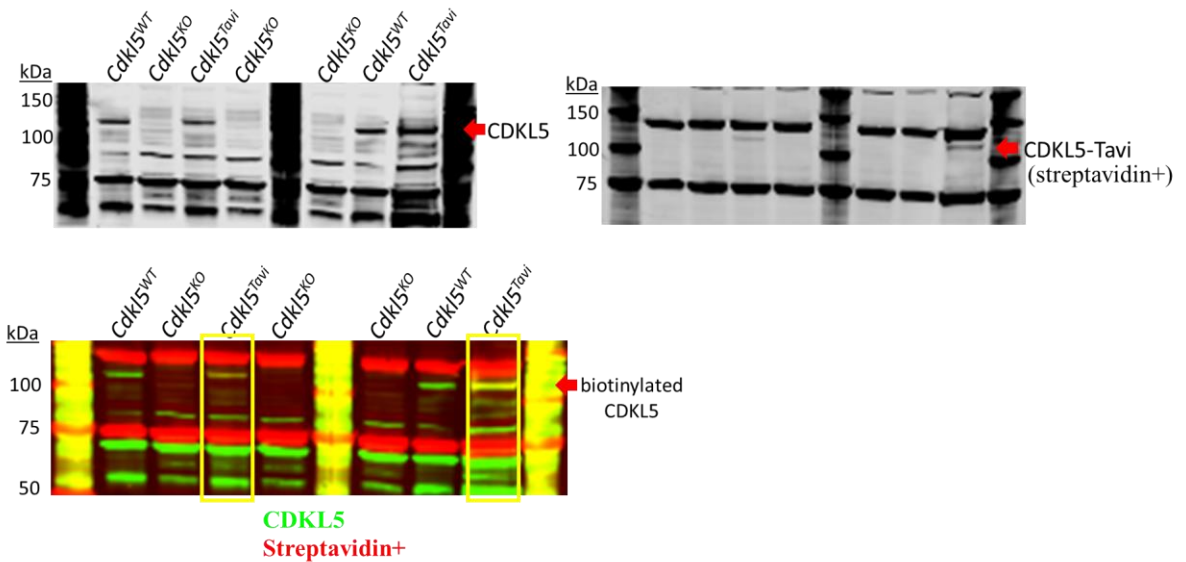
a



b



c



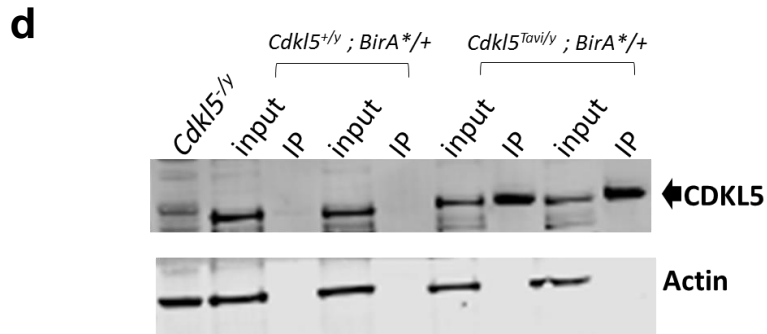


Figure 1. Generation and characterization of CDKL5-TAVI mice.

(a) Diagram of Tavi-tagged CDKL5 showing the kinase domain and amino acid sequence of the TAVI tag (TEV protease cleavage site plus biotinylation consensus sequence). **(b)** Breeding strategy to biotinylate the TAVI tag in a Cre-dependent manner. **(c)** Representative western blots showing the conditions in which the TAVI tag is biotinylated using whole-brain tissue lysates from male mice. Top left: Blot was probed with antibody to the CDKL5 N-terminus, highlighting the presence of CDKL5 in both wild-type and CDKL5-TAVI tissues; Top right: Blot was probed with streptavidin for detection of biotinylated proteins, demonstrating a biotinylated CDKL5 product only in CDKL5-TAVI; *BirA*^{+/+}; Cre mice (asterisk denotes endogenous biotinylated products detectable from brain lysate at 75kDa and 150kDa). Bottom: overlay of CDKL5 antibody (green) and streptavidin (red) staining demonstrating the overlap of biotinylated CDKL5 product. **(d)** Representative western blot demonstrating the enrichment of CDKL5 protein from mouse brain tissues using streptavidin-coated beads in CDKL5-TAVI; *BirA*^{*} mice, but not *BirA*^{*}-only mice.

BIBLIOGRAPHY

- Akamine, S., Ishizaki, Y., Sakai, Y., Torisu, H., Fukai, R., Miyake, N., . . . Ohga, S. (2018). A male case with CDKL5-associated encephalopathy manifesting transient methylmalonic acidemia. *Eur J Med Genet*, *61*(8), 451-454. doi:10.1016/j.ejmg.2018.03.003
- Akhmanova, A., & Steinmetz, M. O. (2015). Control of microtubule organization and dynamics: two ends in the limelight. *Nature Reviews Molecular Cell Biology*, *16*(12), 711-726. doi:10.1038/nrm4084
- Amaral, D. G., Scharfman, H. E., & Lavenex, P. (2007). *The Dentate Gyrus: A Comprehensive Guide to Structure, Function, and Clinical Implications* (Vol. 163): Elsevier.
- Amendola, E., Zhan, Y., Mattucci, C., Castroflorio, E., Calcagno, E., Fuchs, C., . . . Gross, C. T. (2014). Mapping pathological phenotypes in a mouse model of CDKL5 disorder. *PLoS One*, *9*(5), e91613. doi:10.1371/journal.pone.0091613
- Ang, C. W. (2005). Hippocampal CA1 Circuitry Dynamically Gates Direct Cortical Inputs Preferentially at Theta Frequencies. *Journal of Neuroscience*, *25*(42), 9567-9580. doi:10.1523/jneurosci.2992-05.2005
- Ang, C. W., Carlson, G. C., & Coulter, D. A. (2006). Massive and Specific Dysregulation of Direct Cortical Input to the Hippocampus in Temporal Lobe Epilepsy. *26*(46), 11850-11856. doi:10.1523/jneurosci.2354-06.2006
- Antic, S., & Zecevic, D. (1995). Optical signals from neurons with internally applied voltage-sensitive dyes. *Journal of Neuroscience*, *15*(2), 1392-1405. doi:10.1523/JNEUROSCI.15-02-01392.1995
- Archer, H. L., Evans, J., Edwards, S., Colley, J., Newbury-Ecob, R., O'Callaghan, F., . . . Osborne, J. (2006). CDKL5 mutations cause infantile spasms, early onset seizures, and severe mental retardation in female patients. *J Med Genet*, *43*(9), 729-734. doi:10.1136/jmg.2006.041467
- Arellano, J. I. (2007). Ultrastructure of dendritic spines: correlation between synaptic and spine morphologies. *1*(1), 131-143. doi:10.3389/neuro.01.1.1.010.2007
- Bahi-Buisson, N., & Bienvenu, T. (2012). CDKL5-Related Disorders: From Clinical Description to Molecular Genetics. *Mol Syndromol*, *2*(3-5), 137-152. doi:10.1159/000331333
- Bahi-Buisson, N., Kaminska, A., Boddaert, N., Rio, M., Afenjar, A., Gerard, M., . . . Bienvenu, T. (2008). The three stages of epilepsy in patients with CDKL5 mutations. *Epilepsia*, *49*(6), 1027-1037. doi:10.1111/j.1528-1167.2007.01520.x
- Bahi-Buisson, N., Nectoux, J., Rosas-Vargas, H., Milh, M., Boddaert, N., Girard, B., . . . Bienvenu, T. (2008). Key clinical features to identify girls with CDKL5 mutations. *Brain*, *131*(Pt 10), 2647-2661. doi:10.1093/brain/awn197
- Bahi-Buisson, N., Villeneuve, N., Caietta, E., Jacqueline, A., Maurey, H., Matthijs, G., . . . Bienvenu, T. (2012). Recurrent mutations in the CDKL5 gene: genotype-phenotype relationships. *Am J Med Genet A*, *158A*(7), 1612-1619. doi:10.1002/ajmg.a.35401
- Baltussen, L. L., Negraes, P. D., Silvestre, M., Claxton, S., Moeskops, M., Christodoulou, E., . . . Ultanir, S. K. (2018). Chemical genetic identification of CDKL5 substrates reveals its role in neuronal microtubule dynamics. *The EMBO Journal*, e99763. doi:10.15252/embj.201899763

- Baltussen, L. L., Rosianu, F., & Ultanir, S. K. (2018). Kinases in synaptic development and neurological diseases. *Prog Neuropsychopharmacol Biol Psychiatry*, *84*(Pt B), 343-352. doi:10.1016/j.pnpbp.2017.12.006
- Barbiero, I., De Rosa, R., & Kilstrup-Nielsen, C. (2019). Microtubules: A Key to Understand and Correct Neuronal Defects in CDKL5 Deficiency Disorder? *Int J Mol Sci*, *20*(17), 4075. doi:10.3390/ijms20174075
- Barbiero, I., Valente, D., Chandola, C., Magi, F., Bergo, A., Montefonfrio, L., . . . Kilstrup-Nielsen, C. (2017). CDKL5 localizes at the centrosome and midbody and is required for faithful cell division. *Sci Rep*, *7*(1), 6228. doi:10.1038/s41598-017-05875-z
- Bartnik, M., Derwinska, K., Gos, M., Obersztyn, E., Kolodziejaska, K. E., Erez, A., . . . Stankiewicz, P. (2011). Early-onset seizures due to mosaic exonic deletions of CDKL5 in a male and two females. *Genet Med*, *13*(5), 447-452. doi:10.1097/GIM.0b013e31820605f5
- Bates, D., Machler, M., Bolker, B., & Walker, S. (2015). Fitting Linear Mixed-Effects Models Using lme4. *J. Stat. Soft.*, *67*, 1-48.
- Bayés, À., Collins, M. O., Croning, M. D. R., Van De Lagemaat, L. N., Choudhary, J. S., & Grant, S. G. N. (2012). Comparative Study of Human and Mouse Postsynaptic Proteomes Finds High Compositional Conservation and Abundance Differences for Key Synaptic Proteins. *PLoS One*, *7*(10), e46683. doi:10.1371/journal.pone.0046683
- Beconi, M. G., Howland, D., Park, L., Lyons, K., Giuliano, J., Dominguez, C., . . . Pacifici, R. (2011). Pharmacokinetics of memantine in rats and mice. *PLoS Currents*, *3*.
- Benke, T. A., & Kind, P. C. (2020). Proof-of-concept for a gene replacement approach to CDKL5 deficiency disorder. *Brain*, *143*(3), 716-718. doi:10.1093/brain
- Berg, A. T., Langfitt, J. T., Testa, F. M., Levy, S. R., DiMario, F., Westerveld, M., & Kulas, J. (2008). Global cognitive function in children with epilepsy: a community-based study. *Epilepsia*, *49*(4), 608-614. doi:10.1111/j.1528-1167.2007.01461.x
- Berg, A. T., Zelko, F. A., Levy, S. R., & Testa, F. M. (2012). Age at onset of epilepsy, pharmacoresistance, and cognitive outcomes: a prospective cohort study. *Neurology*, *79*(13), 1384-1391. doi:10.1212/WNL.0b013e31826c1b55
- Bermejo, M. K., Milenkovic, M., Salahpour, A., & Ramsey, A. J. (2014). Preparation of Synaptic Plasma Membrane and Postsynaptic Density Proteins Using a Discontinuous Sucrose Gradient. *Journal of Visualized Experiments*(91). doi:10.3791/51896
- Bertani, I., Rusconi, L., Bolognese, F., Forlani, G., Conca, B., De Monte, L., . . . Kilstrup-Nielsen, C. (2006). Functional consequences of mutations in CDKL5, an X-linked gene involved in infantile spasms and mental retardation. *J Biol Chem*, *281*(42), 32048-32056. doi:10.1074/jbc.M606325200
- Bhaskar, P. T., & Hay, N. (2007). The Two TORCs and Akt. *Developmental Cell*, *12*(4), 487-502. doi:10.1016/j.devcel.2007.03.020
- Bienvendu, T. (2002). ARX, a novel Prd-class-homeobox gene highly expressed in the telencephalon, is mutated in X-linked mental retardation. *Human Molecular Genetics*, *11*(8), 981-991. doi:10.1093/hmg/11.8.981
- Bourgeron, T. (2015). From the genetic architecture to synaptic plasticity in autism spectrum disorder. *Nature Reviews Neuroscience*, *16*(9), 551-563. doi:10.1038/nrn3992
- Calfa, G., Hablitz, J. J., & Pozzo-Miller, L. (2011). Network hyperexcitability in hippocampal slices from Mecp2 mutant mice revealed by voltage-sensitive dye imaging. *Journal of Neurophysiology*, *105*, 1768-1784.

- Caligioni, C. S. (2009). Assessing reproductive status/stages in mice. *Curr Protoc Neurosci, Appendix 4*, Appendix 4I. doi:10.1002/0471142301.nsa04is48
- Canning, P., Park, K., Goncalves, J., Li, C., Howard, C. J., Sharpe, T. D., . . . Leroux, M. R. (2018). CDKL Family Kinases Have Evolved Distinct Structural Features and Ciliary Function. *Cell Rep*, 22(4), 885-894. doi:10.1016/j.celrep.2017.12.083
- Carlson, G. C., & Coulter, D. A. (2008). In vitro functional imaging in brain slices using fast voltage-sensitive dye imaging combined with whole-cell patch recording. *J Neurosci*, 28(2), 249-255. doi:10.1038/nprot.2007.539
- Chabbert, D., Caubit, X., Roubertoux, P. L., Carlier, M., Habermann, B., Jacq, B., . . . Gubellini, P. (2019). Postnatal Tshz3 Deletion Drives Altered Corticostriatal Function and Autism Spectrum Disorder-like Behavior. *Biological Psychiatry*, 86(4), 274-285. doi:10.1016/j.biopsych.2019.03.974
- Chandran, V., Gao, K., Swarup, V., Versano, R., Dong, H., Jordan, M. C., & Geschwind, D. H. (2017). Inducible and reversible phenotypes in a novel mouse model of Friedreich's Ataxia. *Elife*, 6. doi:10.7554/elife.30054
- Chao, H.-T., Chen, H., Samaco, R. C., Xue, M., Chahrour, M., Yoo, J., . . . Zoghbi, H. Y. (2010). Dysfunction in GABA signalling mediates autism-like stereotypies and Rett syndrome phenotypes. *Nature*, 468(7321), 263-269. doi:10.1038/nature09582
- Chen, Q., Zhu, Y. C., Yu, J., Miao, S., Zheng, J., Xu, L., . . . Xiong, Z. Q. (2010). CDKL5, a protein associated with rett syndrome, regulates neuronal morphogenesis via Rac1 signaling. *J Neurosci*, 30(38), 12777-12786. doi:10.1523/JNEUROSCI.1102-10.2010
- Chung, W., Choi, S. Y., Lee, E., Park, H., Kang, J., Park, H., . . . Kim, E. (2015). Social deficits in IRSp53 mutant mice improved by NMDAR and mGluR5 suppression. *Nature Neuroscience*, 18(3), 435-443. doi:10.1038/nn.3927
- Costales, J., & Kolevzon, A. (2016). The therapeutic potential of insulin-like growth factor-1 in central nervous system disorders. *Neuroscience & Biobehavioral Reviews*, 63, 207-222. doi:10.1016/j.neubiorev.2016.01.001
- Coulter, D. A., & Carlson, G. C. (2007). Functional regulation of the dentate gyrus by GABA-mediated inhibition. *Progress in Brain Research*, 163. doi:10.1016/s0079-6123(07)63014-3
- Coulter, D. A., Yue, C., Ang, C. W., Weissinger, F., Goldberg, E., Hsu, F.-C., . . . Takano, H. (2011). Hippocampal microcircuit dynamics probed using optical imaging approaches. *J Neurosci*, 31(8), 1893-1903. doi:10.1111/jphysiol.2010.202184
- Creson, T. K., Rojas, C., Hwaun, E., Vaissiere, T., Kilinc, M., Jimenez-Gomez, A., . . . Rumbaugh, G. (2019). Re-expression of SynGAP protein in adulthood improves translatable measures of brain function and behavior. *Elife*, 8. doi:10.7554/elife.46752
- Deacon, R. M. (2006). Assessing nest building in mice. *Nature Protocols*, 1(3), 1117-1119. doi:10.1038/nprot.2006.170
- Deal, R. B., & Henikoff, S. (2010). A Simple Method for Gene Expression and Chromatin Profiling of Individual Cell Types within a Tissue. *Developmental Cell*, 18(6), 1030-1040. doi:10.1016/j.devcel.2010.05.013
- Della Sala, G., Putignano, E., Chelini, G., Melani, R., Calcagno, E., Michele Ratto, G., . . . Pizzorusso, T. (2016). Dendritic Spine Instability in a Mouse Model of CDKL5 Disorder Is Rescued by Insulin-like Growth Factor 1. *Biol Psychiatry*, 80(4), 302-311. doi:10.1016/j.biopsych.2015.08.028

- Demarest, S., Pestana-Knight, E. M., Olson, H. E., Downs, J., Marsh, E. D., Kaufmann, W. E., . . . Benke, T. A. (2019). Severity Assessment in CDKL5 Deficiency Disorder. *Pediatr Neurol*, *97*, 38-42. doi:10.1016/j.pediatrneurol.2019.03.017
- Demarest, S. T., Olson, H. E., Moss, A., Pestana-Knight, E., Zhang, X., Parikh, S., . . . Benke, T. A. (2019). CDKL5 deficiency disorder: Relationship between genotype, epilepsy, cortical visual impairment, and development. *Epilepsia*, *60*(8), 1733-1742. doi:10.1111/epi.16285
- Dengler, C. G., & Coulter, D. A. (2016). Normal and epilepsy-associated pathologic function of the dentate gyrus. *Prog Brain Res.*, *226*, 155-178. doi:10.1016/bs.pbr.2016.04.005
- Devinsky, O., Verducci, C., Thiele, E. A., Laux, L. C., Patel, A. D., Filloux, F., . . . Friedman, D. (2018). Open-label use of highly purified CBD (Epidiolex(R)) in patients with CDKL5 deficiency disorder and Aicardi, Dup15q, and Doose syndromes. *Epilepsy Behav*, *86*, 131-137. doi:10.1016/j.yebeh.2018.05.013
- Devinsky, O., Vickrey, B. G., Cramer, J., Perrine, K., Hermann, B., Meador, K., & Hays, R. D. (1995). Development of the quality of life in epilepsy inventory. *Epilepsia*, *36*(11), 1089-1104. doi:10.1111/j.1528-1157.1995.tb00467.x
- Dierssen, M. (2012). Down syndrome: the brain in trisomic mode. *Nature Reviews Neuroscience*, *13*(12), 844-858. doi:10.1038/nrn3314
- Djurisic, M., Brott, B. K., Saw, N. L., Shamloo, M., & Shatz, C. J. (2018). Activity-dependent modulation of hippocampal synaptic plasticity via PirB and endocannabinoids. *Molecular Psychiatry*. doi:10.1038/s41380-018-0034-4
- Dubos, A., Pannetier, S., & Hanauer, A. (2008). Inactivation of the CDKL3 gene at 5q31.1 by a balanced t(X;5) translocation associated with nonspecific mild mental retardation. *Am J Med Genet A*, *146A*(10), 1267-1279. doi:10.1002/ajmg.a.32274
- Engel Jr., J. (2012). *Seizures and Epilepsy*: Oxford University Press.
- Evans, J. C., Archer, H. L., Colley, J. P., Ravn, K., Nielsen, J. B., Kerr, A., . . . Clarke, A. J. (2005). Early onset seizures and Rett-like features associated with mutations in CDKL5. *Eur J Hum Genet*, *13*(10), 1113-1120. doi:10.1038/sj.ejhg.5201451
- Fairless, A. H., Katz, J. M., Vijayvargiya, N., Dow, H. C., Kreibich, A. S., Berrettini, W. H., . . . Brodtkin, E. S. (2013). Development of home cage social behaviors in BALB/cJ vs. C57BL/6J mice. *Behavioural Brain Research*, *237*, 338-347. doi:10.1016/j.bbr.2012.08.051
- Fehr, S., Downs, J., Ho, G., de Klerk, N., Forbes, D., Christodoulou, J., . . . Leonard, H. (2016). Functional abilities in children and adults with the CDKL5 disorder. *Am J Med Genet A*, *170*(11), 2860-2869. doi:10.1002/ajmg.a.37851
- Fehr, S., Leonard, H., Ho, G., Williams, S., de Klerk, N., Forbes, D., . . . Downs, J. (2015). There is variability in the attainment of developmental milestones in the CDKL5 disorder. *J Neurodev Disord*, *7*(1), 2. doi:10.1186/1866-1955-7-2
- Fehr, S., Wilson, M., Downs, J., Williams, S., Murgia, A., Sartori, S., . . . Christodoulou, J. (2013). The CDKL5 disorder is an independent clinical entity associated with early-onset encephalopathy. *Eur J Hum Genet*, *21*(3), 266-273. doi:10.1038/ejhg.2012.156
- Fehr, S., Wong, K., Chin, R., Williams, S., de Klerk, N., Forbes, D., . . . Leonard, H. (2016). Seizure variables and their relationship to genotype and functional abilities in the CDKL5 disorder. *Neurology*, *87*(21), 2206-2213.

- Feng, G., Mellor, R. H., Bernstein, M., Keller-Peck, C., Nguyen, Q. T., Wallace, M., . . . Sanes, J. R. (2000). Imaging Neuronal Subsets in Transgenic Mice Expressing Multiple Spectral Variants of GFP. *Neuron*, *28*(1), 41-51. doi:10.1016/s0896-6273(00)00084-2
- Fernandez, F., & Garner, C. C. (2007). Over-inhibition: a model for developmental intellectual disability. *30*(10), 497-503. doi:10.1016/j.tins.2007.07.005
- Ferraro, T. N., Smith, G. G., Schwebel, C. L., Doyle, G. A., Ruiz, S. E., Oleynick, J. U., . . . Buono, R. J. (2010). Confirmation of multiple seizure susceptibility QTLs on chromosome 15 in C57BL/6J and DBA/2J inbred mice. *Physiol Genomics*, *42A*(1), 1-7. doi:10.1152/physiolgenomics.00096.2010
- Figueiredo, C. P., Clarke, J. R., Ledo, J. H., Ribeiro, F. C., Costa, C. V., Melo, H. M., . . . Ferreira, S. T. (2013). Memantine Rescues Transient Cognitive Impairment Caused by High-Molecular-Weight A Oligomers But Not the Persistent Impairment Induced by Low-Molecular-Weight Oligomers. *Journal of Neuroscience*, *33*(23), 9626-9634. doi:10.1523/jneurosci.0482-13.2013
- Flurkey, K., Brandvain, Y., Klebanov, S., Austad, S. N., Miller, R. A., Yuan, R., & Harrison, D. E. (2007). PohnB6F1: a cross of wild and domestic mice that is a new model of extended female reproductive life span. *J Gerontol A Biol Sci Med Sci*, *62*(11), 1187-1198. doi:10.1093/gerona/62.11.1187
- Fuccillo, M. V. (2016). Striatal Circuits as a Common Node for Autism Pathophysiology. *Frontiers in Neuroscience*, *10*. doi:10.3389/fnins.2016.00027
- Fuchs, C., Medici, G., Trazzi, S., Gennaccaro, L., Galvani, G., Berteotti, C., . . . Ciani, E. (2019). CDKL5 deficiency predisposes neurons to cell death through the deregulation of SMAD3 signaling. *Brain Pathol*, *29*(5), 658-674. doi:10.1111/bpa.12716
- Fuchs, C., Trazzi, S., Torricella, R., Viggiano, R., De Franceschi, M., Amendola, E., . . . Ciani, E. (2014). Loss of CDKL5 impairs survival and dendritic growth of newborn neurons by altering AKT/GSK-3beta signaling. *Neurobiol Dis*, *70*, 53-68. doi:10.1016/j.nbd.2014.06.006
- Gadalla, K. K. E., Vudhironarit, T., Hector, R. D., Sinnett, S., Bahey, N. G., Bailey, M. E. S., . . . Cobb, S. R. (2017). Development of a Novel AAV Gene Therapy Cassette with Improved Safety Features and Efficacy in a Mouse Model of Rett Syndrome. *Molecular Therapy - Methods & Clinical Development*, *5*, 180-190. doi:10.1016/j.omtm.2017.04.007
- Gandal, M. J., Edgar, J. C., Ehrlichman, R. S., Mehta, M., Roberts, T. P. L., & Siegel, S. J. (2010). Validating γ Oscillations and Delayed Auditory Responses as Translational Biomarkers of Autism. *Biological Psychiatry*, *68*(12), 1100-1106. doi:10.1016/j.biopsych.2010.09.031
- Gao, Y., Irvine, E. E., Eleftheriadou, I., Naranjo, C. J., Hearn-Yeates, F., Bosch, L., . . . Mazarakis, N. D. (2020). Gene replacement ameliorates deficits in mouse and human models of cyclin-dependent kinase-like 5 disorder. *Brain*, *143*(3), 811-832. doi:10.1093/brain/awaa028
- Garg, S. K., Liroy, D. T., Cheval, H., McGann, J. C., Bissonnette, J. M., Murtha, M. J., . . . Mandel, G. (2013). Systemic Delivery of MeCP2 Rescues Behavioral and Cellular Deficits in Female Mouse Models of Rett Syndrome. *Journal of Neuroscience*, *33*(34), 13612-13620. doi:10.1523/jneurosci.1854-13.2013
- Gholizadeh, S., Arsenault, J., Xuan, I. C. Y., Pacey, L. K., & Hampson, D. R. (2014). Reduced Phenotypic Severity Following Adeno-Associated Virus-Mediated Fmr1 Gene Delivery in Fragile X Mice. *39*(13), 3100-3111. doi:10.1038/npp.2014.167

- Goebbels, S., Bormuth, I., Bode, U., Hermanson, O., Schwab, M. H., & Nave, K.-A. (2006). Genetic targeting of principal neurons in neocortex and hippocampus of NEX-Cre mice. *genesis*, *44*(12), 611-621. doi:10.1002/dvg.20256
- Goffin, D., Allen, M., Zhang, L., Amorim, M., Wang, I. T. J., Reyes, A.-R. S., . . . Zhou, Z. (2012). Rett syndrome mutation MeCP2 T158A disrupts DNA binding, protein stability and ERP responses. *Nature Neuroscience*, *15*(2), 274-283. doi:10.1038/nn.2997
- Goldberg, E. M., & Coulter, D. A. (2013). Mechanisms of epileptogenesis: a convergence on neural circuit dysfunction. *Nature Reviews Neuroscience*, *14*(5), 337-349. doi:10.1038/nrn3482
- Guy, J., Gan, J., Selfridge, J., Cobb, S., & Bird, A. (2007). Reversal of Neurological Defects in a Mouse Model of Rett Syndrome. *Science*, *315*(5815), 1143-1147. doi:10.1126/science.1138389
- Habib-E-Rasul Mullah, S., Komuro, R., Yan, P., Hayashi, S., Inaji, M., Momose-Sato, Y., . . . Sato, K. (2013). Evaluation of Voltage-Sensitive Fluorescence Dyes for Monitoring Neuronal Activity in the Embryonic Central Nervous System. *The Journal of Membrane Biology*, *246*(9), 679-688. doi:10.1007/s00232-013-9584-1
- Han, S., Tai, C., Westenbroek, R. E., Yu, F. H., Cheah, C. S., Potter, G. B., . . . Catterall, W. A. (2012). Autistic-like behaviour in Scn1a+/- mice and rescue by enhanced GABA-mediated neurotransmission. *Nature*, *489*(7416), 385-390. doi:10.1038/nature11356
- Hanefeld, F. (1985). The clinical pattern of the rett syndrome. *7*(3), 320-325. doi:10.1016/s0387-7604(85)80037-1
- Harris KM, S. J. (1989). Dendritic spines of CA1 pyramidal cells in the rat hippocampus: serial electron microscopy with reference to their biophysical characteristics. *Journal of Neuroscience*, *9*(8), 2982-2997. doi:10.1523/JNEUROSCI.09-08-02982.1989
- He, A., Ma, L., Huang, Y., Zhang, H., Duan, W., Li, Z., . . . Xiang, D. (2020). CDKL3 promotes osteosarcoma progression by activating Akt/PKB. *Life Science Alliance*, *3*(5), e202000648. doi:10.26508/lsa.202000648
- Hector, R. D., Dando, O., Landsberger, N., Kilstrup-Nielsen, C., Kind, P. C., Bailey, M. E., & Cobb, S. R. (2016). Characterisation of CDKL5 Transcript Isoforms in Human and Mouse. *PLoS One*, *11*(6), e0157758. doi:10.1371/journal.pone.0157758
- Hector, R. D., Kalscheuer, V. M., Hennig, F., Leonard, H., Downs, J., Clarke, A., . . . Cobb, S. R. (2017). *CDKL5* Variants. *Neurology Genetics*, *3*(6). doi:10.1212/NXG.0000000000000200
- Hensch, T. K. (2004). CRITICAL PERIOD REGULATION. *Annual Review of Neuroscience*, *27*(1), 549-579. doi:10.1146/annurev.neuro.27.070203.144327
- Huang, G., Chen, S., Chen, X., Zheng, J., Xu, Z., Doostparast Torshizi, A., . . . Shi, L. (2019). Uncovering the Functional Link Between SHANK3 Deletions and Deficiency in Neurodevelopment Using iPSC-Derived Human Neurons. *Frontiers in Neuroanatomy*, *13*. doi:10.3389/fnana.2019.00023
- James, Aceti, M., Thomas, Emin, Shi, Y., Nicholas, . . . Rumbaugh, G. (2012). Pathogenic SYNGAP1 Mutations Impair Cognitive Development by Disrupting Maturation of Dendritic Spine Synapses. *151*(4), 709-723. doi:10.1016/j.cell.2012.08.045
- Jaworski, J., Kapitein, L. C., Gouveia, S. M., Dortland, B. R., Wulf, P. S., Grigoriev, I., . . . Hoogenraad, C. C. (2009). Dynamic microtubules regulate dendritic spine morphology and synaptic plasticity. *Neuron*, *61*(1), 85-100. doi:10.1016/j.neuron.2008.11.013

- Jeste, S. S., & Nelson, C. A. (2009). Event Related Potentials in the Understanding of Autism Spectrum Disorders: An Analytical Review. *Journal of Autism and Developmental Disorders*, 39(3), 495-510. doi:10.1007/s10803-008-0652-9
- Jhang, C. L., Huang, T. N., Hsueh, Y. P., & Liao, W. (2017). Mice lacking cyclin-dependent kinase-like 5 manifest autistic and ADHD-like behaviors. *Hum Mol Genet*, 26(20), 3922-3934. doi:10.1093/hmg/ddx279
- Johnson, B. S., Zhao, Y.-T., Fasolino, M., Lamonica, J. M., Kim, Y. J., Georgakilas, G., . . . Zhou, Z. (2017). Biotin tagging of MeCP2 in mice reveals contextual insights into the Rett syndrome transcriptome. *Nature Medicine*, 23(10), 1203-1214. doi:10.1038/nm.4406
- Joy, R. M., & Albertson, T. E. (1993). NMDA receptors have a dominant role in population spike-paired pulse facilitation in the dentate gyrus of urethane-anesthetized rats. *604(1-2)*, 273-282. doi:10.1016/0006-8993(93)90379-2
- Kalscheuer, V. M., Tao, J., Donnelly, A., Hollway, G., Schwinger, E., Kubart, S., . . . Gecz, J. (2003). Disruption of the serine/threonine kinase 9 gene causes severe X-linked infantile spasms and mental retardation. *Am J Hum Genet*, 72(6), 1401-1411. doi:10.1086/375538
- Kameshita, I., Sekiguchi, M., Hamasaki, D., Sugiyama, Y., Hatano, N., Suetake, I., . . . Sueyoshi, N. (2008). Cyclin-dependent kinase-like 5 binds and phosphorylates DNA methyltransferase 1. *Biochem Biophys Res Commun*, 377(4), 1162-1167. doi:10.1016/j.bbrc.2008.10.113
- Kang, H. J., Kawasawa, Y. I., Cheng, F., Zhu, Y., Xu, X., Li, M., . . . Šestan, N. (2011). Spatio-temporal transcriptome of the human brain. *Nature*, 478(7370), 483-489. doi:10.1038/nature10523
- Kang, J., & Kim, E. (2015). Suppression of NMDA receptor function in mice prenatally exposed to valproic acid improves social deficits and repetitive behaviors. *8*. doi:10.3389/fnmol.2015.00017
- Katayama, S., Sueyoshi, N., & Kameshita, I. (2015). Critical Determinants of Substrate Recognition by Cyclin-Dependent Kinase-like 5 (CDKL5). *Biochemistry*, 54(19), 2975-2987. doi:10.1021/bi501308k
- Kilstrup-Nielsen, C., Rusconi, L., La Montanara, P., Ciceri, D., Bergo, A., Bedogni, F., & Landsberger, N. (2012). What we know and would like to know about CDKL5 and its involvement in epileptic encephalopathy. *Neural Plast*, 2012, 728267. doi:10.1155/2012/728267
- Kim, J. Y., Bai, Y., Jayne, L. A., Hector, R. D., Persaud, A. K., Ong, S. S., . . . Pabla, N. S. (2020). A kinome-wide screen identifies a CDKL5-SOX9 regulatory axis in epithelial cell death and kidney injury. *Nature Communications*, 11(1). doi:10.1038/s41467-020-15638-6
- Kolc, K. L., Sadleir, L. G., Scheffer, I. E., Ivancevic, A., Roberts, R., Pham, D. H., & Gecz, J. (2019). A systematic review and meta-analysis of 271 PCDH19-variant individuals identifies psychiatric comorbidities, and association of seizure onset and disease severity. *Mol Psychiatry*, 24(2), 241-251. doi:10.1038/s41380-018-0066-9
- Komarova, Y., De Groot, C. O., Grigoriev, I., Gouveia, S. M., Munteanu, E. L., Schober, J. M., . . . Akhmanova, A. (2009). Mammalian end binding proteins control persistent microtubule growth. *Journal of Cell Biology*, 184(5), 691-706. doi:10.1083/jcb.200807179
- Krey, J. F., Paşca, S. P., Shcheglovitov, A., Yazawa, M., Schwemberger, R., Rasmusson, R., & Dolmetsch, R. E. (2013). Timothy syndrome is associated with activity-dependent dendritic retraction in rodent and human neurons. *16(2)*, 201-209. doi:10.1038/nn.3307
- La Montanara, P., Hervera, A., Baltussen, L. L., Hutson, T. H., Palmisano, I., De Virgiliis, F., . . . Di Giovanni, S. (2020). Cyclin-dependent-like kinase 5 is required for pain signaling in

- human sensory neurons and mouse models. *Science Translational Medicine*, 12(551), eaax4846. doi:10.1126/scitranslmed.aax4846
- La Montanara, P., Rusconi, L., Locarno, A., Forti, L., Barbiero, I., Tramarin, M., . . . Landsberger, N. (2015). Synaptic synthesis, dephosphorylation, and degradation: a novel paradigm for an activity-dependent neuronal control of CDKL5. *J Biol Chem*, 290(7), 4512-4527. doi:10.1074/jbc.M114.589762
- Laketa, V., Simpson, J. C., Bechtel, S., Wiemann, S., & Pepperkok, R. (2006). High-Content Microscopy Identifies New Neurite Outgrowth Regulators. *Molecular Biology of the Cell*, 18(1), 242-252. doi:10.1091/mbc.e06-08-0666
- Lee, E., Lee, J., & Kim, E. (2017). Excitation/Inhibition Imbalance in Animal Models of Autism Spectrum Disorders. *Biological Psychiatry*, 81(10), 838-847. doi:10.1016/j.biopsych.2016.05.011
- Lein, E. S., Hawrylycz, M. J., Ao, N., Ayres, M., Bensinger, A., Bernard, A., . . . Jones, A. R. (2007). Genome-wide atlas of gene expression in the adult mouse brain. *Nature*, 445(7124), 168-176. doi:10.1038/nature05453
- Lenth, R. V. (2016). Least-Square Means: The RPackage lsmeans. *J. Stat. Soft.*, 69, 1-33.
- Leterrier, C., Vacher, H., Fache, M. P., d'Ortoli, S. A., Castets, F., Autillo-Touati, A., & Dargent, B. (2011). End-binding proteins EB3 and EB1 link microtubules to ankyrin G in the axon initial segment. *Proc Natl Acad Sci U S A*, 108(21), 8826-8831. doi:10.1073/pnas.1018671108
- Li, L., Liu, C., Amato, R. J., Chang, J. T., Li, W., & Li, W. (2014). CDKL2 promotes epithelial-mesenchymal transition and breast cancer progression. *5(21)*, 10840-10853. doi:10.18632/oncotarget.2535
- Liang, J. S., Huang, H., Wang, J. S., & Lu, J. F. (2019). Phenotypic manifestations between male and female children with CDKL5 mutations. *Brain Dev*, 41(9), 783-789. doi:10.1016/j.braindev.2019.05.003
- Liang, J. S., Shimojima, K., Takayama, R., Natsume, J., Shichiji, M., Hirasawa, K., . . . Yamamoto, T. (2011). CDKL5 alterations lead to early epileptic encephalopathy in both genders. *Epilepsia*, 52(10), 1835-1842. doi:10.1111/j.1528-1167.2011.03174.x
- Lin, C., Franco, B., & Rosner, M. R. (2005). CDKL5/Stk9 kinase inactivation is associated with neuronal developmental disorders. *Hum Mol Genet*, 14(24), 3775-3786. doi:10.1093/hmg/ddi391
- Loi, M., Trazzi, S., Fuchs, C., Galvani, G., Medici, G., Gennaccaro, L., . . . Ciani, E. (2020). Increased DNA damage and apoptosis in CDKL5-deficient neurons. *Molecular Neurobiology*, 57, 2244-2262.
- López-Rivera, J. A., Pérez-Palma, E., Symonds, J., Lindy, A. S., McKnight, D. A., Leu, C., . . . Lal, D. (2020). A catalogue of new incidence estimates of monogenic neurodevelopmental disorders caused by de novo variants. *Brain*, 143(4), 1099-1105. doi:10.1093/brain/awaa051
- Lupori L, S. G., Fuchs, C, Mazziotti R, Stefanov A, Putignano E, Napoli D, Strettoi E, Ciani E, Pizzorusso T. (2019). Site-specific abnormalities in the visual system of a mouse model of CDKL5 deficiency disorder. *Human Molecular Genetics*, 28(17), 2851-2861. doi:10.1093/hmg/ddz102
- M. Elia, M. F., R. Ferri, A. Spalletta, M. Bottitta, G. Calabrese, M. Carotenuto, S.A. Musumeci, M. Lo Giudice, M. Fichera. (2008). CDKL5 mutations in boys with severe encephalopathy and early-onset intractable epilepsy. *Neurology*, 71, 997-999.

- Mangatt, M., Wong, K., Anderson, B., Epstein, A., Hodgetts, S., Leonard, H., & Downs, J. (2016). Prevalence and onset of comorbidities in the CDKL5 disorder differ from Rett syndrome. *Orphanet J Rare Dis*, *11*(1), 39. doi:10.1186/s13023-016-0418-y
- Mari, F., Azimonti, S., Bertani, I., Bolognese, F., Colombo, E., Caselli, R., . . . Landsberger, N. (2005). CDKL5 belongs to the same molecular pathway of MeCP2 and it is responsible for the early-onset seizure variant of Rett syndrome. *Hum Mol Genet*, *14*(14), 1935-1946. doi:10.1093/hmg/ddi198
- McGraw, C. M., Samaco, R. C., & Zoghbi, H. Y. (2011). Adult Neural Function Requires MeCP2. *Neuron*, *69*(6), 186-186. doi:10.1016/j.neuron.2011.06.039
- McKhann, G. M., 2nd, Wenzel, H. J., Robbins, C. A., Sosunov, A. A., & Schwartzkroin, P. A. (2003). Mouse strain differences in kainic acid sensitivity, seizure behavior, mortality, and hippocampal pathology. *Neuroscience*, *122*(2), 551-561. doi:10.1016/s0306-4522(03)00562-1
- Mei, D., Marini, C., Novara, F., Bernardina, B. D., Granata, T., Fontana, E., . . . Guerrini, R. (2010). Xp22.3 genomic deletions involving the CDKL5 gene in girls with early onset epileptic encephalopathy. *Epilepsia*, *51*(4), 647-654. doi:10.1111/j.1528-1167.2009.02308.x
- Mei, Y., Monteiro, P., Zhou, Y., Kim, J. A., Gao, X., Fu, Z., & Feng, G. (2016). Adult restoration of Shank3 expression rescues selective autistic-like phenotypes. *Nature*, *530*(7591), 481-484. doi:10.1038/nature16971
- Merriam, E. B., Millette, M., Lombard, D. C., Saengsawang, W., Fothergill, T., Hu, X., . . . Dent, E. W. (2013). Synaptic regulation of microtubule dynamics in dendritic spines by calcium, F-actin, and drebrin. *J Neurosci*, *33*(42), 16471-16482. doi:10.1523/JNEUROSCI.0661-13.2013
- Mertz, J., Tan, H., Pagala, V., Bai, B., Chen, P. C., Li, Y., . . . Peng, J. (2015). Sequential Elution Interactome Analysis of the Mind Bomb 1 Ubiquitin Ligase Reveals a Novel Role in Dendritic Spine Outgrowth. *Mol Cell Proteomics*, *14*(7), 1898-1910. doi:10.1074/mcp.M114.045898
- Mirzaa, G. M., Paciorkowski, A. R., Marsh, E. D., Berry-Kravis, E. M., Medne, L., Alkhateeb, A., . . . Das, S. (2013). CDKL5 and ARX mutations in males with early-onset epilepsy. *Pediatr Neurol*, *48*(5), 367-377. doi:10.1016/j.pediatrneurol.2012.12.030
- Monory, K., Massa, F., Egertová, M., Eder, M., Blaudzun, H., Westenbroek, R., . . . Lutz, B. (2006). The Endocannabinoid System Controls Key Epileptogenic Circuits in the Hippocampus. *Neuron*, *51*(4), 455-466. doi:10.1016/j.neuron.2006.07.006
- Montini, E., Andolfi, G., Caruso, A., Buchner, G., Walpole, S. M., Mariani, M., . . . Franco, B. (1998). Identification and characterization of a novel serine-threonine kinase gene from the Xp22 region. *Genomics*, *51*(3), 427-433. doi:10.1006/geno.1998.5391
- Mulcahey, P. J., Tang, S., Takano, H., White, A., Davila Portillo, D. R., Kane, O. M., . . . Coulter, D. A. (2020). Aged heterozygous Cdkl5 mutant mice exhibit spontaneous epileptic spasms. *Exp Neurol*, *332*, 113388. doi:10.1016/j.expneurol.2020.113388
- Muller, A., Helbig, I., Jansen, C., Bast, T., Guerrini, R., Jahn, J., . . . Kluger, G. (2016). Retrospective evaluation of low long-term efficacy of antiepileptic drugs and ketogenic diet in 39 patients with CDKL5-related epilepsy. *Eur J Paediatr Neurol*, *20*(1), 147-151. doi:10.1016/j.ejpn.2015.09.001
- Munoz, I. M., Morgan, M. E., Peltier, J., Weiland, F., Gregorczyk, M., Brown, F. C., . . . Rouse, J. (2018). Phosphoproteomic screening identifies physiological substrates of the CDKL5 kinase. *EMBO J*, *37*(24), e99559. doi:10.15252/embj.201899559

- Muñoz, I. M., Morgan, M. E., Peltier, J., Weiland, F., Gregorczyk, M., Brown, F. C., . . . Rouse, J. (2018). Phosphoproteomic screening identifies physiological substrates of the CDKL 5 kinase. *The EMBO Journal*, *37*(24), e99559. doi:10.15252/embj.201899559
- Nawaz, M. S., Giarda, E., Bedogni, F., La Montanara, P., Ricciardi, S., Ciceri, D., . . . Kilstrup-Nielsen, C. (2016). CDKL5 and Shootin1 Interact and Concur in Regulating Neuronal Polarization. *PLoS One*, *11*(2), e0148634. doi:10.1371/journal.pone.0148634
- Nemos, C., Lambert, L., Giuliano, F., Doray, B., Roubertie, A., Goldenberg, A., . . . Philippe, C. (2009). Mutational spectrum of CDKL5 in early-onset encephalopathies: a study of a large collection of French patients and review of the literature. *Clin Genet*, *76*(4), 357-371. doi:10.1111/j.1399-0004.2009.01194.x
- Okuda, K., Kobayashi, S., Fukaya, M., Watanabe, A., Murakami, T., Hagiwara, M., . . . Tanaka, T. (2017). CDKL5 controls postsynaptic localization of GluN2B-containing NMDA receptors in the hippocampus and regulates seizure susceptibility. *Neurobiol Dis*, *106*, 158-170. doi:10.1016/j.nbd.2017.07.002
- Okuda, K., Takao, K., Watanabe, A., Miyakawa, T., Mizuguchi, M., & Tanaka, T. (2018). Comprehensive behavioral analysis of the Cdkl5 knockout mice revealed significant enhancement in anxiety- and fear-related behaviors and impairment in both acquisition and long-term retention of spatial reference memory. *PLoS One*, *13*(4), e0196587. doi:10.1371/journal.pone.0196587
- Olson, H. E., Demarest, S. T., Pestana-Knight, E. M., Swanson, L. C., Iqbal, S., Lal, D., . . . Benke, T. A. (2019). Cyclin-Dependent Kinase-Like 5 Deficiency Disorder: Clinical Review. *Pediatr Neurol*, *97*, 18-25. doi:10.1016/j.pediatrneurol.2019.02.015
- Olson, H. E., & Poduri, A. (2012). CDKL5 mutations in early onset epilepsy: Case report and review of the literature. *Journal of Pediatric Epilepsy*, *1*, 151-159.
- Ozonoff, S., Heung, K., Byrd, R., Hansen, R., & Hertz-Picciotto, I. (2008). The onset of autism: patterns of symptom emergence in the first years of life. *Autism Research*, *1*(6), 320-328. doi:10.1002/aur.53
- Paciorkowski, A., Seltzer, L., & Neul, J. (2018). *Developmental Encephalopathies In: Swaiman's Pediatric Neurology* (6 ed.). Philadelphia: Mosby.
- Paoletti, P., Bellone, C., & Zhou, Q. (2013). NMDA receptor subunit diversity: impact on receptor properties, synaptic plasticity and disease. *Nature Reviews Neuroscience*, *14*(6), 383-400. doi:10.1038/nrn3504
- Pchitskaya, E., Kraskovskaya, N., Chernyuk, D., Popugaeva, E., Zhang, H., Vlasova, O., & Bezprozvanny, I. (2017). Stim2-Eb3 Association and Morphology of Dendritic Spines in Hippocampal Neurons. *Sci Rep*, *7*(1), 17625. doi:10.1038/s41598-017-17762-8
- Pederick, D. T., Richards, K. L., Piltz, S. G., Kumar, R., Mincheva-Tasheva, S., Mandelstam, S. A., . . . Thomas, P. Q. (2018). Abnormal Cell Sorting Underlies the Unique X-Linked Inheritance of PCDH19 Epilepsy. *Neuron*, *97*(1), 59-66 e55. doi:10.1016/j.neuron.2017.12.005
- Peikes, T., Hartley, J. N., Mhanni, A. A., Greenberg, C. R., & Appendino, J. P. (2019). Reflex Seizures in a Patient with CDKL5 Deficiency Disorder. *Can J Neurol Sci*, *46*(4), 482-485. doi:10.1017/cjn.2019.29
- Pizzo, R., Gurgone, A., Castroflorio, E., Amendola, E., Gross, C., Sassoe-Pognetto, M., & Giustetto, M. (2016). Lack of Cdkl5 Disrupts the Organization of Excitatory and Inhibitory Synapses and Parvalbumin Interneurons in the Primary Visual Cortex. *Front Cell Neurosci*, *10*, 261. doi:10.3389/fncel.2016.00261

- Qin, C., Ren, L., Ji, M., Lv, S., Wei, Y., Zhu, D., . . . Xu, J. (2017). CDKL1 promotes tumor proliferation and invasion in colorectal cancer. *Volume 10*, 1613-1624. doi:10.2147/ott.s133014
- Reim, D., Distler, U., Halbedl, S., Verpelli, C., Sala, C., Bockmann, J., . . . Schmeisser, M. J. (2017). Proteomic Analysis of Post-synaptic Density Fractions from Shank3 Mutant Mice Reveals Brain Region Specific Changes Relevant to Autism Spectrum Disorder. *Front Mol Neurosci*, *10*, 26. doi:10.3389/fnmol.2017.00026
- Ricciardi, S., Kilstrup-Nielsen, C., Bienvenu, T., Jacqueline, A., Landsberger, N., & Broccoli, V. (2009). CDKL5 influences RNA splicing activity by its association to the nuclear speckle molecular machinery. *Hum Mol Genet*, *18*(23), 4590-4602. doi:10.1093/hmg/ddp426
- Ricciardi, S., Ungaro, F., Hambrock, M., Rademacher, N., Stefanelli, G., Brambilla, D., . . . Broccoli, V. (2012). CDKL5 ensures excitatory synapse stability by reinforcing NGL-1-PSD95 interaction in the postsynaptic compartment and is impaired in patient iPSC-derived neurons. *Nat Cell Biol*, *14*(9), 911-923. doi:10.1038/ncb2566
- Riva, V., Cantiani, C., Mornati, G., Gallo, M., Villa, L., Mani, E., . . . Molteni, M. (2018). Distinct ERP profiles for auditory processing in infants at-risk for autism and language impairment. *Scientific Reports*, *8*(1). doi:10.1038/s41598-017-19009-y
- Roberts, T. P. L., Khan, S. Y., Rey, M., Monroe, J. F., Cannon, K., Blaskey, L., . . . Edgar, J. C. (2010). MEG detection of delayed auditory evoked responses in autism spectrum disorders: towards an imaging biomarker for autism. *Autism Research*, n/a-n/a. doi:10.1002/aur.111
- Rosner, M., Siegel, N., Valli, A., Fuchs, C., & Hengstschläger, M. (2010). mTOR phosphorylated at S2448 binds to raptor and rictor. *38*(1), 223-228. doi:10.1007/s00726-008-0230-7
- Rothwell, P. E., Fuccillo, M. V., Maxeiner, S., Hayton, S. J., Ozgun, G., Lim, B. K., . . . Sudhof, T. C. (2014). Autism-associated neuroligin-3 mutations commonly impair striatal circuits to boost repetitive behaviors. *Cell*, *158*(1), 198-212. doi:10.1016/j.cell.2014.04.045
- Rubenstein, J. L. R., & Merzenich, M. M. (2003). Model of autism: increased ratio of excitation/inhibition in key neural systems. *Genes, Brain and Behavior*, *2*(5), 255-267. doi:10.1034/j.1601-183x.2003.00037.x
- Rui, Y., Myers, K. R., Yu, K., Wise, A., De Blas, A. L., Hartzell, H. C., & Zheng, J. Q. (2013). Activity-dependent regulation of dendritic growth and maintenance by glycogen synthase kinase 3 β . *4*. doi:10.1038/ncomms3628
- Rusconi, L., Salvatoni, L., Giudici, L., Bertani, I., Kilstrup-Nielsen, C., Broccoli, V., & Landsberger, N. (2008). CDKL5 expression is modulated during neuronal development and its subcellular distribution is tightly regulated by the C-terminal tail. *J Biol Chem*, *283*(44), 30101-30111. doi:10.1074/jbc.M804613200
- Ruzankina, Y., Pinzon-Guzman, C., Asare, A., Ong, T., Pontano, L., Cotsarelis, G., . . . Brown, E. J. (2007). Deletion of the Developmentally Essential Gene ATR in Adult Mice Leads to Age-Related Phenotypes and Stem Cell Loss. *Cell Stem Cell*, *1*(1), 113-126. doi:10.1016/j.stem.2007.03.002
- Saby, J. N., Peters, S. U., Roberts, T. P. L., Nelson, C. A., & Marsh, E. D. (2020). Evoked potentials and EEG analysis in Rett syndrome and related developmental encephalopathies: towards a biomarker for translational research. *Frontiers in Integrative Neuroscience*, *14*. doi:10.3389/fnint.2020.00030
- Sacha, & Valakh, V. (2015). Excitatory/Inhibitory Balance and Circuit Homeostasis in Autism Spectrum Disorders. *Neuron*, *87*(4), 684-698. doi:10.1016/j.neuron.2015.07.033

- Sankoorikal, G. M. V., Kaercher, K. A., Boon, C. J., Lee, J. K., & Brodtkin, E. S. (2006). A Mouse Model System for Genetic Analysis of Sociability: C57BL/6J Versus BALB/cJ Inbred Mouse Strains. *Biological Psychiatry*, *59*(5), 415-423. doi:10.1016/j.biopsych.2005.07.026
- Sartori, S., Di Rosa, G., Polli, R., Bettella, E., Tricomi, G., Tortorella, G., & Murgia, A. (2009). A novel CDKL5 mutation in a 47,XXY boy with the early-onset seizure variant of Rett syndrome. *Am J Med Genet A*, *149A*(2), 232-236. doi:10.1002/ajmg.a.32606
- Sekiguchi, M., Katayama, S., Hatano, N., Shigeri, Y., Sueyoshi, N., & Kameshita, I. (2013). Identification of amphiphysin 1 as an endogenous substrate for CDKL5, a protein kinase associated with X-linked neurodevelopmental disorder. *Arch Biochem Biophys*, *535*(2), 257-267. doi:10.1016/j.abb.2013.04.012
- Shin, E., Kashiwagi, Y., Kuriu, T., Iwasaki, H., Tanaka, T., Koizumi, H., . . . Okabe, S. (2013). Doublecortin-like kinase enhances dendritic remodelling and negatively regulates synapse maturation. *4*, 1440. doi:10.1038/ncomms2443
- Shipton, O. A., & Paulsen, O. (2014). GluN2A and GluN2B subunit-containing NMDA receptors in hippocampal plasticity. *Philosophical Transactions of the Royal Society B: Biological Sciences*, *369*(1633), 20130163. doi:10.1098/rstb.2013.0163
- Smith CM, H. T., Finger JH, Bello SM, McCright IJ, Xu J, Baldarelli RM, Beal JS, Campbell JW, Corbani LE, Frost PJ, Lewis, JR, Giannatto SC, Miers DB, Shaw DR, Kadin JA, Richardson JE, Smith CL, Ringwald M. (2019). The mouse Gene Expression Database (GXD): 2019 update. *Nuclei Acids Res.*, *47*, D774-779.
- Solazzi, R., Fiorini, E., Parrini, E., Darra, F., Dalla Bernardina, B., & Cantalupo, G. (2018). Diaper changing-induced reflex seizures in CDKL5-related epilepsy. *Epileptic Disord*, *20*(5), 428-433. doi:10.1684/epd.2018.0999
- Spratt, P. W. E., Ben-Shalom, R., Keeshen, C. M., Burke, K. J., Clarkson, R. L., Sanders, S. J., & Bender, K. J. (2019). The Autism-Associated Gene Scn2a Contributes to Dendritic Excitability and Synaptic Function in the Prefrontal Cortex. *Neuron*, *103*(4), 673-685.e675. doi:10.1016/j.neuron.2019.05.037
- Stosser, M. B., Lindy, A. S., Butler, E., Retterer, K., Piccirillo-Stosser, C. M., Richard, G., & McKnight, D. A. (2018). High frequency of mosaic pathogenic variants in genes causing epilepsy-related neurodevelopmental disorders. *Genet Med*, *20*(4), 403-410. doi:10.1038/gim.2017.114
- Straube, A., & Merdes, A. (2007). EB3 regulates microtubule dynamics at the cell cortex and is required for myoblast elongation and fusion. *Curr Biol*, *17*(15), 1318-1325. doi:10.1016/j.cub.2007.06.058
- Symonds, J. D., Zuberi, S. M., Stewart, K., McLellan, A., O'Regan, M., MacLeod, S., . . . Wilson, M. (2019). Incidence and phenotypes of childhood-onset genetic epilepsies: a prospective population-based national cohort. *Brain*, *142*(8), 2303-2318. doi:10.1093/brain/awz195
- Szafranski, P., Golla, S., Jin, W., Fang, P., Hixson, P., Matalon, R., . . . Stankiewicz, P. (2015). Neurodevelopmental and neurobehavioral characteristics in males and females with CDKL5 duplications. *Eur J Hum Genet*, *23*(7), 915-921. doi:10.1038/ejhg.2014.217
- Tang, S., Terzic, B., Wang, I. J., Sarmiento, N., Sizov, K., Cui, Y., . . . Coulter, D. A. (2019). Altered NMDAR signaling underlies autistic-like features in mouse models of CDKL5 deficiency disorder. *Nat Commun*, *10*(1), 2655. doi:10.1038/s41467-019-10689-w
- Tang, S., Wang, I. J., Yue, C., Takano, H., Terzic, B., Pance, K., . . . Zhou, Z. (2017). Loss of CDKL5 in Glutamatergic Neurons Disrupts Hippocampal Microcircuitry and Leads to Memory

- Impairment in Mice. *J Neurosci*, 37(31), 7420-7437. doi:10.1523/JNEUROSCI.0539-17.2017
- Tao, J., Van Esch, H., Hagedorn-Greife, M., Hoffmann, K., Moser, B., Raynaud, M., . . . Kalscheuer, V. M. (2004). Mutations in the X-linked cyclin-dependent kinase-like 5 (CDKL5/STK9) gene are associated with severe neurodevelopmental retardation. *Am J Hum Genet*, 75(6), 1149-1154. doi:10.1086/426460
- Tauboll, E., Sveberg, L., & Svalheim, S. (2015). Interactions between hormones and epilepsy. *Seizure*, 28, 3-11. doi:10.1016/j.seizure.2015.02.012
- Trazzi, S., De Franceschi, M., Fuchs, C., Bastianini, S., Viggiano, R., Lupori, L., . . . Ciani, E. (2018). CDKL5 protein substitution therapy rescues neurological phenotypes of a mouse model of CDKL5 disorder. *Human Molecular Genetics*, 27(9), 1572-1592. doi:10.1093/hmg/ddy064
- Van Esch, H., Jansen, A., Bauters, M., Froyen, G., & Fryns, J. P. (2007). Encephalopathy and bilateral cataract in a boy with an interstitial deletion of Xp22 comprising the CDKL5 and NHS genes. *Am J Med Genet A*, 143(4), 364-369. doi:10.1002/ajmg.a.31572
- Velíšková, J., Velíšek, L., Mareš, P., & Rokyta, R. (1990). Ketamine suppresses both bicuculline- and picrotoxin-induced generalized tonic-clonic seizures during ontogenesis. *Pharmacology Biochemistry and Behavior*, 37(4), 667-674. doi:10.1016/0091-3057(90)90544-r
- Wang, D. D., & Kriegstein, A. R. (2008). GABA Regulates Excitatory Synapse Formation in the Neocortex via NMDA Receptor Activation. 28(21), 5547-5558. doi:10.1523/jneurosci.5599-07.2008
- Wang, I. T., Allen, M., Goffin, D., Zhu, X., Fairless, A. H., Brodtkin, E. S., . . . Zhou, Z. (2012). Loss of CDKL5 disrupts kinome profile and event-related potentials leading to autistic-like phenotypes in mice. *Proc Natl Acad Sci U S A*, 109(52), 21516-21521. doi:10.1073/pnas.1216988110
- Wang, X., Bey, A. L., Katz, B. M., Badea, A., Kim, N., David, L. K., . . . Jiang, Y.-H. (2016). Altered mGluR5-Homer scaffolds and corticostriatal connectivity in a Shank3 complete knockout model of autism. *Nature Communications*, 7(1), 11459. doi:10.1038/ncomms11459
- Weaving, L. S., Christodoulou, J., Williamson, S. L., Friend, K. L., McKenzie, O. L., Archer, H., . . . Gecz, J. (2004). Mutations of CDKL5 cause a severe neurodevelopmental disorder with infantile spasms and mental retardation. *Am J Hum Genet*, 75(6), 1079-1093. doi:10.1086/426462
- Wong, R. O. L., & Ghosh, A. (2002). Activity-dependent regulation of dendritic growth and patterning. *Nature Reviews Neuroscience*, 3(10), 803-812. doi:10.1038/nrn941
- Yang, M., & Crawley, J. N. (2009). Simple Behavioral Assessment of Mouse Olfaction. *Current Protocols in Neuroscience*, 48(1). doi:10.1002/0471142301.ns0824s48
- Yennawar, M., White, R. S., & Jensen, F. E. (2019). AMPA Receptor Dysregulation and Therapeutic Interventions in a Mouse Model of CDKL5 Deficiency Disorder. *J Neurosci*, 39(24), 4814-4828. doi:10.1523/JNEUROSCI.2041-18.2019
- Yizhar, O., Fenno, L. E., Prigge, M., Schneider, F., Davidson, T. J., O'Shea, D. J., . . . Deisseroth, K. (2011). Neocortical excitation/inhibition balance in information processing and social dysfunction. *Nature*, 477(7363), 171-178. doi:10.1038/nature10360
- Young, P., Qiu, L., Wang, D., Zhao, S., Gross, J., & Feng, G. (2008). Single-neuron labeling with inducible Cre-mediated knockout in transgenic mice. *Nat Neurosci*, 11(6), 721-728. doi:10.1038/nn.2118

- Zeisel, A., Munoz-Manchado, A. B., Codeluppi, S., Lonnerberg, P., La Manno, G., Jureus, A., . . . Linnarsson, S. (2015). Cell types in the mouse cortex and hippocampus revealed by single-cell RNA-seq. *Science*, *347*(6226), 1138-1142. doi:10.1126/science.aaa1934
- Zhou, A., Han, S., & Zhou, Z. J. (2017). Molecular and genetic insights into an infantile epileptic encephalopathy - CDKL5 disorder. *Front Biol (Beijing)*, *12*(1), 1-6. doi:10.1007/s11515-016-1438-7
- Zhu, Y.-C., & Xiong, Z.-Q. (2019). Molecular and Synaptic Bases of CDKL5 Disorder. *Developmental Neurobiology*, *79*(1), 8-19. doi:10.1002/dneu.22639
- Zhu, Y. C., Li, D., Wang, L., Lu, B., Zheng, J., Zhao, S. L., . . . Xiong, Z. Q. (2013). Palmitoylation-dependent CDKL5-PSD-95 interaction regulates synaptic targeting of CDKL5 and dendritic spine development. *Proc Natl Acad Sci U S A*, *110*(22), 9118-9123. doi:10.1073/pnas.1300003110
- Zhu, Y. C., & Xiong, Z. Q. (2019). Molecular and Synaptic Bases of CDKL5 Disorder. *Dev Neurobiol*, *79*(1), 8-19. doi:10.1002/dneu.22639
- Zoghbi, H. Y., & Bear, M. F. (2012). Synaptic Dysfunction in Neurodevelopmental Disorders Associated with Autism and Intellectual Disabilities. *Cold Spring Harbor Perspectives in Biology*, *4*(3), a009886-a009886. doi:10.1101/cshperspect.a009886